ALMA MATER STUDIORUM
UNIVERSITÀ DI BOLOGNA

DOTTORATO DI RICERCA IN

CHIMICA

Ciclo 37

Settore Concorsuale: 03/C1 - CHIMICA ORGANICA

Settore Scientifico Disciplinare: CHIM/06 - CHIMICA ORGANICA

NICKEL CATALYSIS FOR ADVANCED SYNTHETIC STRATEGIES AND CARBON DIOXIDE VALORISATION

Presentata da: Riccardo Giovanelli

Coordinatore Dottorato

Cristina Puzzarini

Supervisore

Marco Bandini

Co-supervisore

Marco Lucarini

Esame finale anno 2025

Index

I *Abstract*

During my PhD studies great efforts have been dedicated at the *kernel* development of new synthetic paradigms aimed at CO_2 valorisation as C1 synthon. To this end the efficacy of nickel homogenous catalysis has been successfully mastered and exploited, moreover; within the general boundaries of nickel catalysed cross-electrophile coupling a valuable and innovative synthetic pathway for trifluoromethyl carbinols was also developed.[i]

The Introduction part of this manuscript starts with a short but due section regarding the environmental aspects of carbon dioxide pollution, which out of necessity represent the current interpretative key of our generation.

The text evolves through the analysis of possible academic uses of CO_2 rather than industrial ones, this section takes advantage of an accurate analysis of carbon dioxide employment in place of carbon monoxide for laboratory scale applications and preparation of carbonyl containing chemicals.

Introduction goes on unfolding nickel catalysis history and early achievements like Kumada and Heck cross coupling reactions. From this early organic synthesis masterpieces achieved through the deployment of nickel (and palladium) catalysis the focus is then posed on the rection modality and along this line cross electrophile couplings have then been introduced. At this stage an arbitrarily choice has been made to approach smoothly the final themes of this work. Indeed, examples of carboxylation under cross electrophilic conditions and a general framework on trifluoromethylations provides a recount for the topic while paving the way to Results and Discussion part.

The second section of the manuscript is dedicated at punctual description of the work carried out during these three years, herein a short iterative scheme articulated in consistent literature review – reaction development – conclusion has been adopted for all three presented works. The first synthetic methodology is directed at the preparation of the ketone moiety embedded in a tetralone based scaffold with a second CO_2 molecule incorporation giving rise also at a carboxylic group. The focal point of the work revolves around the activation exerted by $AlCl_3$ onto carbon dioxide and its synergy with nickel catalysis for the consecutive forging of three *C-C* σ-bonds. Proper mechanism investigation and dedicated experiments have been carried out to formulate a consistent mechanism proposal and to support the dual role of $AlCl_3$ as activator of CO_2 and as oxygen atom scavenger.

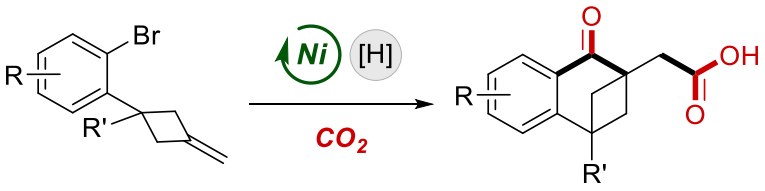

The second project developed deals with lactams and lactones preparation, for this transformation employing carbon dioxide more synthetic methodologies are available, but many of them rely on redox neutral cyclization, thus limiting the choice on suitable starting materials; while many others require carbon dioxide activation or evolves CO during the reaction course. The devised methodology developed within our research group successfully bypasses CO based intermediates, nickel cross-electrophilic conditions open to $2e^-$ *reductive cyclizations* as effective reaction channel. $AlCl_3$ again plays a dual key role in the activation of CO_2 and for the generation of carbamate-like *transient protecting group*, proper experimental and theoretical investigations have been furnished to draw an eligible reaction mechanism.

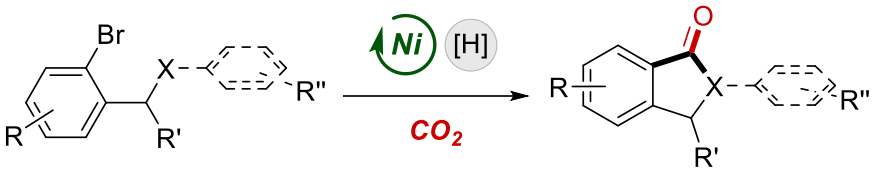

Finally, nickel catalysis has been put to work for the development of α-aryl-α-trifluoromethyl alcohols synthesis, as matter of fact since its infancy fluorination chemistry is of great interest for pharmaceuticals preparations. This red thread was followed to progressively show C-CF_3 bond forging methodologies in the Introduction part, up to the available reaction classes for proper α-aryl-α-trifluoromethyl carbinols moiety preparation in the relative Literature Review section. It is here just before the conclusion that the metal catalysed strategy we developed is discovered as a field breakthrough for the reaction modality and for the exploitation of a reagent never used before to accomplish the desired transformation (*N*-trifluoroethoxyphtalimide). The synthetic methodology is capable to merge aryl iodides and the C-centered radical derived from *N*-trifluoroethoxyphtalimide under nickel cross electrophilic conditions, delivering a large series of products also with biological relevance in high yields and under mild reaction conditions.

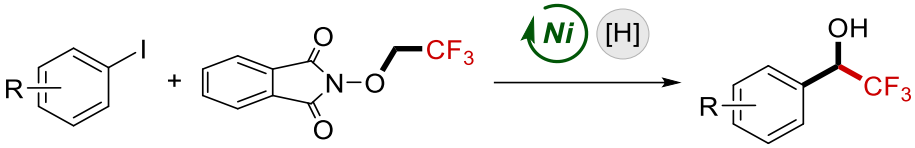

II *Abbreviations*

NZE: Net Zero Emission

IEA: International Energy Agency

IPCC: International Panel on Climate Change

GWP: Global Warming Potential

GHG: Green House Gases

EJ: Exajoule

PV: Photovoltaics

EVs: Electric Vehicles

Gt: Giga tonnes

CRS: Carbon Removal Strategies

GW: Giga Watt

EOR: Enhanced Oil Recovery

CCS: Carbon Capture Storage

CCU: Cabon Capture and Utilization

Mt: Mega tonnes

LA: Lewis Acid

LB: Lewis Base

FLP: Frustrated Lewis Pair

LUMO: Lowest Unoccupied Molecular Orbital

SOMO: Single Occupied Molecular Orbital

HOMO: Highest Occupied Molecular Orbital

SET: Single Electron Transfer

PC: Photocatalyst

R&D: Research and Discovery

CDI: Carbonyldiimidazole

$BMImBF_4$: Butylmethylimidazole tetrafluoroborate

TBD: 1,5,7-Triazabicyclo[4.4.0]dec-5-ene

THF: Tetrahydrofurane

EWG: Electronwithdrawing

EDG: Electrondonating

DME: 1,2-Dimethoxyethane

DMF: *N*,*N*-Dimethylformamide

PTA: 1,3,5-Triaza-7-phosphatricyclo[3.3.1.1^{3,7}]decane

NMP: *N*-Methyl-2-Pyrrolidone

CDT: 1,5,9-Cyclododecatriene

COD: 1,5-Cyclooctadiene

OA: Oxidative Addition

TM: Transmetallation

RE: Reductive Elimination

XEC: Cross Electrophile Coupling

Bpy: Bipyridine

CVE: Constant Voltage Electrolysis

BOx: BisOxazoline

BiOx: Bi-Oxazoline

PyrOx: Pyridine-Oxazoline

PyBOx: Pyridine-Bisoxazoline

PhOx: Phosphinooxazoline

TMSCl: Trimethylsilylchloride

HFIP: Hexafluoroisopropanol

HAA: Hydrogen Atom Abstraction

XAT: Halogen Atom Abstraction

DMPK: Drug Metabolism and Pharmacokinetics

BINAP: 2,2′-Bis(diphenylphosphino)-1,1′-binaphthyl

CSA: Camphorsulphonic Acid

DCM: Dichloromethane

$TBABF_4$: Tetrabutylammonium Tetrafluoroborate

CCE: Constant Current Electrolysis

DMSO: Dimethylsulphoxide

DMA: *N*,*N*-Dimethylacetamide

MO: Molecular Orbital

BDE: Bond Dissociation Energy

$TMSCF_3$: Trimethyl(Trifluoromethyl)silane

TFAA: Trifluoroacetic Anhydride

TFSP: Trifluoromethylsulfonyl pyridinium salt

DoM: Direct *orto*-Metallation

DMAD: Dimethylacetylenedicarboxylate

MP: Methylpyruvate

STAB: Sodium Triacetoxyborohydride

CFL: Compact Fluorescent Light

eChem: Electrochemical(ly)

PMSH: Polymethylhydrosiloxane

DBU: 1,8-Diazabiciclo[5.4.0]undec-7-ene

FeTPP: Iron(tetraporphyrinato) chloride

TEA: Triethylamine

MOFs: Metal Organic Frameworks

n.d.: Not Detected

N.R.: No Reaction

n.q.: Nearly Quantitative

DPPA: Diphenylphosphoryl azide

MBH: Morita Baylis Hillman

DFT: Density Functional Theory

p-TSA: *para*-Toluensulphonic Acid

NHPI: *N*-Hydroxyphtalimide

DCC: Dicyclohexylcarbodiimide

DMAP: *N*,*N*-dimethylaminopyridine

BHT: Butyrratedhydroxytoluene

TS: Transition State

XRD: X-Ray Diffractometry

ORTEP: Oak Ridge Thermal Ellipsoid Plot

CDM: Concerted Deprotonation-Metallation

dppp: Diphenylphosphino propane

TM: Transition Metal

ACN: Acetonitrile

TFA: Trifluoroacetic Acid

SM: Starting Material

FDA: Food and Drug Administration

TDAE: Tetrakis Dimethylamino Ethylene

XylBINAP: 2,2'-Bis[di(3,5-xylyl)phosphino]-1,1'-binaphthyl

DAIPEN: 1,1-Bis(4-methoxyphenyl)-3-methyl-1,2-butanediamine

TFE: 2,2,2-Trifluoroethanole

TEMPO: 2,2,6,6-Tetramethylpiperidine-1-oxyl

MS: Molecular Sieves

PCM: Polarizable Continuum Model

m.p.: melting point

FC: Flash Chromatography

TLC: Thin Layer Chromatography

1 Introduction

1.1 CO_2 Environmental Perspective

In this initial part of the introduction a remark on environmental CO_2 levels build-up is provided. A short examination then of possible solution to reach a NZE scenario (Net Zero Emission) for one of the most polluting sectors (energy sector), as sorted by IEA (International Energy Agency) and IPCC (Internation Panel on Climate Change) is unfolded. This first part is at the edge of climatology science but is due to remind the multifaceted problem of CO_2 to all readers which are kindly invited not to forget the importance of multi disciplinarity collaborations.

1.1.1 Green House Gases Pollution

It is clear that the current global climate crisis it is affecting modern society at all levels and that the main driver for a more sustainable social development is represented by more conscious choices from people on their lifestyles. Among all, chemists and the greater scientific community, jointly to industry, should play a leading role regarding the information of public and at the same time pursue the transition from the fossil fuel era to a more sustainable demand/offer energy age. This is a fundamental step required to all countries which are currently trying to address the sustainability goals posed by the Internation Panel on Climate Change (IPCC) during the several international deals and agreements such as Montréal (1987), Rio de Janeiro (1992), Kyoto (1997), Paris (2015).

In about two hundred years the energy gained from the fossil fuels has led humankind to some of its greatest achievements. This has also triggered what many people have named *Anthropocene* which is referred to the extent of the impact of human activity over the entire globe. In this frame the most notorious consequence of fossil fuels utilization is the rise of carbon dioxide levels into planet atmosphere, from 280 ppm (parts per million) up to the current value of 420 ppm thus originating the greenhouse effect. Such environmental situation is not going to be sustainable with the required, and always increasing, energy demand from modern society. Currently, we need to boost the changing of most of the present supply chains toward a net zero emission of CO_2 and we should do this as fast as possible thus, to avoid a point of no return from which-on the ecosystem cannot sustain anymore the natural resources demand in terms of cultivable land and water supply.[1,2,3]

It is also worth to recall that environmental scientists are not only keeping an eye over the greenhouse effect triggered by gas emissions which is affecting the *fast* carbon cycle, but they are also concerned about other important biogeochemical flows such as the nitrogen and the phosphorus cycles or the change into the biosphere integrity as well as the freshwater use.[4,5]

The annual global net emission of carbon dioxide is a process taking place on a giga tonnes scale and reported data refers to the net anthropic emissions minus the net anthropic sinks. Other gases possessing a different GWP (global warming potential) from CO_2 are monitored, such as methane, nitrous oxide and a group of fluorinated gases. All together the amounts of GHG (greenhouse gases)

[1] Will Steffen *et al*., *Science* 347,1259855 (**2015**).DOI:10.1126/science.1259855
[2] C. Hansen *et al*.; *Science*, 342, 850-853 (**2013**).DOI:10.1126/science.1244693
[3] Fu Z., Ciais P., Wigneron J.P. *et al.*; *Nat Commun* **15**, 4826 (2024). DOI: 10.1038/s41467-024-49244-7
[4] Wang J., Vilmin L., Mogollón J.M., Beusen A.H.W., van Hoek W.J., Liu X., Pika P.A., Middelburg J.J., Bouwman A.F., *Environ Sci Technol*. **2023**; 57, (36), 13506-13519. DOI: 10.1021/acs.est.3c04230
[5] Xingxing Kuang *et al.*; *Science* 383, eadf0630 (**2024**).DOI:10.1126/science.adf0630

are commonly expressed in CO_2-eq (giga tonnes of CO_2 equivalents) through conversions made *via* the corresponding GWP factors (one for each gas). Different sorting systems are being used across the available literature, but the one reported here, for simplicity is sorting in five main categories (**Tab.1**). Estimation is not an easy task, but most reliable institution and data agree on a value around 59±6,6 Gt/y of GHG emissions (value referred to 2019). Not great results have been achieved lately if a global overlook to the emission is considered, but minor positive signal seem to point in the right direction, complete information may be found in the IPCC (Internation Panel on Climate Change) reports.[6] Unfortunately, all currently operating technologies to diminish or remove CO_2 from the atmosphere are still far to reach a macroscopic abatement effect on a global scale. All the efforts put to work on industrial scale to decrease CO_2 levels and to produce new chemical goods are now operating on a kilo/mega tonnes scale. In fact, the energy related and industry sector (**Tab. 1**, first row) despite being the major contributor to the annual GHG emissions share, accounted for about two thirds of the total emission with little increase from the relative share of 59% recorded in 1990.

Table 1. Global net anthropogenic GHG emissions in 2019 expressed as in the reports from IPCC[6]

GHG category	GHG emissions 2019 ($GtCO_2$-eq/y)	Percentage
CO_2 Fossil Fuel and Industry	38.0	64%
CO_2 Land Use, Land-Use Change and Forestry	6.6	11%
Methane	11.0	18%
Nitrous Oxide	2.7	5%
Fluorinated gases	1.4	2%
Total Amount	**59.7**	**100%**

Among western countries different agendas stemming from international agreements to abate CO_2 emission has been approved during last three decades. Nevertheless, the fixed goals that each country is supposed to achieve are often moved down or only partially accomplished due to several reasons which remains beyond scientific horizons.

1.1.2 The Energy Sector: a case study for carbon dioxide removal strategies

Data reported by IPCC investigation and analysis are meant to be used by policymakers in different contexts. A closely look can indeed be taken over the energy sector since its share of GHG emissions has been of 37 Gt of CO_2, accounting for about two third of the total in 2023 also according to IEA update report made in 2023 '*Net Zero Roadmap. A Global Pathway to Keep the 1.5°C Goal in Reach"*.[7]

In the original report released in 2021 by the same agency a NZE Scenario (Net-Zero Emission by 2050) has been defined: *"to show what is needed across the main sectors by various actors, and by when, for the world to achieve net-zero energy related and industrial process CO_2 emissions by 2050"*.[8] In the updated version of this document the main goals have been slightly revised, a full list

[6] IPCC, 2023: Summary for Policymakers. In: Climate Change 2023: Synthesis Report. DOI: 10.59327/IPCC/AR6-9789291691647.001
[7] IEA (2023), Net Zero Roadmap: A Global Pathway to Keep the 1.5 °C Goal in Reach, IEA, Paris https://www.iea.org/reports/net-zero-roadmap-a-global-pathway-to-keep-the-15-0c-goal-in-reach
[8] IEA (2021), Net Zero by 2050, IEA, Paris https://www.iea.org/reports/net-zero-by-2050

is provided (**Tab. 2**).[9,10] Moreover many forecasts for trends of GHG emissions cuts has been drawn, here reported there is a plot against an analogue trend drawn in the eventuality of a low international cooperation case for emissions cuttings (**Figure 1**, top). As might be seen the difference is enormous and is not possible not to have international cooperation to achieve the fixed goals. IEA has compared few GHG emissions scenarios against the NZE, but in the IPCC reports more than 90 different scenarios can be found which consider more parameters and different endpoint temperature (2100) for global warming. It is worth to mention the emission drop for electricity sector which is expected to become almost a non-emitting contributor in about 20 years, with a steep decrease which is two to three times greater than the reduction rates for industry and transport sectors.

Figure 1. GHG emissions drops in the NZE scenario *vs* a low international cooperation case (top). Detailed GHG emission curve with the contribution of CO_2 removal actions (bottom left). Main contribution in GHG emission drop to 2050 in the overall energy sector (bottom right).

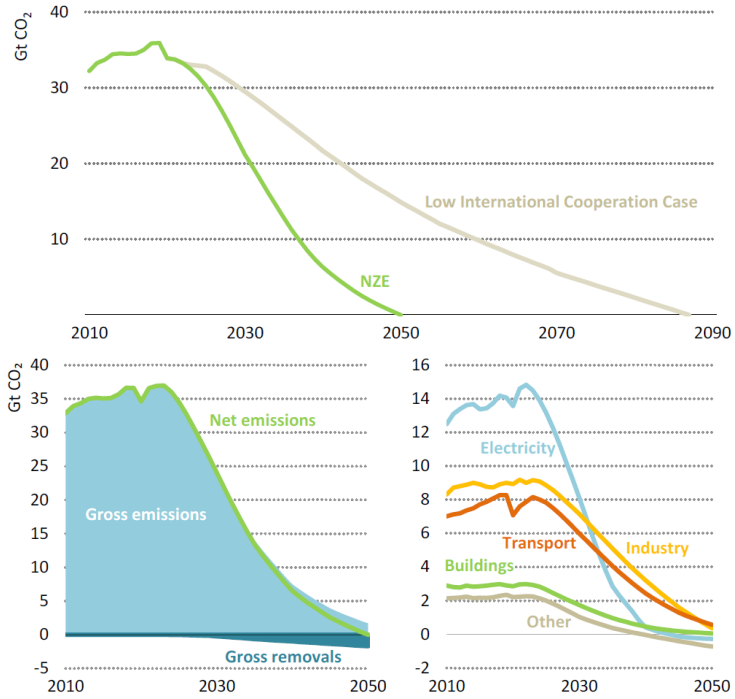

Regarding the target posed by the NZE from to 2021 to 2023 a slight increase of the total energy sector emissions is the most important data, the share for unabated fossil fuels has received a minor change from 58% to 63% but the target for 2050 is always at 11%; thus has also led to a revised value for the total energy consumption, shifted from 390 to 410 EJ for 2030.The forecast to 2050 has instead changed for solar PV capacity addition which have increased from 630 GW to 820 GW. This data is in line with a non-negligible rise of electricity shares in total final consumption from 28% (2030) to 53% (2050) for the latest scenario values which points toward a large electrification of different sectors. It is also reasonable a revised value of battery capacity installed shifted from 590 GW (2021) to 1020 GW (2023) for 2030 stage to ensure a secure power supply. Regarding the wind capacity

[9] As far as 2023,168 countries out of 198 have submitted their NDC (National Determined Contribution), which are climate action plans to cut emissions and adapt to climate impacts, to the UNFCCC (United Nations Framework Convention of Climate Change) after the Paris Agreement subscription in 2015.
[10] EU has submitted its second NDCs update to the UNFCCC, in the document it is recalled the EU regulation 2023/857 which sets a 40% GHG emission reduction by 2030 with respect to 2005 levels, and the emissions reductions shares by country (Italy: 43,7%).

additions, a slight decrease is reported for the 2030 forecast, probably due to the solar PV compensation. The EVs (electric vehicles) sale shares are supposed to grow a little then the previously reported one both in 2030, from 60% to 90%, and in 2050 from 65% to 95%. The hydrogen related technologies have been overestimated in 2021 but in both scenarios contribution the related market not expected to undergo through major revolutions. The total CO_2 removal data from 2023, 0.2 Gt (2030) and 1.7 Gt (2050), has not been substantially modified since 2021 but it is directly connected to the CRS (Carbon Removal Strategies) which are still an underdeveloped field with widespread applications requiring more hard knowledges about CO_2.

Table 2. Change in selected indicators for the NZE Scenario between 2021 and 2023. Both scenarios are relative to 1.4°C increase in the temperature by 2100 and are also consistent with IPCC Scenario C1. Unabated fossil fuels include also the ones used for non-energy purposes.

	2021 IEA target		**2023 IEA target**	
	2030	**2050**	**2030**	**2050**
Total net energy sector CO2 emissions (Gt)	21.1	0.0	24.0	0.0
Share of unabated fossil fuels in total energy supply (%)	58%	11%	62%	11%
Total final consumption (EJ)	390	340	410	340
Solar PV capacity additions (GW)	630	630	820	820
Wind capacity additions (GW)	390	350	320	350
Share of EVs in car sales (%)	60%	90%	65%	95%
Total CO_2 capture (Gt)	1.8	7.7	1.0	6.1
Total CO_2 removal (Gt)	0.3	1.9	0.2	1.7
Installed stationary battery capacity (GW)	590	3100	1020	4200
Share of electricity in total final consumption (%)	26%	49%	28%	53%
Share of H_2 and H_2-based fuels in total final consumption	2%	10%	1%	8%

The outlined series of data should clear out every doubt about how much we're short on time to take actions to reach NZE scenario collaborating with other countries and on a policies side as well as on technical developments.[11,12]

[11] Kramer, G., Haigh, M.; *Nature* **462**, 568–569 (2009).
[12] Cherp, A., Vinichenko, V., Tosun, J. *et al.*; *Nat Energy* **6**, 742–754 (2021).

1.2 Carbon Dioxide Utilization in Industry and Academia

This introduction section aims at highlighting *industrial and academic* carbon dioxide utilization as two faces of the same coin. The great disparity in handleable gas volumes naturally leads to the illustration of chemistries in stark contrast to each other regarding the intricacies of chemical processes. An initial use by sector for industrial application is briefly provided, and then urea synthesis is described, since it is a carbonylation process completely based on the use of CO_2. Academic uses of greenhouse gas are indeed sorted after the affordable class of compounds; this has been done presenting a CO_2 *vs* CO based procedures for the synthesis of the same targets thus to better spot advantages and drawbacks in each case.

1.2.1 Industrial Carbon Dioxide Uses

Nowadays the operating industrial uses for CO_2 concern the EOR process (Enhanced Oil Recovery) or the direct mineralization as inorganic carbonates into exhausted natural gas fields, which are converted into deep geological storages. These two strategies can be generally identified as CCS (Carbon Capture Storage) processes. Otherwise, the synthesis of four main chemicals: urea, polycarbonates, salicylates/cyclic carbonates and methanol are the only industrialized processes using CO_2 on a relevant scale (**Tab. 3**). In the last 15 years few companies have also implemented a CO_2 capturing units as downstream transformations into their plants for the synthesis of methanol. This latter strategy is generally labelled as CCU (Carbon Capture Utilization).

Table 3. Global chemical goods production in which CO_2 is used as a process feedstock.[13]

Chemical good	Annual scale production	CO_2 captured
Urea	150 Mt	112 Mt
Methanol	107 Mt	2 Mt
Cyclic carbonates	80 kt	40 kt
Salicylates	70 kt	30 kt
Total Amount	**250.15 Mt**	**114.07 Mt**

In the grand view of the fast carbon cycle (**Fig. 2**), CCS and CCU are included in the CRS (Carbon Removal Strategies) and should be the main drivers for the abatement of CO_2 levels in the atmosphere and represent a key step in the transition to an environmentally sustainable circular economy. A long time would occur to debate whether actual technologies have a chance to reach on time a relevant modification of equilibria of the fast carbon cycle, altered from humankind activities during the last century. Data reported below can indeed give an idea of emissions magnitude order in the atmosphere.

[13] Fasihi, M., and Breyer, C.; *Energy Environ. Sci.*, **2024**, 17, 3503-3522

Figure 2. Number in yellow shows fluxes of carbon in Gt/y between atmosphere and lands or oceans. Numbers in red highlight the unbalance created by humankind activity per year. White numbers show instead stored amounts of carbon ascribed to the slow carbon cycle.[14]

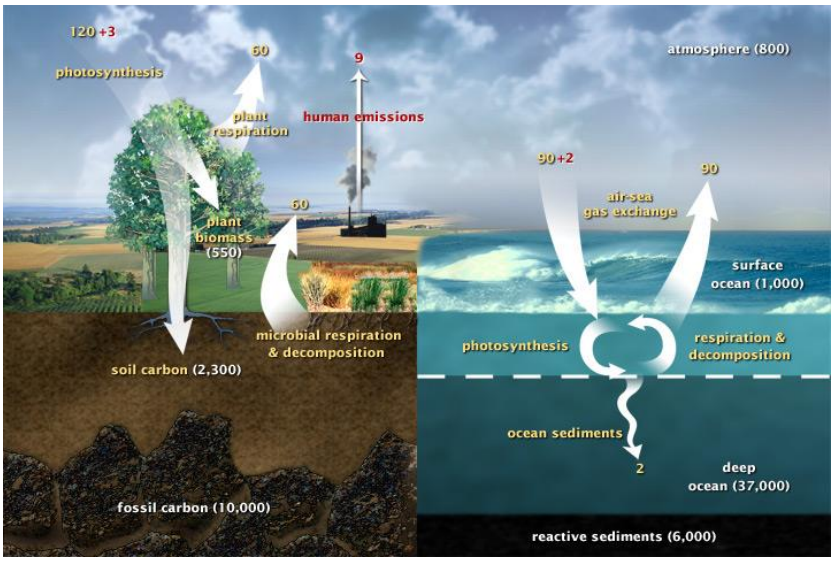

Urea as mentioned above is one of the four main chemicals produced from CO_2 and is the only carbonylation reaction. Urea was first isolated in the second half of 18th century by Hilaire Rouelle, although it has already been noticed earlier by others (Herman Boerhaave), and it has been the first synthetized organic compound in 1828[15]. The first urea preparation due to the work of Friedrich Wöhler which upon mixing inorganic compound (silver cyanate and ammonium chloride) obtained the desired target, later in 1870 A. I. Bessarov achieved urea synthesis from CO_2 and ammonia (**Sch. 1**).

Nowadays urea production is estimated to be around 150 million of tonnes yearly, it is still based on Bessarov chemical transformation, and the industrial synthesis was appointed firstly in 1922 by Carl Bosch and Wilhelm Meiser, but efficient plants have only been developed between the forties and the sixties of the last century.[16,17]

Scheme 1. First urea synthesis by Wöhler from inorganic compound (top), CO_2 based synthesis process from Bessarov still at the base of modern industrial preparation.

Wölher synthesis $\quad AgNCO + NH_4Cl \longrightarrow (NH_2)_2CO + AgCl$

Bessarov synthesis $\quad CO_2 + NH_3 \longrightarrow NH_2C(O)ONH_4 \longrightarrow (NH_2)_2CO + H_2O$

Modern plants where Bessarov chemistry is put to work are equipped thus to carry out the condensation step leading to ammonium carbamate with heat release, here the cooling of the reaction is the easiest way to enhance product formation along with the settings of high pressure so that both reagents and products are maintained in the liquid phase. The second step is ammonium carbamate dehydration: this reaction is slightly endothermic and does not have a great equilibrium constant as

[14] Source: https://earthobservatory.nasa.gov/features/CarbonCycle
[15] Wöhler, F.; (**1828**) *Ann. Phys*., 88: 253-256
[16] Werner, E.A.**;** *J. Chem. Soc., Trans.* **1920**, 117, 1046-1053
[17] Berliner, J. F. T. *Industrial & Engineering Chemistry*, **1936**, 28, 5, 517-522

well as there are no suitable catalysts for the reaction. Urea plants usually operate between 170°C - 220°C and 125 bar - 250 bar with short residence time. Byproducts are biurea originated from two urea molecules condensation and isocyanic acid which may condense into isocyanuric acid (**Sch. 2**). These side reactions are under kinetic control, this highlights the importance of short residence times and a ratio value NH_3/CO_2 of 3 is usually maintained to have less decomposition processes. The water produced in the second step also triggers acid/base equilibria which must be considered.[18]

Scheme 2. Steps for Urea formation (top). Side reactions occurring into urea manufacturing plants (bottom).

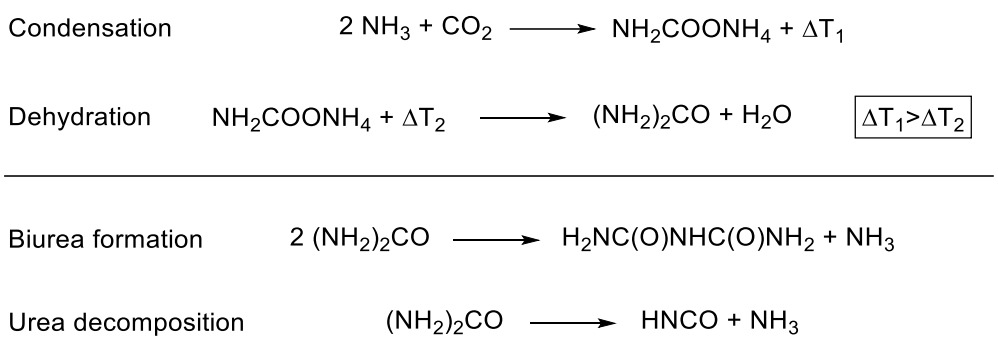

Of the whole annual urea production, about 88% (≈130 Mt/y) is employed in the manufacturing of fertilizers for the agrochemical sector, the CO_2 removed from the atmosphere to sustain such production is about 112 Mt/y. The main countries in the production of urea are China, Russia, United States, and India which covers over half of worldwide production, the principal fertilizers produced beyond urea itself are ammonium nitrate, calcium nitrate, ammonium sulphate and ammonium phosphate. Currently technology leader industries for urea production are Stamicarbon (Netherlands), Snamprogetti (Italy) and Toyo Engineering Corporation (Japan). The utilization of such a large amount of agrochemical fertilizer has also raised attention to the possibility of these nitrogen-based compounds to be a non-negligible source of atmospheric N_2O, but in this sense a more responsible use by the end users of these chemicals represents the crucial factor in lowering the waste production and enhance the achievement of the attended agrochemical results.[19]

In stark contrast with urea, methanol production is still largely sustained by fossil fuels, although access to green methanol is foreseen as one of the next steps for the energetic transition, up to now only one company worldwide is running a plant for CO_2 to methanol conversion; but the strategic location of such a plant over a geothermal site providing energy for the process is the key for successfully running the plant also in terms of costs.

1.2.2 Academic Synthetic Applications of CO_2

Academic research on CO_2 chemistry is a widespread field nowadays. Synthetic utilization of CO_2 rose a long time ago when chemists envisioned into carbon dioxide a versatile C1 synthon suitable for peripheral functionalization (*i.e., carboxylation, carbonylation*) or even structural core elaborations (*i.e., lactonization*) of organic molecules. The early steps undertaken by organic chemists

[18] Meessen, J.; *Chemie Ingenieur Technik*, **2014**, 86,12, 2180-2189
[19] Kanter, D.R., Chodos, O., Nordland, O. *et al.*; *Nat Sustain* **3**, 956–963 (2020). DOI: 10.1038/s41893-020-0577-7

were toward the activation of such inert gas, this was initially done with stoichiometric strong nucleophiles (*i.e., organometallic reagents*), then many other activation strategies emerged and currently CO_2 activation methods are largely dominated by catalytic strategies. Carbon dioxide can be activated via several methods: electrochemically[20] or via photoredox catalysis,[21] but also through classical polar chemistry with nucleophile heteroatoms attack (*i.e. amines or alcohols*), by coordination to a metal center or by coordination to Lewis acid or bases (if LA and LB sites are within the same molecule then the activation method is identified as FLP which stands for Frustrated Lewis Pair).[22] Less common activation methods can indeed involve ionic liquids or carrying CO_2 to supercritical conditions.[23]

Currently carbon dioxide activation and utilization are mainly developed within the field of chemical catalysis, as defined by IUPAC,[24] herein catalytic heterogenous methods are generally employed when hydrogenation of CO_2 to CO, CH_3OH, HCHO and C_{2-3} products are targeted, this represents a hot topic for material and inorganic chemists but lies beyond the purpose of this manuscript. Catalytic homogenous activation strategies are indeed frequently deployed by organic chemists to prepare within one step high added value chemicals, elevating the complexity of a desired organic scaffold while avoiding harsh reaction conditions. In all cases CO_2 activation is promoted by a catalyst in modern synthetic procedures so that the use of stoichiometric additives or harsh organometallic reagents can be avoided (**Fig. 3** top). In most of the illustrated activation modes of CO_2 the initial linear molecular geometry is lost after the coordination or reduction events leading to differently polarized or reduced species which show considerable bended angles (**Fig. 3** middle). For example, at the increase of the bending angle the bond lengths also increase with a decrease in energy of the LUMO orbital, this situation can be triggered by most of the activation methods and naturally favours a single electron reduction which gives CO_2 radical anion with the LUMO being now a SOMO at relatively high energy and a molecular angle of about 135°. The radical anion is more reactive and thus its SOMO – LUMO gap is the smallest, if a second single electron reduction occurs and a proton is captured a formate anion is produced, now with a smaller molecular angle of 130°, similar bond lengths but a higher HOMO – LUMO gap accounting for a slightly lower reactivity. Nowadays the acquisition of this kind of information takes relative efforts through computation but the first studies on CO_2 used to rely on indirect reactivity proofs, only in the luckiest cases an organometallic species with a CO_2 molecule could be isolated and characterized. This is the case of Aresta[25] who reported the first metal-CO_2 complex, Herskovitz[26] has elucidated the structure of iridium-osmium binuclear complex with carbon dioxide; and Collins[27] has contributed by shedding light on a phosphine ligated iridium complex structure with two dimerized CO_2 molecules coordinated to the metal center (**Fig. 3**

[20] Sun, G.Q., Liao, L.L., Ran, C.K., Ye, J.H., and Yu, D.G.; *Accounts of Chemical Research* **2024** 57 (18), 2728-2745.
[21] Zhang, W., Chen, Z., Jiang, Y.X. *et al.*; *Nat Commun* **14**, 3529 (2023)
[22] Corona, H., Pérez-Jiménez, M., de la Cruz-Martínez, F., Fernández, I., Camposj, J., *Angew. Chem. Int. Ed.* **2022**, *61*, e202207581
[23] Behr, A., *Angew. Chem. Int. Ed. Engl.* 271, **1988**, 661-678
[24] *IUPAC Compendium of Chemical Terminology*, 3rd ed. International Union of Pure and Applied Chemistry; 2006.
[25] Aresta, M., Nobile, C.F., Albano, V.G., Forni, E. and Manassero, M., *J. Chem. Soc. Chem. Commun* **1975**, 636-637
[26] Herskovitz, T., Guggenberger, L.J., *J. Am. Chem. Soc.* **1976**G, 98, 1615.
[27] Audett, J. D., Collins, T. J., Santarsiero, B. D., and Spies, G. H., *J. Am. Chem. Soc.* **1982**, 104, 7353

bottom).[28] The activation modes involving transition metal coordination are by far the most investigated one due to the large number of reported procedures where homogeneous as well as heterogeneous *d-block* elements are the active catalysts. The reported modes are only qualitative representations through which CO_2 can be activated by one metallic center, yet more metal centers may be involved in the activation process and often polar solvents strongly influence the aggregation of different reactants.

Figure 3. Hydrogenation methodologies, frequently carried out over heterogeneous catalysts (top left). Homogenous catalysts are usually elected for small organic molecule functionalization with CO_2, also organometals can activate carbon dioxide but homogeneous catalysis aims at replacing these reactants (top right). Activation methods for CO_2 molecule (middle). Early example of CO_2 enclosed in organometallic complexes successfully characterized (bottom).

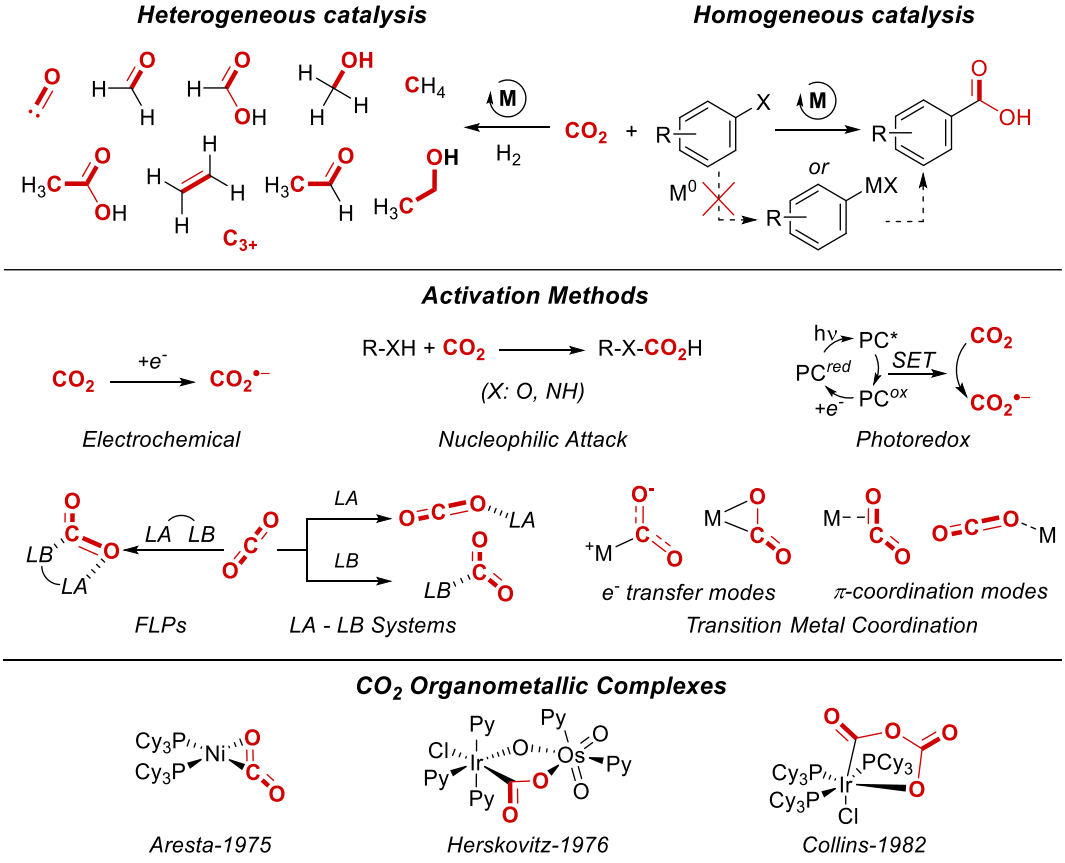

Catalytic carboxylation reactions are a well-established type of transformation and will be disclosed later in the manuscript where cross-electrophile couplings will be presented. Next couple of chapters will be dedicated to carbonylation chemistry since this transformation occurs with classical nucleophile-electrophile polar chemistry.

1.2.2.1 Carbonylations for small organic molecules

Carbonylation reactions are a very large class of transformations where a CO fragment is incorporated into a molecular scaffold over a reactive C-X bond or by reaction with alkynes/alkenes (Oxo-synthesis) in presence of a nucleophile (NuH). Elementary organometallic steps have been extensively elucidated, herein is reported a general mechanism example for nickel catalyzed olefin

[28] Álvarez, A., Borges, M., Corral-Pérez, J.J., Olcina, J.G., Hu, L., Cornu, D., Huang, R., Stoian, D., Urakawa, A., *ChemPhysChem.* **2017**, 18, 3135 – 3141

carbonylation. General agreement is met toward a reactivity scale of feasible transition metals employed for industrially relevant hydroformylations, to date only rhodium and cobalt have found widespread application in industrial carbonylative processes (**Fig. 4**). Chemical industries have also learnt how to properly manipulate CO to efficiently get the desired products by mean of homogeneous as well as heterogeneous catalysis. Nevertheless, higher safety standards and cost effectiveness would be met if CO replacement could turn a feasible solution along with new cheap transition metal catalysed system development. Unfortunately, in industrial relevant processes, CO replacement with other carbonyl sources can indeed result a highly challenging task since a feedstock switch is usually linked to equipment substitution or modifications; thus, in rare cases operative plants are dismantled or shut down exclusively for manufacturing process innovations.[29,30,31,32]

Figure 4. Classical organometallic steps in olefins nickel catalysed carbonylation, branched product is not depicted but *n-/iso-* products ratio is always carefully evaluated (left), industrial relevant carbonylation processes (right).

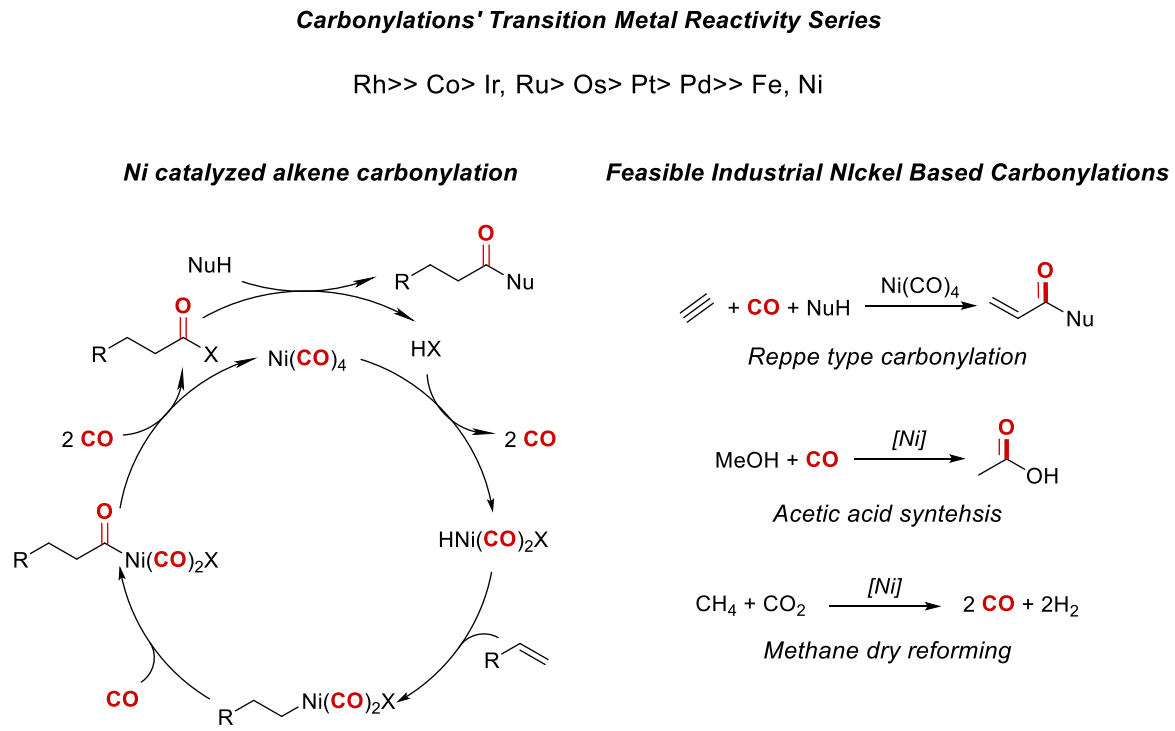

Modern academic solution for hydroformylations indeed, span across the employment of different transition metals as well as CO surrogates, a large share of published methodologies doesn't meet the basic requirements to be scaled up into industrially relevant processes. This undoubtedly represent the *kernel* of pure scientific advancement, and every reader is invited to reason where a continuity solution between academic and industrial realities should be located.

Regarding academic and small *R&D* production of new chemical structures, the available portfolio for CO moiety introduction is large. Nickel along with other metals such as Zn, V, Mn, Cr, Pd, Co,

[29] X.F. Wu, M. Beller; Transition Metal Catalyzed Carbonylation Reactions; **2013**; ISBN : 978-3-642-39015-9
[30] Franke, R., Selent, D., Börner, A., *Chem. Rev.* **2012**, 112, 11, 5675–5732
[31] Field, C.B., Mach, K.J., *Science* **356**, 706-707 (2017)
[32] Parsapur, R.K., Chatterjee, S., and Huang, K.W., *ACS Energy Lett.* **2020**, 5, 9, 2881–2885

Rh, Cu, Fe, Ir and Ru were shown to perform transformations such as those accomplished on larger scale but using CO_2 as CO surrogate while achieving comparable if not better results.

This point will be discussed in the following pages due the considerable efforts and results achieved from academics in shifting the chemical paradigms for a future replacement of CO with CO_2. Such goal would reduce operators' exposure to risky handling of CO or phosgene, while avoiding other chemicals such as CDI (carbonyldiimidazole) and reactions like the Vilsmeier-Haak or Pauson-Khand, utilization of which would only result in larger wastes production.[33,34,35,36]

Conceptually the replacement of CO with CO_2 demands a stoichiometric reductant which act as intermediate or as a final oxygen atom scavenger from carbon dioxide, the need for a final reductant cannot be overcome if CO_2 is employed in place of CO. When "CO" unit is delivered a smart way to classify different processes is based on atoms involved into newly formed chemical bonds (**Fig. 5**).

Figure 5. General concepts depicting the need of stoichiometric reductant for CO_2 and its role as final oxygen atom scavenger (top), functional groups commonly accessed through CO_2 based carbonylation (bottom).

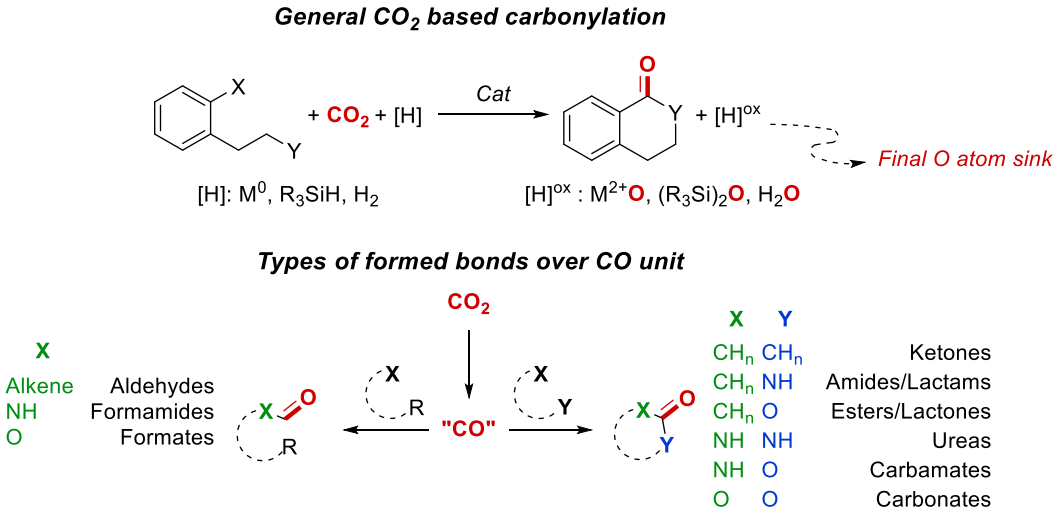

Proofs that moving from CO to CO_2 utilization in current synthetic organic methodologies development is a flourishing topic can be verified by setting up research through common chemical data banks. Let us demand a general ***route A*** able to furnish for example diphenylurea by using carbon monoxide to be found online, meanwhile an alternative ***route B*** is asked to use carbon dioxide in place of CO to get the same product. The illustrated protocols are within the firsts results one can get from available literature, considering the fast updates in the fields (**Fig. 6**).

[33] Wang, L., Sun, W., Liu, C., *Chin. J. Chem.* **2018**, 36, 353−362
[34] Wang, S., and Xi, X., *Chem. Soc. Rev.* **2019**, 48, 382
[35] Song, L., Jiang, Y.X., Zhang, Z., Gui, Y.Y., Zhou, X.Y., and Yu, D.G., *Chem. Commun.* **2020**, 56, 8355
[36] Peng, J.B., Wu, F.P., Wu, X.F., *Chem. Rev.* **2019**, 119, 4, 2090–2127

Figure 6. Synthetic methodologies emerging from literature research for the synthesis of diphenylurea employing carbon monoxide or carbon dioxide alternatively as reagents.

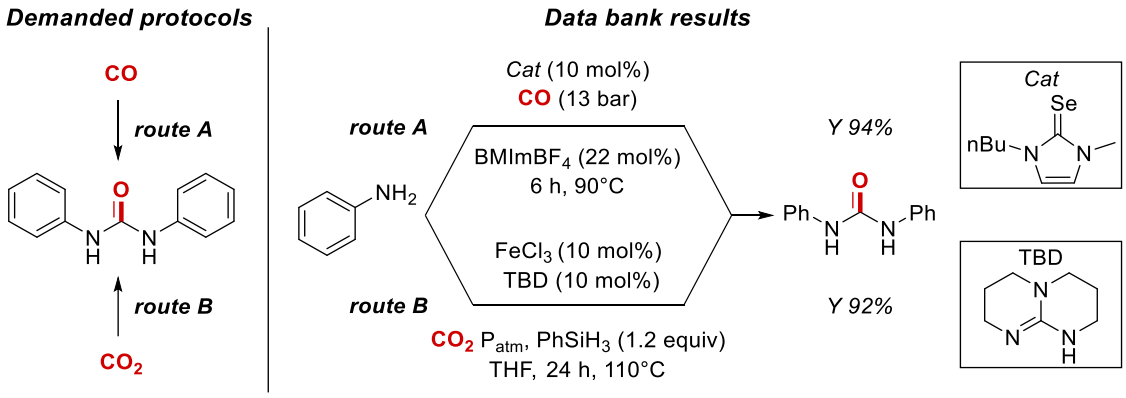

In CO-based procedures less chemicals are used, thus a higher atom economy can be highlighted, but this is might in general be true for most of the procedures which directly uses CO in place of CO_2 since one oxygen atom needs to be scavenged from the latter kind of procedures. The gas handling is much easier and safe in the case of CO_2 based procedure which doesn't require to operate CO at 13 bars. Reaction times are shorter for CO based procedure than those with CO_2, as well as slightly lower temperature are employed 90°C vs 110°. Regarding reaction components used in catalytic amounts $BMImBF_4$/selenium-based system was reported to be reused few times without significant yield drop, on the other hand TBD proofed to be a mandatory additive while $FeCl_3$ was shown to greatly improve yield. Silane reductant is also needed to afford the product in *route B*. The scope of the transformations is a major point which mark a superior performance for the CO_2 based strategy beyond already mentioned safety issues. CO procedure is limited to anilines while in CO_2 based protocol high yields are achieved with differently substituted aniline all ring positions and EWG as EDG substituents are tolerated; primary, secondary amines and benzyl amine can be reacted smoothly; only *orto*-amino benzylamine showed a double formylation instead of affording the expected cyclic mono-formylated product.[37,38]

Quinolinones are also a frequently targeted class of products when carbonylation with CO_2 are attempted, these lactams can also be prepared from CO so that a comparison can be made as for former examples. Quinolin-2-(*1H*)-one **I** has been prepared in 2017 by Jiao and colleagues via an oxidative intermolecular carbonylation with rhodium catalysis, herein authors disclosed how catalytically active rhodium complex delivers the CO moiety on the aniline nitrogen, then activates the α-CH bond to form a cyclometalated intermediate capable to capture the alkyne and giving the product with a chemoselectivity of about 4:1 in favour of the desired product which account for the reported yields.[39] Unfortunately, authors don't report any intramolecular experiment which would have been even better to compare to the methodology reported by Yu and co-workers. The CO_2 based strategy developed by Yu although reporting a narrower substrate scope, 33 examples against 62 furnished by Jiao *et al.* shows an easier set of conditions and a higher yield for the selected example (**Fig. 7**). The main advantages offered by the latter protocol remain the absence of any transition metal

[37] Zhao, Y., Guo, X., Si, Z., Hu, Y., Sun, Y., Liu, Y., Ji, Z., You, J., *J. Org. Chem.* **2020**, 85, 20, 13347–13353
[38] Fengshou, T., Yahong, C., Xiaofang, W., Peng, L., Shiwei, L., *Journal of Chemistry*, **2015**, 210806, 5 pages, 2015. DOI: 10.1155/2015/210806
[39] Li, X., Pan, J., Wu, H., and Jiao, N., *Chem. Sci.* **2017**,8, 6266-6273

catalyst but the use of cheap sodium tert-butoxide for CO_2 activation and avoiding a mixture of CO and oxygen which may set the stage for dangerous scenarios.[40]

Figure 7. Strategies to prepare quinolin-2-(*1H*)-ones either from CO or CO_2.

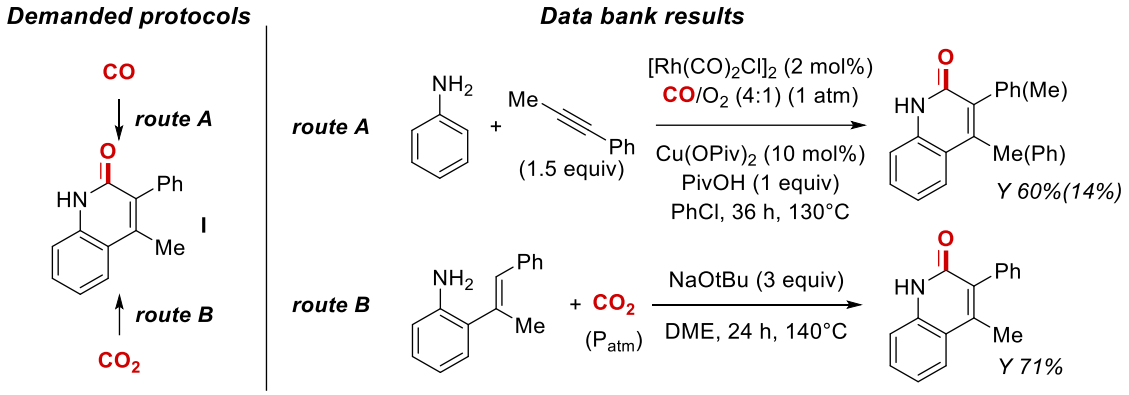

With CO_2-based carbonylation also ketones can be prepared through two C-C bond formations as illustrated in (**Fig. 5**), Ali and colleagues in 2018[41] have developed α-aryl propargyl ketones synthetic methodology via CO while groups of Qi and Jiang have jointly developed a different synthetic route from CO_2 back in 2021 (**Fig. 8**).[42] Starting materials are the same, both strategies exploit palladium chemistry, even the base employed is the same. Thus, an analysis of the transformation scope is needed, in the case of CO protocol higher yields are generally achieved (up to 96%) and 19 analogues have been prepared from aromatic and aliphatic alkynes. In CO_2 based reactions 35 analogues are presented with yields reaching 80% and under close catalytic conditions more than 20 analogues of 2-alkyliden-3-oxindoles are synthetized. The macro picture emerging from these two protocols says that slightly higher yields are achieved when carbon monoxide is employed but only if high pressure equipment is used, while incorporation of carbonyl moiety through carbon dioxide utilization can be done under milder conditions, lower this way safety risks.

Figure 8. Gas-based differentiation in palladium catalyzed Sonogashira cross-coupling strategies to access α-aryl propargyl ketones.

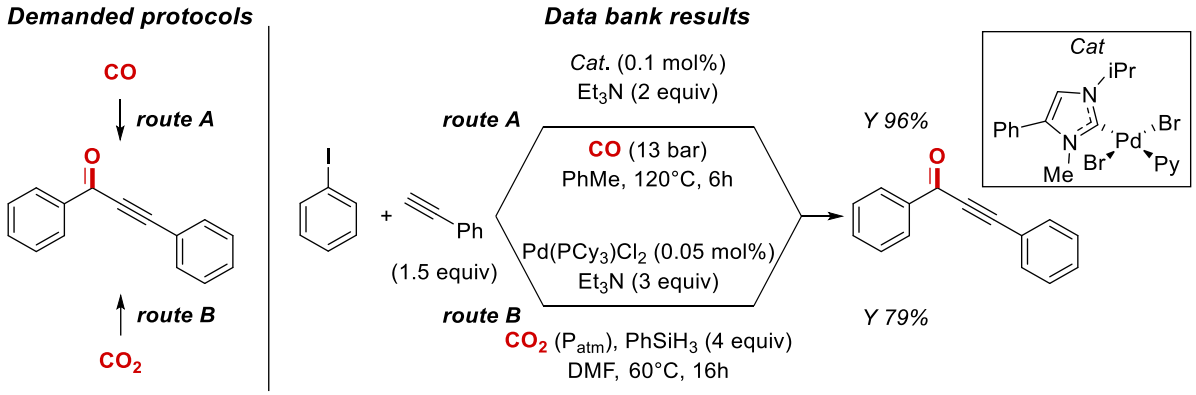

[40] Zhang, Z., Liao, L.L., Yan, S.S., Wang, L., He, Y.Q., Ye, J.H., Li, J., Zhi Y.G., Yu, D.G., *Angew. Chem. Int. Ed.* **2016**, 55, 7068

[41] Ibrahim, M., Malik, I., Mansour, W., Sharif, M., Fettouhi, M., El Ali, B., *Appl Organometal Chem*. **2018**; 32:e4280. DOI: 10.1002/aoc.4280

[42] Xiong, W., Wu, B., Zhu, B., Tan, X., Wang, L., Wu, W., Qi, C., Jiang, H., *ChemCatChem,* **2021**, *13*, 2843.

Reported mechanisms for aryl-propargylic ketone have been described for both procedures by Ali or Qi and Jiang and give a good example of the hurdles the CO_2 based strategies must face when transition metal complex catalysis comes into play. In both cases the organometallic steps engaged by palladium catalyst are the same, namely: *oxidative addition, migratory insertion, alkyne transmetallation* and *eliminative reduction.* When CO is replaced with CO_2 the silane mediated reduction step (**Fig. 9** blue square) needs to match to some extent the rate of the catalytic cycle so that no CO poisoning of the catalyst can happen, neither homocoupling nor generation of biaryls can take place in the reaction mixture via bimolecular off-cycle pathways.

Figure 9. Organometallic mechanism proposed from authors for aryl-propargylic ketone formation with CO_2 (left) and CO (right).

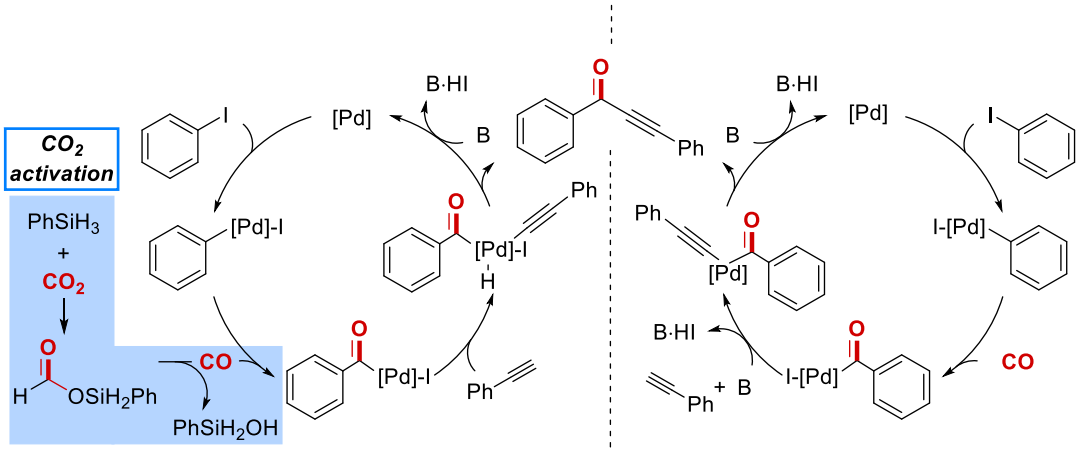

1.2.2.2 Formylation reactions

Other common building block of utmost importance in organic chemistry are aldehydes. As illustrated in former examples let us consider the preparation of *n*-nonenal as a model aldehyde and seek in the literature a preparation based on CO and a synthesis from CO_2.[43,44] The first procedure (*route A*) displays a good yield of 85% but authors have reported a conversion about 10%, this jointly with a *l:b* (*linear: branched*) ratio of 60:40 already constitute non-negligible hurdle and can easily lead to discard this synthetic route, at least for this specific substrate. Sun and colleagues with a CO_2 based strategy have instead reported a set of conditions which give 99% conversion of initial alkene with a recorded yield of 96% and even better *l:b* ratio of 85:15. Moreover a small scope of alkene have been investigated for the latter methodology and even considering the need of a cocatalyst (PTA) and stoichiometric quantities of acetic anhydride the synthetic strategy exploiting CO_2 result a better alternative than the CO-based one by far, regarding both yields and scope assessment (**Fig. 10**).

[43] Bhagade,S.S., Chaurasia, S.R. and Bhanage, B.M., *Catalysis Today*, **2018**, vol. 309, p. 147 - 152
[44] Hua, K., Liu, X., Wei, B., Shao, Z., Deng, Y., Zhong, L., Wang, H. and Sun, Y., *Green Chem*. **2021**, 23, 8040–8046

Figure 10. Synthetic methodologies reported in literature for *n*-nonenal , employing CO (top) and CO_2 (bottom).

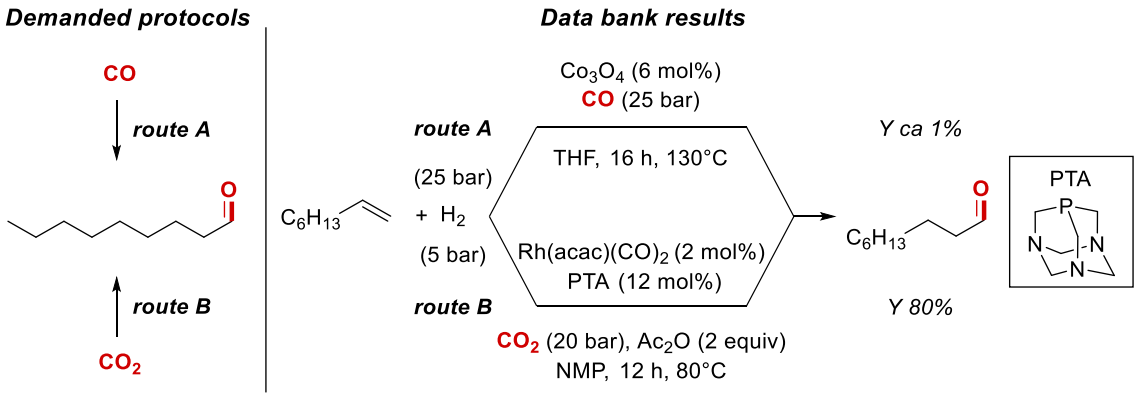

Figure 11. Reported mechanism from Sun and co-worker for the CO_2 alkene hydroformylation, both cycles are supposed to participate in the generation of the product.

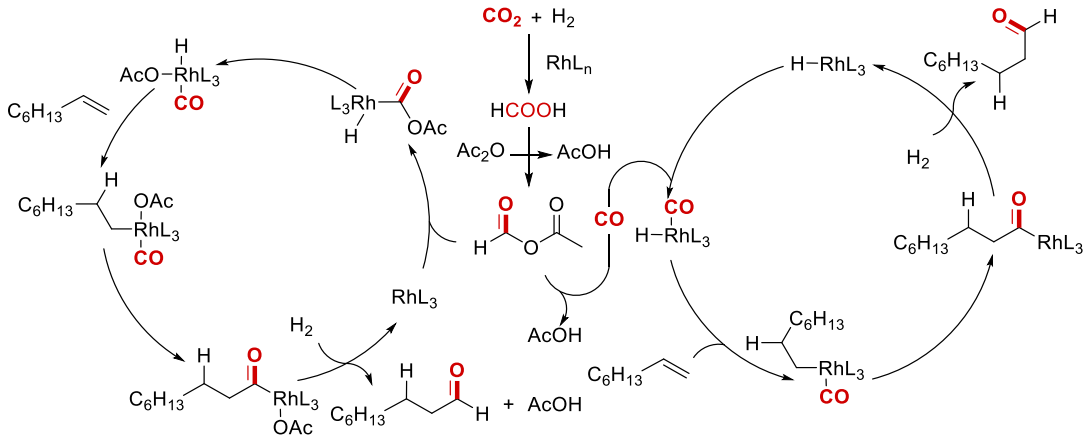

Rhodium complexes are employed also for direct homogeneous CO_2 hydrogenation purposes,[45] here a catalytically competent rhodium species has been wisely adopted for the generation of acetylformate within the reaction mixture. At this stage rhodium intermediates RhL_3 or L_3Rh-H can either coordinate a free CO molecule generated as depicted above (**Fig. 11**) or the acetylformate itself to afford an acylrhodium or a monocarbonyl rhodium complex respectively. The resulting carbonyl rhodium organometallic intermediates are then capable to undergo the classic stepwise *coordination-insertion* step onto the olefin before performing the hydrogenation with molecular H_2 to get the product and regenerate the respective rhodium resting species.

It is worth noting that rhodium-based catalysts can indeed achieve good performances in formylation reactions both with CO and CO_2. In closely related carbonylation of internal alkenes with CO indeed, Beller and co-workers reported linear *n*-nonanol preparation, but intermediate aldehydes were in

[45] Gassner, F. and Leitner, W., *J. Chem. Soc., Chem. Commun.* **1993**, 1465-1466

some cases observed with good yields and *l:b* ratios. However further examples will be illustrated to make clear the broader applicability of CO_2 as carbonylating agent rather than CO.[46]

Preparation of *N*-formyl-*N*-methyl aniline can lastly well represent a benchmark reaction within this formylation framework. A procedure published in 2019 from Jung and Jang[47] uses carbon monoxide at elevated pressure and temperature to enhance the formation of an active carbonylating species between the gas and the base additive (TBD). Authors have shown in the experimental section that also the preformed carbonylatig adduct ([TBD_2---CO]) can afford the *N*-formylated product series but with diminished yields. This first CO based methodology can deliver the formyl group over primary, secondary and aromatic amines for which 18 examples have been reported. The latter synthetic strategy from Chen and He[48] employs a low carbon dioxide pressure, neat condition and a sub-stoichiometric amount of ionic liquid. Similar when not higher yields are recorded under reaction conditions with CO_2, and the investigated portfolio of substrates resemble the former one with 15 examples reported and yields up to 99% (**Fig.12**). The mechanism for the generation of the formamides is ascribed at the formation of a transient complex between CO and TBD for route A protocol. In the second case a silylformate intermediate from CO_2 and the reductant is observed, the subsequent attack by the substrate gives the product and the silanol; authors reported a stabilization during silylformate generation due to a bromide coordination.

Figure 12. Formylation of *N*-methyl-aniline procedures with basic activation of CO in the first case (top) and ionic liquid CO_2 activation in the second case (bottom).

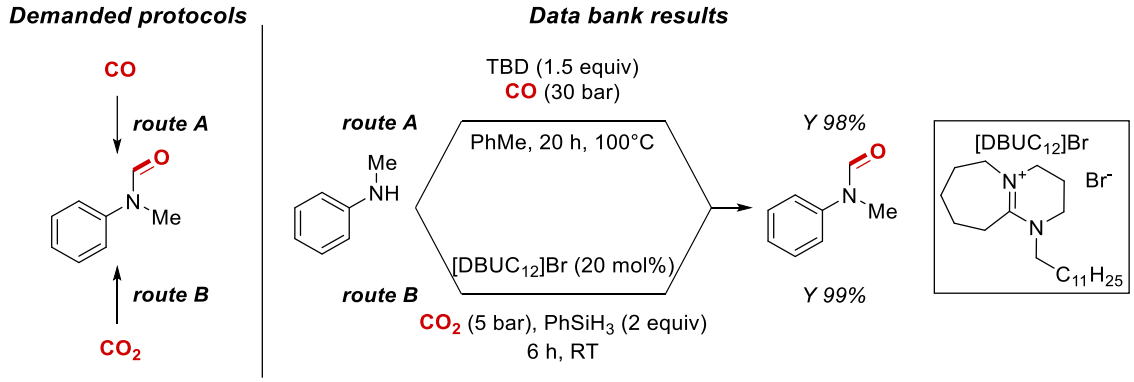

In conclusion of this section about carbonylation chemistry, synthetic methodologies for the construction of ketones, lactams and ureas were reported thus to highlight the potentiality of CO_2 over CO as current and future carbonyl source for the synthesis of small organic molecules aimed at small scales production.

Formylation examples capable for valuable functional groups preparation have been shown, such as formamides and aldehydes either via silane or hydrogen-based CO_2 reduction. Selected examples have been chosen to give a sequential overview on the chances to forge simultaneously differently hybridized C-C, C-X and C-H bonds.

[46] Fleischer, I., Dyballa, K.M., Jennerjahn, R., Jackstell, R., Franke, R., Spannenberg, A., and Beller, M., *Angew. Chem. Int. Ed.* **2013**, 52, 2949 –2953
[47] Noh, H.W., An, Y., Lee, S., Jung, J., Son, S.U., Jang, H.Y., *Adv. Synth. Catal.* **2019**, *361*, 3068.
[48] Li, X.Y., Fu, H.C., Liu, X.F., Yang, S.H., Chen, K.H., He, L.N., *Catalysis Today* 356 (**2020**) 563–569

The way the works were shown has been appointed to enhance how far CO_2 based methodologies have come in the field of carbonylation, nevertheless many other possible ways to embed carbonyl group into organic scaffolds remains unaddressed. From these early synthetic methodologies' development, future outlooks may lead to rethink countless synthetic routes in total synthesis or medicinal chemistry libraries preparation in ways that are not totally clear yet today.

1.3 Nickel catalysis: a broad spectrum of applications

This last introductive section of the manuscript has been conceived to cover different, but selected, types of transformations for which nickel has been largely employed. The basis of nickel organometallic chemistry is initially illustrated, the text follows then the chronological applications in first cross coupling reactions of organonickel complexes (*Kumada and Heck*). Among different nickel catalysed methodologies, cross-electrophile couplings have then been considered due to the relevance for projects presentation. Last part deals instead with freely chosen type of reactions (*carboxylations and trifluoromethylation*) which sets final boundaries for the unfolding of Results and Discussion chapter. Unfortunately, some classic cross coupling like Suzuki-Miyaura or Negishi reactions as well as nickel photoredox catalysed processes will not be disclosed due to space reasons but will be cited at need.

1.3.1 Origins of organonickel chemistry

Nickel was first discovered in 1751 by the Swedish mineralogist Axel Fredrik Cronstedt while he was working to copper extraction from a mineral source. For this reasons nickel has been known also as *Kupfernickel* which stands for "Devil's copper", referring to its naturally occurrence along with copper ores as minor impurity to be removed. It took until 1890 for nickel to enter the realm of organic chemistry when Ludwig Mond, Carl Langer and Friedrik Quincke published the synthesis of nickel tetracarbonyl[49] In 1900 then Mond, a German born chemist patented a purification method (named after himself, Mond process) for nickel from its crude ores which exploited the conversion into gaseous nickel tetracarbonyl and then back to the metallic form, thus obtaining a highly pure metallic nickel. This process for sure had in impact on industrial and academic research for nickel chemistry, but organic chemists generally agree in considering 1960 as *Annus mirabili* since it was first published the preparation of the 18e$^-$ complex, nickel bis(cyclo-octadiene) by Günther Wilke (**Fig. 13**).[50]

Figure 13. Steps of Mond purification process (top left). Wilke synthesis of $Ni(COD)_2$ (top right). Early discovered zerovalent nickel complexes after $Ni(COD)_2$ (bottom).

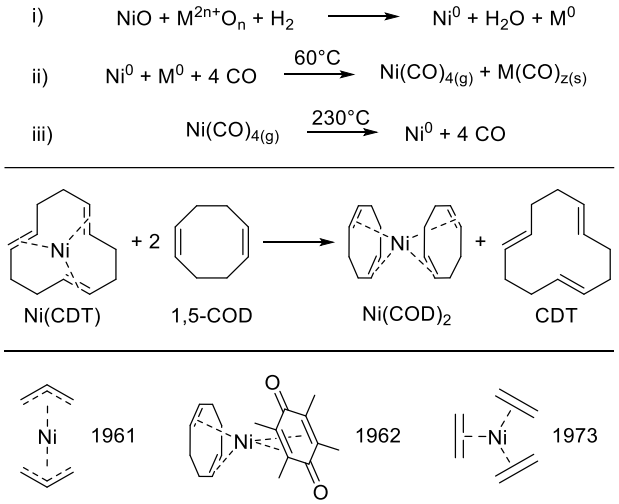

[49] Mond, L., Langer. C., Quincke, F., *J. Chem. SOC*.**1890**. 749
[50] Bunning, E., Cremer, E., Inhoffen, H.H., Kienitz, H., Klever, E., *Angew. Chem.* **1960**, *72*, 565–593.DOI: 10.1002/ange.19600721611

The research carried out by Wilke and co-workers was dealing with the optimization/replacement of Ziegler catalyst for olefin oligomerization based on titanium. Due to the instability shown by nickel cyclo-dodecatriene under certain conditions they reacted this compound with two equivalents of cyclo-octadiene to move from a sixteen-electron complex to an eighteen electron one, which could in theory display higher stability. What they could observe was a nice yellow crystalline compound, correctly identified as nickel bis(cyclo-octadiene) or simply $Ni(COD)_2$. This new compound didn't perform better than Ziegler catalyst for olefin polymerization but gave to organic chemist a new nickel compound which later played a key role in many transformations.

The following year Wilke and Bogdanovic reported the preparation of the zerovalent bis-π-allyl-nickel.[51] In 1962 the preparation of a new zerovalent nickel complex was reported by Schrauzer and colleagues where they managed to replace one of the two cyclooctadiene with a duroquinone molecule; but the strength of this new ligand was considerably higher than those of COD itself limiting this way the replacement of this ligand only with stronger and more nucleophilic ones.[52] In 1973 Wilke again, reported the preparation of tris ethylene nickel ($Ni(C_2H_4)_3$) finally paving the way for a widespread interest into organonickel chemistry.[53,54]

1.3.2 Cross couplings are merged with nickel chemistry

The aim of next couple of sections will not to be exhaustiveness about the freely chosen methodologies, since this would take too long, but rather illustrate how these organic masterpiece transformations were born and what reaction can be achieved considering the latest advancement for such methodologies, on this behalf the hope is to capture readers attention and thus trigger an independent survey of the literature.

1.3.2.1 Kumada Coupling

Cross coupling reactions have emerged as a powerful tool in organic chemistry also prompted by the discovery of all those organometallic complexes shown above, that has been going on since second part of the 20th century. Nevertheless, a detailed survey of the literature issued before 1972 can reveal, to the most careful readers, that cross coupling reactions weren't a sudden breakthrough but represented the most advanced version of a well-known chemistry. Indeed, stoichiometric coupling reactions between organometals complexes and organic halides were known since the discoveries made by Victor Grignard, for many years chemists investigated the effects sorted by the addition of exogenous metals to Grignard coupling reactions. Under these premises the first catalytic cross coupling reaction as we define it today was reported in 1971 by Kochi,[55] when catalytic amounts of copper halides were shown to catalyse the coupling of alkyl Grignard reagents with alkyl halides.

Although the first zerovalent nickel complexes were known for more than ten years it was only in 1972, another *Annus Mirabilis,* when Makoto Kumada[56] and R. J. P. Corriu[57] independently reported

[51] Wilke, G., Bogdanovič, B., *Angew. Chem.* 73 (**1961**) 756
[52] Schrauzer, G. N. and Thyret, H., *Z.*, *Naturforsch., B: J. Chem. Sci.* **1961**, 16, 353– 356, DOI: 10.1515/znb-1961-0601
[53] Fischer, K., Jonas, K. and Wike, G., *Angew. Chem*. 85 (**1973**) 620
[54] Wilke, G., *Angew. Chem. Int. Ed. Engl.* **1988**, 27: 185-206
[55] Kochi, J.K. and Tamura, M., *J. Am. Chem. Soc*. **1971**, 93, 6, 1485–1487
[56] Tamao, K., Sumitani, K. and Kumada, M., *J. Am. Chem. Soc,* **1972,** 94, 4374-4376
[57] Corriu, R.J.P. and Masse, J.P., *Journal of the Chemical Society, Chemical Communications* (3): 144a. DOI: 10.1039/C3972000144A

the first use of nickel catalyst for the coupling between aryl/alkenyl Grignard reagents with aryl/alkenyl halides, with a non-trivial interpretation of the reaction mechanism considered how long ago this purpose was made. Newly unravelled potentialities of nickel catalysis were then known, from this point onward nickel (along with palladium) has been used as catalysts in different classes of organic transformations such as: cross-electrophile couplings, photoredox catalysis and in electrocatalysis. What couldn't be foreseen at that time was probably that the first reactions reported by Kochi, Kumada or Heck in the early seventies wouldn't then have marked the end of an era but rather the beginning of a new one.

Kumada-Corriu original cross coupling mechanism description perfectly accounts for the observed products but doesn't involve any redox event for the nickel catalyst, where oxidation state of +2 is considered to go unchanged all along the reaction pathway (**Fig. 14**). Variations and modification of original reaction conditions has given to organic chemists a powerful tool to forge C-C bonds from a plethora of organic precursors while doing so, also new mechanistic pictures have emerged. For example, under conditions reported in 2018 from Cornella and co-worker, during the scope assessment an inverted *l:b* selectivity was achieved for the addition of secondary Grignard reagent over aryl fluorides.[58] Nevertheless, it is worth to note the changes on the mechanism proposal across fifty years of developments for this reaction.

Figure 14. Mechanistic pictures for Kumada-Corriu cross coupling made by Kumada in 1972 (left) and a modern example from 2018 made by Cornella (right).

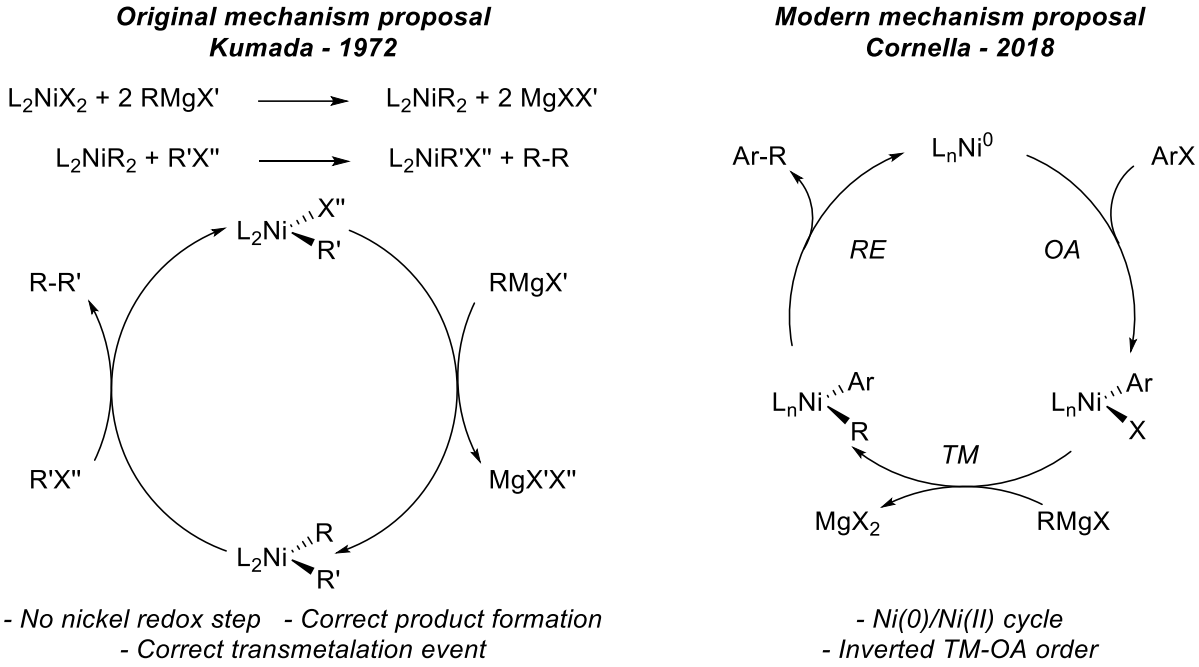

Interesting Kumada coupling procedures have appeared since the seventies, for example conditions to couple aryl trimethylammonium salts and aryl Grignard have been disclosed by Wenkert[59] and co-workers to be feasible under nickel catalysis. Then improved conditions from analogue family salts

[58] Kiso, Y., Tamao, K., Kumada, M., *Journal of Organometallic Chemistry*, 50 (**1973**) C12-C14
[59] Wenkert, E., Han, A.I. and Jenny, C.J., *J. Chem. Soc., Chem. Commun*. **1988**, 975

appeared later under palladium catalysed conditions due to the work of Reeves[60] and colleagues, here better yields and slightly broader substrates tolerance were determined. Lately one interesting set of conditions for the coupling of tertiary alkyl Grignard reagents with alkenyl bromides was published by Mazet[61] group, authors have gained in this case a wide substrate scope and good to high yields except for few sluggishly reactive scope entries. Nickel is the main transition metal employed along with palladium but examples using other transition metals can be found in literature (**Fig. 15**).

Figure 15. Original substrate scope investigated by Kumada in 1972 (top), examples for trialkylaryl ammonium salts cross coupling under palladium r nickel catalysis alternatively (middle), modern example of Kumada coupling, affording a considerable number of products, from low reactive tertiary alkyl Grignard reagents (bottom).

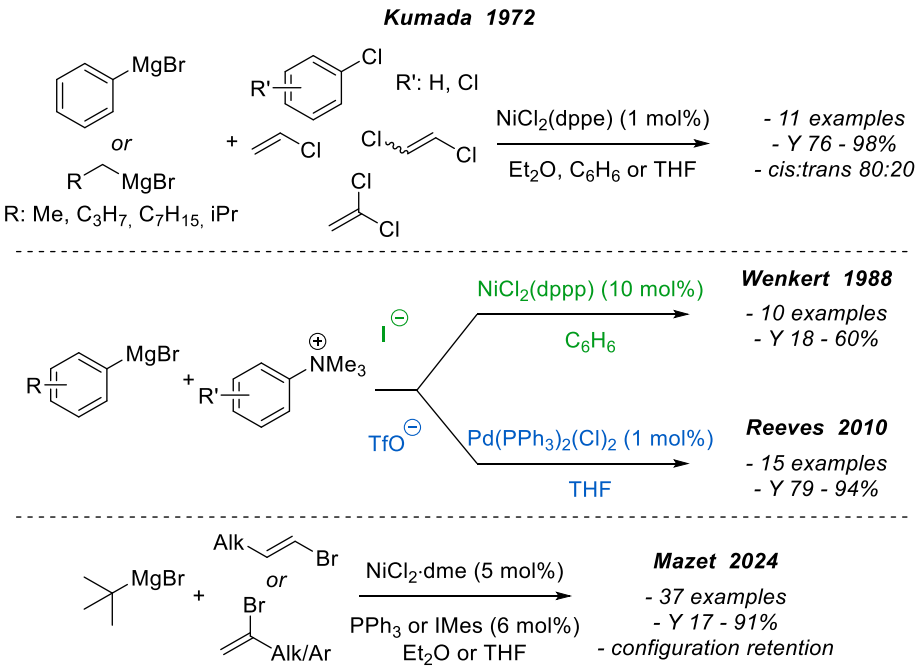

1.3.2.2 Mizoroki-Heck Coupling

In February 1971, while Kumada and Corriu were developing their procedures another organic chemistry masterpiece was published by the Mizoroki group, the reaction enabled for the coupling of iodobenzene onto olefins substrates by means of palladium dichloride salt.[62] The Japanese research group had correctly identified the product but in the work a detailed reaction mechanism as well as a wide substrate scope were not provided unfortunately. Less than a year later in January 1972 Heck and Nolley showed a procedure where aryl, benzyl and vinyl halides could be reacted under milder conditions with palladium acetate and a series of olefins to get the same products.[63] In the latter paperwork precise suggestion on the mechanism were presented, a wider series of coupling partners was investigated, and a clearer background picture was furnished. In fact, Heck and Nolley report that this procedure should overcome and replace the use of organomercury, -tin and -lead compounds in addition reactions over alkenyl halides (**Sch. 3**). To some extent the approach they followed is the

[60] Reeves, J.T., Fandrick, D.R., Tan, Z., Song, J.J., Lee, H., Yee, N.K., and Senanayake, C.H., *Org. Lett.* **2010**, 12, 19, 4388–4391
[61] Li, K., Zu, B., and Mazet, C., *Org. Lett*. **2024**, 26, 28, 6047–6052
[62] Mizoroki, T., Mori, K., Ozaki, A., *Bull. Chem. Soc. Jap*., 44, 581(**1971**)
[63] Heck, R.F., Nolley Jr, J.P., *J. Org. Chem*. **1972**, 37, 14, 2320–2322

same from Kumada and Corriu where upon mixing little amounts of transition metal halide salts to a mixture of organometallic reagent with a second organic halide the isolation of coupling product proved to be efficient.

Scheme 3. Original coupling scheme appeared on the *Bulletin of the chemical Society of Japan* in 1971 from Mizoroki group (top). Mechanism as reported in the original illustration by Heck in 1972 (bottom). Both groups clearly state the need for a base to neutralize the formed HX species and to achieve catalyst regeneration.

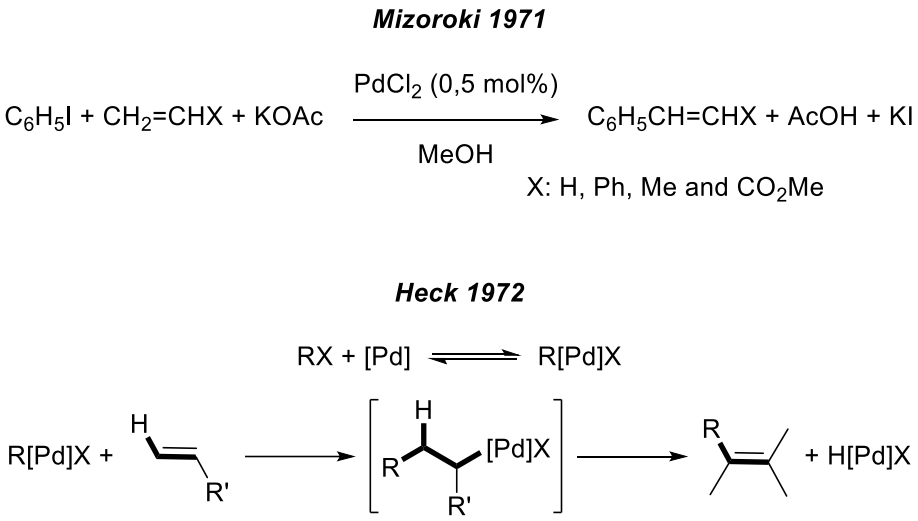

Soon this protocol gets the common name of Mizoroki-Heck coupling/reaction, and many other procedures have appeared in literature as it has been for Kumada cross coupling. The two major drawbacks from the original reaction conditions were the main limitation to aryl iodides partners with rare employment of bromides and chlorides and *cis: trans* olefin isomerization issues when a pure regioisomer was used as feedstock. These problems were readily solved by Heck who presented in 1974 an updated set of conditions where the use of *in situ* generated $(PPh_3)_2PdCl_2$ by adequate amount addition of triphenylphosphine, along with the choice of an appropriate base and tuning of solvent as well as temperature made possible to react electron-rich and electron-poor bromoarenes with styrene and methyl acrylate.[64] Issues regarding olefin isomerization and configuration were also readily unraveled through the use of silver or thallium salts.

Nowadays several other transition metals[65] such as iron,[66] copper,[67,68,69] cobalt, [70] platinum, iridium ruthenium, gold[71] and nickel are known to catalyse this reaction, here we will disclose in greater detail nickel-based protocols. [72]

[64] Dieck, H.A., Heck, R.F., *J. Am. Chem. Soc.* **1974**, 96, 4, 1133-1136
[65] Alisha, M., Philip, R.M., Anilkumar, G., *Eur. J. Org. Chem.* **2022**, e202101384.
[66] Xiong, H., Li, Y., Qian, B., Wei, R., Van der Eycken, E.V., and Bao, H., *Org. Lett*. **2019**, 21, 776–779
[67] Suresh, I., Chinnasamy, R., Sarkar, A. and Wadgaonkar, P.P., *Tetrahedron Lett*. **1997**, 38, 46, 8113-8116
[68] Gholivand, K., Salami, R., Farshadfar, K., Butcher, R.J., *Polyhedron* **2016**, 119, 267–276
[69] Tian, M.Q., Wang, C., Hu, X.H., and Loh, T.P., *Org. Lett*. **2019**, 21, 6, 1607–1611
[70] Srivastava, A.K., Satrawala, N., Ali, M., Sharma, C. and Joshi, R.K., *Tetrahedron Lett*. **2019**, 60, 151283
[71] Bhoyare, V.W., Sosa Carrizo, E.D., Chintawar, C.C., Gandon, V. and Patil, N.T., J. *Am. Chem. Soc*. **2023**, 145, 16, 8810–8816
[72] Huang, X., Teng, S., Chi, Y.R., Xu, W., Pu, M., Wu, Y.D. and Zhou, J.S., *Angew. Chem. Int. Ed.* **2021**, 60, 2828–2832

Ban group in 1979 implemented an intramolecular Heck cyclization specifically for the cyclization of chloroarene **II**. They used a MeMgBr as reductant to generate the active low valent nickel species, and they illustrate a correct mechanism for oxidative addition and subsequent migratory insertion, elimination steps through which product is formed in high yield. [73]

A second example of nickel catalyzed Heck coupling is from Pallini group in 1981, where β-bromostyrene is added onto potassium 3-butenoate, from the reaction of pure (Z) or (E) olefin only mixtures of two stereoisomers could be isolated in both cases; unfortunately this report only account for the specific formation of this targeted polyolefin.[74] In 1986 instead Umani-Ronchi and co-workers[75] achieved Heck coupling of aryl iodides, bromides and chlorides with styrene and ethyl acrylate with discrete yields, $Ni(PPh_3)_2Cl_2$ was used as pre-catalyst instead of $Ni(PPh_3)_4$ (**Fig. 16**). The major drawbacks were the low reactivity of chlorides, which were tested but could only give the addition byproduct and the low control over olefin regioisomeric ratios.

Figure 16. First nickel catalyzed Heck reactions from Ban (top), Pallini (middle) and Umani-Ronchi (bottom) groups.

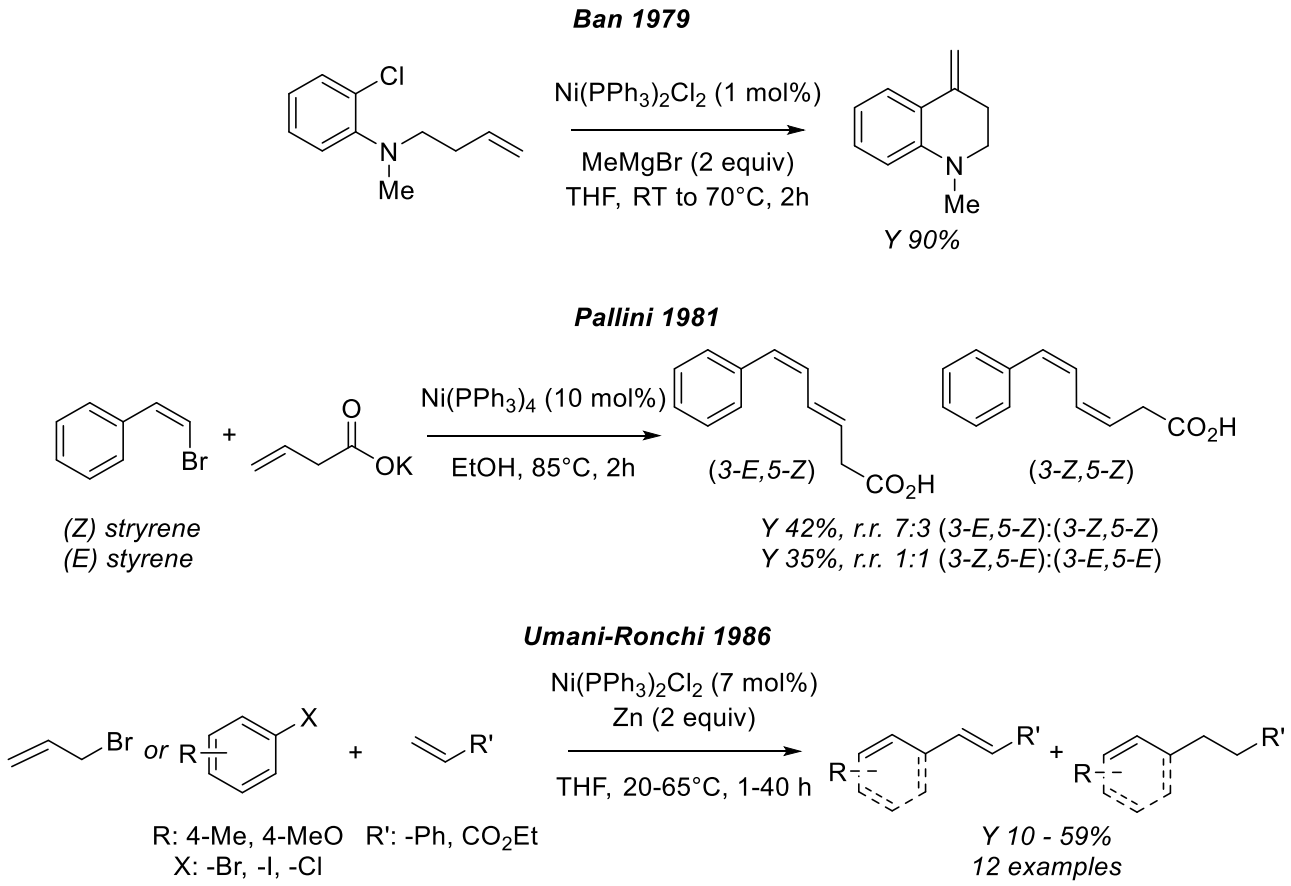

[73] Mori, M., Kudo, S. and Ban, Y., *J. Chem. Soc., Perkin Trans.* 1, **1979**, 771-774

[74] Chiusoli, G.P., Salerni, G., Giroldini, W., Pallini, L., *Journal of Organometallic Chemistry*, 219, (**1981**) C16-C20

[75] Boldrini, G.P., Savoia, D., Tagliavini, E., Trombini, C., Umani-Ronchi, A., *Journal of Organometallic Chemistry* 301, (**1986**) C62-C64

Nevertheless, since its discovery Heck coupling has greatly evolved and publications regarding DFT/mechanistic investigations[76,77] application in target synthesis,[78,79] and reviews[80,81,82] have regularly appeared. Most advanced reports on nickel catalyzed Heck reaction have pursued really challenging synthetic goals, to the extent that just an olefin moiety needs to be preserved along with the delivered unsaturated framework for these procedures to be addressed as Heck reaction if compared to original works from the seventies. Halide partners can be replaced with many other functional groups namely: pseudohalides, ether or sulphonates; palladium catalysts are often substituted by nickel-based ones and nitrogen-based ligands have been used in place of phosphines regularly, especially in nickel catalyzed protocols.

Intermolecular Heck coupling is the classic way to execute the reaction but over the years intramolecular versions seem to have become more popular, until a few years ago when a refreshed interest in intermolecular Heck reactions has risen again due to the better development of enantiocontrolled processes. Few examples to account for this trend: an α-arylcyclopentanalkylidene intramolecular cyclization from Jarvo group is reported.[83] Afterwords is instead presented a recent intermolecular Heck reaction from Zhou group.[84] In the first illustrated transformation the scope isn't much wide, but good to high yields and excellent *ee* are achieved under the easily accessible dichloronicklel-bis(tricyclohexylphosphine) moreover, the enetiomeric control is perfectly dictated by the starting material and no loss of stereochemical information takes place during the reaction. Meanwhile in the protocol developed by Zhou and co-workers aryl pseudo halides react with vinylether and vinylamine under catalytic conditions set by a nickel dichloride-phosphine chiral complex, the developed system is able to furnish a wide range of Heck-type products in moderate to high yields and with high to excellent *ee* (**Fig. 17**).

[76] Sperger, T., Sanhueza, I.A., Kalvet, I. and Schoenebeck, F., *Chem. Rev*. **2015**, 115, 17, 9532–9586
[77] Palladino, C., Fantoni, T., Ferrazzano, L., Muzzi, B., Ricci, A., Tolomelli, A. and Cabri, W., *ACS Catal.* **2023**, 13, 18, 12048–12061
[78] Endo, A., Yanagisawa, A., Abe, M., Tohma, S., Kan, T., Fukuyama, T., *J. Am. Chem. Soc*. **2002**, 124, 23, 6552–6554
[79] Bolt, Y.V., Dubinnyi, M.A., Litvinenko, V.V., Kotlobay, A.A., Belozerova, O.A., Zagitova, R.I., Shmygarev, V.I., Yatskin, O.N., Guglya, E.B., Kublitski, V.S., Baranov, M.S., Yampolsky, I.V., Kaskova, Z.M. and Tsarkova, A.S., *Org. Lett*. **2023**, 25, 26, 4892–4897
[80] Cabri, W., Candiani, I., *Acc. Chem. Res.* **1995**, 28, 1, 2–7
[81] Beletskaya, I.P. and Cheprakov, A.V., *Chem. Rev.* **2000**, 100, 8, 3009–3066
[82] Bhakta, S., Ghosh, T., *Adv. Synth. Catal.* **2020**, *362*, 5257
[83] Harris, M.R., Konev, M.O., and Jarvo, E.R., *J. Am. Chem. Soc.* **2014**, 136, 22, 7825–7828
[84] Huang, X., Teng, S., Chi, Y. R., Xu, W., Pu, M., Wu, Y.D., Zhou, J. S., *Angew. Chem. Int. Ed.* **2021**, 60, 2828.

Figure 17. Jarvo's and Zhou's methodologies are representative on how far nickel catalyzed Heck reactions have come nowadays.

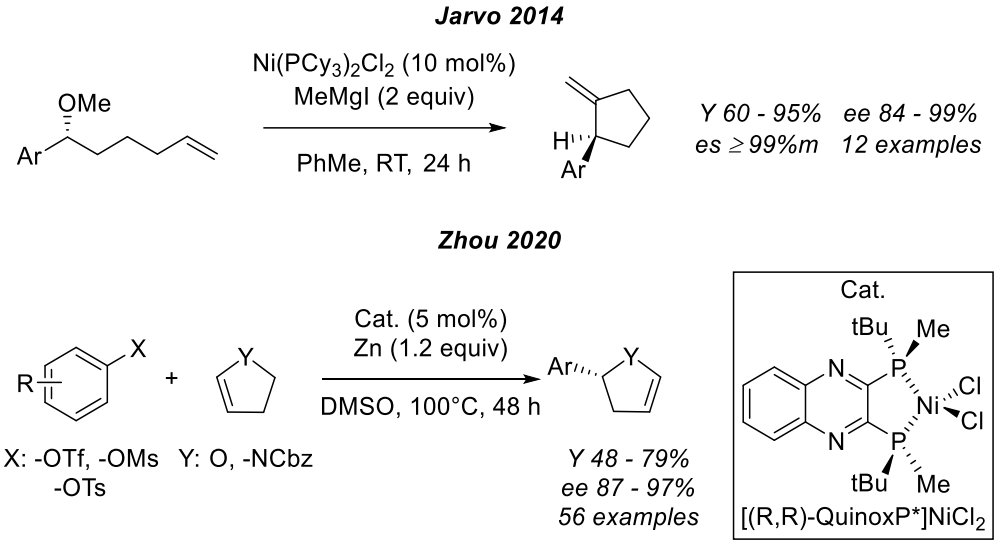

1.3.3 Cross-electrophile Couplings

Cross-electrophile coupling reactions (XEC) emerged as a powerful tool to sew together two electrophiles, to accomplish such a shift from classical cross coupling chemistry the pivotal role of a reducing agent to sustain the process had to be identified.[85] This was recognized in 1977 when seminal work from Kumada appeared as improvement of 1971 Semmelhack's stoichiometric version of biaryls preparation via zerovalent organonickel reagent.[86] The employment of nickel in XECs this early, set the stage for its dominance over other transition metal.[87]

Semmelhack and colleagues original paper reported biaryls formation upon mixing one equivalent of aryl halide with half equivalent of $Ni(COD)_2$ in DMF, the protocol proved to be efficient so any reducing agent was ever tried to be added to the reaction mixture, hence no possibility to lower the stoichiometric amount of nickel could be guessed.[88] From this 'pitfall' in 1977 Kumada and colleagues while seeking milder synthetic conditions to get biaryls than classical Ulmann type ones, were able to prepare biaryls but *catalytically in nickel*.[89] This was possible since they were aware of Semmelhack *stoichiometric* protocol and they also knew that *in situ* preparation of zerovalent nickel complexes from $Ni(PPh_3)Cl_2$ by reduction with zinc dust was feasible due to a work of Kende group.[90] Hence, Kumada correctly guessed the possibility to generate cross-electrophile products with a zerovalent nickel precursor and a reductant while operating *catalytically in nickel*; they were not immediately able to depict a reaction mechanism but, they claim that no organozinc species seem to be involved and zinc powder was responsible to reduce some Ni(II) species. Moreover, they could

[85] Lucas, E., Jarvo, E., *Nat Rev Chem* 1, 0065 (**2017**). https://doi.org/10.1038/s41570-017-0065
[86] Semmelhack, M.F., Helquist, P.M., Jones, L.D., *J. Am. Chem. Soc.* **1971**, 93, 22, 5908–5910
[87] Tasker, S., Standley, E. and Jamison, T., *Nature,* 509, 299–309 (**2014**)
[88] In the case of Semmelhack report in 1971 the purpose of using $Ni(COD)_2$ for biaryl preparation was to overcome limitation posed by copper catalyzed Ulmann coupling (usually T ≥ 200°); stoichiometric conditions with nickel already represented a great improvement thus we can imagine that no reason was envisioned to further investigate on other feasible mechanisms.
[89] Zembayashi, M., Tamao, K., Yoshida, J., Kumada, M., Tetrahedron Lett. **1977**, 4089.
[90] Kende, A.S., Liebeskind, L.S., Braitsch, D.M., Tetrahedron Lett.**1975**, 3375.

observe a significant acceleration of the reaction rate by adding potassium iodide, giving so almost 50 years ago the basis to discuss halogen atom exchange mechanism which is still today a debated phenomenon (halogen atom effects) among others.[91]

In 1981 Mukaiyama group developed the synthesis of asymmetric ketones from pyridyl-carboxylate esters and aryl iodides by mean of stoichiometric zinc as reductant and $Ni(PPh_3)Cl_2$ in catalytic amounts. The targeted asymmetric ketones were previously accessible only through addition of organolithium, -copper, -cadmium or Grignard reagents onto carbonyl containing precursors (such as activated esters, carboxylic acids and acyl halides) which required the preparation of the titled organometallic reagents prior to the use.[92] The targeted ketones are highly interesting still today and modern preparation via XEC will be disclosed, but at the time this chemistry was being developed they represented an outlying class of targets since all the interest was about replacing Ullmann's conditions for biaryls synthesis (**Fig. 18**).

Figure 18. Kumada original conditions for biaryls synthesis, chlorides were tested but didn't react (top left), Mukaiyama asymmetric ketones synthesis (top right), Colon and Kelsey coupling protocol where they also highlight a feasible nickel catalytic cycle (bottom left), Perichon electrochemical biaryl formation under CVE (bottom right).

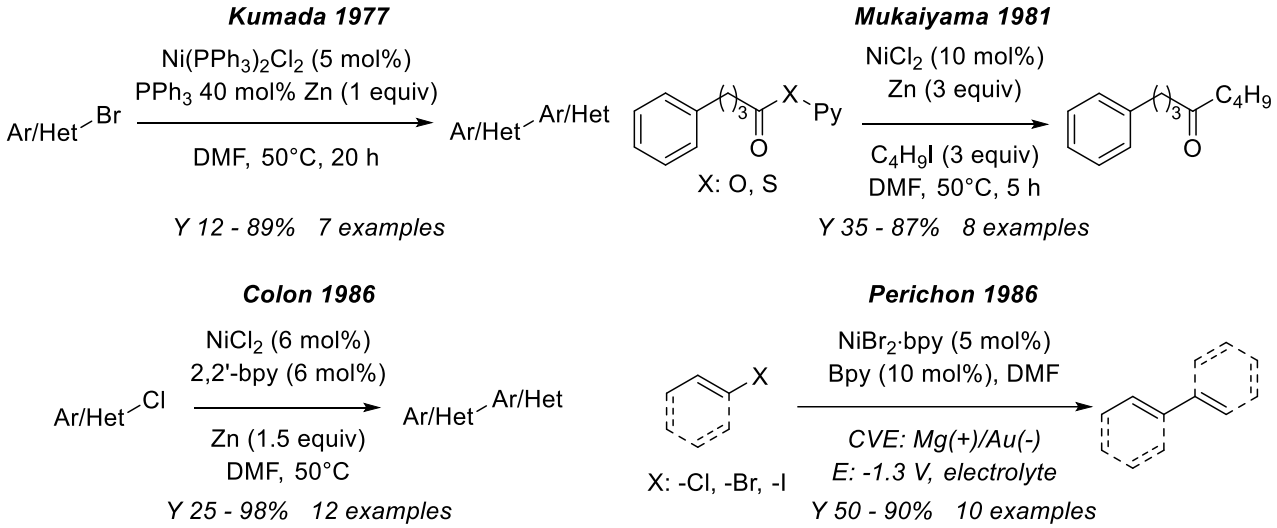

Colon and Kelsey from Union Carbide[93] company laboratories in 1986 moved to nickel-bipyridine complexes as catalyst again for biaryls preparation, they were able to react aryl chlorides which proved to poorly react under Kumada conditions. The main goal achieved by this group was indeed a clear overview of the proposed mechanisms, already including Ni(II)/Ni(IV) as well as Ni(I)/Ni(III) catalytic intermediates.[94] In this case Colon and Kelsey supposed that a Ni(I)/Ni(III) cycle, already hypothesized by electrochemical studies of Bontempelli *et al.*[95] could be operative under reaction conditions they've employed, although what they claim was: "*Considering the diverse conditions and observations reported, it is unlikely that one mechanism is operating under all reaction conditions*".

[91] Prinsell, M.R., Everson, D.A. and Weix, D.J., *Chem. Commun.*, **2010**,46, 5743-5745
[92] Onaka, M., Matsuoka, Y. and Mukaiyama, T., *Chemistry Letters*, **1981**, 531-534.
[93] Colon, I. and Kelsey, D.R., *J. Org. Chem*. **1986**, 51, 14, 2627–2637
[94] Tsou, T.T. and Kochi, J.K., *J. Am. Chem. Soc*. **1979**, 101, 25, 7547–7560
[95] Schiavon, G., Bontempelli, G. and Corain, B., *J. Chem. Soc., Dalton Trans.*, **1981**, 1074-1081

During 1986 also Perichòn group published XEC procedure where reductive conditions were provided via an electrochemical equipment.[96] Perichon and colleagues were mainly devoted to unravelling electrochemical behaviours of organometallic complexes, already in 1980 they were aware of the possibility for nickel complexes to accomplish different transformations with organic reactant partners such as organic halides.[97] Nevertheless, even if this group properly exploited electrochemical techniques they ended up with the same conclusion of Colon and Kelsey, they agree on an initial reduction of Ni(II) source to a catalytically active Ni(0) species (being this step executed electrochemically or not), but then subsequently remarked the elusive nature of the steps occurring between the oxidative addition and the reductive elimination step.[98,99]

In almost 50 years XEC methodologies have found widespread applications in synthetic organic chemistry and target synthesis, with time initially valuable homocoupling products turned out to be one of the undesired side products when different electrophiles have been subjected to XECs conditions.[100] The evolution of XEC has indeed grown tremendously, and today wide classes of electrophiles can react *intra-* or *intermolecularly* to deliver highly functionalized organic scaffolds. Although palladium[101,102,103,] cobalt[104,105,106] titanium[107] and iron[108] have been used in proficient ways for XECs, the elected metal for these reactions remains nickel by far.[109] Its intrinsic propensity to access different oxidation states ($Ni^{0\text{-}IV}$) and the great tunability of its ligand families such as phosphine, bipyridines, Box, BiOx, PyrOx, PyBOx, PhOx and others, has enabled nickel complexes to achieve highly sophisticated transformations.[110] Nickel paramagnetic nature always poses great challenges to whoever aspires at giving punctual events unfolding around the catalytic center, but a lot of interesting reports have shed light on many XECs aspects which can be evaluated *ad hoc* whenever a new reaction is developed.[111,112,113,114,115]

Shu and Zhao in 2023 have documented about a protocol to forge C(sp^3)-C(sp^3) bond, the sophistication level of nickel catalysis was dictated primarily from the BOx ligand (Bis-Oxazoline) and from an accurate choice of conditions.[116] The mechanism reported present two possible reaction

[96] Troupel, M., Rollin, Y., Sibille, S., Perichon, J., Fauvarque, J.F., *Journal of Organometallic Chemistry*, **1980**, 202(4), pp. 435–446
[97] In 1981 Bontempelli group already achieved XEC products electrochemically. See ref. 95
[98] Tsou, T.T. and Kochi, J.K., *J. Am. Chem. Soc.* **1979**, 101, 21, 6319–6332
[99] Nakamura, A., Otsuka, S., *Tetrahedron Letters* No. 5, pp 463 - 466, **1974**.
[100] Everson, D.A. and Weix, D.J., *J. Org. Chem.* **2014**, 79, 11, 4793–4798
[101] Krasovskiy, A., Duplais, C., Lipshutz, B.H., *J. Am. Chem. Soc*. **2009**, 131, 43, 15592–15593
[102] Bhonde, V.R., O'Neill, B.T., Buchwald, S.L., *Angew. Chem. Int. Ed.* **2016**, 55, 1849
[103] Manna, K., Jana, R., *Org. Lett*. **2023**, 25, 2, 341–346
[104] Gomes, P., Fillon, H., Gosmini, C., Labbé, E., Périchon, J., *Tetrahedron,* 58 (**2002**) 8417–8424
[105] Xing, D., Liu, J., Cai, D. *et al., Nat Commun.* 15, 4502 (**2024**)
[106] Gao, M. and Gosmini, C., *Org. Chem. Front.* **2024**,11, 3557-3561
[107] Xie, H., Wang, S., Wang, Y., Guo, P. and Shu, X.Z., *ACS Catal*. **2022**, 12, 2, 1018–1023
[108] Lin, Y., Zou, L., Bai, R., Ye, X.Y., Xie, T. and Ye, Y., *Org. Chem. Front.* **2023**,10, 3052-3060
[109] Kranthikumar, R., *Organometallics,* **2022**, 41, 6, 667–679
[110] Chernyshev, V.M. and Ananikov, V.P., *ACS Catal.* **2022**, 12, 2, 1180–1200
[111] Cornella, J., Gómez-Bengoa, E., Martin, R., *J. Am. Chem. Soc.* **2013**, 135, 5, 1997–2009
[112] Su, Z.M., Deng, R. and Stahl, S.S., *Nat. Chem.* (**2024**). DOI: 10.1038/s41557-024-01627-5
[113] Lin, Q., Spielvogel, E.H., Diao, T., *Chem* (**2023**), DOI: 10.1016/j.chempr.2023.02.010
[114] Dawson, G.A., Lin, Q., Neary, M.C., Diao, T., *J. Am. Chem. Soc.* **2023**, 145, 37, 20551–20561
[115] Dawson, G.A., Spielvogel, E.H., Diao, T., *Acc. Chem. Res.* **2023**, 56, 24, 3640–3653
[116] Zhao, W.T., Shu, W., *Sci. Adv.* 9, eadg9898 (**2023**). DOI: 10.1126/sciadv.adg9898

pathways, as in many other cases authors didn't declare which one is most likely to be operative in the titled methodology.

A few years earlier in 2016 Reisman and colleagues appointed a reductive coupling procedure between α-chloronitriles and a wide series of heteroaryl iodides. This represented and alternative route for α,α-disubstituted nitriles preparation rather than traditional palladium catalyzed Suzuki-Miyaura reaction or nickel catalyzed Negishi cross coupling. In this case the mechanism has not been deeply investigated, just radical trapping experiments were performed, radical species generated from the nitrile partner have been recognized. Thus, if the cycles proposed by Shu are supposed to be valid also under Reisman conditions for example, a reasonable mechanism hypothesis would involve the *Oxidative Addition – Radical Capture – Reductive Elimination - Halide Abstraction* pathway (**Fig 19 a**).[117,118,119]

Figure 19 a. Shu XEC protocol for C(sp^3)-C(sp^3) fragment coupling with a tentative two-pathway mechanism (top). Reisman conditions for the synthesis of α,α-disubstituted nitriles (bottom).

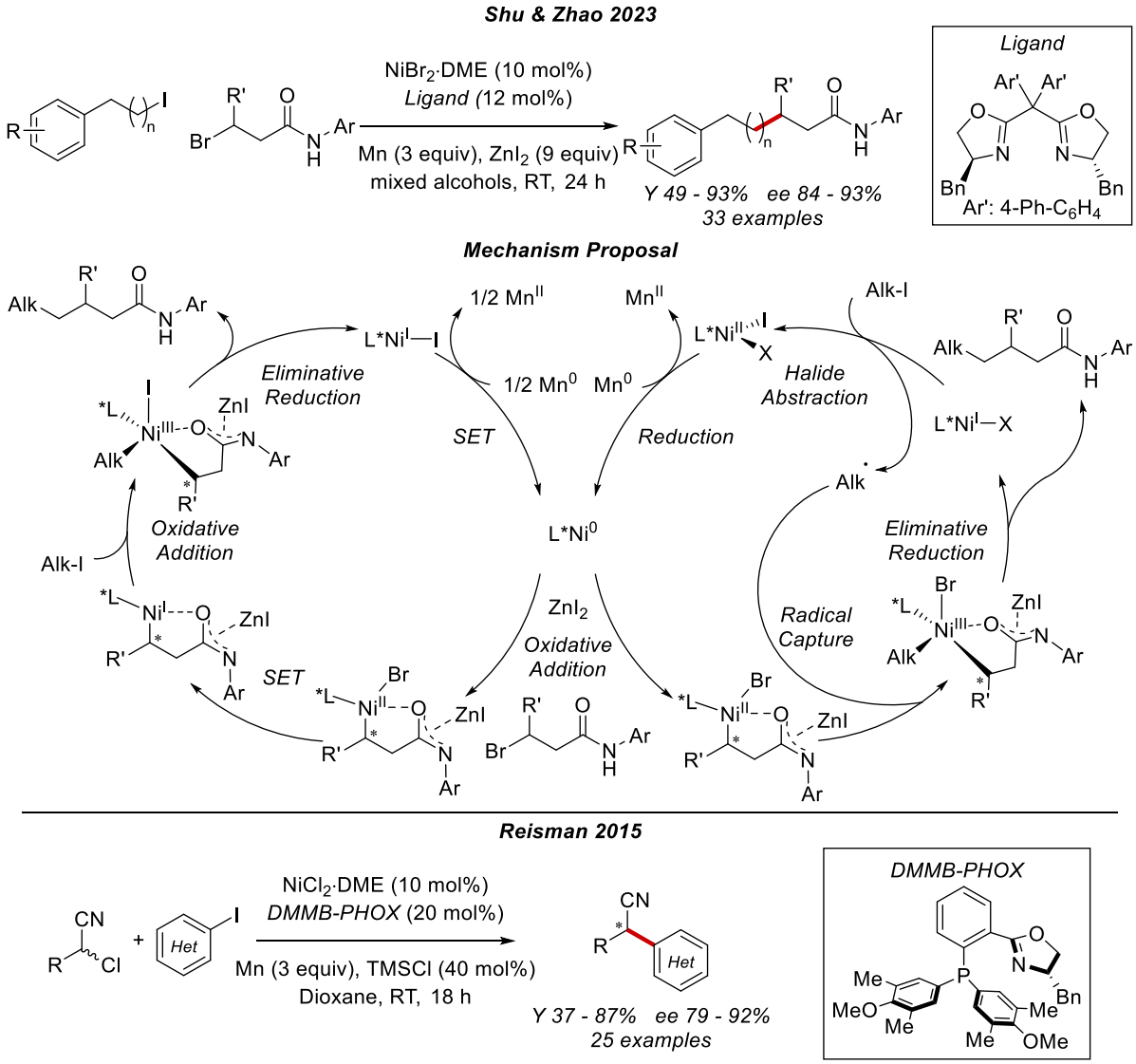

[117] Kadunce, N.T., Reisman, S.E., *J. Am. Chem. Soc*. **2015**, 137, 33, 10480–10483
[118] He, A., Falck, J.R., *J. Am. Chem. Soc*. **2010**, 132, 8, 2524–2525
[119] Choi, J., Fu, G.C., *J. Am. Chem. Soc.* **2012**, 134, 22, 9102–9105

The ability of nickel to mediate reductive cyclization is also noteworthy, this peculiarity is '*an inherited characteristic'* from the early developments as polymerization catalysts which always give nickel a good propensity to coordinate olefins. Over time a variety of [2+2], [4+4] and [2+2+2] cycloadditions have become amenable transformations under nickel catalysis.[120] This characteristic of nickel is frequently exploited in XEC chemistry to shape highly valuable molecular architectures. Under these conditions isomerization and migration steps are often crucial for the observed reaction outcomes.

A 1,6-enyne reductive cyclization with aryl iodides or alkyl bromides alternatively is reported from Kong and Shen. *(Z)*-allyl acetates are demanded for the arylation reaction to occur as shown also in other works. Then Kong and Shen investigated the possibility for alkyl bromides to undergo the same process, it turned out that primary allyl acetate could give access to tetrahydropyrrole rather than tetrahydropyridine, but no enantioselective versions of the process could be developed. The employment of secondary stereo-defined allylacetate has indeed enabled the development of an alkylative enantiospecific version of the cyclization reaction. In the alkylative cyclization the electronic nature of ligand played a key role. (**Fig. 19 b**).[121]

Figure 19 b. Kong and Shen conditions for nickel reductive arylative and alkylative cyclizations.

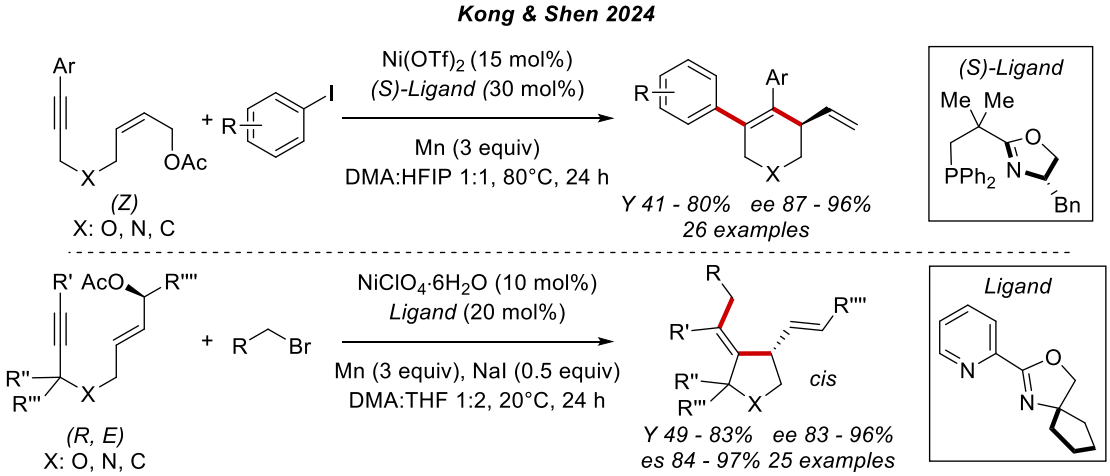

As a last example a nickel based photoredox catalysis approach to XEC is presented. About ten years ago MacMillan and co-workers indeed, found a way to merge aryl and alkyl halides by matching an iridium based photoredox cycle with a nickel based organometallic cycle, in what is generally termed as metallaphotoredox strategy.

The illustrated transformation (**Fig 20**) with the relative mechanism proposal clearly opens to a new series of strategic coupling developments via light triggered activation modes. In the reported methodology the nickel organometallic cycle begins with a classical oxidative addition of a low valent nickel species, meanwhile the out-sphere bromide anion is oxidized to a neutral radical from the photocatalyst reductive quenching. This so formed radical promotes a parallel hydrogen abstraction from tris(trimethylsilyl)silane generating a stabilized silyl radical which owes the right characteristics to accomplish halogen abstraction from C(sp^3)-Br bonds. This event generates the corresponding alkyl radical which is captured by the [Ni(II)]Ar to produce the intermediate Alk[Ni(III)]Ar. The final

[120] Montgomery, J., *Angew. Chem. Int. Ed.,* 43, 3890–3908 (**2004**)
[121] Liu, W., Xing, Y., Yan, D. *et al., Nat Commun* 15, 1787 (**2024**)

reductive elimination gives the product and the SET between the [Ni(I)] and the iridium photocatalyst restores the metal catalyst. The sophistication achieved in this transformation is remarkable and is certainly the highest among illustrated XECs, the common element with previous methodologies, which cannot be escaped, is the presence of a stoichiometric reductant.

In this specific case the use of a hydride-based reductant sets the need for a basic additive since after the HAA (Hydrogen Atom Transfer) step any proto-demetalation event must be avoided in the nickel catalytic cycle. This synthetic methodology is derived directly from earlier examples of dual catalytic metallaphotoredox reaction where the photocatalyst reductive quenching occurring *via* SET (Single Electron Transfer) is exploited for the *oxidative* activation of different organic partners such as phenols,[122] or to accomplish a XEC between tertiary alcohols with primary unactivated alkyl bromides.[123]

Figure 20. Dual photoredox catalysis for XEC of aryl bromides and alkyl bromides, tris(trimethylsilyl)silane is used as final reductant. HAA (Hydrogen Atom Abstraction), XAT (Halogen Atom Transfer).

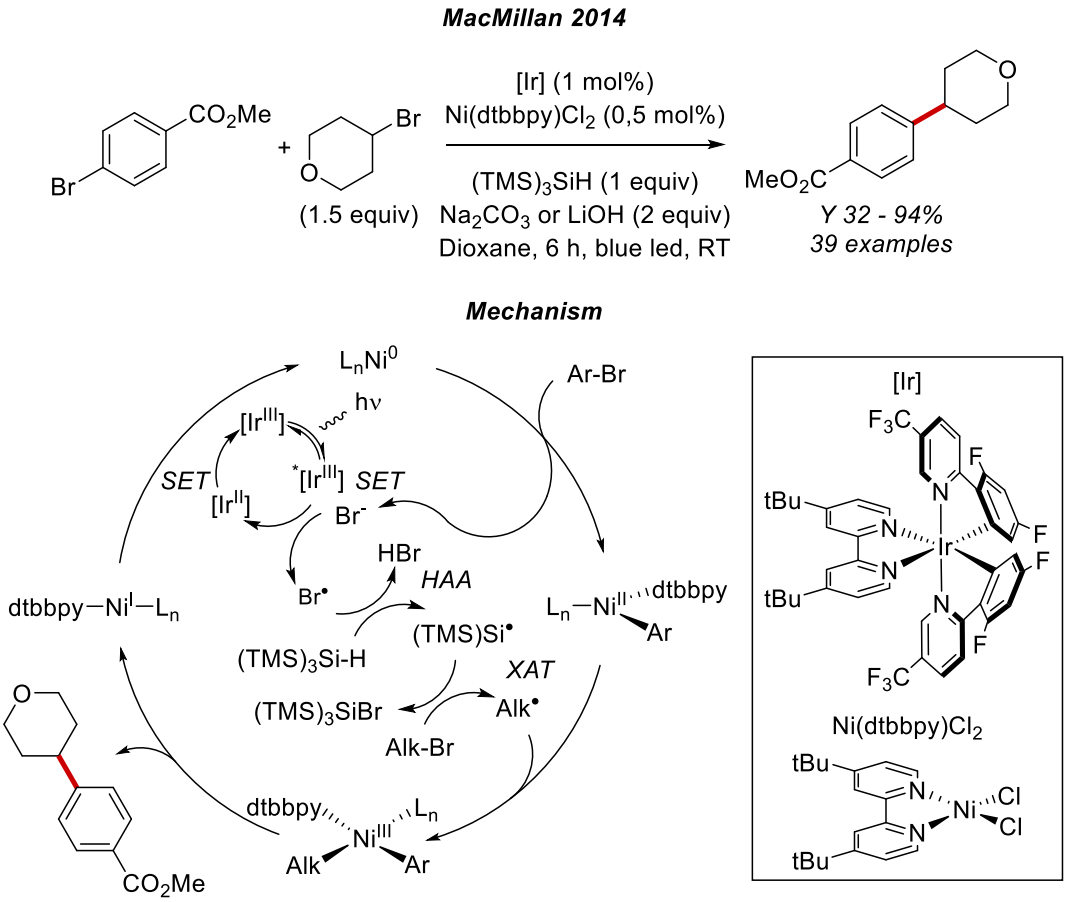

The main modes through which a XEC reaction can be developed have been illustrated. The author kindly readdresses interested readers to the literature where many XECs following these approaches

[122] Terrett, J., Cuthbertson, J., Shurtleff, V. *et al.*, *Nature* 524, 330–334 (**2015**).
[123] Gould, C.A., Pace, A.L., MacMillan, D.W.C., *J. Am. Chem. Soc.* **2023**, 145, 30, 16330–16336

are available, by mean of which a large topological space of differently hybridized carbon-carbon bonds has been accessed.[124,125,126,127,128,129]

1.3.3.1 Carboxylation Reactions

The unlocked possibility of coupling organic halides with themselves first and with other electrophiles then, has soon led to the use of carbon dioxide as second electrophile in XECs.[130,131,132,133] Preparation of carboxylic acids and their derivatives from CO_2 was possible for a long time by means of organometallic reagents, but when cross-electrophile approach for the construction of organic scaffolds was discovered then chemists turned their attention at chemical and electrochemical reductive strategies for direct CO_2 trapping over organic halides, led among other reasons to the considerably larger pool availability of these latter reagents if compared to organometallic ones. An early example for this, is an elegant electrocatalyzed carboxylation of benzyl chlorides mediated by a Co-Salen complex reported from Périchon and co-workers in 1985 (**Fig. 21**).[134]

Figure 21. Cobalt-Salen electrocatalysed carboxylation from Périchon group.

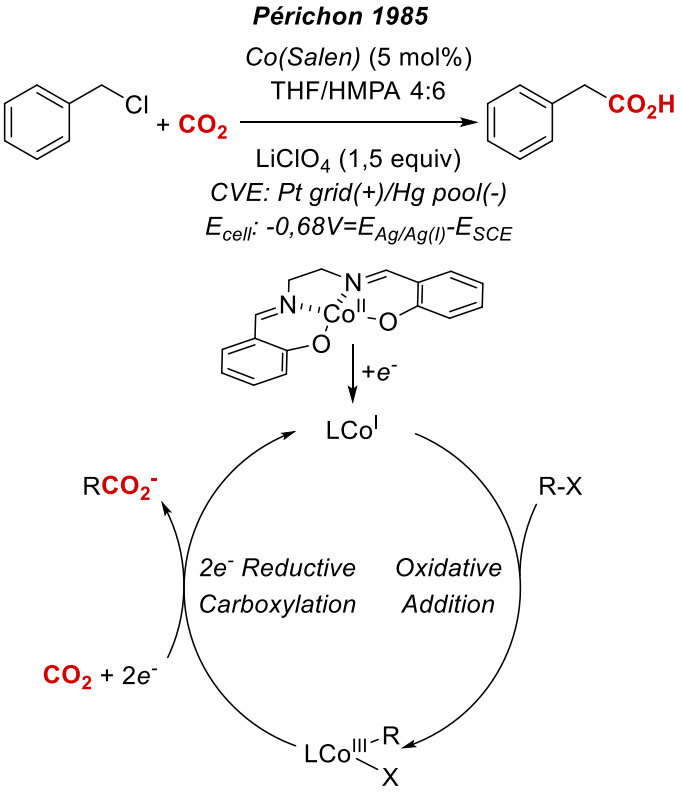

[124] Hamby, T.B. *et al. Science* 376, 410-416 (**2022**)
[125] Twilton, J., Johnson, M.R., Sidana, V. *et al.*, *Nature* 623, 71–76 (**2023**)
[126] Balaraman, K., Wolf. C., *Sci. Adv.* 8, eabn7819 (**2022**). DOI: 10.1126/sciadv.abn7819
[127] Ni, S. *et al.*, *Sci. Adv.*5, eaaw9516 (**2019**). DOI: 10.1126/sciadv.aaw9516
[128] Zhang, W., Lu, L., Zhang, W. *et al.*, *Nature* 604, 292–297 (**2022**)
[129] Juliá-Hernández, F., Moragas, T., Cornella, J., Martin, R., *Nature* 545, 84–88 (**2017**)
[130] Jutand, A. and Négri, S., *Eur. J. Org. Chem.* 4, 1811–1821 (**1998**).
[131] Torii, S. *et al.*, *Chem. Lett.* 15, 169–172 (**1986**)
[132] Jutand, A., Négri, S. and Mosleh, A., *J. Chem. Soc. Chem. Commun*. 23, 1729–1730 (**1992**).
[133] Jutand, A. and Négri, S., *Synlett* 6, 719–721 (**1997**)
[134] Folest, J.C., Duprilot, J.M., Périchon, J., *Tetrahedron Letters*, Vol.26, No.22, pp 2633-2636,**1985**

They provide a strategy for benzyl-, allylic- and other few chlorides carboxylation where a Co(II)-Salen precatalyst is reduced to a nucleophilic Co(I)-Salen which undergoes oxidative addition with the organic halide, authors then comprehensibly describe a one-step simultaneous two electron reduction-carboxylation event leading to product generation and catalyst regeneration. In this case the electrochemical set up is designed for the oxidative half-reaction of the cell to take place at Hg pool.

Recently electrochemical carboxylation example came from Skrydstrup and Rosas-Hernàndez, they developed a palladium catalyzed protocol to deliver carboxylic group onto aryl- and heteroaryl-bromides and fluorosulphonates in a divided cell equipment with an additional third chamber in the glassware dedicated to the development of $^{12}CO_2$ but also $^{13}CO_2$ as well as $^{14}CO_2$. This radiolabeling strategy results in an undoubtedly added value for drug candidate synthesis aimed at DMPK (Drug Metabolism and Pharmacokinetics) studies. The focal point in this case was also the reaction speed under palladium catalysis due to the rapid decay time in case of $^{14}CO_2$ evolution upon acidolysis and incorporation from $Ba^{14}CO_3$. While accomplishing such a goal, authors have also clearly investigated the unfolding events surrounding palladium catalyst for the titled process. Carboxylation begins with anionic $[(BINAP)Pd^0Cl]^-$ **III** undergoing oxidative addition and SET to form the neutral pivotal [(BINAP)Pd(I)Ar] intermediate **IV**, then a carboxylative migratory insertion can occur directly on this intermediate (neutral pathway) or on a further reduced $[(BINAP)Pd^0Ar]$-*ate* species **V** (anionic pathway). Subsequently for the anionic pathway the release of the product with catalyst regeneration is promptly achieved since two reductive events have already occurred, while for the neutral pathway the product release is observed and then a final SET event regenerate the catalyst while giving the second mole of electrons to the process. [135] While the palladium catalyzed half-reaction takes place in the cathodic chamber the radiolabeled precursor salt delivers the different isotopic analogues of $^{12}CO_2$ upon reaction with CSA (camphorsulphonic acid) from the third chamber and the electron releasing oxidation of DMF with ascorbic acid or ethanol proceeds in the anodic chamber (**Fig. 22**).

Nickel among other metals played a significant role for carboxylation reactions development, in the past couple of decades the known ability for nickel catalyst to easily access odd oxidation states with respect to palladium has dictated its larger application in XEC carboxylation with simple metal reductants.[136] An example of this is from Martin and Yorimitsu groups where they jointly developed a reductive carboxylation strategy for aryl sulphonium salts. They generate the starting material *in situ* by adding MeOTf in DCM solution followed by drying out of all volatiles, this so formed sulphonium salt then readily enters the nickel catalytic cycle for which also the role played by the reductant (zinc dust) has been thoroughly assessed.[137] Then Martin group, reported another nickel catalyzed carboxylation of primary alkyl bromides and sulphonates under closely related conditions.[138]

[135] Batista, G.M.F., Ebenbauer, R., Day, C. *et al., Nat Commun* 15, 2592 (**2024**)
[136] Leon, T., Correa, A., Martin, R., *J. Am. Chem. Soc*. **2013**, 135, 4, 1221–1224
[137] Yanagi, T., Somerville, R.J., Nogi, K., Martin, R., Yorimitsu, H., *ACS Catal*. **2020**, 10, 3, 2117–2123
[138] Liu, Y., Cornella, J., Martin, R., *J. Am. Chem. Soc.* **2014**, 136, 32, 11212–11215

Many other XECs with CO_2 have been conducted under transition metal catalysis,[139,140,141,142,143] electrocatalysis[144] or photoredox catalysis.[145,146]

Figure 22. Palladium catalyzed protocol aimed at electrochemical radiolabeling of arene and heteroarenes with the provided mechanism (top). Nickel mediated carboxylations (bottom).

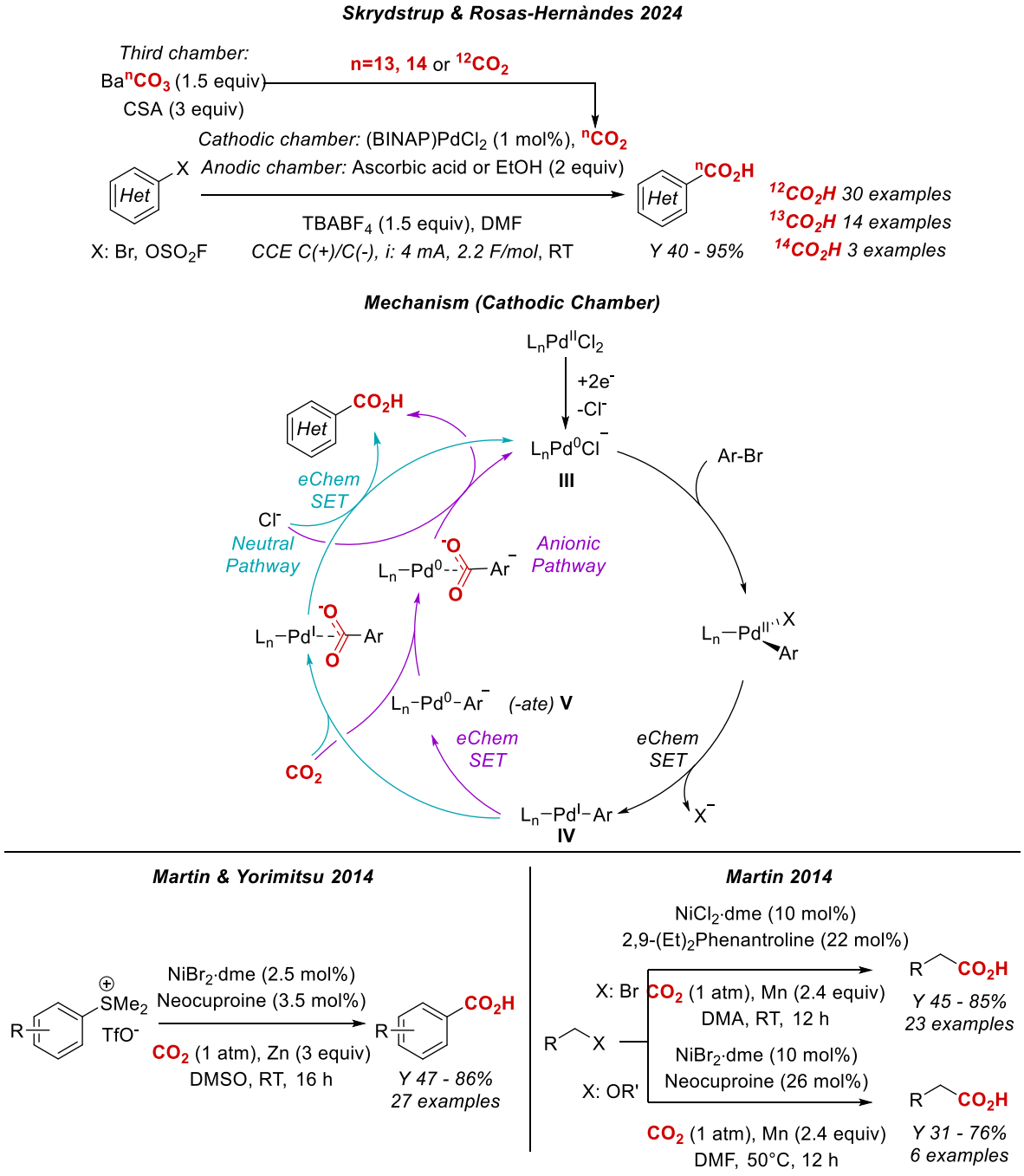

[139] Correa, A., Martin, R., *J. Am. Chem. Soc.* 131, 15974–15975 (**2009**)
[140] Bhunia, S.K., Das, P., Nandi, S., R Jana*Org. Lett.* 21, 4632–4637 (**2019**)
[141] Nogi, K., Fujihara, T., Terao, J., Tsuji, Y., *J. Org. Chem.* 80, 11618–11623 (**2015**)
[142] Tran-Vu, H., Daugulis, O., *ACS Catal.* 3, 2417–2420 (**2013**)
[143] Correa, A., Leon. T., Martin, R., *J. Am. Chem. Soc.* 136, 1062–1069 (**2014**)
[144] Sun, G.Q., Zhang, W., Liao, L.L. *et al*., *Nat Commun* **12**, 7086 (2021). DOI: 10.1038/s41467-021-27437-8
[145] Shimomaki, K., Murata, K., Martin, R., Iwasawa, N., *J. Am. Chem. Soc.* 139, 9467–9470 (**2017**)
[146] Meng Q.Y., Wang, S., König, B., *Angew. Chem. Int. Ed.* 56, 13426–13430 (**2017**)

1.3.3.2 Trifluoromethylations

This brief section regarding trifluoromethylation reactions is aimed at introducing background knowledge on general fluorination and trifluoromethylation chemistry. Covering this whole branch of developed methodologies would be out of reach for this manuscript. Useful information on trifluoromethylating reagents, trifluoromethyl radical fragment studies and some examples on how C(sp^3)-CF_3 and C(sp^2)-CF_3 can be forged with modern photochemical and electrochemical techniques will be given to help in the drawing of a more complete picture over trifluoromethylation chemistry which will be completed in the final part of this thesis.

It was early understood that the nature of perfluorinated organic compounds was quite different from other molecule families. Although perfluororganic compounds have gained large interest in other sectors such as polymer chemistry (*i.e.,* Teflon), a considerable amount of literature has been produced to gain insights on trifluoromethyl radical rather than the corresponding anion or cation, this is because of its higher reactivity and its extended employment in synthetic organic chemistry. For years it was commonly believed that radical species were too unstable to be usefully employed in organic synthesis, but the above-mentioned studies have changed this perspective, nowadays radical species are commonly manipulated at need from organic chemists. Among perfluoroalkyl organic fragments, elucidation of the structure of lighter homolog and reactivity has represented a challenging task. Nevertheless, good control of CF_3 synthon and precursors reactivities is now easier than in the past both from an empirical and a theoretical point of view.[147]

Sequential replacement of hydrogen atoms with fluorine ones leading from methyl to trifluoromethyl fragment marks a change within the physicochemical properties of the synthon. Basics consideration about CF_3 radical reactivity should be the following:

- Small fluorine atom size makes electronic effects prominent rather than sterics

- Fluorine lone pairs in $2p_F$ orbitals can hyperconjugate with $\sigma^*_{C\text{-}F}$

- Fluorine lone pairs in $2p_F$ orbitals can stabilize the radical onto carbon centered SOMO

- Fluorine lone pairs $2p_F$ generating some of the CF_3 MO have both stabilizing and destabilizing interaction, a general evaluation is complex!

- Geometry distortions are caused by F-atom electronic effects, and such distortions show back modifications on MO energies.

Investigation of fluoromethyl radical series' thermodynamic stability historically followed a general approach, this was based upon evaluation of C-H BDEs of heteroatom bearing hydrocarbon and then assuming a linear correlation might account for stability/reactivity scale of the corresponding radicals (**Sch. 4**).[148]

[147] Dolbier Jr., W.R., *Topics in Current Chemistry, Vol. 192* (Ed.1), Springer, Heidelberg, **1997**, pp. 97–163
[148] Berger, R., Resnati, G., Metrangolo, P., Weber, E. and Hulliger, J., *Chem. Soc. Rev.*, **2011**,40, 3496-3508

Scheme 4. Classical approach for radical stability/reactivity pattern evaluation

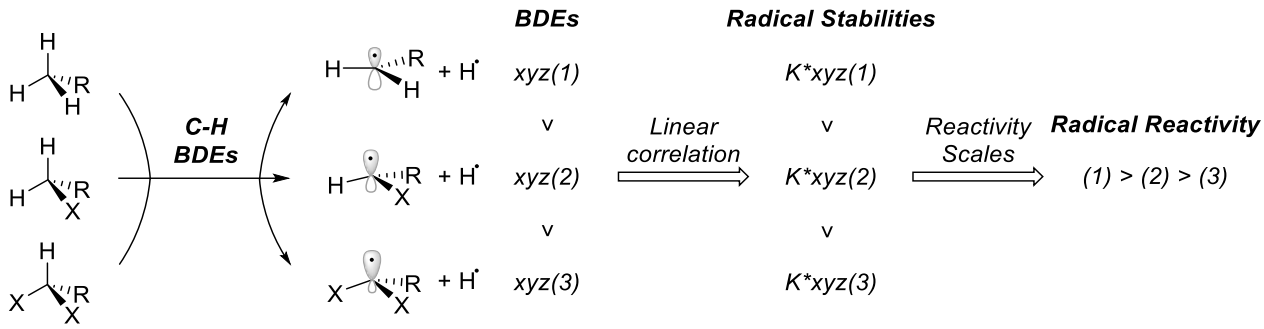

.

This approach applied at reactivity investigation of fluoromethane radicals, has led to the observation of both linear and non-linear trends in $CH_{3-n}F_n$ radical properties due to the above-mentioned effects caused by fluorine atoms, all these peculiar behaviours are termed as *"fluorine effects"*.[149]

So globally, electronic and steric effects triggered by fluorine atoms presence show reciprocal influences on each other, effects of increased fluorine atoms are non-additive and explanation for properties trends might consider all these aspects to furnish valid explanations of empirical results and physico-chemical properties trends (**Sch. 5**).[150,151,152]

Scheme 5. Some trends in fluoromethyl radical properties.

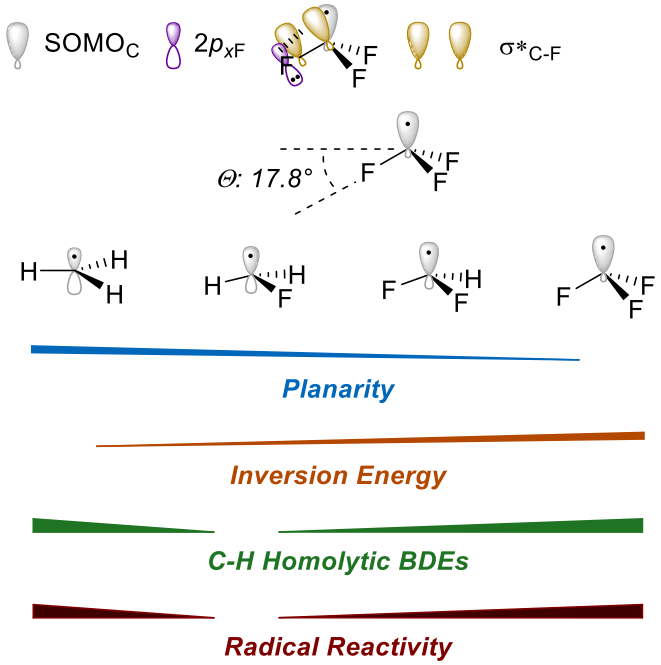

Trifluoromethylation reactions have always represented among synthetic organic chemists a highly challenging as well as interesting goal. Since early reports appeared between XIX and XX century

[149] O'Hagan, D., *Chem. Soc. Rev.* **2008**, 37, 308-319
[150] Bernardi, F., Cherry, W., Shaik, S. and Epiotis, N.D., *J. Am. Chem. Soc*. **1978**, 100, 5, 1352–1356
[151] Studer, A., *Angew. Chem. Int. Ed*. **2012** 51: 8950-8958
[152] Kirsch, P., *Modern Fluoroorganic Chemistry: Synthesis, Reactivity, Applications*, Wiley-VCH, Weinheim, **2004**

the interest in the CF_3 fragment has been related to medicinal chemistry.[153] Although the reasons to develop new trifluoromethylations today are still posed from pharmaceutical industries demand, the true *leitmotiv* of progresses in this field is dictated by the development of new CF_3 containing reagents; since is largely preferable following a *building block approach* rather than pursuing *direct C-F bond construction* multiple times. To make an easy distinction between these two approaches and considered that CF_3I has been discovered in 1948, then 1950 can be considered as arbitrary reference date from which on the *building block approach* has become the main way to introduce the CF_3 group onto organic scaffolds (**Fig. 23**).

In first instance, before 1950 fluorinations and trifluoromethylations were performed with inorganic KHF_2, SbF_3, SbF_5, SF_4 or other fluorine-based precursors, under these circumstances' pioneers were able to prepare, for example benzotrifluoride, acyl fluorides or some trifluoromethyl alkane when no commercial trifluoromethyl precursors were available.[154,155] Although some literature work appeared since trifluoroiodomethane discovery, it was only around 1960 when the escalade to trifluoromethyl precursors began with the spreading of relatively reactive CF_3I as CF_3 source.[156] CF_3I (also known as Freon) original synthesis from 1948, employs carbon tetraiodide and iodiumpentafluoride. Twenty years after its first preparation, in 1969 freon was used to prepare a series of trifluoromethylated aromatic compounds, opening this way to the *building block approach* while obviating at the need to forge C-F directly on the desired organic scaffold.[157] Fluoroform reactivity remained indeed less explored especially due to major difficulties regarding its handling.[158,159]

Figure 23. Fluorination/trifluoromethylation strategies before 1950, when especially CF_3 precursors were highly limited or unknown (top). Main trifluoromethyl precursors developed until $TMSCF_3$ preparation and methylfluoride the first synthetized organofluoride in history (bottom).

[153] Swarts, F., (**1892**). *Acad. Roy. Belg*. 3 (24): 474
[154] Lehmann, F., *Archiv f. experiment. Pathol. u. Pharmakol* 130, 250–255 (**1928**)
[155] Hasek, W.R., Smith, W.C. and Engelhardt, V.A., *J. Am. Chem. Soc.* **1960**, 82, 3, 543–551
[156] Haszeldine, R.N., *J. Chem. Soc.* **1949**, 2856–2861
[157] Kobayashi, Y., Kumadaki, I., *Tetrahedron Letters*. (**1969**), 10 (47): 4095–4096
[158] Prakash, G.K.S. *et al.*, *Science* 338,1324-1327 (**2012**)
[159] Lee, H.J., Joo, J.U., Yim, S.J. *et al.*, *Nat Commun* 14, 1231 (**2023**)

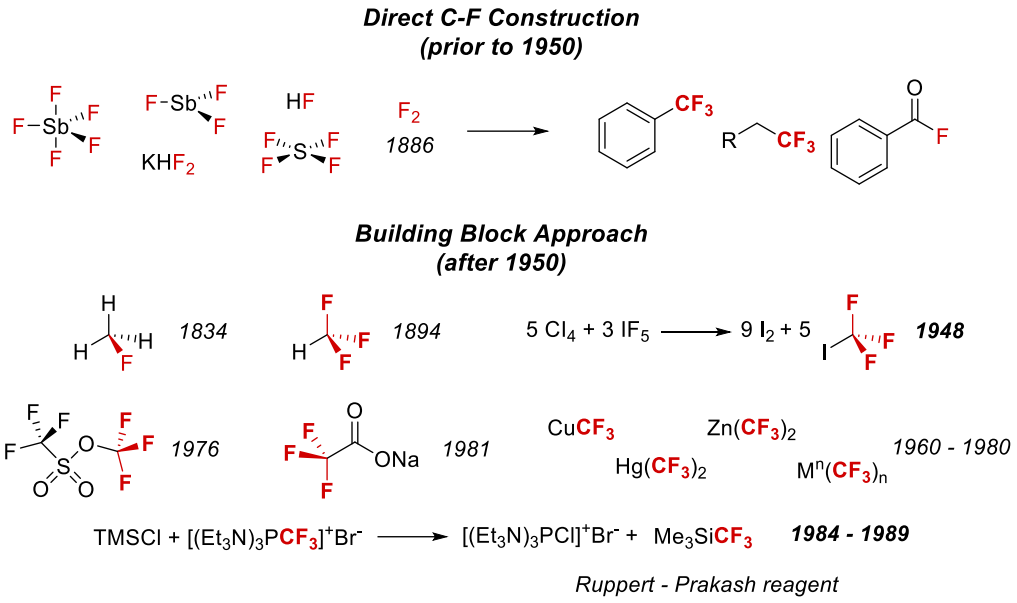

Afterwards, between the '60 and the mid '80 of the last century trifluoromethyltrifate,[160] for example, was also explored but since cross coupling chemistry was arising, efforts from several research group have been directed at unravelling stable metal-CF_3 complexes, by testing different metals all across the periodic table, especially copper.[161] The main envisioned chemistry for such trifluoromethide metal complexes was indeed focusing on triggering ligand metathesis, so that CF_3 anion could potentially access organometallic coupling reactions in a straightforward manner. Yet some of these procedures worked, none of them were free from drawbacks, the main of which being decomposition to metal-fluoride and CF_2 carbene via α-elimination as in the case of [$LiCF_3$]; thus, trifluoromethylations could not fully flourish yet.[162,163,164]

For another 20 years no new reagents became popular as CF_3 precursors, until 1984 - 1989 when Ingo Rupert and Surya Prakash synthetized and successfully employed $TMSCF_3$ (trifluoromethyltrimethylsilane) setting the modern paradigms in trifluoromethylation chemistry. $TMSCF_3$ soon became popular as Ruppert-Prakash reagent and is widely recognized as the first popular CF_3 building block, from 1990 onward all newly developed trifluoromethylating reagents as a final proof of their genuine reactivity are usually tested against $TMSCF_3$ on new transformations or in classical benchmark reactions.[165,166] In the same period Wakselman group synthetized a really common trifluoromethylating reagent, CF_3SO_2Na which have also been named after one of the authors, Bernard Langlois. Sodium triflinate is also currently considered one of the original benchmark reagents for trifluoromethylations (**Fig. 23**).[167]

[160] a) Olah, G.A., Ohayama, T., *Synthesis* **1976**, 319. b) Taylor, S.L. and Martin, J.C., *j. Org. Chem,* **1987**, 52, 4147 - 4156
[161] Folléas, B., Marek, I., Normant, J.F., Saint-Jalmes, L., *Tetrahedron,* 56, 2, 7, **2000**, 275-283
[162] Wiemers, D.M. and Burton, D.J., *J. Am. Chem. Soc.* **1986**, 108, 832
[163] Kondratenko, NV., Vechirko, E.P., Yagupolskii, L.M., *Synthesis* **1980**; 1980(11): 932-933. DOI: 10.1055/s-1980-29276
[164] Matsui, K., Tobita, E., Ando, M., Kondo, K., *Chemistry Letters*, 10, 12, **1981**, 1719–1720
[165] Ruppert, I., Schlich, K., Volbach, W., *Tetrahedron Letters*, (**1984**), 25 (21): 2195–2198
[166] Prakash, G.K.S., Krishnamurti, R. and Olah, G.A., *J. Am. Chem. Soc.* (**1989**) 111 (1): 393–395
[167] Langlois, B.R., Laurent, E., Roidot, N., *J. Org. Chem*., **1989**, 54, 2452-3

In the last 35 years an extensive series of trifluoromethyl precursors have been reported from different research groups. At the sight of an organic chemist, all these reagents may be divided into three classes, namely: *nucleophilic* (CF_3^-), *radical* ($CF_3^\bullet$) or *electrophilic* (CF_3^+). Even if modern photoredox and electrochemical transformations can indeed change the native electronic properties of a given CF_3 fragment, these three categories are used to pick a suited trifluoromethylating agent considering the type of transformation at work and the electronic nature of the substrate.

Among these reagents also a great span of costs is covered, with the cheapest displaying an easier molecular structure such as Langlois' reagent, TFAA or Chen's reagent priced around 500€ - 1000€/Kg or less, while the most expensive such as Umemoto (III) and Shibata (I) for example, being priced up to 1000 times more 100€ - 1000€/g (**Fig. 24**).

Figure 24. Trifluoromethylating reagents developed in the last 35 years.

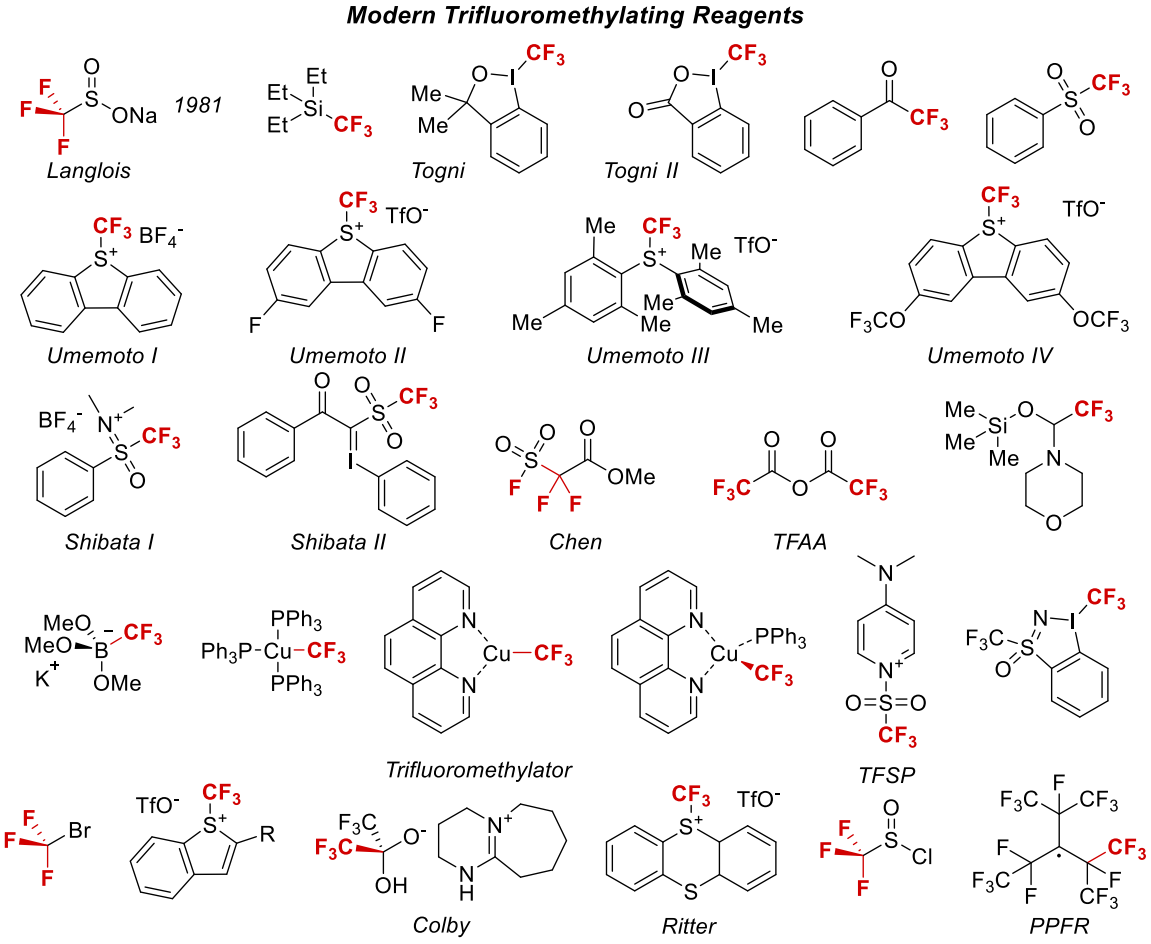

Modern synthetic organic strategies have achieved great efficiencies in trifluoromethylation of reluctantly reactive substrate. A neat example of this is a report by Studer and co-workers about *m*-CH functionalization of pyridines, quinolines and isoquinolines either via radical or ionic pathway,

introduction of EWG groups in such a position is still a poorly addressed transformation.[168] Indeed the main functionalization strategies for the elected substrates are DoM (Direct o-Metallation),[169] radical Minisci-type reactions[170] and S_NAr on *N*-activated pyridines.[171] The reported strategy is capable to functionalize the challenging *m*-position regardless of the nature of the substituents on the heteroaromatic ring via deraomatization-rearomatization sequence, a known approach which although needs to be carefully evaluated since unstable intermediate or energetically favoured byproducts can be formed.[172,173,174] Cheap CF_3I is the trifluoromethyl precursor for which a renewed interest has been lately triggered by photoredox, electrochemical and flow technologies. Studer and colleagues have prepared dearomatized azaheterocycles stable intermediates upon condensation of DMAD (dimethyl-acetylenedicarboxylate) and MP (methylpiruvate), then a light stimulus has triggered C-I bond homolysis in CF_3I so that a CF_3 radical could attack the intermediate in the designed position. A final acidic work-up of the reaction mixture gives the product in moderate to high yields. The illustrated sequence not only allows trifluoromethylations and perfluoroalkylations but can also be used to deliver a series of different anions onto azaheterocycles' *m*-position such as: -Cl, -Br, -I, -NO_2, -SPh, -SePh and -D. (**Fig. 25**).[175]

Figure 25. Studer's conditions for perfluoroalkylation of azaheterocycles' *m*-position (top). MacMillan copper mediated photoredox trifluoromethylation of heteroaryl bromides with Umemoto III reagent (bottom).

[168] Das, R., Kapur, M., *Asian J. Org. Chem*. **2018**, 7, 1217
[169] Nakao, Y., *Synthesis* 2011, 3209–3219 (**2011**)
[170] Proctor, R.S.J., Phipps, R.J., *Angew. Chem. Int. Ed.* 58, 13666–13699 (**2019**)
[171] Bull, J.A., Mousseau, J.J., Pelletier, G. and Charette, A.B., *Chem. Rev*. **2012**, 112, 5, 2642–2713
[172] Zhou, X.Y., Zhang, M., Liu, Z., He, J.H., Wang, X.C., *J. Am. Chem. Soc.* **2022**, 144, 32, 14463–14470
[173] Wübbolt, S., Oestreich, M., *Angew. Chem. Int. Ed.* 54, 15876–15879 (**2015**)
[174] Bertuzzi, G., Bernardi, L., Fochi, M., *Catalysts* 8, 632 (**2018**)
[175] Cao, H., Cheng, Q., Studer, A., *Science* 378,779-785 (**2022**)

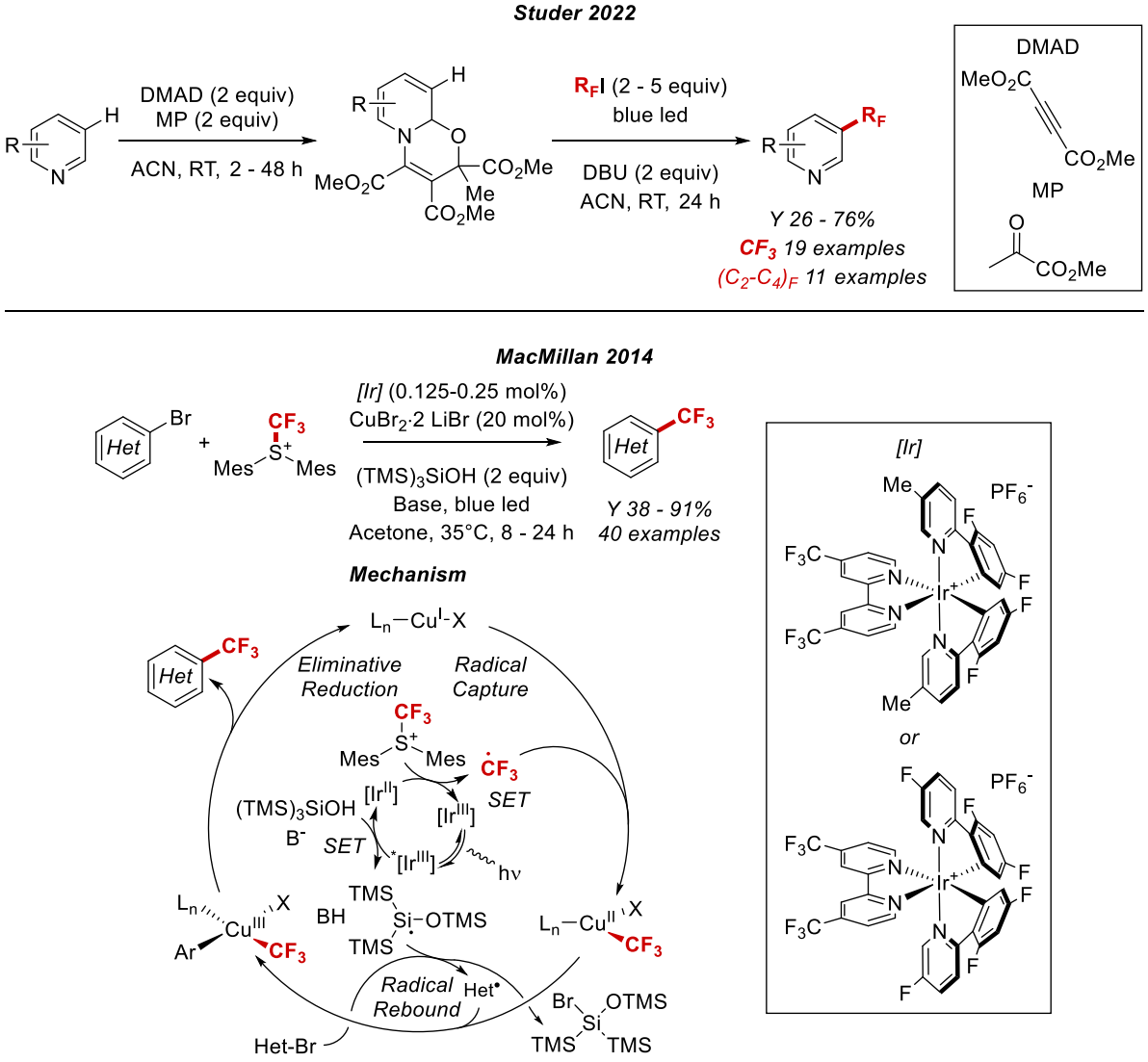

Another valuable synthetic methodology to forge C(sp^2)-CF_3 bonds via photoredox copper catalysis has been reported by MacMillan group. Since organocopper intermediates reluctantly undergo two electron oxidative addition events if compared to nickel and palladium, and such a process has been computationally identified as kinetically disfavoured, the main hurdle is to access more reactive organocopper(III) species.[176,177] The main disclosure of this work has been the scouting of two sequential radical generation steps matching with the photocatalyst redox cycle. Hence the two open-shell reactive radical species ($CF_3^{\bullet}$, $Het^{\bullet}$), generated from the iridium photocatalyst promptly react *via* sequential radical capture with the organocopper intermediates up to the formation of an Ar[Cu(III)]CF_3 which could fastly engage an eliminative reduction to give the product.[178]

Many other methodologies have appeared lately to forge a series of C(sp^2)-CF_3 bonds starting from (hetero)aryl (pseudo)halides or C(sp^2)-H bond activation, a series of different trifluoromethylating

[176] Jones, G.O., Liu, P., Houk, K.N., Buchwald, S.L., *J. Am. Chem. Soc.* 132, 6205–6213 (**2010**)
[177] Giri, R., Brusoe, A., Troshin, K., Wang, J.Y., Font, M., Hartwig, J.F., *J. Am. Chem. Soc.* 140, 793–806 (**2018**)
[178] Le, C., Chen, T.Q., Liang, T., Zhang, P., MacMillan, D.W.C., *Science* 360,1010-1014 (**2018**)

reagents has been used to this aim.[179,180] Many disclosed procedures take advantage of photocatalyzed strategies to access interesting new reactivity pathways; while other works are likely focused also on the development of highly attractive reaction set ups such as photo-flow or electro-flow apparatuses.[144,181,182,183,184,185]

The intrinsic value for C(sp^3)-C(sp^3) bond formation when applied to trifluoromethylation becomes even more valuable since it can give access to three-dimensional fluorinated carbon-based organic scaffolds, which are indeed valuable targets in medicinal chemistry. To this aim Governeur group reported a hydrocarbofunctionalization *via* ruthenium based photoredox catalysis for simple alkenes. In this transformation the oxidative quench of the photocatalyst generates CF_3 radical, which attacks the olefin, methanol then provides the terminal proton for the product formation via *HAT* and the subsequent oxidation to formaldehyde takes place with the restoration of the catalyst.[186] Investigators have also ascertained the source of the proton through deuterium labelled experiments. Gaunt and co-workers haven instead studied a tricomponent reaction starting from DMSO solution of CF_3I. They figured out a protocol where a fast condensation between secondary amines and aldehydes could deliver the corresponding enamine, a light source capable to homolitically cleave CF_3-I bond provided at least an initial source of radical CF_3, such a radical is supposed to add to the enamine leading to the formation of an unstable a-amino radical which can be converted to the final iminium ion intermediate either through a *SET* mechanism or *XAT*- α-elimination sequence. The titled iminium ion can then furnish the desired product through reductive work up with STAB (sodium triacetoxyborohydride).[187] A third example accounting for C(sp^3)-C(sp^3) bond formation is indeed an alkene electrochemical dicarbofunctionalization reported in 2023. Within Zeng research group the envisioned tri-component transformation relied on reduction of trifluoromethylthiantrenium triflate reagent introduced by Ritter group[188] to generate the CF_3 radical, which chemoselectively attack the terminal olefins' position to give a linear alkyl radical intermediate captured then from the azaheterocycle. The final heterocycle radical intermediate upon deprotonation and single electron transfer generates the product and closes the redox neutral transformation (**Fig. 26**).[189]

Reported synthetic methodologies are just an example of the wide variety of developed trifluoromethylations. Many more can be found in literature, differing by CF_3 source, employed catalytic systems and targeted bonds type formations.[190,191]

---

[179] Tsuruta, T., Spinnato, D., Won Moon, H., Leutzsch, M. and Cornella, J., *J. Am. Chem. Soc.* **2023**, 145, 47, 25538–25544
[180] Nagib, D.A., Scott, M.E. and MacMillan, D.W.C., *J. Am. Chem. Soc.* **2009**, 131, 10875–10877
[181] Wu, X.F., Neumann, H., Beller, M., *Chem. Asian J.* (**2012**), 7: 1744-1754
[182] Bhaskaran, R.P., Babu, B.P., *Adv. Synth. Catal.* **2020**, *362*, 5219
[183] Lin, D., Coe, M., Krishnamurti, V., Ispizua-Rodriguez, X., Prakash, G.S.K., *Chem. Rec.* **2023**, 23, e202300104
[184] Sumii, Y., Shibata, N., *Chem. Rec.* **2023**, 23, e202300117
[185] Shaw, R., Sihag, N., Bhartiya, H. and Ramu, M., Yadav*Org. Chem. Front.* **2024**,11, 954-1014
[186] Mizuta, S., Verhoog, S., Engle, K.M., Khotavivattana, T., O'Duill, M., Wheelhouse, K., Rassias, G., Médebielle, M. and Gouverneur, V., *J. Am. Chem. Soc.* **2013**, 135, 7, 2505–2508
[187] Kolahdouzan, K., Kumar, R. and Gaunt, M.J., *Chem. Sci.*, **2020**,11, 12089-12094
[188] Jia, H., Häring, A.P., Berger, F., Zhang, L. and Ritter, T., *J. Am. Chem. Soc.* **2021**, 143, 7623– 7628
[189] Xiang, F., Wang, D., Xu, K. and Zeng, C.C., *Org. Lett*. **2024**, 26, 1, 411–415
[190] Wu, F.P., Yuan, Y., Wu, X.F., *Angew. Chem*. **2021**, 133, 25991 –25996
[191] Jang, J., Seong Hwang, H., Jeong, H. and Cho, E.J., *Chem. Sci.*, **2024**, Advance Article. DOI: 10.1039/D4SC06780K

Figure 26. Modern examples for hydro-, amino- and carbo-trifluoromethylation for C(sp^3)-C(sp^3) building.

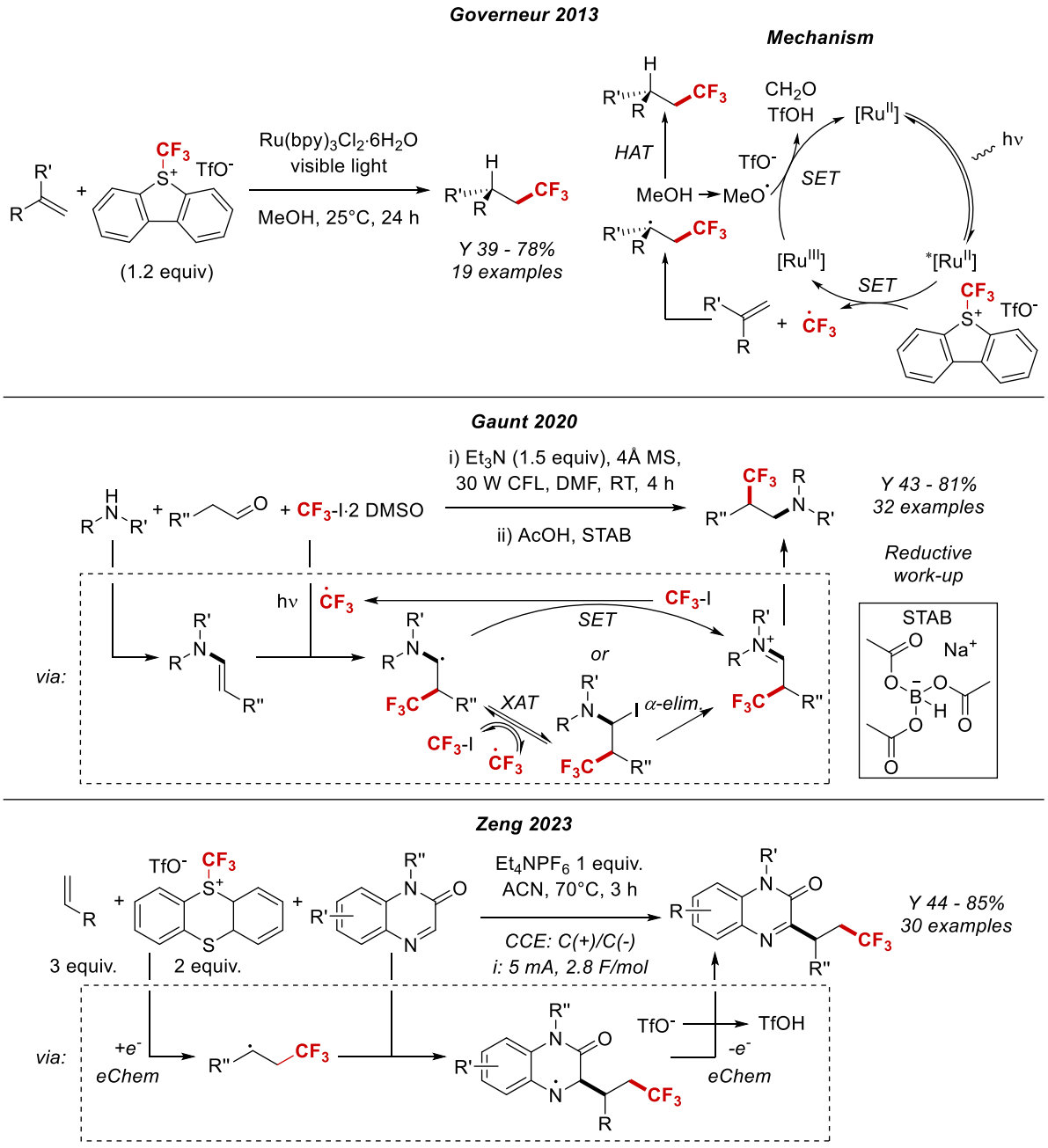

2 Aim of the Thesis

The following chapters will illustrate the organic synthetic methodologies developed during my PhD. To enhance a harmonic structure, only projetcs related to nickel catalysis will be disclosed. Hence, a double CO_2 capture for tandem carbonylation-carboxylation sequence and carbonylative preparation of benzolactams and benzolactones procedures will regard nickel catalysis and CO_2 valorisation; the third project will instead give due disclosure at α-aryl-α-trifluoromethyl alcohols preparation via nickel catalyzed XEC. As in the introduction part, CO_2 chemistry will cover two out of three projects since its use in modern synthetic organic methodologies has been a pivotal element within this PhD program. The third project is going to be presented afterwards thus tracing the same order followed in the introduction part (**Sch. 6**). During this PhD I also had room to engage in electrochemically driven C-H functionalization and in gold catalyzed manipulations of strained ring systems. Nevertheless, these works have been freely cited but not included, the first being an electrosynthetic strategy and the latter being still in an early phase during the preparation of this thesis.[192,193,194,195,196]

Scheme 6. Nickel catalysed synthetic methodologies for CO_2 valorisation and trifluoromethylated fragment delivery.

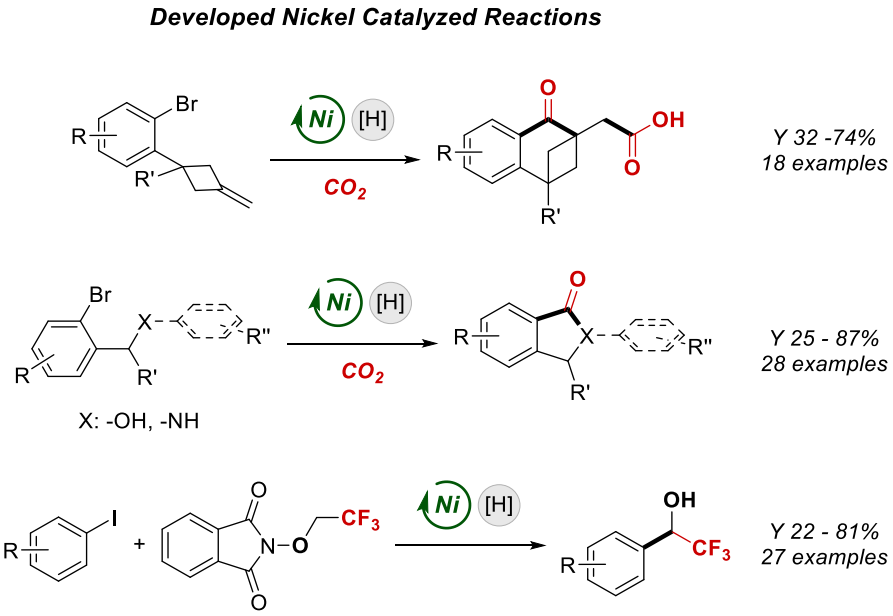

[192] Giovanelli, R., Lombardi, L., Pedrazzani, R., Monari, M., Castiñeira-Reis, M., Silva-López, C., Bertuzzi, G. and Bandini, M., *Org. Lett*. **2023**, 25, 38, 6969–6974
[193] Giovanelli, R., Monda, G., Kiriakidi, S., Silva-López, C., Bertuzzi, G., Bandini, M., *Chem. Eur. J.*, **2024**, 30, e202401658. DOI: 10.1002/chem.202401658
[194] Lombardi, L., Cerveri, A., Giovanelli, R., Castiñeira-Reis, M., Silva-López, C., Bertuzzi, G., Bandini, M., *Angew. Chem. Int. Ed.* **2022**, *61*, e202211732; *Angew. Chem.* **2022**, *134*, e202211732
[195] Giovanelli, R., Bertuzzi, G., Bandini, M., *ChemCatChem* **2023**, 15, e202300827
[196] Rapisarda, L., Fermi, A., Ceroni, P., Giovanelli, R., Bertuzzi, G. and Bandini, M., *Chem. Commun.*, **2023**,59, 2664-2667

3 Results and Discussion

3.1 Double CO_2 incorporation in a Carbonylation/Carboxylation Sequence

3.1.1 Research Context and Literature Review

The incorporation of CO_2 into added value organic vectors has achieved prominent results in many sectors such as energy storage and new material development.[197,198,199,200,201] Catalytic carboxylative reactions have lately greatly contributed to the appointment of mild condition and site-selective processes for highly added-value products manufacturing, displaying the full catalytic capabilities of several transition metals.[202,203,204,205,206]

Formerly illustrated carbonylative processes (see 1.2.2) were aiming to prove CO_2 performances as carbon monoxide surrogate besides its conversion methods to CO synthon. Herein a due disclosure will focus on poorly addressed CO_2 based carbonylation transformations and a fruitful discussion will lead into the first undertaken PhD project. In this sense a literature survey, of available synthetic methodologies to date, enables to draw a framework where different development degrees can be identified based upon atomic bonds formation relative to CO unit (**Sch. 7**).

Scheme 7. General approach to CO_2 based carbonylative protocols.

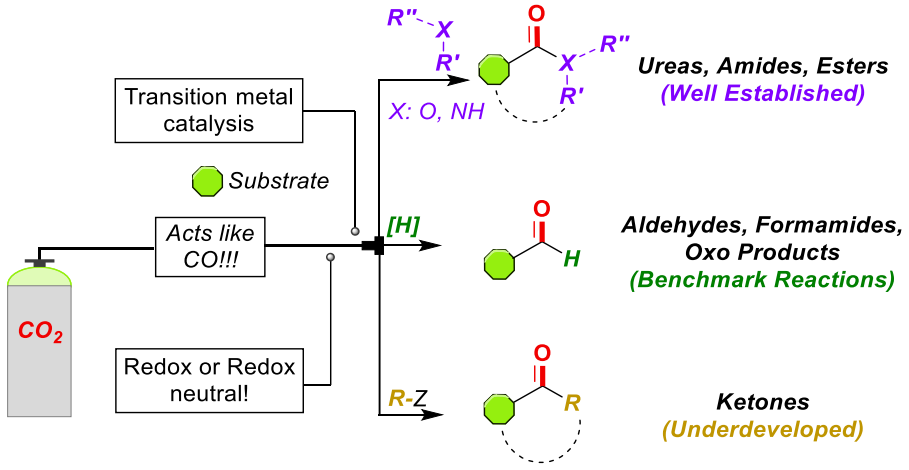

Synthesis of aldehydes, formamides and oxo-products are among the most targeted kind of transformations within CO_2 valorisation. For such reaction both silane as well as hydrogen can be

[197] Nielsen, D.U., Hu, X.M., Daasbjerg, K. *et al.*, *Nat Catal* 1, 244–254 (**2018**)
[198] Liu, Q., Wu, L., Jackstell, R., Beller, M., *Nat Commun* 6, 5933 (**2015**)
[199] Song, Q.W., Zho, Z.H. and He, L.N., *Green Chem.* **2017**,19, 3707-3728
[200] Robert, M., *ACS Energy Lett*. **2016**, 1, 1, 281–282
[201] Modak, A., Bhanja, P., Dutta, P., Chowdhury, B. and Bhaumik, A., *Green Chem.* **2020**,22, 4002-4033
[202] Tortajada, A., Juliá-Hernández, F., Börjesson, M., Moragas, T., Martin, R., *Angew. Chem. Int. Ed.* **2018**, 57, 15948
[203] Ackermann, L., *Angew. Chem. Int. Ed.* **2011**, 50, 3842
[204] Yan, S.S., Fu, Q., Liao, L.L., Sun, G.Q., Ye, J.H., Gong, L., Bo-Xue, Y.Z., Yu, D.G., *Coord. Chem. Rev.* **2018**, 374, 439
[205] Fujihara, T., Tsuji, Y., *Front. Chem.* **2019**, 7, 430
[206] Ran, C.K., Liao, L.L., Gao, T.Y., Gui, Y.Y., Yu, D.G., *Curr. Opin. Green Sus. Chem.* **2021**, 32, 100525

used as reductants with a series of transition metal complexes as catalysts. Conversely ureas, amides but also esters have been largely involved in redox neutral transformations, mainly cyclization reactions, where nucleophilic reactive sites (-NH, -OH, -SH) release their protons for water coproduction generally.[207,208,209,210]

On the other hand, ketones are surely the most synthetic challenging products to achieve, especially when operative boundaries, such as those illustrated previously are set, namely: no *in situ* formation of CO but reduction of CO_2 through alternative oxygen atom scavenging pathways, formation of two C-C bonds with bimolecular condensation (cyclization) or trimolecular mechanisms (intermolecular and/or asymmetric products), no overreduction to alcohols or methylene units. With such thermodynamic (O scavenging) and kinetic (reaction molecular order and phases number) hurdles to be overcome, solutions must be creative and effective. To date few examples have appeared in literature and here some will be presented.

The first general approach relies on *in situ* CO generation from bench stable precursors made from CO_2. Skrydstrup group has mastered this type of approach so far, developing the glassware apparatus (COware) and the chemicals needed to effectively trap CO_2 into useful chemicals and then release CO in a controlled environment. First uses of such chemicals have been directed to palladium catalysed Buchwald-Hartwig cross coupling[211,212] and, later-on new conditions enabled asymmetric ketones synthesis. COgen and SilaCOgen are the commercially available CO precursors, they can also be prepared *in-house* as reported below. Due to noteworthy physico-chemical properties such CO precursors, they have quickly found widespread application especially for radiolabelling purposes using $^{n}CO_2$ (n: 11 – 14). COgen and SilaCOgen can release CO under reported conditions and the applicative outlets have been largely explored (**Fig. 27**).[213,214,215,216]

[207] Dalpozzo, R., Della Ca', N., Gabriele, B., Mancuso, R., *Catalysts,* **2019**, *9*(6), 511
[208] Zhang, Y., Zhang, T. and Das, S., *Green Chem.* **2020**,22, 1800-1820
[209] Wang, L., Sun, W., Liu, C., *Chin. J. Chem*. **2018**, 36, 353−362
[210] Song, L., Jiang, Y.X., Zhang, Z., Gui, Y.Y., Zhou, X.Y. and Yu, D.G., *Chem. Commun.* **2020**,56, 8355-8367
[211] Friis, S.D., Taaning, R.H., Lindhardt, A.T. and Skrydstrup, T., *J. Am. Chem. Soc.* **2011**, 133, 45, 18114–18117
[212] Nordeman, P., Friis, S.D., Andersen, T.L., Audrain, H., Larhed, M., Skrydstrup, T., Antoni, G., *Chem. Eur. J.* (**2015**), 21: 17601-17604
[213] Hermange, P., Lindhardt, A.T., Taaning, R.H., Bjerglund, K., Lupp, D. and Skrydstrup, T., *J. Am. Chem. Soc*. **2011**, 133, 15, 6061–6071
[214] Friis, S.D., Taaning, R.H., Lindhardt, A.T. and Skrydstrup, T., *J. Am. Chem. Soc*. **2011**, 133, 45, 18114–18117
[215] Nielsen, D.U., Neumann, K.T., Lindhardt, A.T., Skrydstrup, T., *J Label Compd Radiopharm*. **2018**; 61: 949–987
[216] Friis, S.D., Lindhardt, A.T. and Skrydstrup, T., *Acc. Chem. Res*. **2016**, 49, 4, 594–605

Figure 27. Cogen and SilaCOgen preparation (top) and "activation" methods (bottom). COgen releases carbon monoxide at moderate rate compared to SilaCOgen and operative temperatures can also affect release paces.

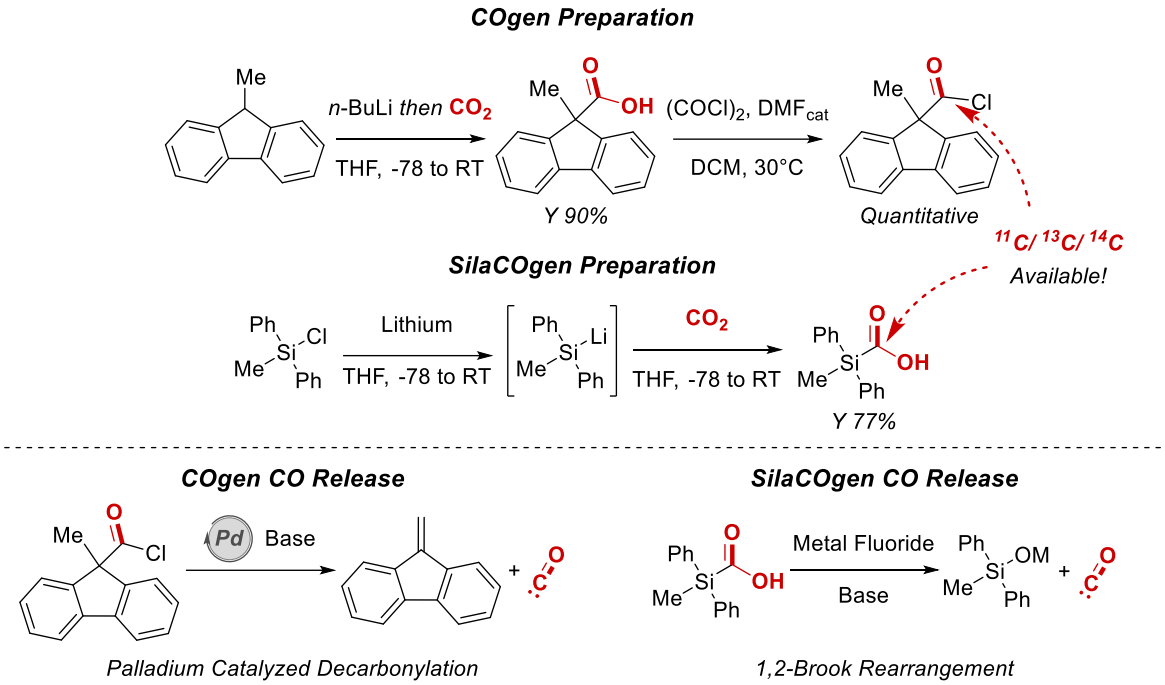

In 2016 asymmetric ketones preparation through SilaCOgen exploitation has been recorded, starting so to cover in such a smart way the pursued transformation highlighted at the beginning of this chapter. The synthetic protocol shown below starts with CO generation through silane reduction triggered by caesium fluoride, generating carbon monoxide for the palladium cycle. A palladium precatalyst performs the first oxidative addition and carbon monoxide insertion up to an acyl-palladium intermediate **I**. Formerly generated siloxane then gives rise to a caesium silanolate upon the attack from another CsF. Such caesium silanolate enters through a copper mediated ligand exchanges series in the palladium cycle and yields an acyl-silanolate palladium(II) complex **II**. A ligand metathesis onto the titled acyl-silanolate palladium(II) leads to the final acyl-aryl palladium(II) **III** which upon reductive elimination generates the products and regenerates the catalyst (Path A). The mechanism can also evolve through bis-silylated organopalladium species **IV**, represented in pathway B which also explains products formation. What has been less investigated are fluoride-involving mechanisms, but available data are sufficient for a clear proposal to be drawn. From the original work both electron-rich and electron-poor silylarenes can be employed. Aryl iodides and bromides can also be used, although halide anion and electronic nature of the ring due to different functional groups needs to be evaluated.[217,218] Few years later a similar protocol was developed from Skrydstrup, Lian and Kramer for asymmetric ketones preparation by using SilaCOgen and palladium catalysis.[219]

[217] Lian, Z., Nielsen, D., Lindhardt, A., Daasbjerg, K. and Skrydstrup, T., *Nat Commun* 7, 13782 (**2016**)
[218] Tymonko, S.A., Smith, R.C., Ambrosi, A., Ober, M.H., Wang, H., Denmark, S.E., *J. Am. Chem. Soc.* 137, 6200–6218 (**2015**)
[219] Li, X., Xu, J., Li, Y., Kramer, S., Skrydstrup, T., Lian, Z., *Adv. Synth. Catal.* **2020**, 362, 4078

Figure 28. Asymmetric ketones preparation via Hiyama-Denmark coupling, implemented with CO_2 to CO conversion.

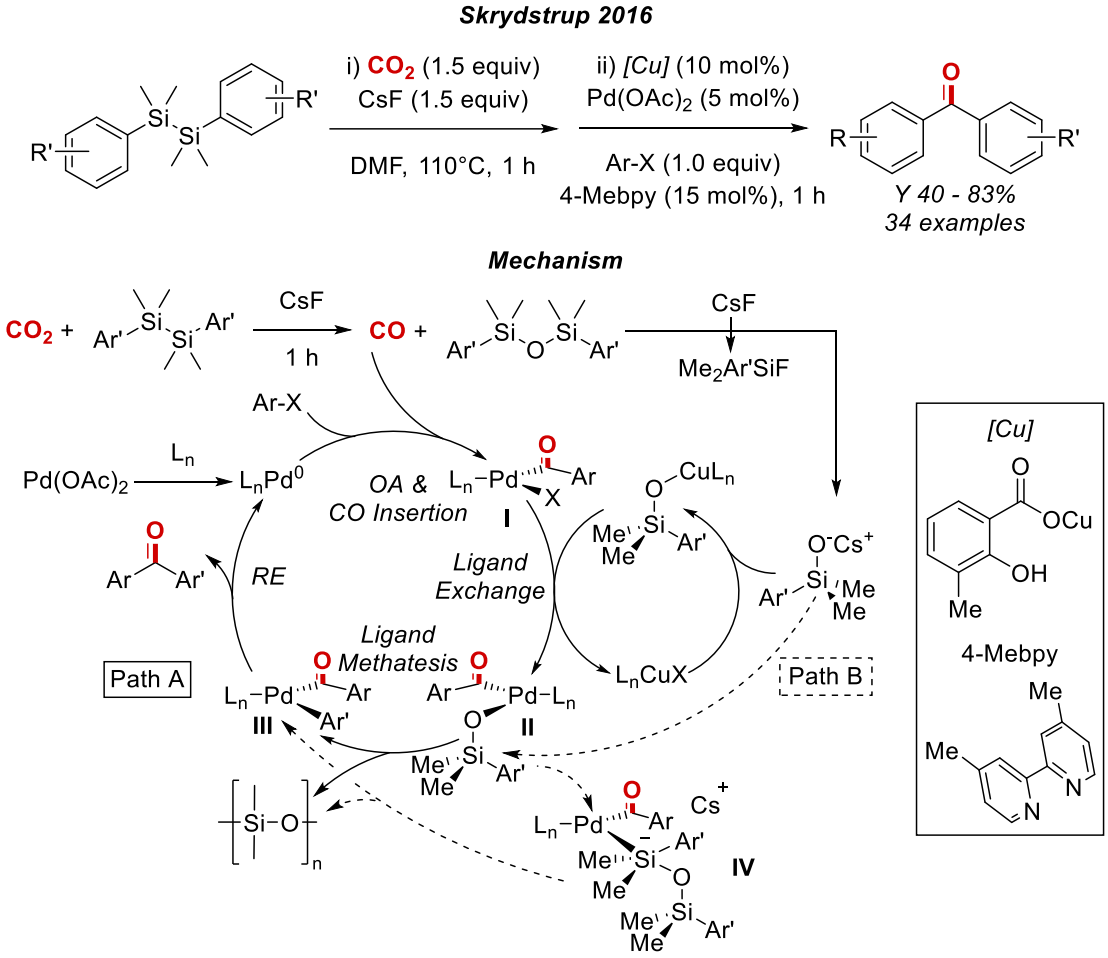

Another interesting synthetic protocol developed to forge two consecutive C-C bonds is reported by Huang, Fang and Li. Starting with cheap 2-halophenols (-Br, -I) and arylacetylene partners, a CO_2 reduction can be engaged via silane mediated reduction to produce aurones. This approach reduces CO_2 through silanes (but also boranes can work), for which many authors propose silyl-formates species to be operative in different kind of carbonylative synthetic methodologies. In the analysed example PMSH (Polymethylhydorsiloxane) is responsible for direct CO_2 reduction to the corresponding formats **V**, which releases CO upon palladium catalyzed decarbonylative action. Additionally, palladium-dppf catalyst is responsible for undergoing oxidative addition onto the halophenols and subsequently insert carbon monoxide. At this stage, a copper free Sonogashira mechanism takes place from the acylpalladium(II) intermediate **VI** by base activation of the alkyne. Thus, a stable propargylic ketone **VII** is formed undergoing a final Pd-mediated intramolecular cyclization to afford products **VIII**. Investigated partners for the reaction account for aryl and heteroaryl alkynes while only electron-poor halophenols are suitable for such a transformation (**Fig. 29**).[220] Only one close methodology from Qi and Jiang also includes 2-haloanilines as starting materials, where palladium catalysis and silanes as reductants have been used. [221] The adopted

[220] Huang, Z., Li, Y., Zhou, J., Zhang, Y., Wu, J., Wu, Y., Zhang, F., Fang, Z., Li, Y., *ChemSusChem* **2023**, 16, e202202365. DOI: 10.1002/cssc.202202365
[221] Xiong, W., Wu, B., Zhu, B., Tan, X., Wang, L., Wu, W., Qi, C., Jiang, H., *ChemCatChem* **2021**, 13, 2843

strategic route to access ketones using CO_2 as CO surrogate, although being a popular one has proved to be efficient and future works might be aimed at expanding the portfolio of substrates undergoing this kind of carbonylative transformation.

Figure 29. Aurones preparation through silane-based reduction of CO_2 to silylformates, and subsequent transformation into CO source.

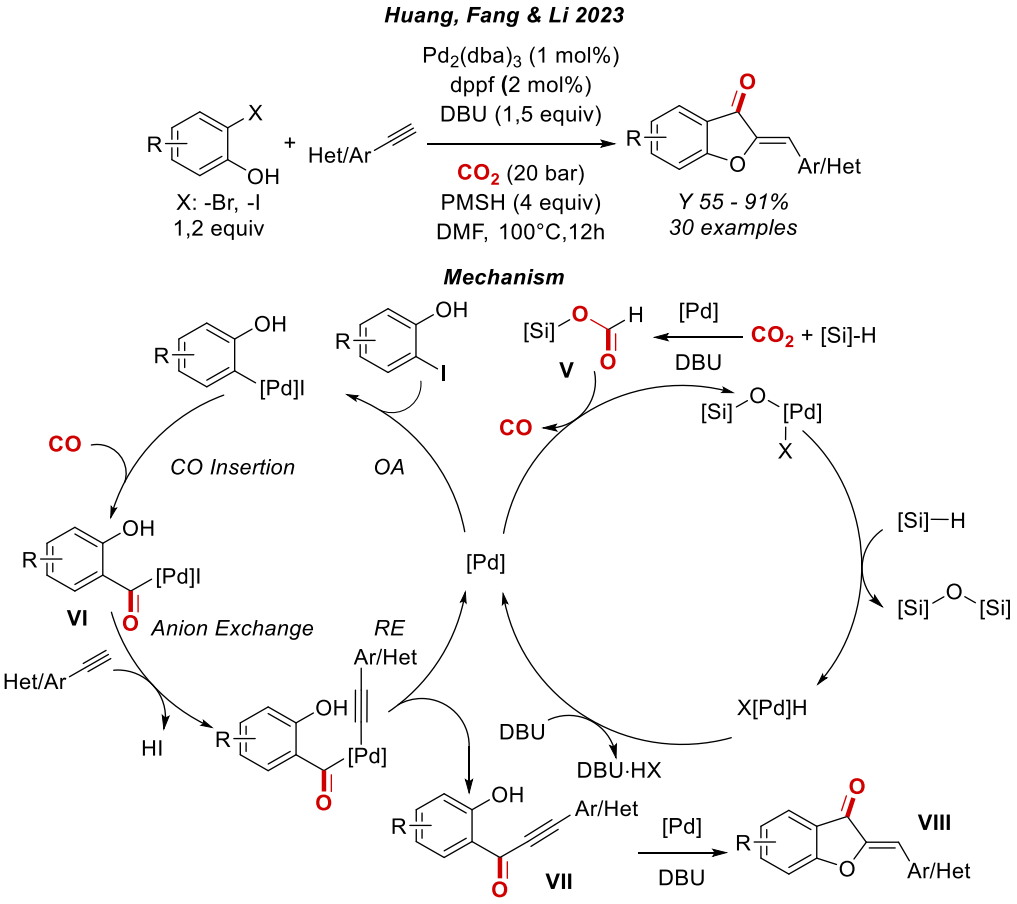

In 2024 an elegant electrochemical approach directed to the preparation of symmetrical ketones from CO_2 was reported by Lloret-Fillol group, relying on an iron/nickel bimetallic system. During mechanism investigations authors suggest that both metallic catalysts can doubly reduce the benzyl chloride to Cl^- and Bn^- anions as well as CO_2 to CO and this hypothesis has not been ruled out. Although, for halide reduction nickel-bpy should be a more competent species rather than FeTPP, while the latter complex seems to perform better CO_2 reduction to CO. The only major mechanistic standpoint is no ketone observation without nickel catalyst being used, so Fe-TPP role in product formation can be excluded. Despite the narrow substrate tolerance displayed by this strategy, competencies of such a protocol to directly access ketones via XEC by means of CO_2 and organic halides represent a highly desirable approach to the displayed synthetic challenge herein presented; indeed, an alternative solution at *in situ* CO generation methods is introduced combined with a non-traditional oxygen atom scavenging strategy (**Fig. 30**). In this electrochemical synthetic methodology several problems have been faced, with the most prominent being dimerization of benzyl fragments, proto-demetallation to toluene and direct carboxylation over ketone formation. Secondly in the overall transformation a triethylamine molecule results as the final sacrificial reductant to balance the

cathodic events occurring in the formation of the desired product; this is in stark contrast with classical reductants employed (usually metal powders, silanes/boranes or gaseous hydrogen are being used).[222]

Figure 30. Lloret-Fillol electrocatalysed synthesis of symmetric ketones via bimetallic catalysis.

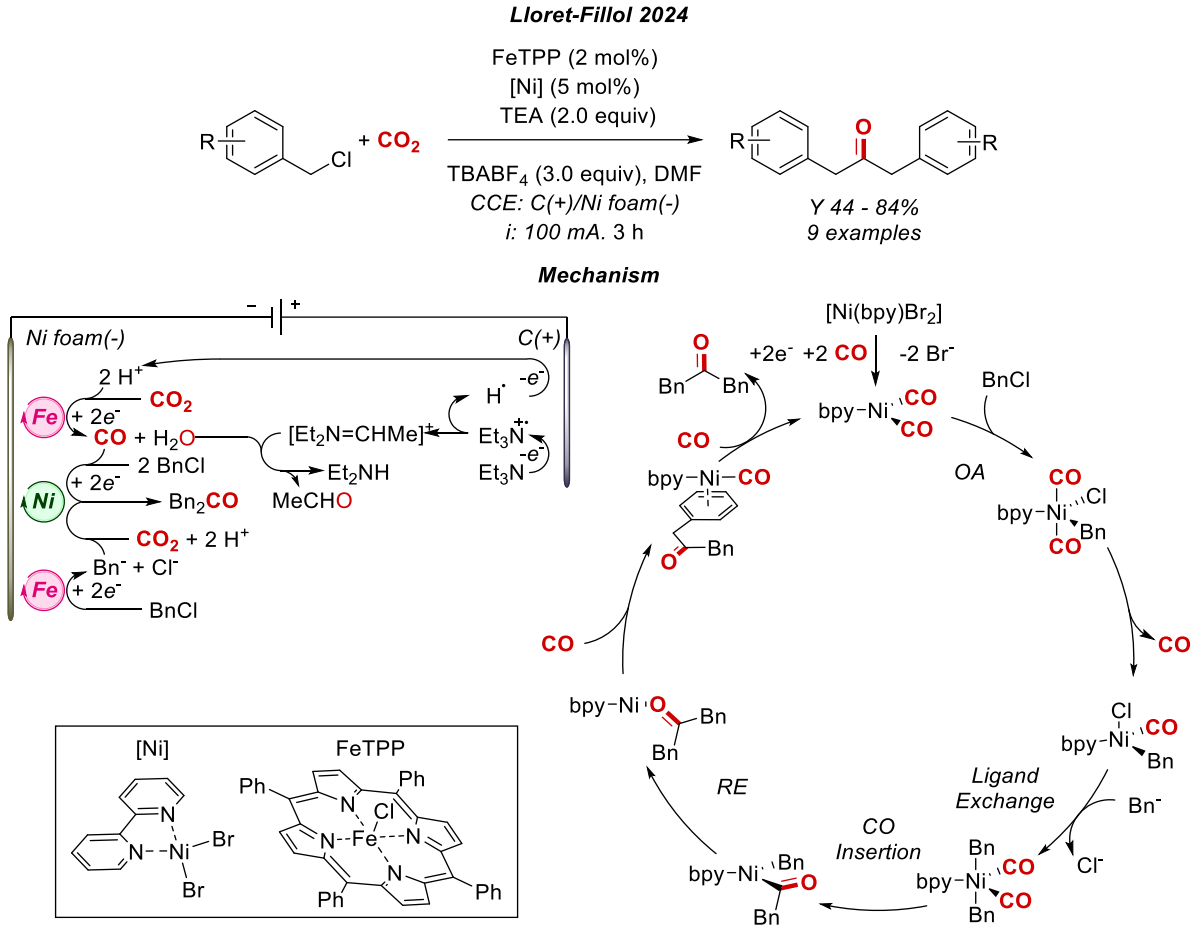

During recent years only a few other methodologies for CO_2 reduction and incorporation into ketones have been known in the scientific community, two of which require MOF preparation and relies over rhodium or palladium/copper catalysis; the third one being an eChem reduction followed by a polymerization of produced CO.[223,224,225]

3.1.2 Work Rationale and Development

The illustrated approaches toward ketones synthesis are summarized below, due to previous works related to CO_2 valorisation carried out in our research group we wondered if a new solution could arise from proper leveraging of carboxylic acids' electrophilic activation chemistry, especially

[222] Sheta, A.M., Fernández, S., Liu, C., Dubed-Bandomo, G.C., Lloret-Fillol, J., *Angew. Chem. Int. Ed.* **2024**, 63, e202403674.DOI: 10.1002/anie.202403674
[223] Shyshkanov, S., Vasilyev, D.V., Abhyankar, K.A., Stylianou, K.C., Dyson, P.J., *Eur. J. Inorg. Chem.* **2022**, e202200037
[224] Fu, S., Yao, S., Guo, S., Guo, G.C., Yuan, W., Lu, T.B., Zhang, Z.M., *J. Am. Chem. Soc*. **2021**, 143, 49, 20792–20801
[225] Dodge, H.M., Natinsky, B.S., Jolly, B.J., Zhang, H., Mu, Y., Chapp, S.M., Tran, T.V., Diaconescu, P.L., Do, L.H., Wang, D., Liu, G. and Miller, A.J.M., *ACS Catal.* **2023**, 13, 7, 4053–4059

through low valent metal species. Such a solution would trace a mark to finally put aside CO chemistry (**Sch. 8**).[226,227,228,229]

Scheme 8. Schematized approaches to ketones synthesis, Skrydstrup approach with bench-stable CO precursors. Lloret-Fillol electrocatalysed, bimetallic strategy. Common CO_2 synthetic routes with traditional reductants. Our new CO-bypassing strategy enabled by nickel catalysis with Lewis acid assistance.

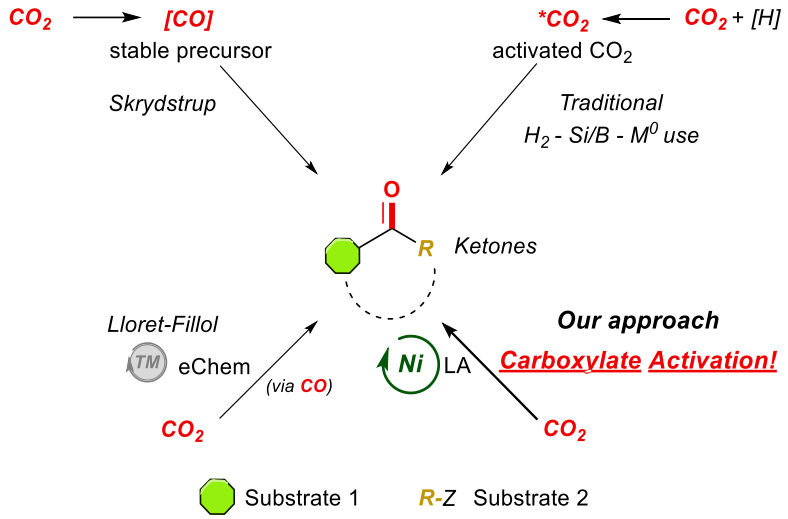

We began to investigate the ability of Lewis acid to electrophilically activate carboxylic acids. Due to its known affinity toward carboxylation chemistry, we initially selected a nickel-based catalysts; a metal powder as reductant avoiding in one time the need of hydrogen/silane manipulation and to go over again known methodologies; and finally, we picked up a scarcely investigated substrates family **(Fig. 31**). The choice of reported cyclobutanealkylidenes was made considering some fundamental requirements such as the need of an easy reactive site toward nickel catalysis (bromide) where nickel could start its cycle. Then we wondered if a sterical restrained/oriented olefin, rather than a plain pendant one) could favour a Heck-like step to occur, while giving rise at the same time to non-trivial molecular structure. With such initial boundaries for a cross-electrophile coupling to be developed we extensively screened reaction conditions, also considering that highly oxophilic LA such as $AlCl_3$ could simultaneously activate CO_2 and work as oxygen atom scavenger.

[226] Deng, X., Guo, J., Zhang, X., Wang, X., Su, W., *Angew. Chem., Int. Ed.* **2021**, 60, 24510
[227] Lundberg, H., Tinnis, F., Selander, N. and Adolfsson, H., *Chem. Soc. Rev.* **2014**, 43, 2714-2742
[228] Taussat, A., Marcia de Figueiredo, R. and Campagne, J.M., *Catalyst,* **2023**, 13, 366
[229] Kumar, V., Rana, A., Meena, C.L., Sharma, N., Kumar, Y., Mahajan, D., *Synthesis,* **2018**, 50, 3902

Figure 31. Tandem carbonylation/carboxylation sequence with observed byproducts

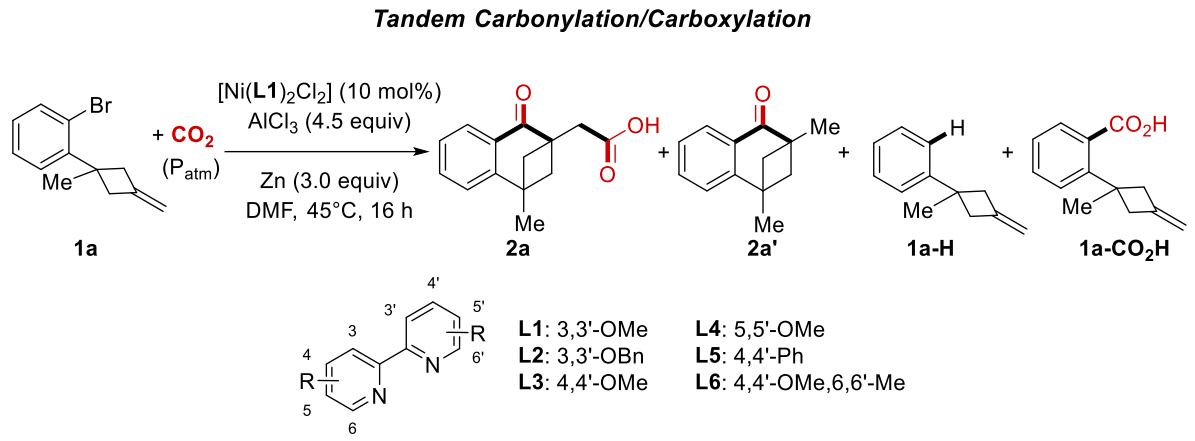

Table 4. [a]All reactions were carried out under CO_2 atmosphere and with dry solvents. [b]Isolated yields after flash chromatography. [c]**1a**/[Ni(**L1**)$_2$Cl$_2$]/Al/Zn, 1/0.1/4.5/3 equiv, [**1a**] = 0.1 M. [d]Variable amounts of proto-debrominated-1a (59–97%) were recorded (^{1}H NMR analysis on the reaction crude). [e]Variable amounts of unreacted **1a** (75–77%) were recorded in the reaction crude. n.d.: not detected, N.R.: no reaction, n.q.: nearly quantitative.

Entry[a]	Deviation from Optimal	SM (%)[b]	Y (%) 2a[b]	Y (%) 2a'[b]	Y (%) 1a-H[b]	Y (%) 1a-CO$_2$H[b]
1	-[c]	traces	**70**	7	21	traces
2	Ni(**L2**)$_2$Cl$_2$	traces	**64**	7	27	2
3	Ni(**L3**)$_2$Cl$_2$	3	**61**	4	21	11
4	Ni(**L4**)$_2$Cl$_2$	traces	**19**	-	46	33
5	Ni(**L5**)$_2$Cl$_2$	7	**15**	5	65	8
6	Ni(**L6**)Cl$_2$	6	**-**	-	89	5
7	Ni(**L1**)$_2$I$_2$	traces	**64**	10	25	0
8	Ni(**L1**)Cl$_2$	traces	**64**	5	25	traces
9	without AlCl$_3$	n.d.	-	-	-[d]	-
10	without Ni(**L1**)$_2$Cl$_2$	-[e]	-	-	-	-
11	N_2 instead of CO_2	n.d.	-	-	-[d]	-
12	CO instead of CO_2	N.R.	**0**	-	-	-
13	DMA instead of DMF	n.a.	**41**	10	n.d.	n.d.
14	Mn instead of Zn	n.a.	**60**	5	n.d.	n.d.

In this synthesis of tetralone-2-acetic acids the use of larger substituents onto nickel ligand scaffold or a position shift on bipyridyl ring system favoured proto-dehalogenation byproducts (**Tab. 4, 2 – 6 entries**). Switching from di-chloro to di-iodo nickel precatalyst and from bi-ligated to mono-ligated nickel species also lowered the product formation with an increase of the de-brominated byproduct **1a-H** (**Tab. 4, 7 – 8 entries**). Proto-dehalogenation also occurred when Lewis acid was excluded from the reaction (**entry 9**) or when N_2 was used in place of CO_2 (**Tab. 4, entry 11**). When no catalyst was used instead (**entry 10**) variable amounts of unreacted **1a** were found. Solvent effect was assessed by using DMA and in such a case product yield almost dropped by 50% (**Tab. 4, entry 13**). Also, manganese was tested as alternative reductant but gave 10% less product **2a** with respect to zinc (**Tab. 4, entry 14**). Due to high water sensitivity of this reaction, as demonstrated by the large amount of

1a-H byproduct always observed, no organic reductants could be used with standard Schlenk technique given their marked hygroscopicity (*i.e.* TBD, DBU).

Other Lewis acids have been investigated ($MgCl_2$, $ZnCl_2$, $Al(OTf)_3$, LiCl and TMSCl) but none of them gave remarkable results. This highlights an already observed propensity of $AlCl_3$ to participate in nickel mediated XEC reactions and its applicability in carboxylative processes.[230,231,232]

Even after a strict control over water content, proto-dehalogenation of **1a** resulted to be one of the most prominent side reactions. That said, the formation of benzoic acid derivatives **1a-CO_2H** through direct ring carboxylation, which no cyclization event followed might be ascribed to ligand electronics/geometry variation (**Tab. 4, entries 1, 3 and 4**). As main mechanistic investigations a $^{13}CO_2$ labelling experiment has been carried out, the corresponding ^{13}C-NMR spectra confirms that both carbonyl and carboxylic moieties are originated from CO_2, ruling out other possible carbonyl sources as DMF (**Fig. 32**).

Figure 32. ^{13}C-NMR spectra of doubly ^{13}C-labelled tetralone derivative.

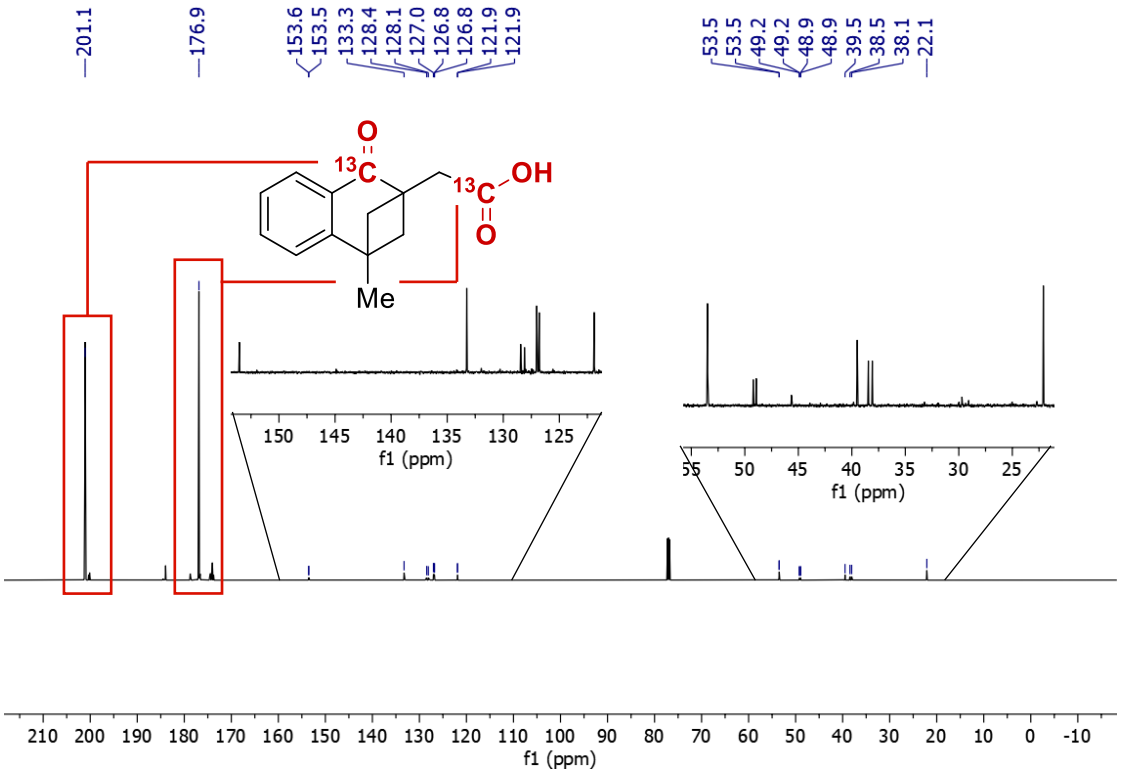

Our attention was then dedicated at investigating the breadth of this transformation (**Fig. 33**), both EDG and EWG substituents could be accommodated on the phenyl ring. Particularly, EDG functional groups commonly showed higher yields (49 – 74%) than EWG substituents (33 – 53%) (**2a - 2g, 2i, 2j**). Two examples of fused cycles were also tested (**2h, 2k**) with good yields recorded. The Me-substituent in **1a** was then replaced with a n-Bu pendant chain (**2l**) and with phenethyl groups (**2m –**

[230] Lombardi. L., Cerveri, A., Ceccon, L., Pedrazzani, R., Monari, M., Bertuzzi, G. and Bandini, M., *Chem. Commun.* **2022**, 58, 4071
[231] Olah, G.A., Török, B., Joschek, J.P., Bucsi, I., Esteves, P.M., Rasul, G., Prakash, G.K.S., *J. Am. Chem. Soc*. **2002**, 124, 38, 11379–11391
[232] Gu, M., Cheng, Z., *Ind. Eng. Chem. Res.* **2014**, 53, 24, 9992–9998

2p) recording yields from 53% to 74%. Finally, aromatic rings could be accommodated at the same quaternary position (**2q, 2r**) despite a moderate recorded yield of 45% for both substrates.

Figure 33. Scope of the transformation, functional groups accommodated on the phenyl ring (blue) and on the quaternary center (brown)

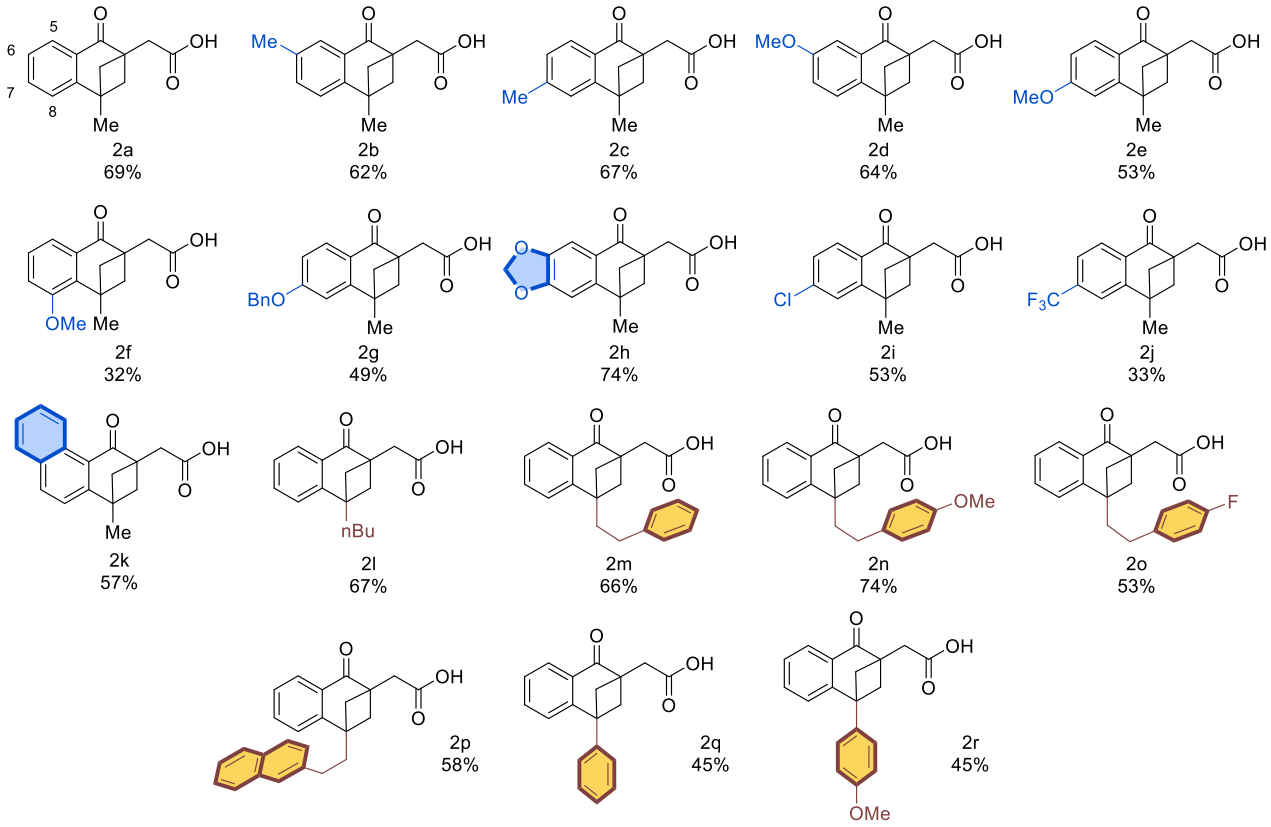

A series of synthetic manipulation of product scaffold was also successfully attempted for both the carboxylic and the carbonyl moieties, whose introduction delivered useful reactive sites for further elaborations. Product **2a** has been converted to the corresponding alcohol by reduction with $NaBH_4$ and then an esterification led to compound **3** in good yield. Under acidic conditions set by p-toluensulphonic acid, then **3** was also converted into the corresponding lactone **4** in 55% yield. A sample of **2a** was then converted into piridazinone **5** in 74% yield through condensation with hydrazine.

Later the carboxylic moiety was further exploited, a Curtius rearrangement was carried out with DPPA (diphenylphosphoryl azide) to form the corresponding carbamate **6** in moderate yield 50%. Finally, a conversion of product **2a** into the redox active ester adduct **7** with *N*-hydroxyphthalimide alkylic scaffold was done with a yield of 51% and this compound under electrochemical conditions was employed as a radical precursor, for the alkylation of a MBH (Morita-Baylis-Hillman) acetate (**8**) to get cinnamate derivative **9** (**Fig. 34**).[196]

The last part of this work was aimed at mechanism elucidation, to do so DFT calculations were performed, and the energetically favoured pathway is displayed below(**Fig. 35**).

Figure 34. Tetralonyl-2-acetic acids products' post functionalization.

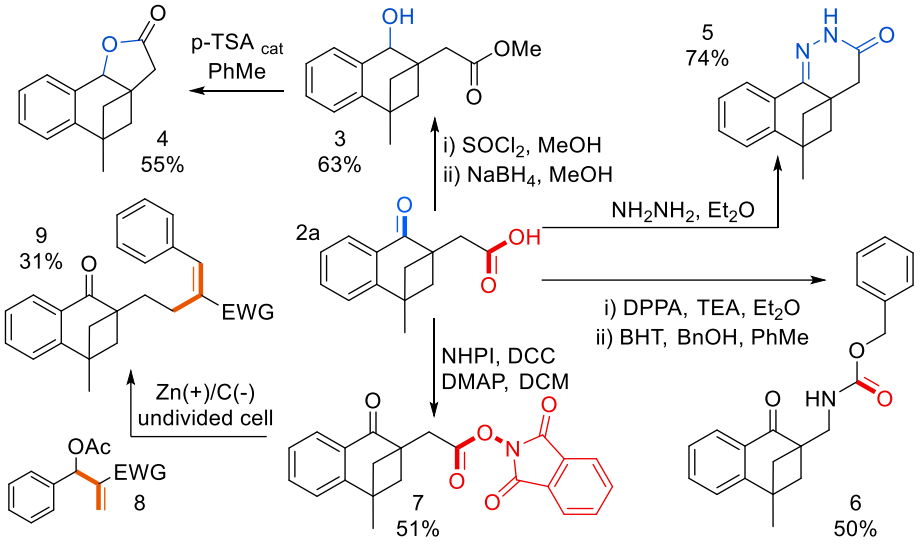

Initially zinc powder converts via SET the nickel (II) precatalyst into a catalytically active nickel(I) species **i**. Then a substrate coordination by **i**, evolves through intermediate **ii** toward the first, largely energetically feasible, transition state represented by the oxidative addition step to **iii** (**TS ii-iii**). From **iii** to **iv** two sequential SET event occurs and then an $AlCl_3$-CO_2 adduct is formed (intermediate **v)**. At this stage the second transition state is encountered, **TS v-vi** leading to organonickel(I) **vi** which is intramolecularly stabilized by the olefin moiety and the carboxylation occurs in a nearly barrierless fashion, with carboxylate **vi** formation resulting in an exothermic step. After coordinative organization of chelating groups around nickel(I) in intermediate **vii**, another $AlCl_3$ coordinates the second CO_2 oxygen leading to **viii**, which lies in the lower point of the energetic profile. Nevertheless, **viii** can go through the most energy demanding step (**TS viii-ix)** where about 40 kcal/mol are required to the olefin moiety to attack the carboxylate and furnish **ix**. This step is possibly the rate determining one, and it is thought it can occur only by assistance of a Lewis acid. One of the oxygen atoms in **ix** is then de-coordinated from aluminium trichloride while the other one is the scavenged to Al oxides upon zinc reduction, during carbonyl group generation (**x – xi**). A final CO_2 capture from the organonickel(I) **xi**, with a nickel-aluminium exchange, accounts for cycle closure.

In the depicted mechanism $AlCl_3$ activates CO_2 in solution through coordination and plays an additional key role in stabilizing **TS v-vi** and **TS viii-ix** of over 20 kcal/mol. Moreover, the effect of the methyl group from the substrate residue was found to exert a further stabilization of about 20 kcal/mol with respect to the tertiary alkylidene cyclobutene analogue. Structural confirmation through XRD (X-Ray Diffractometry) analysis has been performed on crystalline **2a** (**Fig. 36**).[192]

Figure 35. DFT driven mechanism proposal for tandem carbonylation/carboxylation sequence.

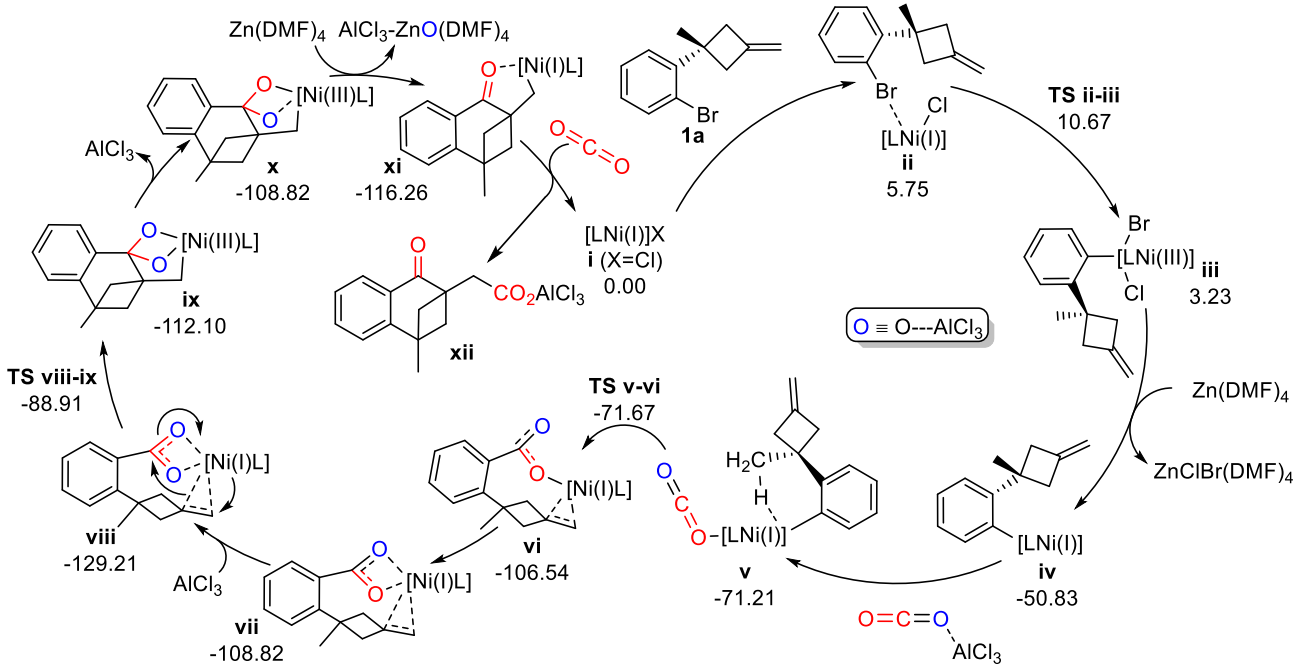

Figure 36. ORTEP drawing of **2a**. Thermal ellipsoid are drawn at 30% of the probability level.

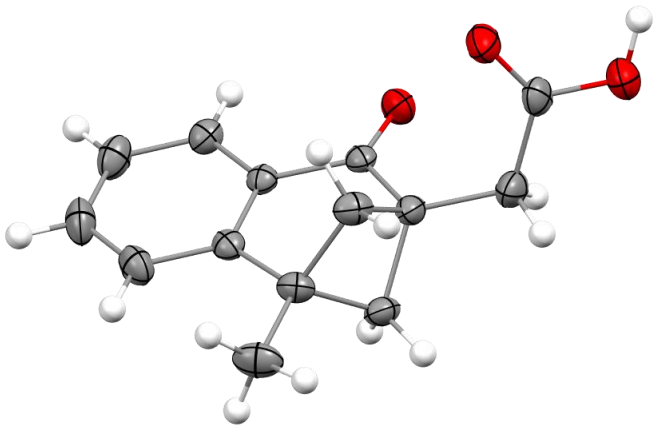

3.1.3 Conclusions

This final scenario has determined the first CO_2 based carbonylation/carboxylation sequence to be developed under nickel catalysed cross-electrophilic conditions. The proposed mechanism is a first of its kind to be documented for ketone formation, where CO is not involved but genuine transformation of CO_2 directly into carbonyl group is achieved under the assistance of $AlCl_3$. This opens to a conceptually new synthetic route (**Sch. 8**). Unequivocal proofs of CO_2 origins have been provided through labelling experiments and computational data helped for an overall mechanism unveiling.

3.2 Synthesis of Benzolactams and Benzolactones

3.2.1 Research Context and Literature Review

Research toward preparation of (benz)amides and (benzo)lactones using CO_2 in place of CO in carbonylation protocols, will be the core of this chapter. To give a better structure some literature examples will be discussed prior the presentation of the second PhD work, thus, to better identify the missing conceptual points that this work is going to cover. Formylation reactions may also give rise to the compound classes herein treated (formamides and formyl esters); thus, considering they have been treated formerly (cap. 2.2.2) and considered that the outcome of formylations represent a quite different chemical entities with respect to (benz)amides and (benzo)lactones, here only consistent synthetic methodology will be reported to draw the state of the art in matter of amide/esters functional group preparation.[233,234]

After proving that carbonyl moiety introduction could be done following a whole new conceptual synthetic pathway in the former chapter, the goal set for the next research was to shift such a paradigm to the preparation of other functional group. Proper leveraging of nickel catalysis and CO_2 chemistry could lead to the preparation of benzolactams and benzolactones in a new straightforward manner. An extensive literature survey showed that lactams and lactones' preparation (but also amides and esters) mainly falls into three synthetic lines: one exploiting palladium/CO synergy; the second one relying on metallacarbonyl as CO sources and the third one accomplishing *redox neutral* carbonylative cyclizations with 4^{th} or 5^{th} row transition metals mainly. Other strategies to install CO moiety are marginal, and among them few reports account for cyanide precursors utilization making them not less potentially harmful than CO deploying ones (**Sch. 9**).[235,236,237,238,239,240,241,242,,243,244]

Carbonylation protocols have been developed since palladium catalysis infancy with early examples from Ban, Stille, Heck and others.[245,246] The electrophilic character of acylpalladium species is the main reason why this metal has been so widely used in combination with CO. The final proof of this can be found in the development of several double carbonylative strategies.[247,248] A valid example is from Heck and colleagues, in 1974 they set up a convenient set of conditions for the carboalkoxylation of aryl-, benzyl- and vinylhalides. Mechanism explanation is readily given by authors stating that a carbon monoxide-palladium complex **IX** undergoes oxidative addition with the organic halide giving

[233] Wu, X.F., Neumann, H. and Beller, M., *Chem. Rev*. **2013**, 113, 1, 1–35
[234] Peng, J.B., Geng, H.Q., Wu, X.F., *Chem.* **2019**, 5, 526-552
[235] Garrou, P.E., Heck, R.F., *J. Am. Chem. Soc.* **1976**, 98, 14, 4115–4127
[236] Marosvölgyi-Haskó, D., Takács, A., Riedl, Z., Kollár, L., *Tetrahedron*, **2011**, 67 ,5 ,1036-1040
[237] Dahl, K., Schou, M., Amini, N., Halldin, C., *Eur. J. Org. Chem*. **2013**: 1228-1231
[238] Brunet, J.J., Sidot, C., Caubere, P., *J. Org. Chem*. **1983**, 48, 8, 1166–1171
[239] Foà, M., Francalanci, F., Bencini, E., Gardano, A., *Journal of Organometallic Chemistry,* **1985**, 285, 1–3, 293-303
[240] Wu, X., Mahalingam, A.K., Wan, Y., Alterman, M., *Tetrahedron Letters*, **2004**, 45, 24, 4635-4638
[241] Prasad, P.K, Sudalai, A., *Adv. Synth. Catal.* **2014**, 356: 2231-2238
[242] Mahendar. L., Satyanarayana, G., *J. Org. Chem*. **2016**, 81, 17, 7685–7691
[243] Meyer, N., Seebach, D., *Chem. Ber*. **1980**, 113: 1304-1319
[244] Wang, Z., Yin, Z., Wu, X.F., *Chem. Commun.* **2018**, 54, 4798–4801
[245] Mori, M., Chiba, K., Ban, Y., *J. Org. Chem*. **1978**, 43, 9, 1684–1687
[246] Cowell, A., Stille, J.K., *J. Am. Chem. Soc.* **1980**, 102, 12, 4193–4198,
[247] Tanaka, M., Kobayashi, T.A. and Sakakura, T., *J. Chem. Soc., Chem. Commun.*, **1985**, 837-838
[248] Das, D., Bhanage, B.M., *Adv. Synth. Catal.* **2020**, 362, 3022

X, then a CO migratory insertion occurs. This so formed acyl palladium species **XI** is attacked by the alcohols within palladium coordination sphere and the reductive elimination of the product leaves a Pd-halohydridic species **XII** readily regenerated by the base.[249] These steps are currently accepted for this transformation and are commonly found in textbooks highlighting the value of these works (**Fig. 37**).

Scheme 9. Different modes to access amides and esters from CO or its precursors.

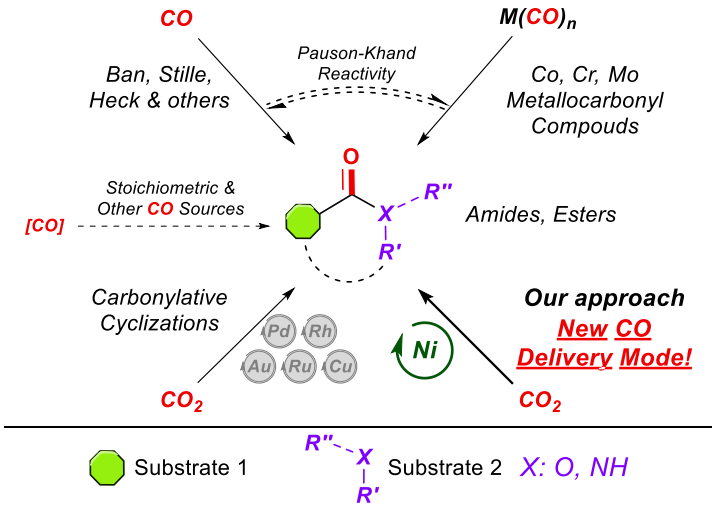

Figure 37. Reproduction of original reaction mechanism proposal made by Heck in 1974.

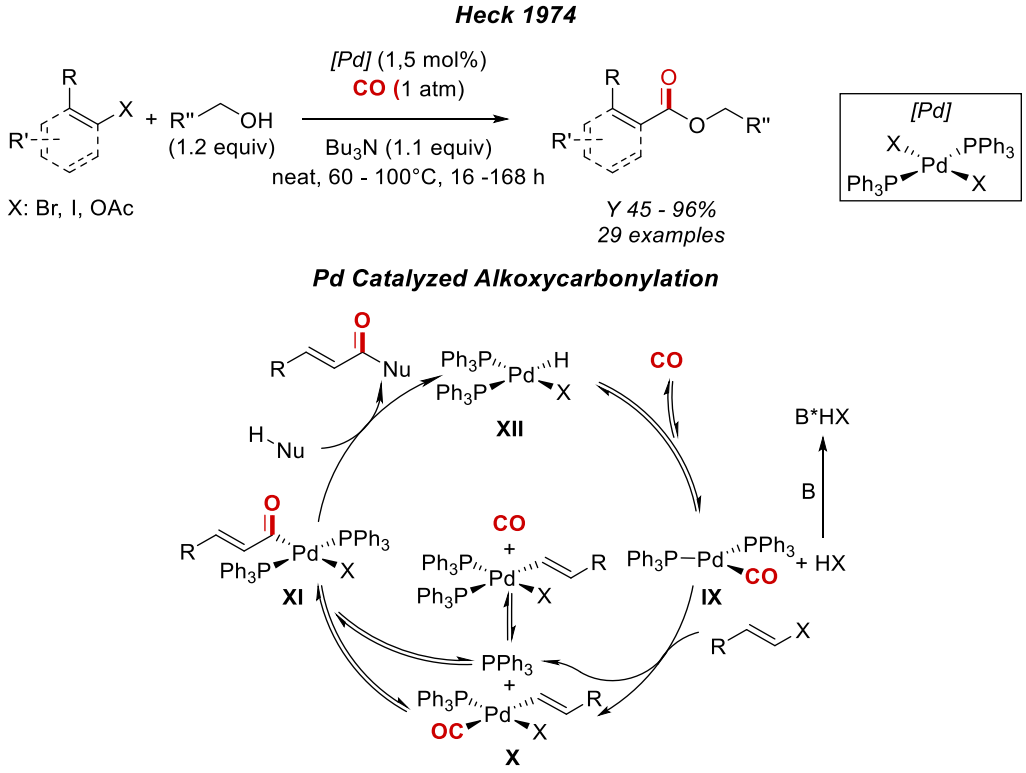

Lactones preparation via CO incorporation have also been unravelled so far, Wang and co-workers have accounted for such a transformation in 2015, they targeted coumarin derivatives synthesis by mean of cobalt(III) catalysis. The high valent Cp*Co(III) engages the starting material to form the

[249]Schoenberg, A., Bartoletti, I., Heck, R.F., *J. Org. Chem.* (**1974**), 39, 3318

alkoxide **XIII**, then either through sequential metalation- deprotonation (*pathway A*) or CDM (Concerted Metallation-Deprotonation) sequence (*pathway B*) an alkenyl-Co(III) complex **XIV** is formed. This intermediate is capable to insert CO and undergoing reductive elimination. A final sacrificial oxidation by Ag/Cu action regenerates the catalyst (**Fig. 38**). Investigation of the transformation scope revealed that both EWG and EDG groups are tolerated in the aromatic ring, two substituents can also be accommodated if one of them is an alkyl short chain; as second olefinic substituents (R'') also a second aryl ring can be introduced but, in this case, only electron-poor rings or unsubstituted moieties have been used in place of methyl groups.[250]

As example for CO cyclization enabled by TM catalysis, it is possible to consider a hetero Pauson-Khand type reaction reported in 2013 by Mukai and colleagues. The devised reaction takes advantage of rhodium catalysis to perform olefin cyclization, in an intramolecular fashion, through a coordinative oxidation leading from Rh(I) to Rh(III). The formed hetero-rhodacycle **XV** undergoes CO insertion and reductive elimination then, affording the product directly. The main drawback highlighted from this synthetic methodology is a limited substrate scope and the high catalyst loading, also considered the price of rhodium sources (**Fig. 39**).[251]

Figure 38. Wang's Cp*Co catalysed coumarin derivatives preparation.

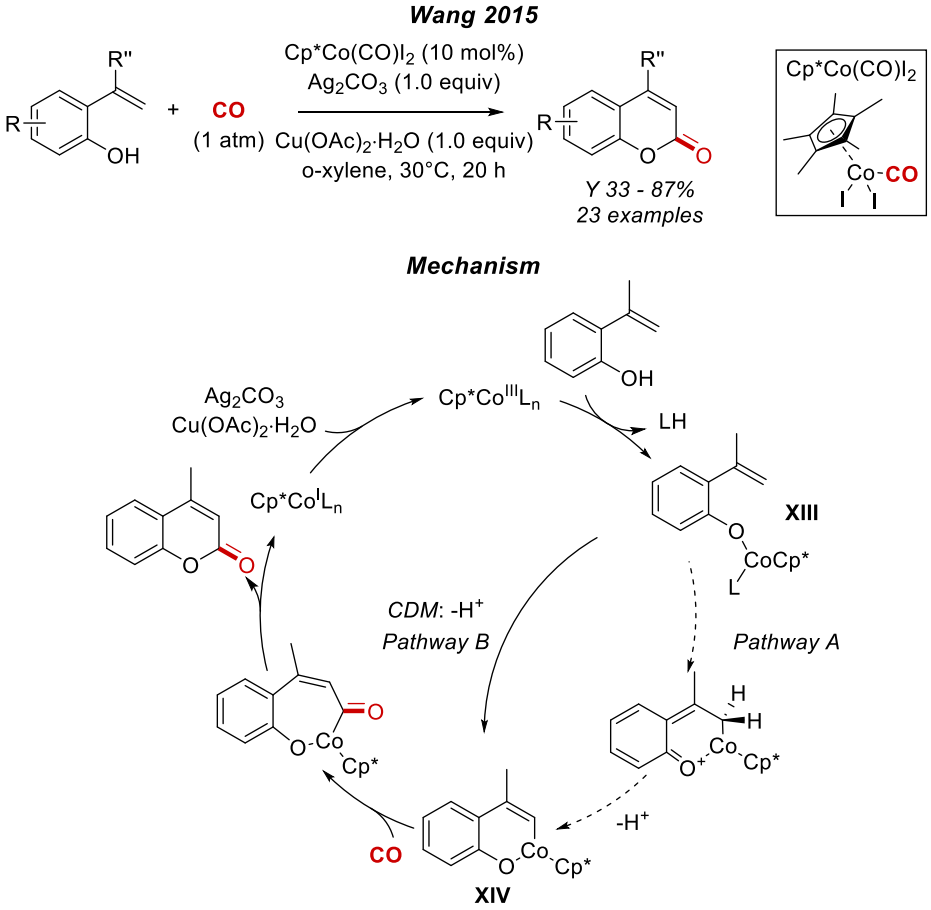

As in the former example CO handling is demanded even if not at high pressures, other known synthetic procedures are available in literature where CO delivery is obtained with transition metals

[250] Grigorjeva, L. and Daugulis, O., *Org. Lett.* **2015**, 17, 5404−5407
[251] Iwata, T., Inagaki, F., Mukai, C., *Angew. Chem. Int. Ed.* **2013**, 52, 11138 –11142

catalytic systems following the mechanistic line herein presented. A last general observation is due when mixing CO ad transition metal catalysts, it regards possible poisoning of catalytically active species either through direct ligand substitution and deactivation or via off-cycles' species production which then furtherly evolve into unproductive lines. Thus, a careful metal catalysts' evaluation should be undertaken in reason of the selected CO source.[252]

Figure 39. Rhodium-carbonyl catalyst triggered cyclization from Mukai group.

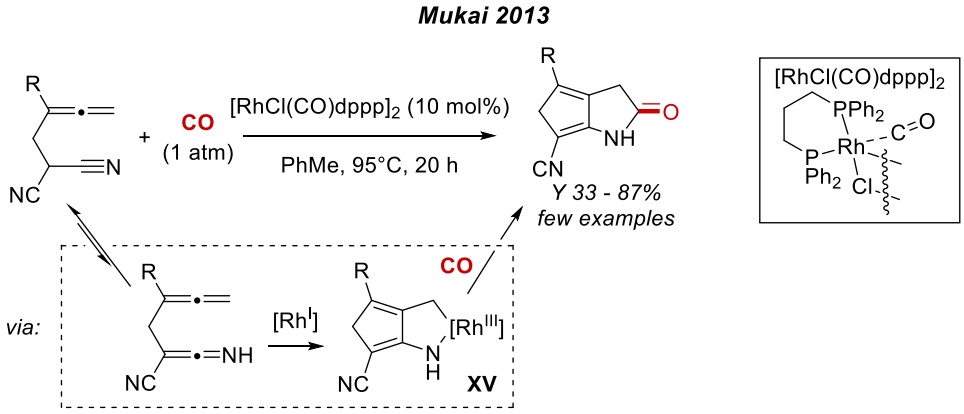

Switching from CO/TM dichotomy exploitation to metallacarbonyl compounds-based methodologies, a report from Iranpoor and Firouzabadi taking advantage of chromium hexacarbonyl is shown below (**Fig. 40a**). Authors achieved amide, ester and even thioester productions from aryl-iodides with the corresponding hetero-nucleophiles. In this protocol, nickel halides are used as precatalysts and, upon reduction, they can engage the coupling steps within all the reaction partners. $Cr(CO)_6$ has been employed as source of CO, such precursor (as other $M(CO)_n$) can lower the propensity of highly reactive nickel intermediates to undergo poisoning or chances to be channelled into catalytic cycle dead-ends. The mechanism proposed in the original article follows a classical Ni(0)/Ni(II) oxidative addition onto the aryl halide to afford intermediate **XVI**, then CO insertion and ligand exchange leads to **XVII** and **XVIII**; reductive elimination ends the sequence. The scope of the envisaged transformation is wide and satisfactory both for the substitution patterns encountered on the aryl halides and for the series of employed nucleophiles.[253]

A slightly different example of metal-carbonyl employment as CO source is from Hu and co-workers who described a reductive carbonylative amide synthesis between nitro compounds as pre-nucleophilic sources and iodoarenes (**Fig. 40b**). Such a synthetic pathway based upon a Ni-bpy catalyst platform also includes a super stoichiometric amount of manganese powder as a reductant in combination with TMSCl as additive. Authors proposed a nickel catalytic cycle perfectly matching the previously reported ones (Ni(0)/Ni(II)). The reductive action of manganese indeed, doesn't perturb nickel catalytic cycle but accounts for nitro compounds reduction to amines (or diazo-dimers, nitroso-compound and hydroxylamine) which can then act as nucleophilic partners onto the acylnickel species as illustrated above (**Fig. 40a**).[254]

[252] Y. Hoshimoto, Y., Ashida, K., Sasaoka, Y., Kumar, R., Kamikawa, K., Verdaguer, X., Riera, A., Ohashi, M., Ogoshi, S., *Angew. Chem. Int. Ed.* **2017**, 56, 8206
[253] Iranpoor, N., Firouzabadi, H., Etemadi-Davan, E., Nematollahi, A. and Firouzi, H.R., *New J. Chem.* **2015**,39, 6445-6452
[254] Cheung, C.W., Ploeger, M.L. and Hu, X., *Chem. Sci.*, **2018**, 9, 655–659

Fig. 40a. Esters, amine and thioester production via $Cr(CO)_6$ CO delivery.

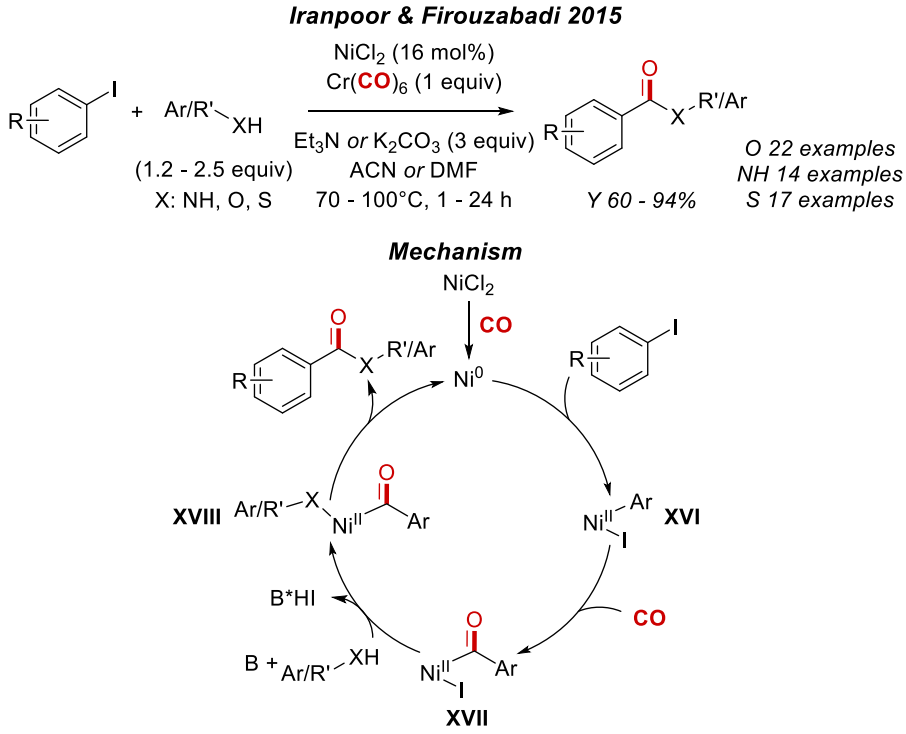

Figure 40b. Hu nitroarene reductive procedure for amide preparation via redox neutral carbonylative cyclization.

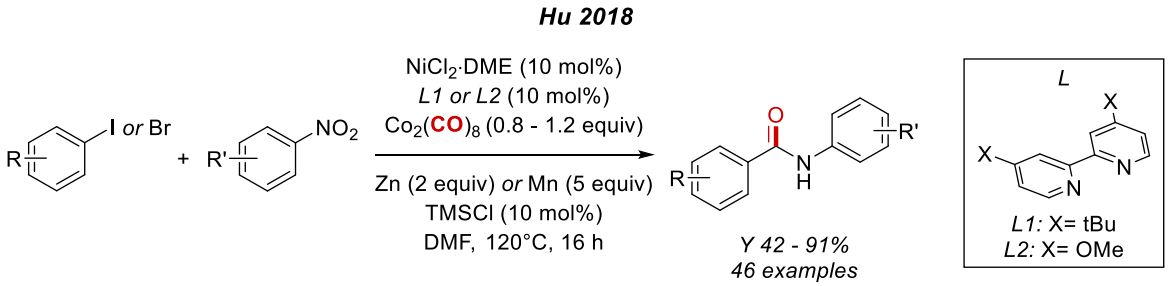

Carbonylative cyclizations have indeed recently faced a tremendous development since the use of CO_2 has been unlocked for these transformations, with the aim to replace CO in first instance and to possibly switch to a renewable coupling synthon as CO_2. The main conceptual turning points triggered by this choice is the need of a reaction system with a high energy content, needed to break one of the C-O bonds in carbon dioxide. Moreover, the electrophilic nature of CO_2 requires for a reactivity review, in contrast with nucleophilic CO. The redox neutral nature of these reactions often obviates the need of a transition metals action. If the substrate displays enough nucleophilic reactive sites (two), then CO_2 can be attacked to form unstable carbamates or carbonates which spontaneously evolves toward the products. Rearrangements have also been exploited from many researchers, frequently via isocyanide incorporation, to achieve the desired C-O bond disconnection.[255,256,257,258]

[255] Mampuys, P., Neumann, H., Sergeyev, S., Orru, R.V.A., Jiao, H., Spannenberg, A., Maes, B.U.W. and Beller, M., *ACS Catal*. **2017**, 7, 8, 5549–5556
[256] Li, X., Benet-Buchholz, J., Escudero-Adán, E.C., Kleij, A.J., *Angew. Chem. Int. Ed.* **2023**, 62, e202217803
[257] Wang, S., Shao, P., Du, G., Xi, C., *J. Org. Chem*. **2016**, 81, 15, 6672–6676
[258] Zhou, Z., Ma, J.G., Gao, J. and Cheng, P., *Green Chem.* **2021**, 23, 5456–5460

Alternatively, if the substrate displays one nucleophilic site and one C-H bond the activation of the latter may require a greater energy input and transition metals' ability to activate such a bond can be deployed (**Sch. 10**).

Scheme 10. Main features of CO_2 based carbonylative cyclizations.

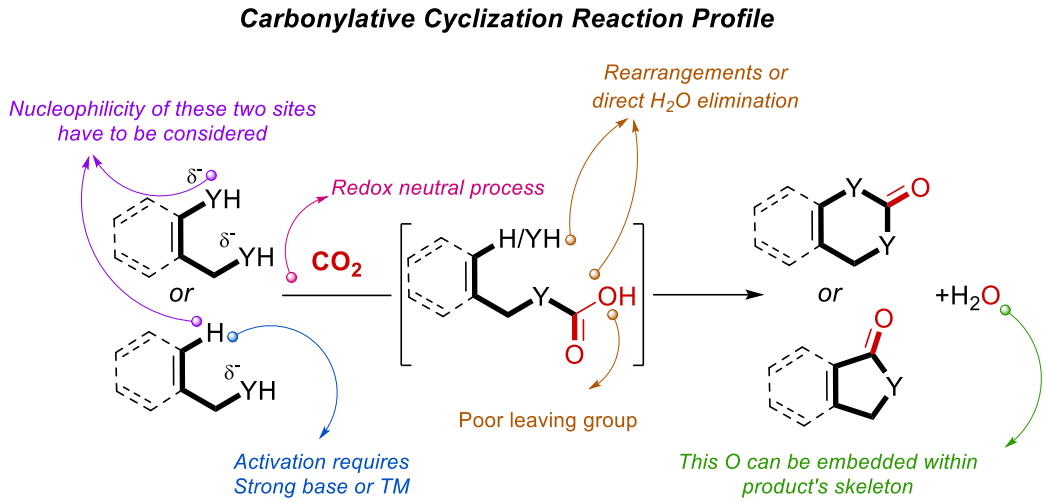

In 2013 a seminal Iwasawa' work described lactones preparation enabled by palladium catalysis which prompted the activation of C-H bond onto a pendant alkenyl fragment. Authors successfully isolated and characterized a vinyl palladium species, thought to be responsible for carbon dioxide trapping. Subsequent concomitant ligand exchange with a new substrate molecule and product ring closure leads back to the active Pd(II) intermediate. As mentioned above no redox events occurs during the reaction course (**Fig. 41**). The phenolic scaffold used has been decorated with different substituents and additional aryl rings have also been added onto the olefin moiety. Iwasawa's group also proved by NMR the existence, in the reaction mixture, of palladacycle **XIX** before CO_2 insertion. This intermediate was also characterized by XRD analysis.[259]

Another synthetic methodology from Yu and Lan's groups was appointed in 2018, where a palladium-based mechanism, analogue to the one proposed by Iwasawa, can afford benzolactones via carbonylation of benzylic alcohols. In this reaction authors identified a slightly harsher reaction conditions' set. The scope assessed for the transformation is indeed wider than the previous one and herein palladium catalyst activates an aryl C(sp^2)-H bond instead of a vinylic one. The main mechanistic steps are reported below and $^{13}C/^{18}O$ labelling experiments ensure for the robustness of such a proposal. Additional DFT calculations showed that two CO_2 molecules add consecutively to form a larger palladacycle **XX**, indeed, calculated energies for other possible palladacycle intermediates lies all higher in energy by several kcal/mol (**Fig. 42**).[260]

Figure 41. One of the first example of redox neutral carbonylative cyclization with CO_2 enabled by palladium catalysis.

[259] Sasano, K., Takaya, J., Iwasawa, N., *J. Am. Chem. Soc*. **2013**, 135, 10954−10957
[260] Vechorkin, O., Hirt, N. and Hu, X., *Org. Lett.* **2018**, 20, 3776−3779

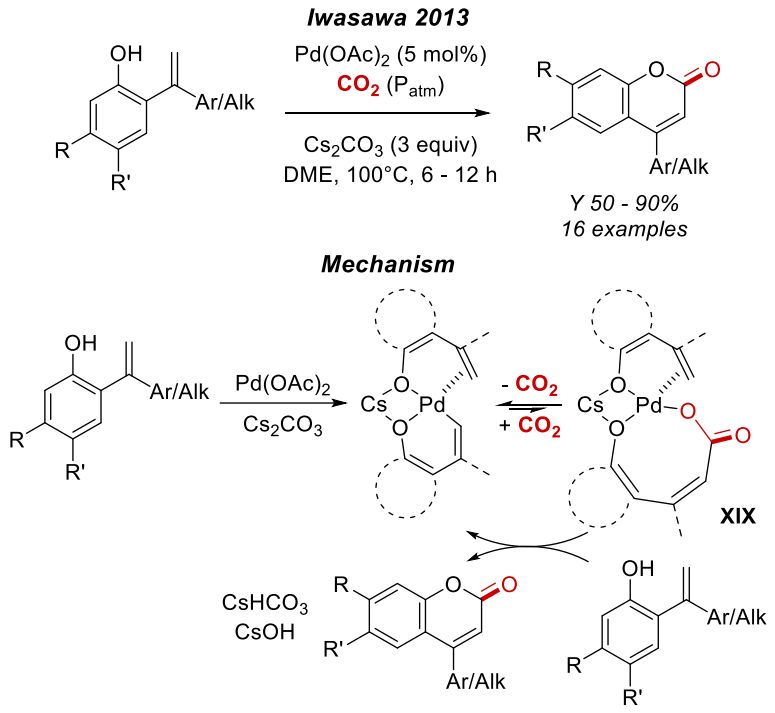

Figure 42. Lan and Yu Palladium catalysed benzolactones preparation through palladium enabled arylic CH activation.

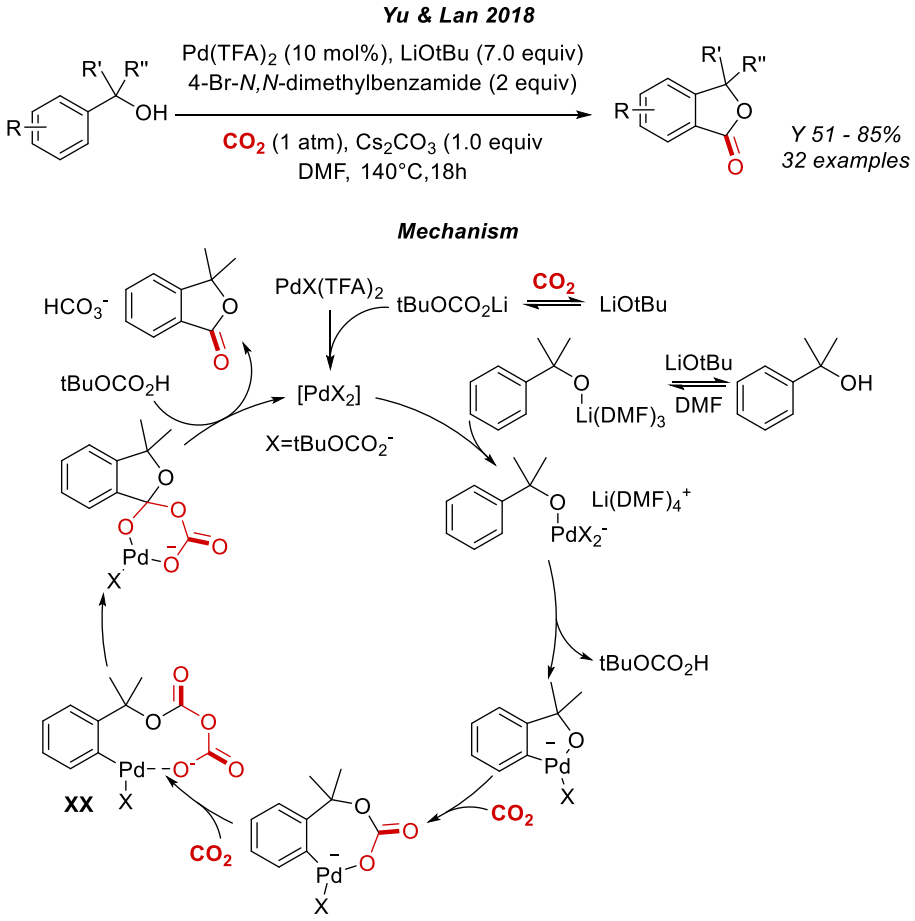

Benzolactams have also been recognized as feasible targets for CO_2 redox neutral carbonylative cyclization. To this aim a work from Cheng's group employed $Pd(PPh_3)_2Cl_2$ as catalyst to perform

the coupling between aryl iodides and *N*-Tosylhydrazones, previously activated by the base. Palladium catalyst accounts for the merging of the two sites reactive toward CO_2, once the open aniline with a pendant olefin **XXI** is delivered, the mechanism evolves to the final product only prompted by the basic additive, while palladium is no longer involved. Thus, the coupling product **XXI** engages CO_2 yielding a deprotonated carbamate which rearrange into isocyante **XXII**, onto this intermediate cyclization occurs and after a final re-aromatization carbonylated product **XXIII** is delivered (**Fig. 43**).

Synthetic methodologies illustrated above (**Fig. 41, 42** and **43**) remains redox neutral, with metal catalysed cross coupling steps are sometimes incorporated to achieve a one pot coupling/carbonylation sequence or to achieve C-H bond activation.[333,261]

Figure 43. Cheng cross coupling/carbonylative synthetic methodology.

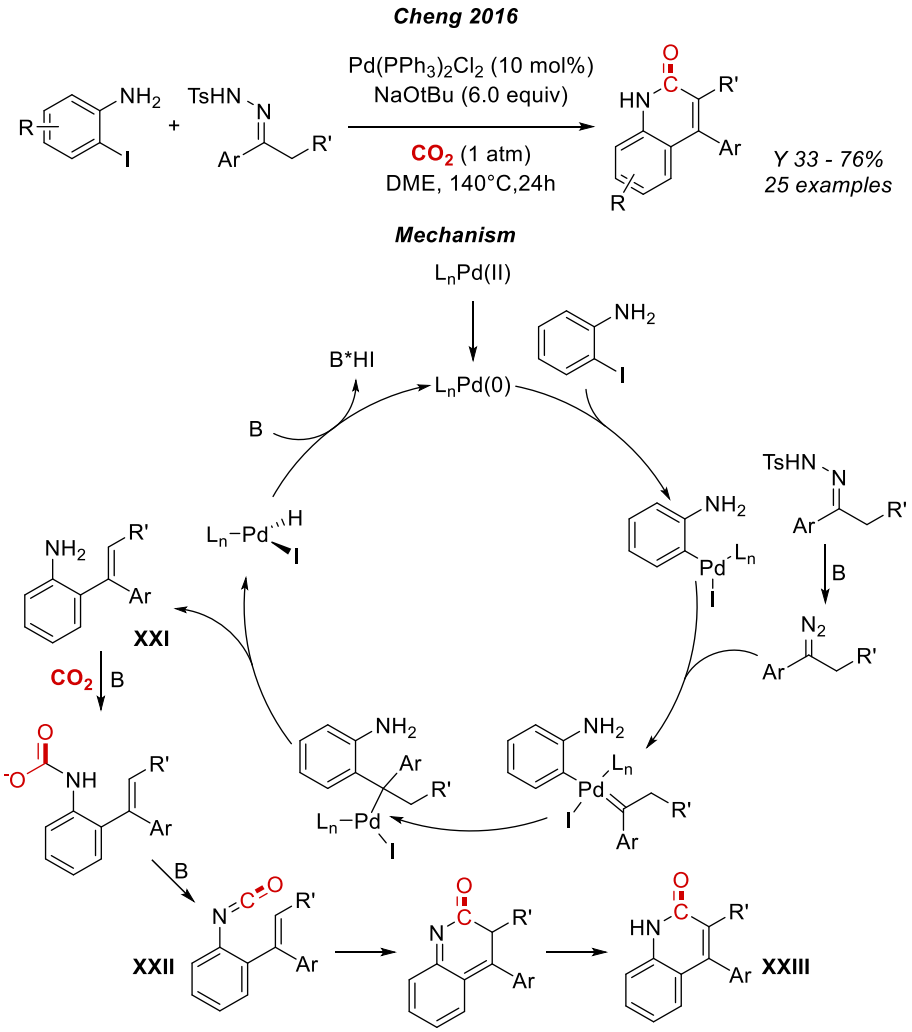

3.2.2 Work Rationale and Development

[261] Wang, B., Sun, S., Yu, J.T., Jiang, Y. and Cheng, J., *Org. Lett.* **2017**, 19, 4319−4322

The possibility to turn one of the nucleophilic sites of substrates, commonly encountered in carbonylative cyclization, into an electrophilic position has been envisioned as the second project of my doctoral studies. This would directly translate into the possibility to deliver carbonyl moieties over a series of seldom explored substrates, upon exploitation of nickel catalysis to activate and direct C-X bonds reactivity (X: halogens, pseudo-halogens, sulphonates) (**Sch. 11**).

Scheme 11. Transition metal carbonylative cyclization of electrophilic sites bearing substrates.

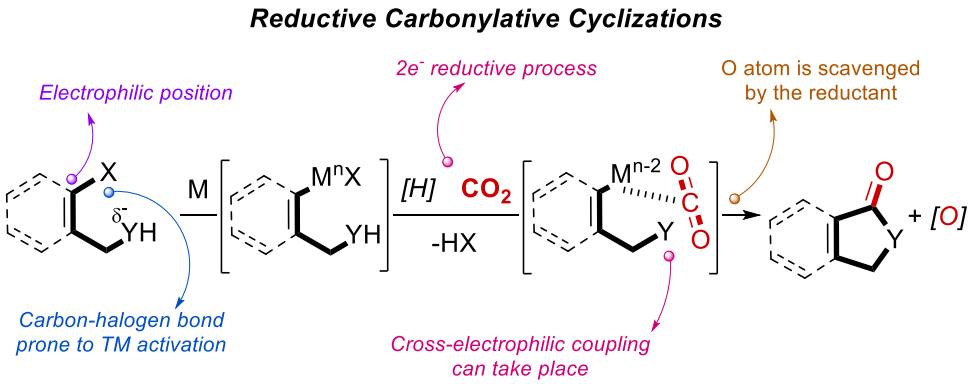

Hence *N*-2-halobenzylanilines were elected as model substrates to be converted into benzolactams, nickel catalysts have been chosen coupled to $AlCl_3$, due to observations made in the former project, to efficiently deliver a CO functional group (**Fig. 44**). Due to the proton onto the substrate which will lead to HX co-production a base additive was added within the reaction mixture to limit hydrodemetalation events occurrence. Under these initial general conditions, a reaction protocol optimization was undertaken.

Figure 44. CO_2-based reductive cross-electrophilic coupling for benzolactams and benzolactones preparation.

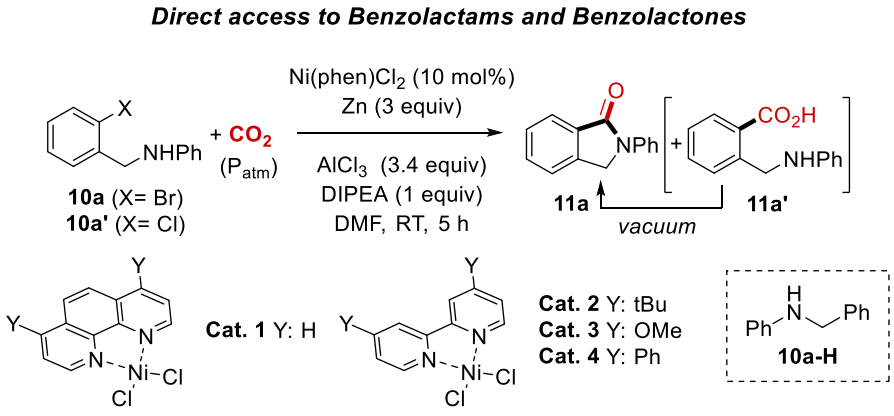

Table 5. [a]All reactions were carried out under rigorous anhydrous conditions (**10a**: 0.1 mmol, 0.1 M), [Ni]: 10 mol%, LA, DIPEA, dry DMF, CO_2 (1 atm), 5 h, rt. [b]Isolated yield after flash

chromatography, upon reaction crude standing under vacuum for 16 h. [c]*N*-Bn-aniline **10a-H** was obtained as predominant product via de-halogenation of **10a**. [d]Large amount of unreacted **10a** was determined in the reaction crude. N.R.: no reaction with a large quantity of **10a-H** recorded in the reaction crude.

Entry[a]	Deviation from Optimal	Y (%)[b]
1	-	**63**
2	w/o base and LA	**N.R.**
3	1.2 equiv. LA	**47**
4	w/o base	**24**[c]
5	**Cat. 2** instead of **Cat. 1**	**48**[d]
6	**Cat. 3** instead of **Cat. 1**	**28**[d]
7	**Cat. 4** instead of **Cat. 1**	**48**
8	$Al(OTf)_3$ instead of $AlCl_3$	**traces**
9	$InCl_3$ instead of $AlCl_3$	**N.R.**
10	Mn instead of Zn	**58**
11	**10a'** instead of **10a**	**N.R.**

First, we ensured the need of a basic additive and of a Lewis acid (**Tab. 5, entry 2**), with no $AlCl_3$ at all no product was observed, indeed the addition of low amounts, gave a poorer yield (**Tab. 5, entry 3**). When no base was used a lower yield was also recorded 24% *vs* 63% (**Tab.5, entry 4** *vs* **entry 1**), in this case considerable production of **10a-H** was recorded thus, confirming that released acidity in the reaction mixture exert a remarkable negative effect if not properly neutralized. Then prior to a large pre-screening (*see Material and Methods*) we decided to test the reported catalysts (**Cat. 2** to **Cat. 4**), in all cases lower yields have been observed, between 28% to 48% (**Tab. 5, entries 5-7**). Then we investigated how Lewis acids nature could affect reaction outcome. For example, aluminium triflate performed poorly, giving just traces of product (**Tab. 5, entry 8**), an in presence of $InCl_3$ no reaction occurred (**Tab. 5, entry 9**). As alternative to zinc, manganese powder was tested as reductant since it is largely used in XEC reactions. In our cases, it worked smoothly, in slightly lower yield (58%). As last parameter we tested -Cl analogue **10a'** of our starting material, which could open to aryl chlorides employment. As no product was observed and **10a'** could be recovered from the reaction mixture, we concluded that only aryl bromides possess the needed reactivity degree (**Tab. 5, entry 11**).

During the optimization phase we observed in reactions crudes spectra (^{1}H-NMR, $CDCl_3$) different amounts of benzoic acid **11a'** derived from direct ring carboxylation along with directly carbonylated product. Different rates for spontaneous ring closure were observed upon reaction standing under vacuum during samples solvent removal, also influenced by electronic character of the aromatic ring. After this observation and a careful literature survey, we found out that interconversion of **11a'** into **11a** was exploited in the early seventies in some mechanistic investigation about *N*-benzyl-anilines metallation with organolithium reagents.[262] In 2023 by mean of completely different synthetic protocols benzoic acid **11a'** was prepared via Pd supported heterogeneous catalysis with MOFs, presence of product **11a** was not reported.[263] In 2012 benzolactones like **11a** were indeed targeted,

[262] Ludt, R.E., Hauser, C.R., *Journal of Organic Chemistry*, **1971**, 36(12), 1607–1613
[263] Liang, J., Wu, L., Li, Z., Liu, Y., Ding, N. and Dong, Z., *RSC Adv.* **2023**,13, 5186-5196

again via a different synthetic route, in this case transformation scope was only partially investigated leaving a considerable portion of accessible molecular architecture unexplored.[264]

With optimal conditions on our hands and with clear reactivity pattern for these rarely synthetized substrates we engaged a scope investigation. Substrates bearing electron-releasing substituents on the halogenated ring were transformed in good to high yields, up to 81% (**11a – 11g**). A naphthyl analogue **11h** showed a satisfactory 78% yield, then electron-withdrawing functional groups were accommodated on the phenyl ring always recording good to high yields from 50 to 86%, for **11i – 11l** substrates. The investigation continued by placing different substituents on the aniline ring (**11m – 11q, 11s – 11u**), a mixed effect arising both from the position and the electronic nature of substituents group was recorded on the reaction yields ranging from 32% up to 87%. Benzylic hydrogens were also replaced with one methyl group along with different electronically diversified aniline rings (**11r, 11w – 11y**), good to high yields were found in these cases (52% to 73%), pointing to a diminished influence of aniline electronics when steric effects are influencing reagents conformation. Finally, a short series of benzolactones **12a – 12e** could also be prepared under the developed catalytic conditions and generally high yields were achieved (58% to 64%) (**Fig. 45**). A total of 29 substrates were successfully subjected to our catalytic conditions, recording moderate to high yields across all the investigated substitution patterns.

Figure 45. Scope for nickel catalyzed carbonylative cross coupling.

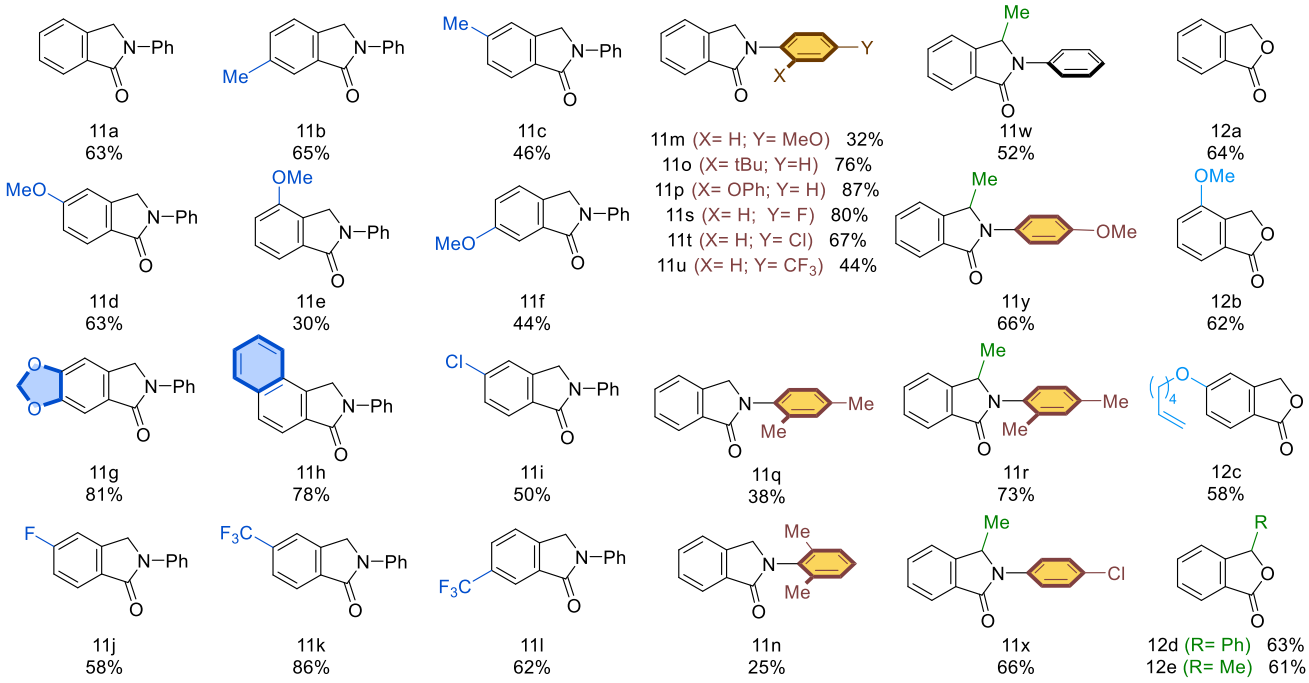

The mechanism investigation began from a simple unclear point dealing with the possibility for the aniline nitrogen to quench the reactivity of organonickel species in the catalytic cycle, and thus lower the yield of the reaction. To answer this question some considerations must be made. In DMF an equilibrium between free CO_2 and a CO_2-$AlCl_3$ adduct is known to occur, providing so an "activated" carbon dioxide reservoir. We first confronted relative energies required to form *a carbamate-like adduct* **xvii** between deprotonated starting material and free CO_2 or CO_2-$AlCl_3$ adduct. The formation

[264] Shi, L., Hu, L., Wang, J., Cao, X., Gu, H., *Org. Lett*. **2012**, 14, 7, 1876–1879

of the latter was found to be much more energetically favoured, resulting in an exergonic process (ΔG= -22.4 kcal/mol) while the carboxylation of anionic **10a**$^-$ with free CO_2 would have demanded an energy input of about 31.5 kcal/mol.

Considering that oxidative addition and ring carboxylation are supposed to be the first events occurring in the catalytic cycle. This finding has prompted us to further investigate the role of $AlCl_3$ during ring carboxylation occurrence. We assumed species **xiv** to be a consistent partner to be confronted with species **xiv'**; which are both anionic species derived from oxidative addition and SET reductions, **xiv'** displays an activated CO_2 molecule on the nitrogen acting as a *dynamic protecting group*.

Calculations showed that CO_2 coordination to complex **xiv** required 7.7 kcal/mol, nevertheless more accurate calculations find out that electronic energy outcome for this step possess a ΔG= -5.7 kcal/mol thus, an entropic factor must account for the positive calculated value. The formation of the C-C bond then requires an additional 8.7 kcal/mol setting TS energy value at 16.4 kcal/mol. Evolution toward species **xvi** then comes with a stabilization of 25.8 kcal/mol.

In parallel when $AlCl_3$ is added, CO_2-protected adduct **xiv'** is engaged into coordination with CO_2-$AlCl_3$ adduct in a barrierless step with some energy release (-3.3 kcal/mol) leading to **xv'**; the C-C bond forming event then proceed ways faster displaying only an overall 6.3 kcal/mol energy barrier and a greater stabilization of the product **xvi'** which lies at -53.7 kcal/mol (**Fig. 46**). These data suggest that the process proceeds more easily via the "protected" intermediate **xv'** and indicate that CO_2-$AlCl_3$ mixture has a twofold role in the present reaction.

Figure 46. Carbamate-like intermediate formation by mean of CO_3-$AlCl_3$ adduct (top). Computated energies for intermediates during carboxylation with or without $AlCl_3$ (bottom).

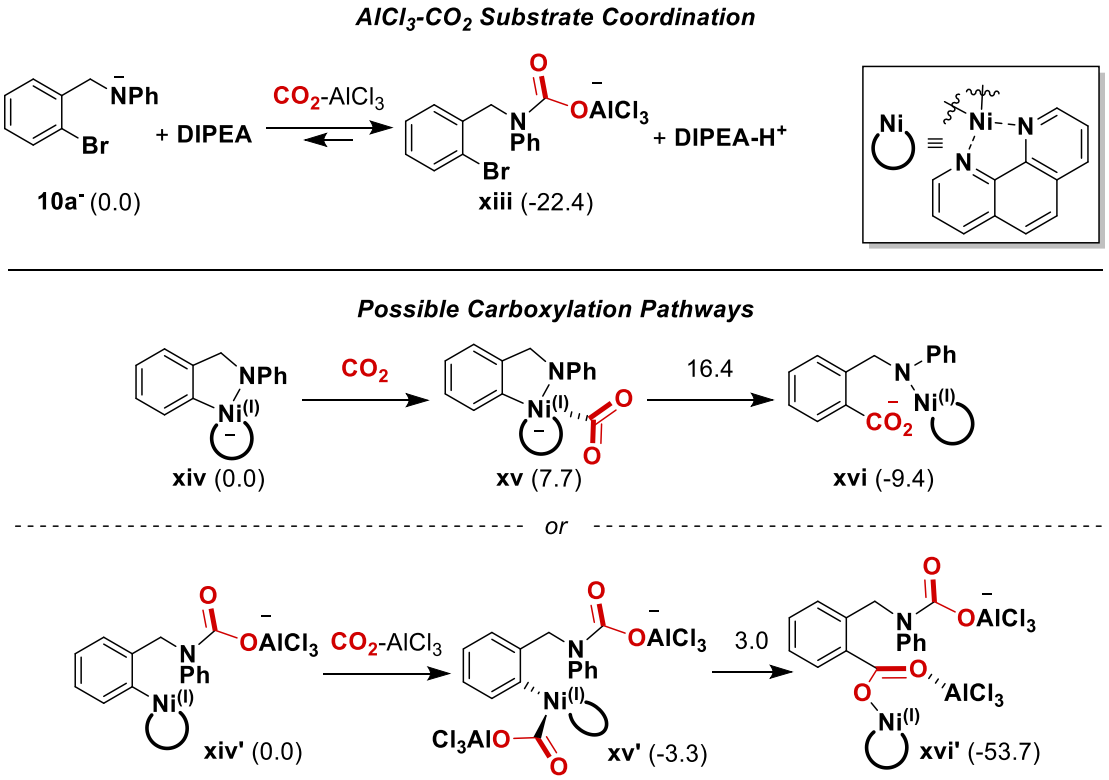

These computational values were then supported by NMR investigation carried out upon mixing starting material **10a** under Ar and under CO_2 respectively, in presence or absence of $AlCl_3$ resulting in two mixtures of **10a**/$AlCl_3$/Ar and **10a**/$AlCl_3$/CO_2, all these four samples were acquired in DMF-d_7, and the results are shown below (**Fig. 47**).

Figure 47. Stacked NMR spectra of starting material **10a** (SM) under Ar (purple), SM under CO_2 (blue), SM and $AlCl_3$ under Ar (green), SM and $AlCl_3$ under CO_2 (red).

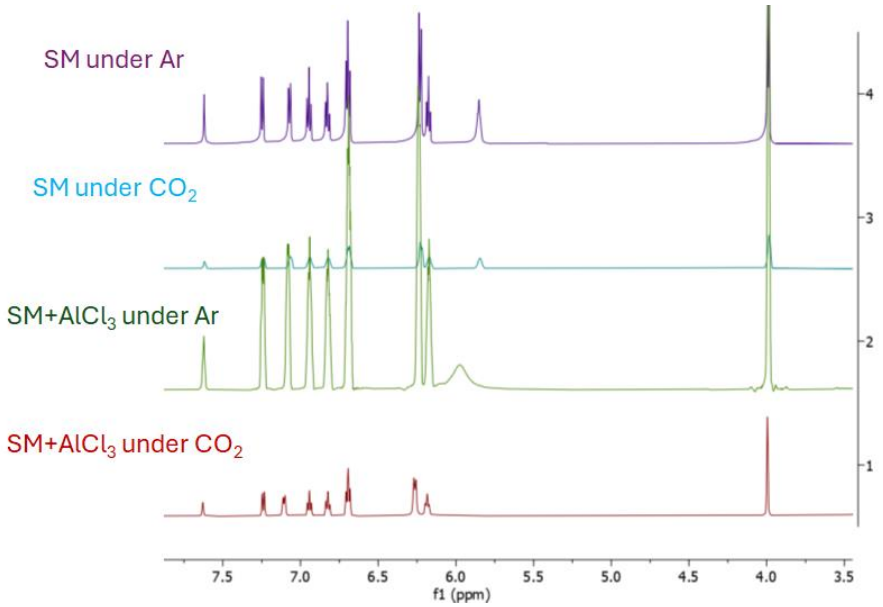

Attention must be paid at the 5.85 lying signal of NH proton, a slightly de-shielding and signal broadening occurred within first two spectra (purple and blue lines). This can only account for a little interaction between **10a** and CO_2. Meanwhile when $AlCl_3$ was added to the samples (green and red traces) the full involvement of NH proton can be hypothesized into the formation of a species like **xvi'**.

Consistently with these findings a catalytic cycle for the reaction is proposed, where a zinc generated Ni(I) species formed upon nickel precatalyst reduction may undergo oxidative addition with a carbamate-like species **xiii**. Two consecutive SET events lead again to a low valent aryl-nickel(I) **xiv'** capable of coordinating and triggering the aromatic ring carboxylation with a CO_2-$AlCl_3$ adduct. This final arylcarboxylate **xvi'** is then prone to undergo the final cyclization step with concomitant catalyst restoration. The *carbamate-like* moiety **xvi'** at this stage accounts also for the variable amounts of acyclic benzoic acid **11a'** observed in reaction crudes; most of which is converted into the desired **11a**, upon *vacuum* treatment (**Fig. 48**).

Finally, a labelling experiment with $^{13}CO_2$ was carried out to ensure the origin of the CO moiety embedded within the product molecular scaffold. The spectra reported, clearly show ^{13}C enrichment in the product upon exposure of starting material under standard reaction conditions and $^{3}CO_2$ (**Fig. 49**).

Figure 48. Proposed catalytic cycle for benzolactams and benzolactones reaction mechanism.

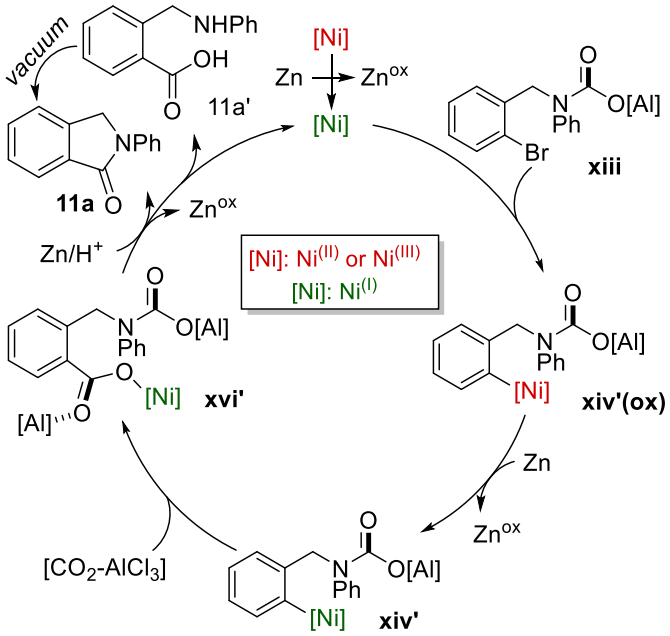

Figure 49. ^{13}C-NMR spectra of ^{13}C enriched product **11a**.

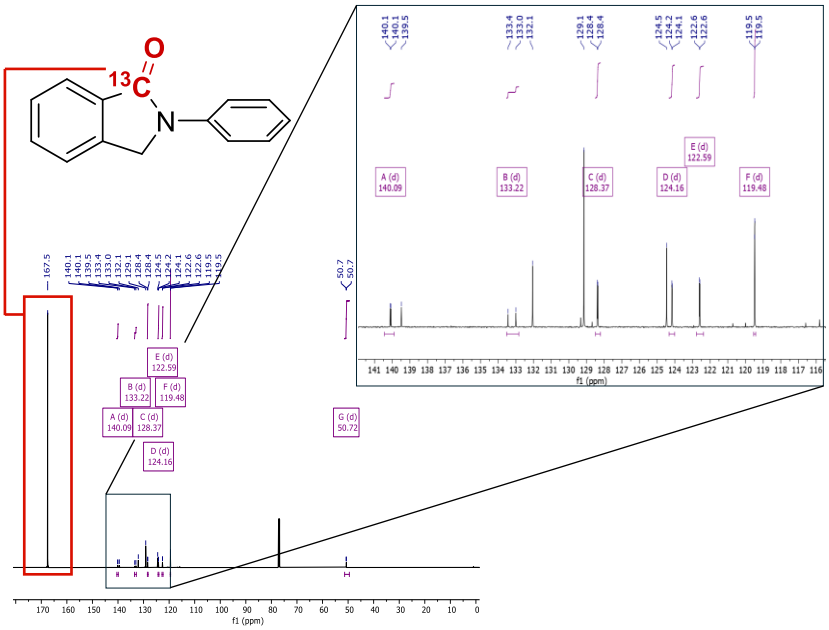

3.2.3 Conclusion

The illustrated methodology for the preparation of benzolactams and benzolactones is one the first accounting for CO_2 utilization as CO surrogate in a two-electron reductive process, unlocking this way a whole new series of possible reaction partners (**Sch. 9** and **11**). This might mark another step for leaving behind toxic CO manipulation (at least on a laboratory scale), surrogates with low atom efficiencies and metallacarbonyl compounds for Pauson-Khand like reactions.

3.3 Direct Access to α-Aryl-α-Trifluoromethyl Benzyl Alcohols

3.3.1 Research Context and Literature Review

As mentioned in the introduction part, in this chapter more details will be presented about the pharmaceutical interest over the CF_3 fragment introduction into drugs. Other methodologies related to the paperwork of the current chapter will be present. Particular attention will be paid at synthetic methodologies for the preparation of α-trifluoromethyl carbinols, expanding this way the range of trifluoromethyl-containing molecular architectures, considering that C(sp^3)-CF_3 and C(sp^2)-CF_3bond forming methodologies have been shown earlier.

Within the small molecule (< 500 Da) drug discovery business, powered by pharmaceutical, which economic volume has been about 55 billion only in 2023, those approved by FDA and containing one fluorine atoms at least accounts for about 20%. Beside the first ever approved drug containing a fluorine atom (Fludrocortisone known as Florinef, 1954) many famous brand names are based upon fluorinated organic architectures. Estimations says that 30% of fluorinated drugs are blockbusters: Fluoxetine known as Prozac® (1986), Levofloxacine known as Levaquin® (1993), Atorvastatine known as Lipitor® (1997), these popular names highlight how deep are the changes brought in from the introduction of fluorine chemistry into the pharmaceutical manufacturing realm. [265,266,267]

Fluorinated homologues of a determined compound which physico-chemical and biological features are known, can have completely different behaviours when placed into biologically relevant conditions. Fluorine-hydrogen exchange mainly influences lipophilicity/lipophobicity, hence solubility, acid-base equilibria and steric/electronics hence modification over binding and target affinity; DMPK properties, conformational and metabolic stability (oxidatively/hydrolytically) may be greatly modified by H/F swapping; these mentioned are just some of the most important parameters traditionally monitored during drug discovery phases (**Fig. 50**).[268]

Let us consider as representative example the group of 55 new drugs approved only in 2023 by FDA for therapeutic treatments, 25 of them (45%) are biologics and 30 are small molecules (55%), among the latter 12 out of 30 contains at least one fluorine atom marking so a 34% of share of small molecule marketed drugs for the year and an overall 22% of share. Between these 12 approved fluoropharmaceutical 6 of them contain a CF_3 group (one candidate has two), one structure presents a CF_2 substitution onto an alkyl chain and five molecules bears one or more F atoms across their structure, with one of them being a ^{18}F tracer for radiopharmaceutical studies (**Fig. 51**).[266,269]

[265] Rizzo, C., Amata, S., Pibiri, I., Pace, A., Buscemi, S. and Palumbo Piccionello, A., *Int. J. Mol. Sci.* **2023**, 24, 7728
[266] Inoue, M., Sumii, Y. and Shibata, N., *ACS Omega* **2020**, 5, 19, 10633–10640
[267] Wang, J., Sánchez-Roselló, M., Aceña, J.L., del Pozo, C., Sorochinsky, A.E., Fustero, S., Soloshonok, V.A. and Liu, H., *Chem. Rev.* **2014**, 114, 4, 2432–2506
[268] Purser, S., Moore, P.R., Swallow, S. and Gouverneur, V., *Chem. Soc. Rev.* **2008**,37, 320-330
[269] Advancing Health Through Innovation: New Drug Therapy Approvals for 2023. https://www.fda.gov/drugs/novel-drug-approvals-fda/novel-drug-approvals-2023

Figure 50. First fluoropharmaceutical approved drug (Florinef) and some worldwide famous examples of fluorine containing drugs.

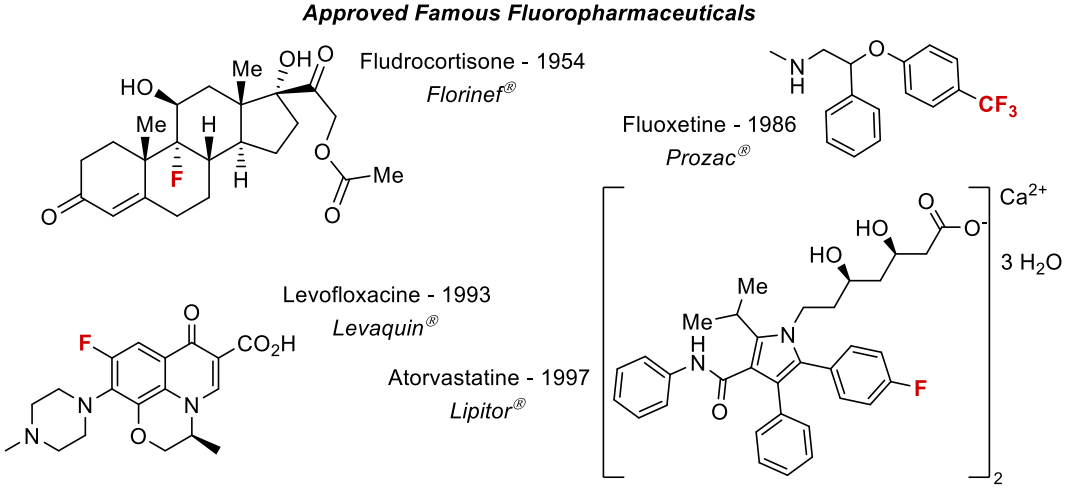

Among the six new trifluoromethylated chemical entities approved in 2023 there are two examples of α-oxy-trifluoromethyl moieties, these peculiar frameworks are rarely seen in fluorinated pharmaceutical compounds; from a literature survey it can be highlighted how over the entire class of fluoropharmaceutical ever approved (ca. 340 small molecules) only five of them displays an α-trifluoromethyl-α-hydroxy group, 9 candidates have a 2,2,2-trifluoroethoxy pendant group and just two have trifluoroacetamide residue embedded into their molecular structure (**Fig. 51**).[270]

Incorporation of α-trifluoromethyl-α-hydroxy group ($F_3CC(H)OH$) seems to be one of the most dramatically underdeveloped yet challenging kind of transformation. Such a situation is probably due to the lack of generally available synthetic tools, attractive for pharmaceutical purposes. Considering that a large share of pharmaceuticals has at least one arene ring, targeting α-trifluoromethyl-α-aryl alcohols preparation would represent a highly desirable goal. With some trifluoromethylation procedure shown in the introduction part and a general overview of trifluoromethylating reagents developed a thoroughly analysis can be made over available methods for α-trifluoromethyl-α-aryl alcohols preparations.

[270] The four approved drugs with α-trifluoromethyl-α-hydroxy group are: Efavirenz, Falecalcitriol, Telotristat Ethyl and Lotilaner. The two compounds with a trifluoroacetyl residue are: Nirmatrelvir and Valrubicine. The eight approved molecules bearing a trifluoroethoxy moiety are: Isoflurane, Desflurane, Sevoflurane, Silodosin, Oteseconazole, Lanzoprazole, Dexlanzoprazole and Flecainide.

Figure 51. Functional group classification for 2023 FDA-approved drugs (top). Bonds classification among CF_3 group containing drugs (bottom).

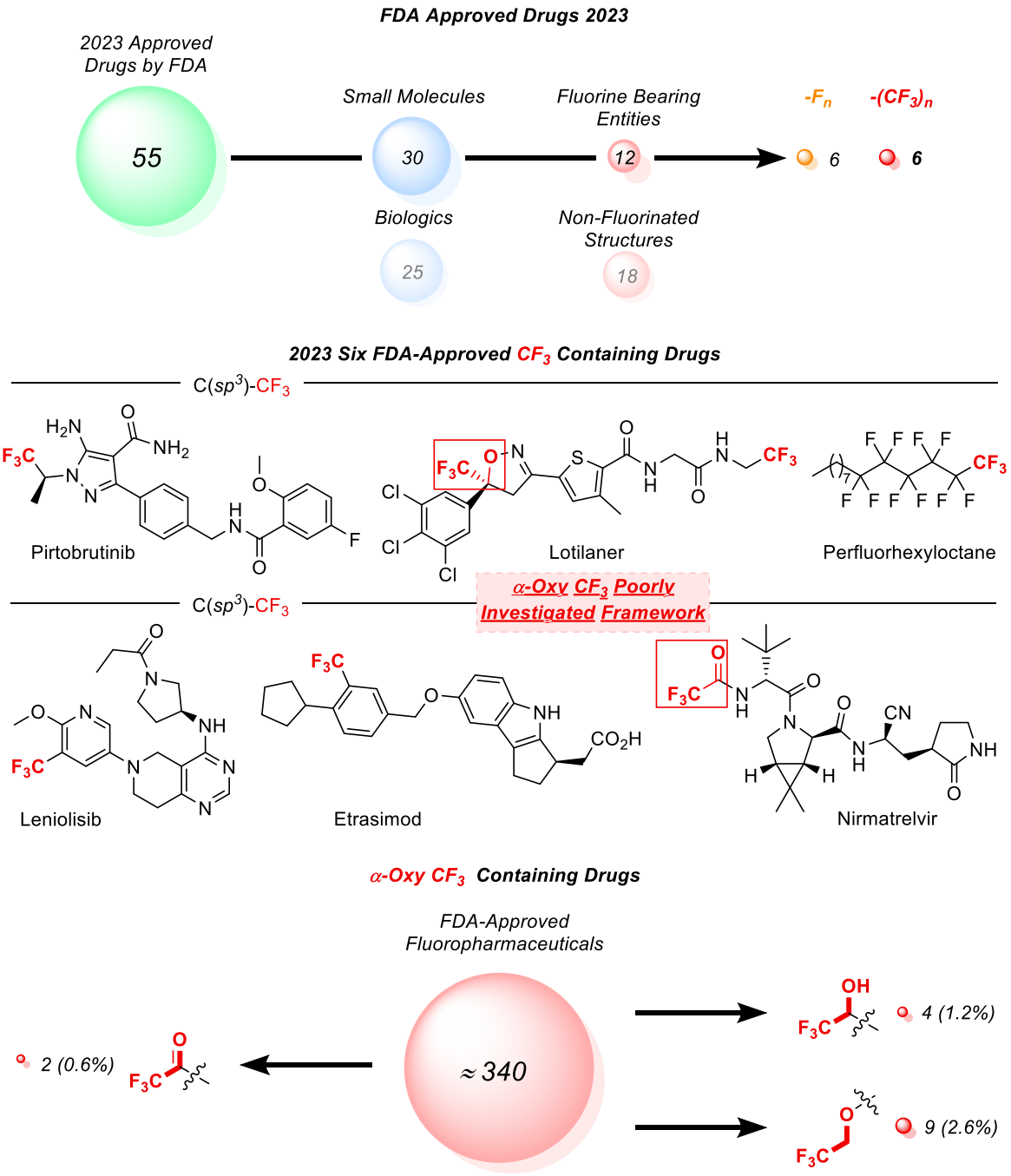

A straightforward strategy unfolds upon using nucleophilic CF_3^- precursors over aldehydes substrates or other oxo products containing carbon centres with the same oxidation state (*Nucleophilic route*). A second approach might involve the hydrogenation of parental trifluoromethyl ketones through accurately selected catalytic systems either based on transition metals or not (*Reduction route*). A third general way to face α-aryl-α-trifluoromethyl alcohols preparation stems from reversed polarity synthons employment. Hence masked electrophilic form of trifluoroacetaldehyde (*i.e. trifluoroalkylacetates, trifluoromethylpyruvates, trifluoroacetaldehyde hemiacetals or hemiaminals, trifluoroacetaldehyde imines and hydrazones*) is functionalized by a variety of nucleophilic reagents (*i.e. organometals)* via S_N2 type mechanism, aldol reactions or fluoral-ene type reactions

(*Electrophilic route*) and the product is readily delivered. Within this depicted generalization it is true that other strategies can effectively lead to the target scaffold, like controlled oxidation or hydrogenation of proper trifluoromethyl olefins; however, despite the considerable number of known procedures to access α-aryl-α-trifluoromethyl alcohols the reader is invited to note the redundant use of electrophilic trifluoroacetaldehydes surrogates or classic (pro)nucleophilic reagents such the Ruppert-Prakash one. It was under this macro environment of available synthetic methodologies that a transition metal catalysed strategy was developed during the PhD program. This advancement surely provided an exclusive reactivity pattern along with the effective introduction of a new stable and easy-to-handle trifluoroacetaldehyde precursor (**Fig. 52**).

Figure 52. Retrosynthetic routes for target preparation.

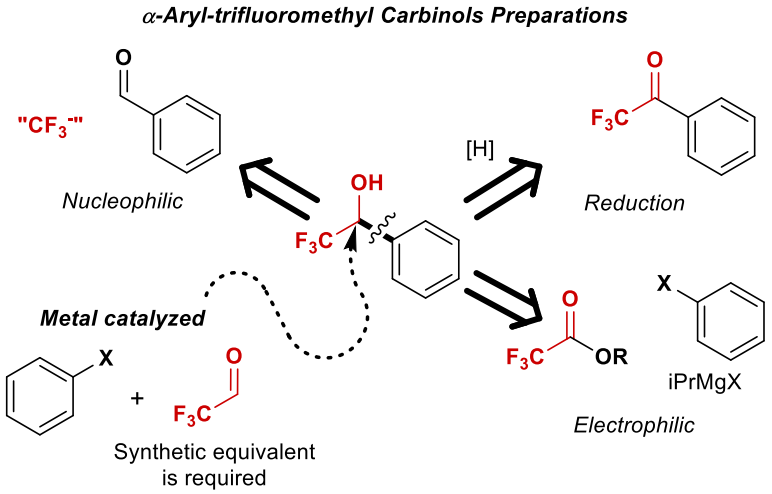

In 2001, Dolbier and Medébielle exploited CF_3I as trifluoromethyl source. Upon its exposure to TDAE (Tetrakis-dimethylaminoethylene) in DMF at -20°C under a sunlamp light stimulus, the formation of trifluoromethyl anion is promoted. Authors claimed this to be the operative mechanism responsible for the active trifluoromethylating species production, which appear as a bright red charge transfer complex in solution. Under the illustrated optimized reaction conditions, aromatic, heteroaromatic and aliphatic aldehydes could be transformed into the corresponding tertiary α-aryl-α-trifluoromethyl alcohols, with the electron-poor ones displaying better performances than the electron-rich ones. Additionally, selected examples of ketones, such as benzophenone and chalcone were converted into the respective quaternary alcohols in 65 – 68% yields respectively (**Fig. 53**).[271]

Figure 53. Nucleophilic trifluoroiodomethane-based protocol triggered by light.

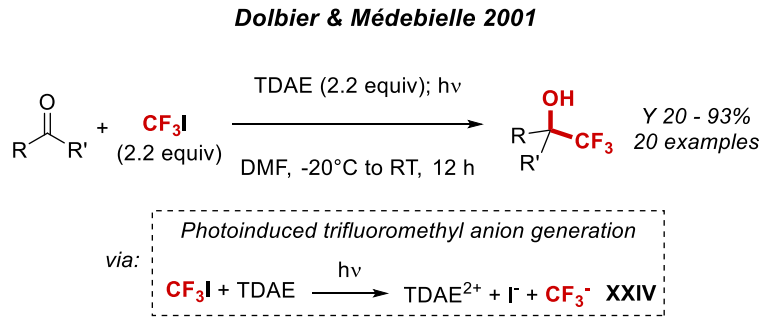

[271] Aït-Mohand, S., Takechi, N., Médebielle, M., Dolbier, W.R., *Org. Lett*. **2001**, 3, 26, 4271–4273

Another example of nucleophilic synthetic methodology to prepare the targeted compounds was disclosed by Shibata and co-workers, in 2009. The authors updated a previously known set of conditions for aldehydes nucleophilic trifluoromethylation based upon the use of Ruppert-Prakash reagent. Through the employment of potassium phenoxide and a chiral C2 crown ether-based catalyst, they unlocked the possibility to selectively attack only one pro-chiral face onto the selected starting material. In this case, only ten substrates have been investigated (aromatic, aliphatic and α,β-unsaturated). The displayed yields were comprised in a good-high range (66% to 91%), while only modest enantiomeric excesses were recorded (as high as 44%) (**Fig. 54**).[272]

Figure 54. Shibata conditions for $TMSCF_3$-based enantioselective trifluoromethylation of aldehydes and ketones.

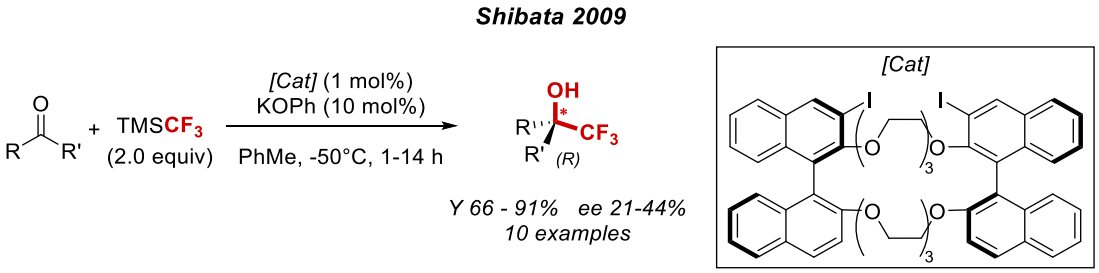

In these couple of examples, the nucleophilic approach for the synthesis of α-aryl-α-trifluoromethyl alcohols seems to be a feasible synthetic route mainly suited to transform aldehydes. Indeed, foreseeable steric issues when it comes to the transformation of more encumbered ketones have been encountered, thus suffering from non-negligible scope limitations. Moreover, in both methodologies the need of low temperatures acts as an indication of parasitic reactions occurrence which might be hard to suppress. Other comparable synthetic methodologies, show the same features of these protocols: modest to good yields, limited substrate scopes, generally good to high enantio/diastereoselectivities.[273,274,275,276]

The second introduced synthetic strategy to prepare α-aryl-α-trifluoromethyl alcohols is by reduction of the parental ketones. Several synthetic protocols have appeared during the last forty years, which showed how metal hydrides, organometals and hydrogen gas can be used to achieve this goal.[277,278,279,280] In 1998, Noyori used a chiral combined ruthenium catalyst bearing xylBINAP and DAIPEN as ligands to induce the correct enantiocontrol over the reduction of several ketones.[281] Aware of the performances exerted in hydrogenations by systems based on alcoholic solvents/bases

[272] Kawai, H., Kusuda, A., Mizuta, S., Nakamura, S., Funahashi, Y., Masuda, H., Shibata, N., *Journal of Fluorine Chemistry,* 130 (**2009**) 762–765
[273] Soloshonok, V.A., Avilov, D.V., Kukhar, V.P., *Tetrahedron Asymmetry*, **1996**, 7, 6, 1547-1550
[274] Chang, Y., Cai, C., *Journal of Fluorine Chemistry*, **2005**, 126, 6, 937 - 940
[275] Zhang, Y., Fujiu, M., Serizawa, H., Mikami, K., *Journal of Fluorine Chemistry,* **2013**, 156, 367-371
[276] Song, J.J., Tan, Z., Reeves, J.T., Gallou, F., Yee, N.K., Senanayake, C.H., *Org. Lett*. **2005**, 7, 11, 2193–2196
[277] Kuroki, Y., Sakamaki, Y., Iseki, K., *Org. Lett*. **2001**, 3, 3, 457–459
[278] von Arx, M., Mallat, T., Baiker, A., *Journal of Catalysis*, **2001**, 202, 1, 169-176
[279] Brüning, F., Nagae, H., Käch, D., Mashima, K., Togni, A., *Chem. Eur. J.* **2019**, 25, 10818
[280] Bao, D.H., Wu, H.L., Liu, C.L., Xie, J.H., Zhou, Q.L., *Angew. Chem. Int. Ed*. **2015**, 54, 8791-8794
[281] Doucet, H., Ohkuma, T., Murata, K., Yokozawa, T., Kozawa, M., Katayama, E., England, A.F., Ikariya, T. and Noyori, R., *Angew. Chem. Int. Ed.* **1998**, 37, 1703−1707

and transition metal catalysts they achieved the reduction of many different substrates. Nevertheless, despite the sophistication level of ligands and the attention posed on the research of optimal conditions only few α-aryl-α-trifluoromethyl ketones could be converted into designed products, although the four furnished examples displayed excellent results (**Fig. 55**).[282]

Figure 55. Ru-xylBINAP/DAIPEN hydrogenation of some trifluoromethyl ketones.

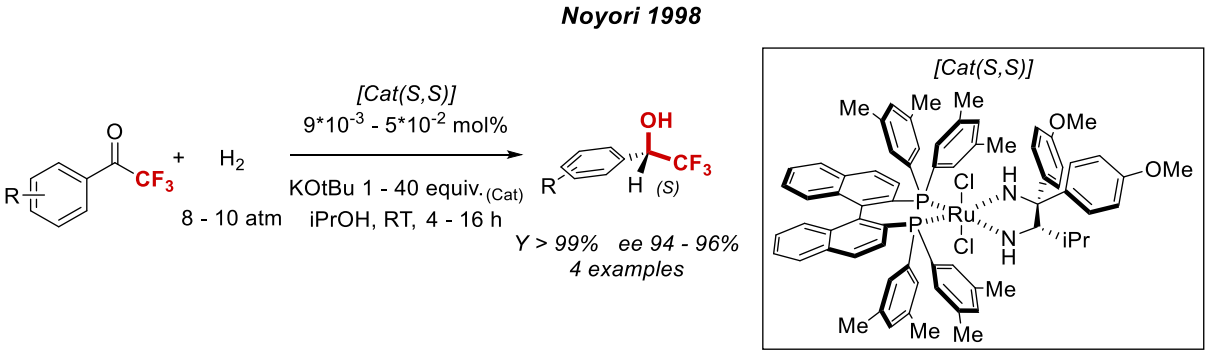

Another reductive strategy to access targeted products was developed by Chong who exploited chiral *(S)*-BINAL-H (previously developed by Noyori)[283] for the reduction of aryl-trifluoromethyl ketones via metal hydride strategy. After a literature confrontation, this paper highlights how the presence of a trifluoromethyl group can modify also well-established reactivities such as those of aluminium hydride-based reductions. Indeed, the stereochemical outcome of the reduction reported below (**Fig. 56**) showed *(S)*-BINAL-H giving the *(S)*-alcohol and *(R)*-BINAL-H giving the *(R)*-alcohol, when unsaturated ketones were used as starting materials. The substitution of a general alkyl group -R with a -CF_3, interestingly, led to observe an inversion of the reaction stereochemical result. These empirical data can be explained considering the two proposed chair-like TS, build upon models proposed by Noyori, where the most favoured structure should be the one presenting the -CF_3 group directed toward the O atom. Among the two proposed structures steric effects are surely into play, but most likely a stronger stabilization is supposed to stem from a π_O-n_{CF3} interaction rather than a π_O- π_{ring} one.[284]

Another feasible way to reduce trifluoromethyl ketones was appointed by Song in 2015 where his group successfully accomplished asymmetric β-hydride transfer from diethyl zinc to these substrate family. They used 1,2-diamino phosphinamide to control the stereoselective profile of the addition, to do so the Lewis acidity of zinc proved essential for carbonyl activation toward the hydride attack. Nevertheless, despite efforts put in the reaction optimization, a narrow scope was presented for the synthetic protocol with high yields and good to high *ee* (**Fig. 57**) over a limited number of productive substrates.[285]

[282] Ohkuma, T., Koizumi, M., Doucet, H., Pham, T., Kozawa, M., Murata, K., Katayama, E., Yokozawa, T., Ikariya, T. and Noyori, R., *J. Am. Chem. Soc*. **1998**, 120, 51, 13529–13530
[283] Noyori, R., Tomino, I., Tanimoto, Y., Nishizawa, M., *J. Am. Chem. Soc.***1984**, 106, 22, 6709-6716
[284] Chong, J.M., Mar, E.K., *J. Org. Chem*. **1991**, 56, 893-896
[285] Huang, H., Zong, H., Bian, G., Song, L., *Tetrahedron: Asymmetry* 26 (**2015**) 835–839

Figure 56. Chong's trifluoromethyl ketones reduction by mean of metal hydride reagent BINAL-H.

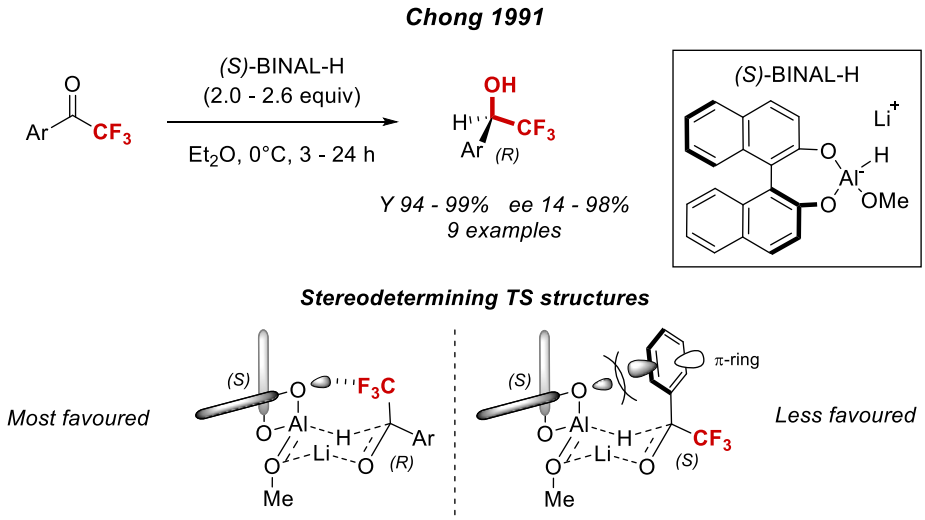

Figure 57. Hydrogenation of trifluoromethyl ketones via asymmetric Lewis acid enhanced β-hydride transfer.

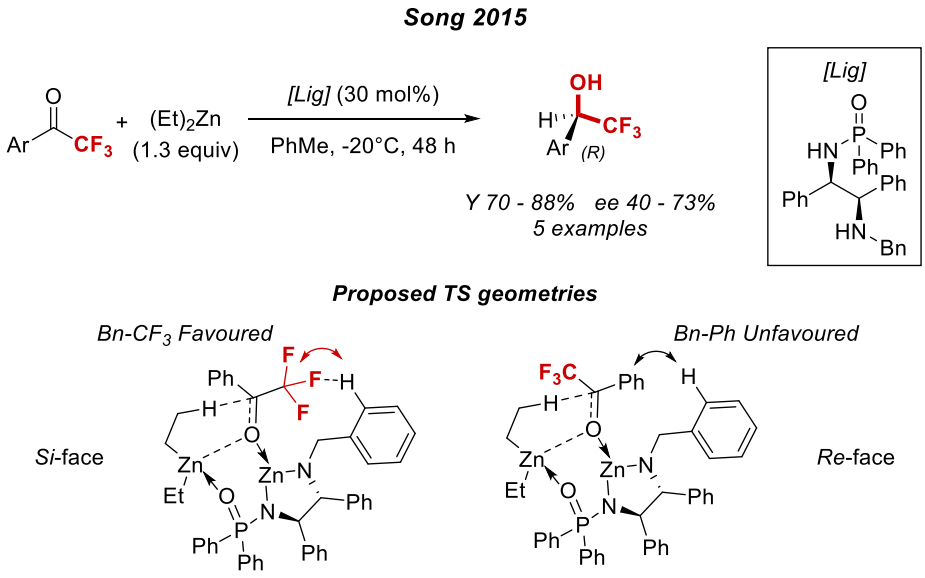

To further extend the topological transformation giving access to α-aryl-α-trifluoromethyl alcohols a *Nucleophilic* synthetic route is going to be presented, to do so different types of nucleophiles, not only organometallic reagents, will be considered along with their associated electrophilic trifluoromethyl bearing partners.

In 2020 Funabiki group disclosed a two-step synthetic procedure for preparation of α-aryl-α-trifluoromethyl alcohols, in the first step a series of aryl iodides have been metalated with turbo Grignard iPrMgCl*LiCl, after the lithiation occurred the unstable intermediated **XXV** was quenched with trifluoroethyl trifluoroacetate. The use of such a highly reactive organometallic reagent set the stage for a fast reaction to occur. The main drawback about this procedure, lies in the handling of air and moisture sensitive organometallic reagents, which might easily be quenched or be pyrophoric.

Beyond practical issues, the procedure displays good to high yields over a good number of transformed substrates (Fig. 58).[286]

Figure 58. Funabiki's direct turbo Grignard addition onto trifluoroethyl trifluoroacetates.

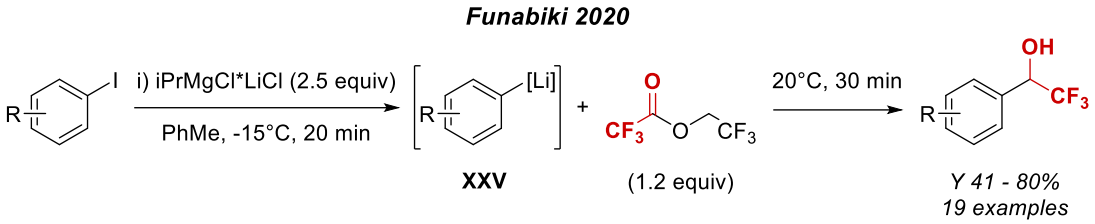

Accounting for the exploration of other nucleophiles, in 2000 Jørgensen and co-workers presented a general procedure for sewing together arenes and glyoxal via asymmetric Friedel-Craft acylation. The general classes of compounds investigated were *N,N*-disubstituted anilines and *orto*-functionalized furanes as arenes, while glyoxal and trifluoromethyl pyruvate were chosen as acylating partners. The reaction was catalysed by a chiral copper species; under a set of optimized conditions the selected bisoxazoline-copper complex proved to be an effective chiral Lewis acid by promoting the formation of compounds **XXVI**, **XXVII** and **XXVIII** in moderate to good yields and with high to excellent *ee*. Below, the feasible structure of the enantiodetermining step, was reported as the authors did in their original work. Here, the copper catalyst activates the trifluoromethyl pyruvate and the chiral information is thus transferred to the approaching arene; unfortunately, only three examples were furnished with electron rich arenes, highlighting this way the main drawback for Friedel-Craft acylation protocols (**Fig. 59**).

Figure 59. Coper catalysed asymmetric Friedel-Craft acylation of trifluoromethyl pyruvate.

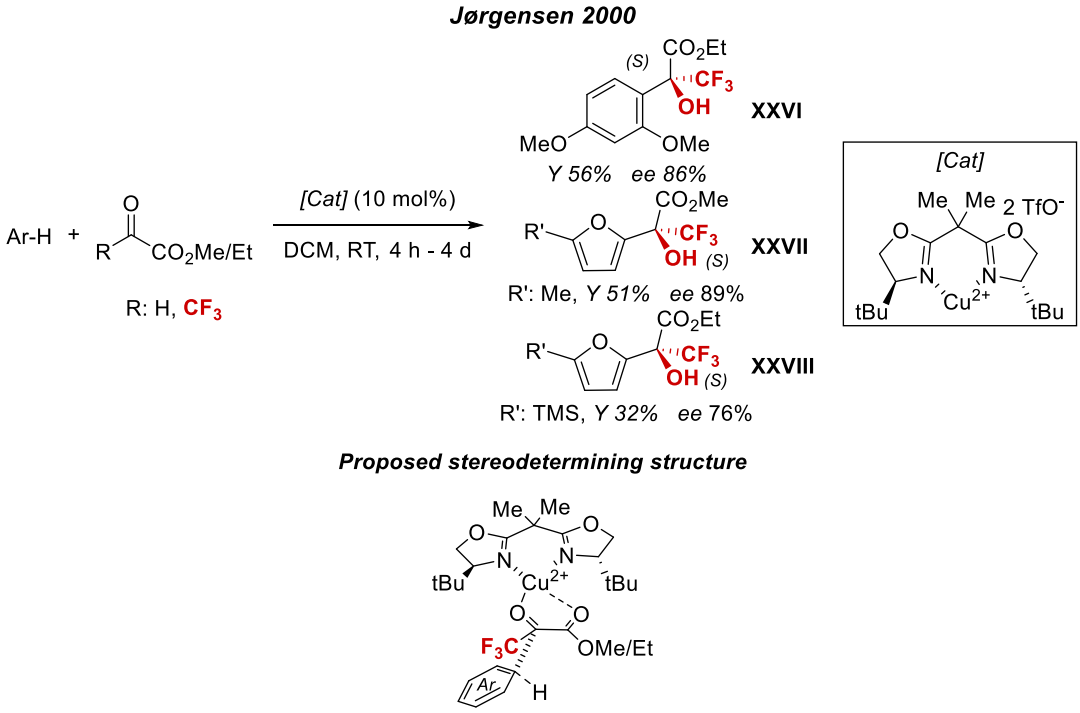

[286] Kani, R., Inuzuka, T., Kubota, Y., Funabiki, K., *Eur. J. Org. Chem.*, **2020**, 4487-4493

Bandini and Umani-Ronchi in 2008 presented an organocatalyzed Henry reaction between trifluoromethyl ketones and CH_3NO_2, where the latter acts as C1 nucleophile.[287] They iteratively investigated different cupreine and quinuclidine-based organocatalysts and found that a 3,5-bistrifluoromethylbenzoate substituents at C9 position (**Fig. 60**) was necessary to achieve satisfactory results. Former examples of such a reaction are claimed to have poor enantiocontrol and long reaction times when other conditions are employed.[288] Under the reaction conditions developed by Bandini and Umani-Ronchi uncontrolled background reactions have been successfully suppressed and high yields and *ee* have generally been achieved. Other research groups investigated analogue transformations but the active catalyst in those cases presented intricated lanthanum based organometallic catalyst whose performances difficultly are worth the efforts for their synthesis.[289]

Figure 60. Bandini and Umani-Ronchi conditions for organocatalyzed CH_3NO_2 addition onto trifluoromethyl ketones.

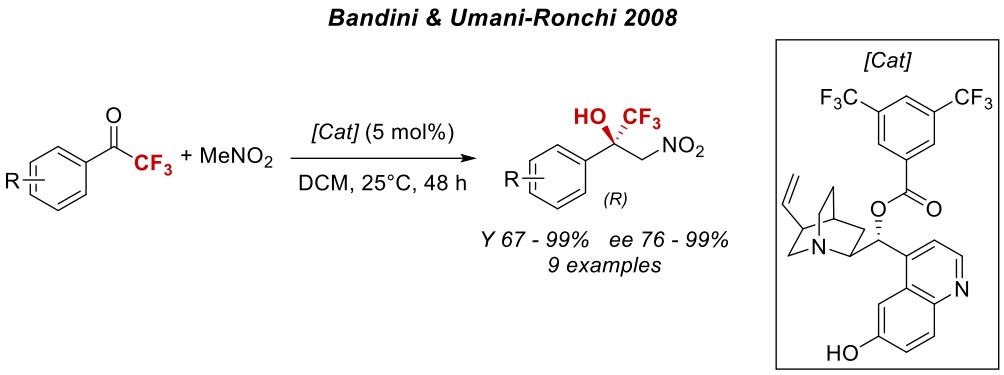

3.3.2 Work Rationale and Development

The presented methodologies have accounted for the three different main approaches toward the synthesis of α-aryl-α-trifluoromethyl alcohols. In 2022, our group interest was raised by the possibility to design a new transition metal catalysed coupling between a trifluoroacetaldehyde surrogate and a largely available compound class. Iodoarenes have been chosen to this aim since they can promptly be involved in many cross-coupling reactions. Then we opted for nickel-based catalysts which are known to have excellent performances in cross-coupling protocols, due to their ability to easily access also odd oxidation states at need. Lately we wondered if proper leveraging of poorly explored redox active ethers chemistry could turn TFE (2,2,2-trifluoroethanol) into a suitable trifluoroacetaldehyde precursor, upon activation and subsequent reduction. Having these main boundaries set we proceeded into the rational design of a feasible XEC mechanism through which the envisioned transformation could unfold. Indeed, phthalimide platform bearing *N*-alkoxy pendant groups (PhthN-OR) should provide an oxygen centered radical fragment, after single electron reduction, this radical species may then evolve via different rearrangements, among which 1,2 HAT can provide the corresponding carbon centered radical. Such a radical is amenable to be captured by arylnickel(II) species, previously generated via oxidative addition of a low valent nickel species over aryl halides, thus furnishing an organonickel(III) intermediate. A final reductive elimination would then account for the desired product formation (**Sch. 12**).

[287] Bandini, M., Sinisi, R., Umani-Ronchi, A., *Chem. Commun.* **2008**, 4360-4362
[288] Misumi, Y., Bulman, R.A. and Matsumoto, K., *Heterocycles*, **2002**, 56, 599
[289] Tur, F., Saa, J.M., *Org. Lett*. **2007**, 9, 24, 5079–5082

Scheme 12. Reactivity events leading to the formation of the desired products exploiting nickel catalysis and *N*-alkoxyphthalimides chemistry. M: transition metal catalyst, *[H]*: reductant.

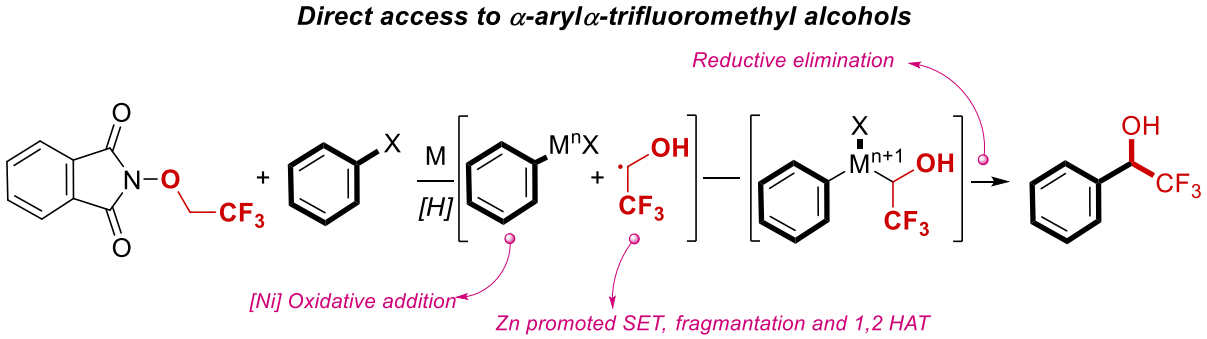

Under these promises we faced the optimization of the newly thought XEC protocol, using 4-iodotoluene as model substrate. We began the investigation (**Tab. 6 entry 1**) by placing *N*-trifluoroethoxyphthalimide **14** with substrate **13a** in a 3:1 ratio along with 10 mol% of catalyst Ni(**L1**)Cl_2, TMSCl (1 equiv), and Zn as reductant in dry DMA. These initial conditions allowed us to recover product **15a** in 36% yield, a good suggestion about the feasibility of the reaction. A performance screening of manganese and TDAE as alternative reductants followed (**Tab. 6 entries 2, 3**): the former gave a 16% yield, the latter gave no product at all. Behaviour investigation of different nitrogen-based ligands followed (**Tab. 6 entries 4-11**), bisoxazoline **L2** and terpyridine ligand **L8** gave poor yields, effects of -Cl vs -Br counter anion were checked with ligand **L3** which showed a remarkable yield (**Tab. 6 entries 5, 6**). Nevertheless, no substantial differences came out. Reaction outcomes with bipyridyl-based ligands **L3 – L7** gave different results based upon their electronic and steric properties, electron-poor ligand **L4** and sterically encumbered ligand **L7** showed poor yield or low selectivity toward the product and variable amounts of dehalogenated starting material (**13a-H**) were recorded. Among electron-rich bipyridyl ligands **L3**, **L5** and **L6** we chose **L5** which showed a yield value of 60% (**Tab. 6 entry 8**). Finally, a series of additives beyond TMSCl was investigated, across all of them NaI enabled us to obtain almost a quantitative yield (**Tab. 6 entry 12**) and in a considerably shorter amount of time (two hours). With the same reaction time but with no sodium iodide the yield dropped at 30% (**Tab. 6 entry 13**) and the developed reaction conditions also gave good results under open air with a 60% of yield (**Tab. 6 entry 14**).

Figure 61. Optimized parameters for trifluoromethylcarbinols preparation, and ligand structures.

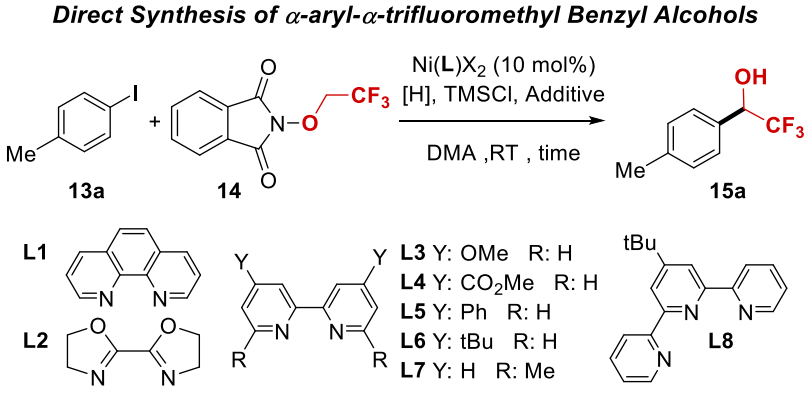

Table 6. [a]All reactions were carried out under N_2 in dry DMA (**13a**/**14**/Ni(**L**)Cl_2/NaI/TMSCl/Zn, 1/3/0.1/1/1/2, [**13a**] = 0.2 M. [b]Determined by ^{19}F NMR on the reaction crude with an internal standard

($CF_3C_6H_5$). In brackets, isolated yields after flash chromatography. [c]The catalytic complex was prepared in situ (**L**/$NiCl_2 \cdot$ DME: 15/10 mol%). [d]Dehalogenative homocoupling of **13 a** was determined as the major product. [e]With reagent grade DMA and under air. [H]: reductant, N.R.: no reaction.

Entry[a]	Ligand	[H]/Additive	Time (h)	Y 15a (%)[b]
1	Ni(**L1**)Cl_2	Zn/-	16	**36**
2	Ni(**L1**)Cl_2	Mn/-	16	**16**
3	Ni(**L1**)Cl_2	TDAE/-	16	**0**
4[c,d]	Ni(**L2**)Cl_2	Zn/-	16	**0**
5[c]	Ni(**L3**)Cl_2	Zn/-	16	**55**
6	Ni(**L3**)Br_2	Zn/-	18	**54**
7[c,d]	Ni(**L4**)Cl_2	Zn/-	16	**8**
8	Ni(**L5**)Cl_2	Zn/-	16	**59**
9[c]	Ni(**L6**)Cl_2	Zn/-	16	**48**
10[c,d]	Ni(**L7**)Cl_2	Zn/-	16	**0**
11[c]	Ni(**L8**)Cl_2	Zn/-	16	**5**
12	Ni(**L5**)Cl_2	Zn/NaI	2	**95(88)**
13	Ni(**L5**)Cl_2	Zn/-	2	**30**
14[e]	Ni(**L5**)Cl_2	Zn/NaI	2	**60**

The beneficial effects of NaI have been debated for long time, iodide anions could speed-up Ni(II) reduction by acting as bridging ligand with solid zinc powder, or by enhancing Zn(II) removal from the surface and enhance better exposure of new Zn(0). It is also plausible that a Cl^-/I^- swapping could favour the formation of highly active catalytic intermediates, such ligand exchange processes is documented to better occur in polar aprotic solvents like DMA.[93,290,291,292,293,294]

With optimized conditions in our hands, we started an investigation of suitable substrates. Electron rich ring substituents could efficiently be accommodated at *meta* and *para* positions among these six analogues were prepared (4-Me **15a**, 3-Me **15b**, 4-OAlly **15c**, 4-OBn **15d**, 4-OMe **15e** and 3-OMe **15f**) with yields from 50 to 64%, one ester analogue (3-OAc **15g**) and one trifluoroacetamide **15j** have successfully been isolated in good yields, 62% and 63% respectively; the latter substituents also remark the robustness of the developed methodology toward acidic residues. Other two N containing functional group were introduced, namely *N,N*-dibenzylamine and *N*-Phthalimide whose corresponding products could be recovered in high yields, **15h** 73% and **15i** 74%; a naphthyl-based trifluoromethylated product **15k** was also obtained in 61% yield (**Fig. 62**). Simple iodobenzene could be transformed into the desired target **15l** with a satisfactory 70% yield. Then a series of electronwithdrawing functional group were investigated, placement of one/two halogens (**15m – 15p**) or one halogen and one -CF_3 group (**15q, 15r**) on the ring led to the isolation of products in somewhat lower yields (43% to 65%) compared to electron-rich arenes. Indeed, 4-CO_2Me **15s** and 4-Acetyl **15t** analogues gave high yields (73% and 68% respectively) which are comparable values to EDG functionalized rings. Then, five examples of substrates desirable for further transformations were

[290] Wang, D. and XU, T., *ACS Catal.* **2021**, 11, 20, 12469–12475
[291] Cassar, L., Foa, M., *Journal of Organometallic Chemistry*, **1973**, 51, 381-393
[292] Zembayashi, M., Tamao, K., Yoshida, J.I., Kumada, M., *Tetrahedron Lett.* **1977**, 18, 4089–4091
[293] Feng, C., Cunningham, D.W., Easter, Q.T., Blum, S.A., *J. Am. Chem. Soc.* **2016**, 138, 35, 11156–11159
[294] Wang, X., Ma, G., Peng, Y., Pitsch, C.E., Moll, B.J., Ly, T.D., Wang, X., Gong, H., *J. Am. Chem. Soc.* **2018**, 140, 43, 14490–14497

subjected to our conditions, and we successfully isolated products **15u** (61%), **15v** (60%), **15w** (43%), **15y** (65%) and **15z** (50%) which can be easily engaged in cross coupling, click chemistry or redox functionalizations; we also isolated product **15x** stemming from 1,4-diodobenzene with a remarkable yield of 73%. Later, we engaged substrates having phenyl rings conjugated with biologically relevant structures; products **15aa**, **15ab** and **15ae** were obtained with 46%, 67% and 32% yields respectively. Lastly three biphenyl-based iodoarenes were collected in 81% (**15ac**) and 58% (**15ad**) yields, **15ac** was prepared on a mmol scale and it is a key intermediate in the synthesis of bioactive compound LP-533401, one iodo-biphenyl substrate could also be functionalized with pentafluoropropyl pendant group (**15ac'**) in a 22% yield. A useful variety of substrates was presented, others, however provided yields lower than 15%, namely: 2-MeO-5-Iodopyridine, 2-iodothiophene, 4-iodophenylacetylene, 4-iodoaniline, 2-iodotluene and methyl-2iodobenzoate. Other three candidates (4-iodophenol, 4-iodobenzaldehyde and 4-iodobenzonitrile) instead did afford the products in good yields but their separation from coproduced phthalimide was not successful neither through flash chromatography nor through mild basic washings.

Afterward we proceeded to shed light on the mechanism at work in the reaction, **13t** and *N*-trifluoroethoxyphthalimide **14** were chosen as substrates in DFT calculations; indeed, Ni(**L3**)Cl_2 was chosen as catalyst due to its simpler structure and having displayed comparable performances to Ni(**L5**)Cl_2 (**Tab. 6 entry 5** *vs* **8**). We have found that nickel(II) precatalyst **xxiii** is reduced to the active resting state **xxiv** (-15.16 kcal/mol) by zinc in an exergonic way, while calculated energies for two electron reduction set nickel(0)-bpy complex energies higher in energy.[295,296,297] Then a reversible substrate coordination takes place and oxidative addition from **xxv** to **xxvi** calculated energy demand is around 4.1 kcal/mol. Organonickel(III) intermediate **xxvi** then promptly engages into a SET event lowering this way its relative free energy to -57.35 kcal/mol in intermediate **xxvii**, at this stage radical **xxii** is captured to form **xxviii** (-71.34 kcal/mol) with a further stabilization. From here reductive elimination takes place yielding the product with a low energy barrier (5.52 kcal/mol) and regenerating **xxiv**.

The reaction for *N*-trifluoroethoxyphthalimide **14** instead began with coordination of $ZnBr_2$ acting as Lewis acid, then proceeded with SET triggered by Zn(0) thus forming radical anion species **xviii**, with a modest energy input the **TS xviii-xix** demanding less than 4 kcal/mol led to **xix**, after electronic reorganization occurred the less energy demanding pathway is the fragmentation of **xix** to O-centered radical **xxi** and phthalimide anion **xx**. To complete the mechanistic picture a quite energy demanding, yet occurring, 1,2 hydrogen shift takes place, the computation says that **TS xxi-xxii** lies at 20.0 kcal/mol but the desired C-centered radical is a bit more stable; within this step assistance of polar DMA is needed.

Figure 62. Trifluoromethylcarbinols scope investigation.

[295] Till, N.A., Oh, S., MacMillan, D.W.C., Bird, M.J., *J. Am. Chem. Soc.* **2021**, 143, 25, 9332–9337
[296] Lin, Q., Fu, Y., Liu, P., Diao, T., *J. Am. Chem. Soc.* **2021**, 143, 35, 14196–14206
[297] Ting, S.I., Williams, W.L., Doyle, A.G., *J. Am. Chem. Soc.* **2022**, 144, 12, 5575–5582

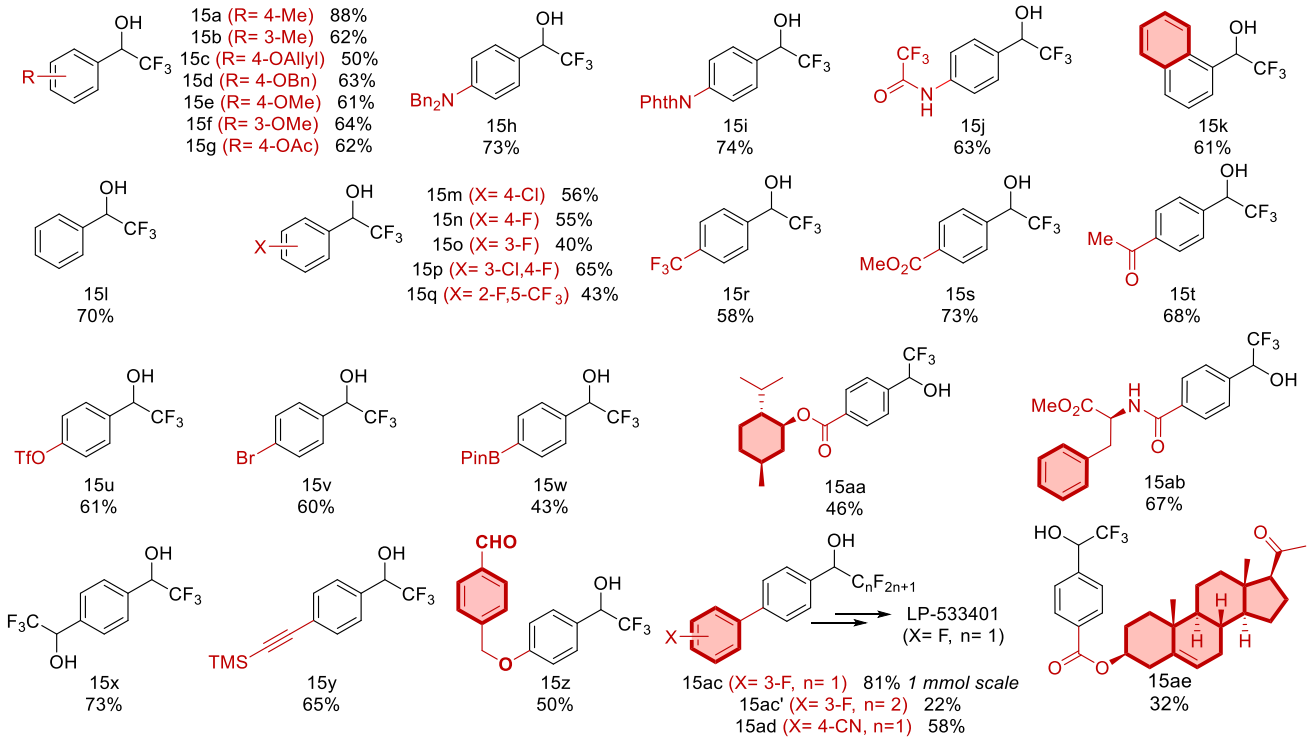

During molecular modelling investigations relative to trifluoroacetaldehyde formation from **xix** to **xixa** were carried out, despite the latter structure being more stable, no saddle points could be found thus ruling out feasible reaction channels for this event.

Figure 63. Proposed mechanistic pathway and DFT calculated energies for intermediates of the cycle.

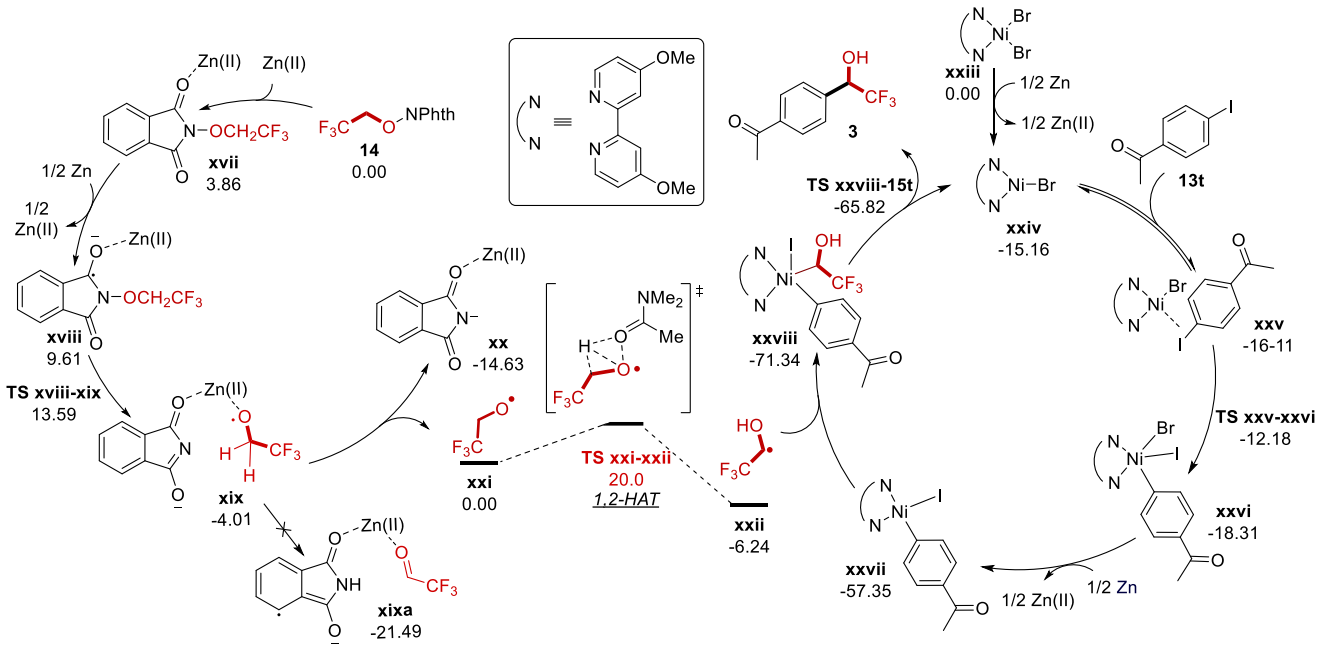

Additionally radical trapping experiments were done to verify presence of **xxi** or **xxii** either, the first experiments took advantage of TEMPO ability to trap radicals, in fact it was used in place of

substrates with *N*-trifluoroethoxyphthalimide **14**, under standard catalytic conditions formation of **xxix,** a TEMPO adduct with **xxii** was observed via GC-MS. Then also a tButyl-acrilate was placed under optimal catalytic conditions once with 10 mol% of nickel catalyst and once without it, in the first case a 35% of **xxx** was isolated, in the second case a 12% yield of the same product **xxx** was again isolated and characterized. These are solid evidence supporting the unfolded mechanism (**Fig. 64**).

Figure 64. Radical trapping experiments.

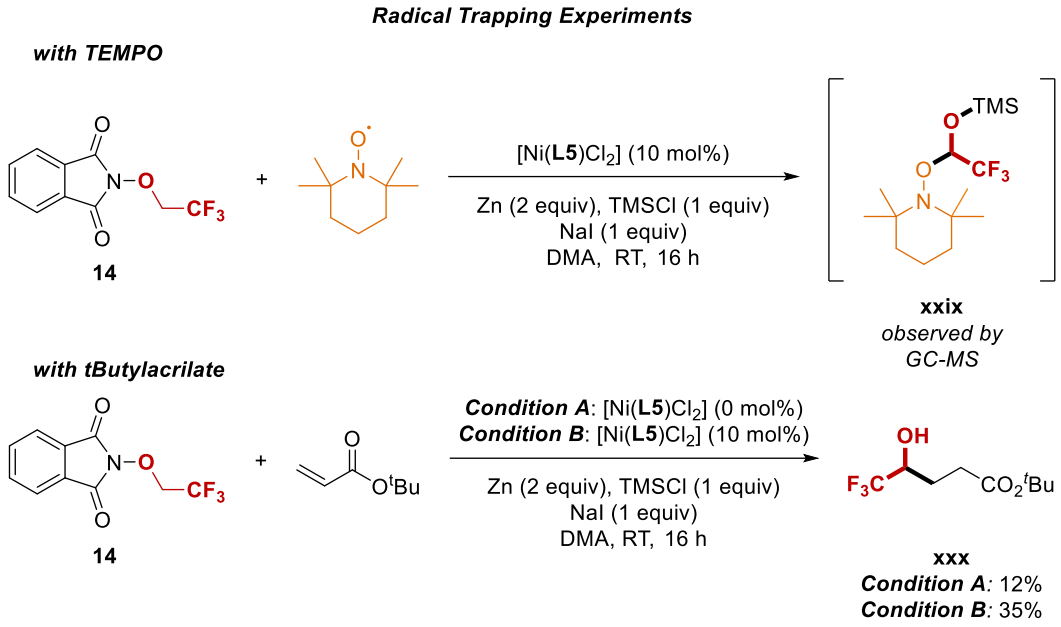

3.3.3 Conclusion

The presented methodology has successfully enabled the preparation of α-aryl-α-trifluoromethyl alcohols, among these also few analogues with biologically relevant scaffolds could be obtained in useful yields. The development of a new bench stable reagent **14** proved successful in *bypassing* the use of hazardous trifluoroacetaldehyde or its common surrogates. Since 2022 new synthetic methodologies exploiting *N*-trifluoroethoxyphthalimide have been published for the preparation of other trifluoromethylcarbinols under photochemical conditions, as of today no other uses of such a reagent under reductive metal catalysed conditions have been recorded.[298,299,300,301]

[298] Boyle, B.T., Dow, N.W., Kelly, C.B. *et* al, Nature, **631**, 789–795 (2024)
[299] Chen, F., Xu, X.H., Chen, Z.H., Chen, Y., Qing, F.L., *Beilstein J. Org. Chem.* **2023,** 19, 1372–1378
[300] Chen, F., Xu, X.H., Chu, L., Qing, F.L., *Org. Lett.* **2022**, 24, 50, 9332–9336
[301] Thakur, A., Gupta, S.S., Dhiman, A.K., Sharma, U., *J. Org. Chem*. **2023**, 88, 4, 2314–2321

4 Final Considerations

The present thesis, which has begun with introduction of CO_2 chemistry and nickel catalysis, has served to collect selected development lines directed at the explanation of dedicated research topics like carbonylation-carboxylation dichotomy and highly attractive trifluoromethylations. Within the manuscript unfolding the author has tried not to get lost in all possible reaction outcomes but rather to highlight the basic concepts which were then corroborated with literature examples. These unveiled research topics were selected and ordered in a way to efficiently introduce the highly progressive works developed during the PhD period. Due to the breadth of the covered topics (environmental CO_2 aspects, cross couplings, cross-electrophile couplings, carbonylation and trifluoromethylations) the following manuscript doesn't aim at exhaustiveness but eventually at being a good reference point to give good guidance at readers while showing achieved academic results during these three years.

Projects dealing with CO_2 based carbonylation chemistry have showed that CO utilization can efficiently be overcome at least for R&D purposes, the novelty in the addressed transformations is indeed remarkable and will hopefully inspire future works along these lines. Trifluoromethylation project on the other hand has established the use bench stable *N*-trifluorothoxyphthalimide, previously seldom recorded, for the preparation of α-aryl-α-trifluoromethyl alcohols in a fruitful way. The illustrated methodology goes beyond simple CF_3 installation but opens at new creative applications for medicinal chemistry and photochemical synthetic methodologies.

5 Methods and Materials

All catalytic transformation were carried out with standard Schlenk Technique.

^{1}H NMR, ^{13}C NMR and ^{19}F NMR spectra were recorded on Varian 400-MR (400 MHz) and a Bruker 600 (600 MHz). Data are reported as follows: chemical shift, multiplicity (s = singlet, d = doublet, dd= double doublet, t = triplet, td = triple doublet, dt = double triplet, q = quartet, sext = sextet, sept = septet, p = pseudo, b = broad, m = multiplet), coupling constants (Hz). Chemical shifts are reported in ppm from TMS with the solvent resonance as the internal standard.

HRMS spectra were obtained with a G2XS QTof mass spectrometer using ESI ionization technique, as specified case by case.

Melting points were determined with a Büchi Melting Point B-540 apparatus and are not corrected.

Chromatographic purification was done with 240-400 mesh silica gel.

Anhydrous solvents were supplied by Sigma Aldrich in Sureseal® bottles and used without any further purification.

During project regarding carbonylation/carboxylation sequence DMF was dried as follows: 4Å molecular sieves (MS) were activated under microwave irradiation for 10 minutes, they were charged in a flask connected to the Schlenk line and dried under vacuum three additional times, then allowed to cool to room temperature. Under a CO_2 flow, commercially available DMF (purchased from Sigma Aldrich, Sureseal® bottle) was transferred to the flask and stored for 72 h. Then, the activation procedure was repeated into another flask with new 4Å MS and the DMF was transferred from the first flask to the second one under a continuous CO_2 flow. After 72 additional hours we directly used the DMF from the latter flask and stored it under CO_2 after every use.

During project for benzolactams and benzolactones preparation DMF was dried the same way as before, but Ar was used as inert gas instead of CO_2.

Commercially available chemicals and (non-anhydrous) solvents were purchased from Sigma Aldrich, Fluorochem and TCI Chemicals and used without any further purification. Zn dust refers to a particle size <10μm, and was purchased from Sigma Aldrich, having ≥98% purity.

Room temperature (RT) refers to the ambient temperature of the laboratory, ranging from 20 °C to 26 °C.

5.1 Double CO_2 Incorporation in a Carbonylation/Carboxylation Sequence

Further relevant information can be found in the SI document of the following work:

Nickel Catalyzed Carbonylation/Carboxylation Sequence via Double CO_2 Incorporation

Riccardo Giovanelli, Lorenzo Lombardi, Riccardo Pedrazzani, Magda Monari, Marta Castiñeira Reis, Carlos Silva López, Giulio Bertuzzi, and Marco Bandini

Organic Letters **2023** *25* (38), 6969-6974

DOI: 10.1021/acs.orglett.3c02394

5.1.1 General crystallographic data

The X-ray intensity data were measured on a Bruker Apex III CCD diffractometer. Cell dimensions and the orientation matrix were initially determined from a least-squares refinement on reflections measured in four sets of 20 exposures, collected in three different ω regions, and eventually refined against all data. A full sphere of reciprocal space was scanned by 0.5° ω steps. The software SMART3 was used for collecting frames of data, indexing reflections and determination of lattice parameters. The collected frames were then processed for integration by the SAINT program,[302] and an empirical absorption correction was applied using SADABS.[303] The structures were solved by direct methods (SIR 2014)[304] and subsequent Fourier syntheses and refined by full-matrix least-squares on F2 (SHELXTL)[305] using anisotropic thermal parameters for all non-hydrogen atoms. The aromatic, methyl and methylene hydrogen atoms were placed in calculated positions, refined with isotropic thermal parameters U(H) = 1.2 Ueq(C) and allowed to ride on their carrier carbons. Molecular drawings were generated using Mercury.[306] Crystallographic data have been deposited with the Cambridge Crystallographic Data Centre (CCDC) with deposition number CCDC 2267379-2267380 Copies of the data can be obtained free of charge via www.ccdc.cam.ac.uk/getstructures.

[302] SMART & SAINT Software Reference Manuals, version 5.051 (Windows NT Version), Bruker Analytical X-ray Instruments Inc.: Madison, Wi, **1998**.
[303] Sheldrick, G. M.; SADABS-2008/1 - Bruker AXS Area Detector Scaling and Absorption Correction, Bruker AXS: Madison, Wisconsin, USA, **2008**.
[304] Burla, M.C., Caliandro, R., Carrozzini, B., Cascarano, G.L., Cuocci, C., Giacovazzo, C., Mallamo, M., Mazzone, A., Polidori, G., *J. Appl. Cryst*. **2015**, 48, 306.
[305] Sheldrick, G.M., *Acta Cryst* C71, **2015**, 3
[306] Macrae, C.F., Sovago, I., Cottrell, S.J., Galek, P.T.A., McCabe, P., Pidcock, E., Platings, M., Shields, G.P., Stevens, J.S., Towler, M., Wood, P.A., *J. Appl. Cryst.*, **2020**, 53, 226

5.1.1.1 Crystal data and structure refinement for $[Ni(L1)_2Cl_2]$

SC-XRD suitable crystals were obtained from layering a saturated solution of $[Ni(\mathbf{L1})_2Cl_2]$ in acetonitrile on toluene in a closed cup vial. Small deep green rhombohedral crystals were observed.

Table 7. [a)] $R_1 = \Sigma||F_o|-|F_c||/\Sigma|F_o|$. [b] $wR_2 = [\Sigma w(F_o^2-F_c^2)^2/\Sigma w(F_o^2)^2]^{1/2}$ where $w = 1/[\sigma^2(F_o^2) + (aP)^2 + bP]$ where $P = (F_o^2 + F_c^2)/3$.

Compound	**$[Ni(L1)_2Cl_2]$**
Formula	$C_{24}H_{24}Cl_2N_4NiO_4 \bullet CH_3CN$
Fw	603.13
T, K	296(2)
λ, Å	0.71073
Crystal symmetry	Triclinic
Space group	P -1
a, Å	10.1973(5)
b, Å	11.0334(5)
c, Å	13.5797(6)
α	101.161(2)
β	106.863(2)
γ	101.404(2)
Cell volume, Å^3	1381.1(1)
Z	2
D_c, Mg m^{-3}	1.450
μ(Mo-K$_\alpha$), mm^{-1}	0.937
F(000)	624
Crystal size/ mm	0.12 x 0.08 x 0.06
θ limits, °	1.626 to 27.000
Reflections collected	18647
Unique obs. Reflections [$F_o > 4\sigma(F_o)$]	5891 [R(int) = 0.0442]
Goodness-of-fit-on F^2	0.885
R_1 (F)[a], wR_2 (F^2) [$I > 2\sigma(I)$][b]	R1 = 0.0596, wR2 = 0.1255
Largest diff. peak and hole, e. Å^{-3}	0.596 and -0.567

Figure 65. ORTEP drawing of **[Ni(L1)$_2$Cl$_2$]**. Thermal ellipsoids are drawn at 30% of the probability level. Solvated acetonitrile molecule removed for clarity.

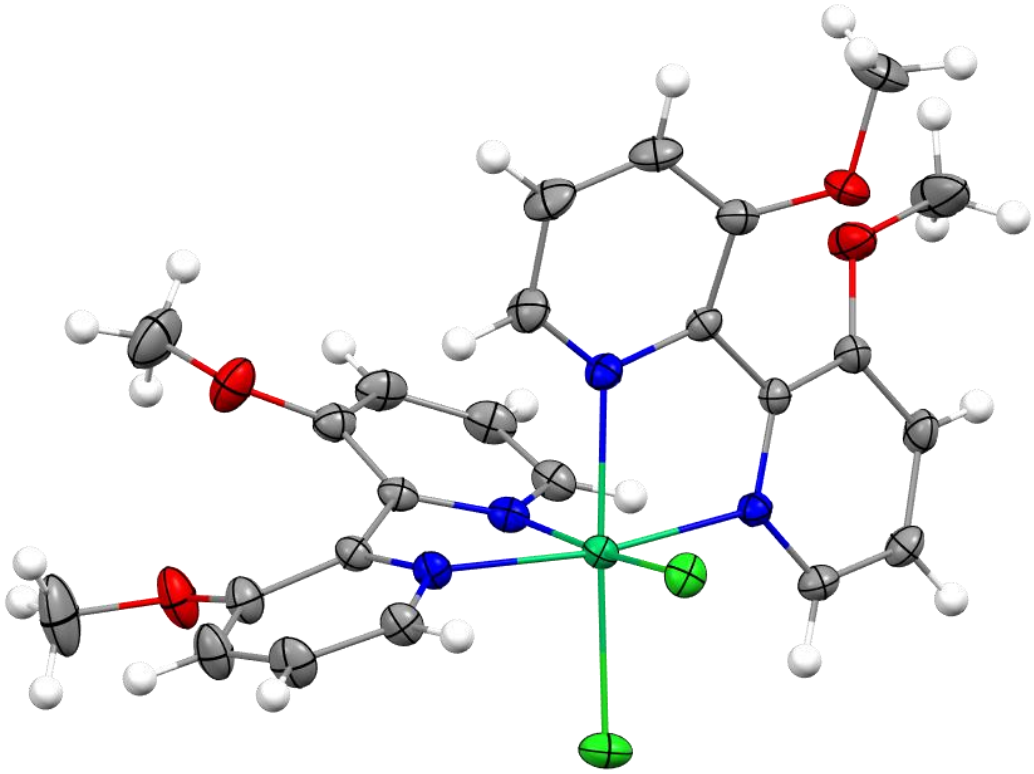

5.1.2 General DFT information

We have used the Density Functional Theory (DFT) in the Kohn-Sham formulation to optimize all the stationary points presented in this manuscript. Geometries of all the stationary points were fully optimized at the M06[307]/def2svpp[308] computational level. The effect of solvent (*N*,*N*-dimethylformamide, abbreviated as DMF) was modelled using the polarizable continuum model (PCM)[309] with the default parameters implemented in the Gaussian 09 package.[310] Explicit solvation was also included in some instances since the solvent has the potential ability to coordinate the metallic center. All geometry optimizations have been optimized using tight convergence criteria in the SCF and requesting a pruned (99.590) grid to guarantee the accuracy of the reported results. Moreover, the calculations were performed considering 1.0 atm and 298 K to simulate the reaction conditions. Frequency analysis was used to establish the nature of all optimized structures as either minima or transition structures. For all stationary points, the stability of the wave function was also examined.[311] When different spin-states are possible for a stationary point those states were explored by running single point energy calculations starting from the optimized structure with the expected multiplicity. Electronic energies for the optimized structures of the different possible multiplicities are specified in the Cartesian section. IRC calculations[312] were conducted for important transition states to ensure their connectivity with the expected reactants and products. When the substrates showed conformational freedom, conformational analysis was performed manually, it must be indicated that only the most stable conformer of each stationary point was considered and reported unless otherwise indicated. The visualization of the reported structures was performed using MOLDEN.[312] The representation of the structures here presented were generated using CYLView.[313] The reduction steps constitute a troublesome point in this research since they involve metallic Zn. We have worked here under the consideration that in the presence of such a coordinating solvent such as DMF part of the metallic Zn will be efficiently solvated and leached in the form of $Zn(DMF)_3$, in

[307] a) Zhao, Y., Truhlar, D.G., *Theor. Chem. Acc.* **2008**, 120, 215. b) Zhao, Y., Truhlar, D.G., *Acc. Chem. Res.* **2008**, 41, 157

[308] a) Weigend, F., *Phys. Chem. Chem. Phys*. **2006**, 8, 1057. b) Weigend, F., Ahlrichs, R., *Phys. Chem. Chem. Phys.* **2005**, 7, 3297.

[309] Tomasi, J., Mennucci, B., Cammi, R., *Chem. Rev*. **2005**, 105, 2999

[310] Gaussian 09, Revision A.02, M. J. Frisch, G. W. Trucks, H. B. Schlegel, G. E. Scuseria, M. A. Robb, J. R. Cheeseman, G. Scalmani, V. Barone, G. A. Petersson, H. Nakatsuji, X. Li, M. Caricato, A. Marenich, J. Bloino, B. G. Janesko, R. Gomperts, B. Mennucci, H. P. Hratchian, J. V. Ortiz, A. F. Izmaylov, J. L. Sonnenberg, D. Williams-Young, F. Ding, F. Lipparini, F. Egidi, J. Goings, B. Peng, A. Petrone, T. Henderson, D. Ranasinghe, V. G. Zakrzewski, J. Gao, N. Rega, G. Zheng, W. Liang, M. Hada, M. Ehara, K. Toyota, R. Fukuda, J. Hasegawa, M. Ishida, T. Nakajima, Y. Honda, O. Kitao, H. Nakai, T. Vreven, K. Throssell, J. A. Montgomery, J. E. Peralta, F. Ogliaro, M. Bearpark, J. J. Heyd, E. Brothers, K. N. Kudin, V. N. Staroverov, T. Keith, R. Kobayashi, J. Normand, K. Raghavachari, A. Rendell, J. C. Burant, S. S. Iyengar, J. Tomasi, M. Cossi, J. M. Millam, M. Klene, C. Adamo, R. Cammi, J. W. Ochterski, R. L. Martin, K. Morokuma, O. Farkas, J. B. Foresman, D. J. Fox, Gaussian, Inc., Wallingford CT.

[311] a) Schlegel, H.B., McDouall, J.J.W., "Do You Have SCF Stability and Convergence Problems?" in Computational Advances in Organic Chemistry: Molecular Structure and Reactivity, Dordrecht: Springer Netherlands, **1991**, pp. 167– 185. b) Bauernschmitt, R., Ahlrichs, R., *J. Chem. Phys.* **1996**, 104, 9047. c) Seeger, R., Pople, J.A., J. Chem. Phys. **1977**, 66, 3045

[312] a) Maeda, S., Harabuchi, Y., Ono, Y., Taketsugu, T., Morokuma, K., *Inter. J. Quantum Chem*. **2015**, 115, 258. b) Fukui, K., *Acc. Chem. Res*. **1981**, 14, 363

[313] CYLview20; C. Y. Legault, Université de Sherbrooke, **2020** (http://www.cylview.org).

agreement with our previous results. Topological analysis of the electron density was done via analysis of the wavefunction using Multiwfn.[314]

[314] Lu, T., Chen, F., *J. Comput. Chem.,* **2012**, 33, 580.

5.1.3 General procedures for starting materials preparation

Substrates **1** were prepared from the corresponding cyclobutanones **MM-1** by a Wittig olefination. Cyclobutanones **MM**-1 are known compounds and were prepared following unmodified literature procedures.[230]

Figure 66. Strating material **1** preparation.

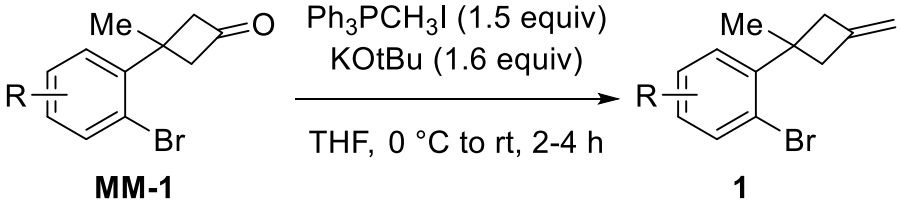

In a heat-gun dried Schlenk flask, under a N_2 atmosphere and magnetic stirring, Ph_3PCH_3I (1.5 equiv., 1.5 mmol, 606 mg) and KOtBu (1.6 equiv., 1.6 mmol, 180 mg) were charged, followed by dry THF (5 mL). The resulting yellow suspension was stirred for 1 h at room temperature and then cooled to 0°C. The desired cyclobutanone S (1 mmol, 1 M solution in THF), was added dropwise under vigorous stirring. After the addition, the reaction was stirred at room temperature and monitored by TLC (100% hexane). When full consumption of S was observed (ca. 2-4 h), saturated NH_4Cl(aq.) (20 mL) was added to the reaction flask and the mixture, transferred to a separatory funnel, was extracted with EtOAc (3x20 mL). The organic phase was dried over Na_2SO_4 and the solvent evaporated in vacuo. The reaction crude was finally purified by flash chromatography on silica gel (FC, 100% n-hex).

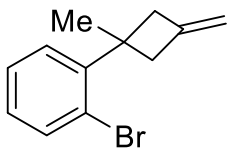

1a. Colourless oil. FC eluent: *n*Hex 100%. Yield = 83% (0.83 mmol, 245.4 mg). **^{1}H NMR** (401 MHz, $CDCl_3$) δ 7.53 (d, *J* = 9.1 Hz, 1H), 7.33 – 7.24 (m, 1H), 7.22 – 7.16 (m, 1H), 7.10 – 7.03 (m, 1H), 4.90 (s, 2H), 3.20 – 3.16 (m, 2H), 2.89 – 2.85 (m, 2H), 1.54 (s, 3H). **^{13}C NMR** (101 MHz, $CDCl_3$) δ 148.2, 144.7, 133.9, 127.9, 127.4, 127.3, 121.7, 106.4, 45.2 (s. 2C), 41.1, 26.8. **HRMS (*ESI)*** m/z: $[M+H]^+$ calcd. for $C_{13}H_{16}Br$ 251.0430; found 251.0439.

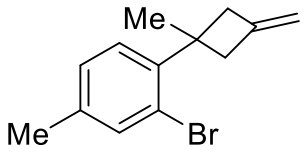

1b. Colourless oil. FC eluent: *n*Hex 100%. Yield = 81% (0.81 mmol, 242.2 mg). **^{1}H NMR** (401 MHz, $CDCl_3$) δ 7.37 (s, 1H), 7.12 – 7.02 (m, 2H), 4.90 (s, 2H), 3.21 – 3.09 (m, 2H), 2.90 – 2.79 (m, 2H), 2.32 (s, 3H), 1.52 (s, 3H). **^{13}C NMR** (101 MHz, $CDCl_3$) δ 145.1, 144.8, 137.3, 134.2, 128.0, 127.6, 121.5, 106.4, 45.2 (2C), 40.6, 26.9, 20.4. **HRMS (*ESI)*** m/z: $[M+H]^+$ calcd. for $C_{13}H_{16}Br$ 251.0430; found 251.0439.

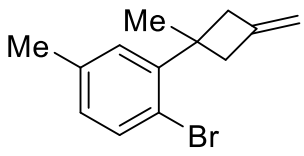

1c. Colourless oil. FC eluent: *n*Hex 100%. Yield = 83% (0.83 mmol, 248.5 mg). **^{1}H NMR** (401 MHz, $CDCl_3$) δ 7.40 (d, *J* = 8.0 Hz, 1H), 6.99 (s, 1H), 6.88 (d, *J* = 8.0 Hz, 1H), 4.90 (s, 2H), 3.24 – 3.09 (m, 2H), 2.93 – 2.78 (m, 2H), 2.32 (s, 3H), 1.53 (s, 3H). **^{13}C NMR** (101 MHz, $CDCl_3$) δ 147.9, 144.8, 137.0, 133.6, 128.7, 128.3, 118.3, 106.3, 45.2 (2C), 40.9, 26.8, 21.0. **HRMS (*ESI)*** m/z: $[M+H]^+$ calcd. for $C_{13}H_{16}Br$ 251.0430; found 251.0435.

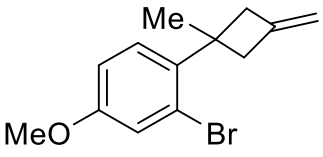

1d. Colourless oil. FC eluent: *n*Hex 100%. Yield = 86% (0.86 mmol, 273.2 mg). **^{1}H NMR** (401 MHz, $CDCl_3$) δ 7.12 – 7.06 (m, 2H), 6.83 (dd, *J* = 8.6, 2.6 Hz, 1H), 4.89 (s, 2H), 3.79 (s, 3H), 3.20 – 3.07 (m, 2H), 2.89 – 2.77 (m, 2H), 1.50 (s, 3H). **^{13}C NMR** (101 MHz, $CDCl_3$) δ 158.1, 144.9, 140.3, 128.2, 121.8, 118.8, 113.3, 106.3, 55.5, 45.3 (2C), 40.3, 27.0. **HRMS (*ESI)*** m/z: $[M+H]^+$ calcd. for $C_{13}H_{16}OBr$ 267.0379; found 267.0367.

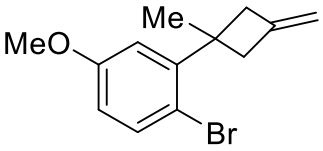

1e Colourless oil. FC eluent: *n*Hex 100%. Yield = 80% (0.83 mmol, 264.0 mg). **^{1}H NMR** (401 MHz, $CDCl_3$) δ 7.42 (d, *J* = 8.7 Hz, 1H), 6.75 (d, *J* = 3.0 Hz, 1H), 6.63 (dd, *J* = 8.7, 3.0 Hz, 1H), 4.92 (s, 2H), 3.81 (s, 3H), 3.24 – 3.09 (m, 2H), 2.93 – 2.76 (m, 2H), 1.54 (s, 3H). **^{13}C NMR** (101 MHz, $CDCl_3$) δ 158.9, 149.4, 144.4, 134.5, 114.3, 112.4, 112.2, 106.5, 55.4, 45.1 (2C), 41.1, 26.7. **HRMS (*ESI)*** m/z: $[M+H]^+$ calcd. for $C_{13}H_{16}OBr$ 267.0379; found 267.0381.

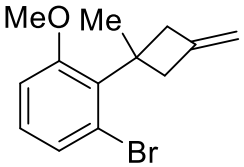

1f. Colourless oil. FC eluent: *n*Hex 100%. Yield = 89% (0.89 mmol, 283.7 mg). **^{1}H NMR** (401 MHz, $CDCl_3$) δ ^{1}H NMR (401 MHz, $cdcl_3$) δ 7.18 (dd, *J* = 8.0, 1.1 Hz, 1H), 7.02 (t, *J* = 8.1 Hz, 1H), 6.83 (dd, *J* = 8.2, 0.9 Hz, 1H), 4.86 (s, 2H), 3.81 (s, 3H), 3.30 – 3.13 (m, 2H), 3.01 – 2.82 (m, 2H), 1.52 (s, 3H). **^{13}C NMR** (101 MHz, $CDCl_3$) δ 158.8, 147.2, 136.3, 127.4, 126.2, 122.5, 110.2, 104.8, 55.4, 47.1 (2C), 40.2, 24.2. **HRMS (*ESI)*** m/z: $[M+H]^+$ calcd. for $C_{13}H_{16}OBr$ 267.0379; found 267.0368.

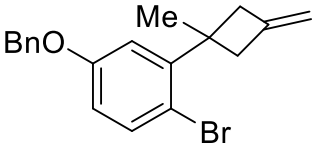

1g. Colourless oil. FC eluent: *n*Hex 100%. Yield = 77% (0.77 mmol, 258.9 mg). **^{1}H NMR** (401 MHz, $CDCl_3$) δ 7.48 – 7.39 (m, 5H), 7.38 – 7.33 (m, 1H), 6.82 (d, *J* = 3.0 Hz, 1H), 6.70 (dd, *J* = 8.7, 3.0 Hz, 1H), 5.05 (s, 2H), 4.90 (s, 2H), 3.20 – 3.09 (m, 2H), 2.89 – 2.80 (m, 2H), 1.52 (s, 3H). **^{13}C NMR** (101 MHz, $CDCl_3$) δ 158.0, 149.4, 144.5, 136.6, 134.5, 128.6 (2C), 128.1, 127.51 (2C), 115.3, 113.30, 112.4, 106.4, 70.2, 45.1 (2C), 41.1, 26.7. **HRMS (*ESI)*** m/z: $[M+H]^+$ calcd. for $C_{19}H_{20}OBr$ 343.0692; found 343.0697

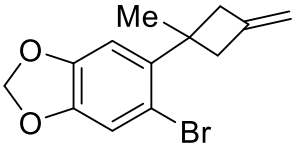

1h. Colourless oil. FC eluent: *n*Hex 100%. Yield = 67% (0.67 mmol, 188.1 mg). **^{1}H NMR** (401 MHz, $CDCl_3$) δ 6.97 (s, 1H), 6.66 (s, 1H), 5.96 (s, 2H), 4.88 (s, 2H), 3.15 – 3.03 (m, 2H), 2.85 – 2.74 (m, 2H), 1.48 (s, 3H). **^{13}C NMR** (101 MHz, $CDCl_3$) δ 147.2, 146.4, 144.5, 141.7, 113.6, 111.7, 107.7, 106.4, 101.6, 45.4 (2C), 41.0, 26.7 **HRMS (*ESI)*** m/z: $[M+H]^+$ calcd. for $C_{14}H_{16}OBr$ 279.0379; found 279.0371.

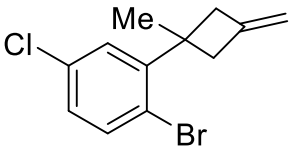

1i. Colourless oil. FC eluent: *n*Hex 100%. Yield = 74% (0.74 mmol, 261.3 mg). **^{1}H NMR** (401 MHz, $CDCl_3$) δ 7.44 (d, *J* = 8.4 Hz, 1H), 7.15 (d, *J* = 2.5 Hz, 1H), 7.04 (dd, *J* = 8.4, 2.6 Hz, 1H), 4.92 (s, 2H), 3.19 – 3.10 (m, 2H), 2.90 – 2.82 (m, 2H), 1.53 (s, 3H). **^{13}C NMR** (101 MHz, $CDCl_3$) δ 150.0, 143.8, 134.9, 133.3, 128.1, 127.5, 119.5, 106.9, 45.0 (2C), 41.0, 26.5. **HRMS (*ESI)*** m/z: $[M+H]^+$ calcd. for $C_{12}H_{13}BrCl$ 270.9884; found 270.9891.

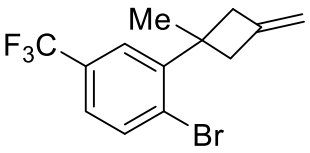

1j. Colourless oil. FC eluent: *n*Hex 100%. Yield = 69% (0.69 mmol, 210.4 mg). **^{1}H NMR** (401 MHz, $CDCl_3$) δ 7.65 (d, *J* = 8.3 Hz, 1H), 7.40 (d, *J* = 1.7 Hz, 1H), 7.31 (dd, *J* = 8.3, 1.9 Hz, 1H), 4.92 (s, 2H), 3.21 – 3.13 (m,

2H), 2.94 – 2.86 (m, 2H), 1.55 (s, 3H). **^{13}C NMR** (101 MHz, $CDCl_3$) δ 149.3, 143.6, 134.5, 129.8 (q, *J* = 32.7 Hz), 125.6 (q, *J* = 1.5 Hz), 124.8 (q, *J* = 3.8 Hz), 124.2 (q, *J* = 3.7 Hz), 124.0 (q, *J* = 273.2 Hz) 107.0, 45.1 (2C), 41.2, 26.5. **^{19}F NMR** (377 MHz, $CDCl_3$) δ -62.6 (s, 3F). **HRMS (*ESI)*** m/z: $[M+H]^+$ calcd. for $C_{13}H_{13}BrF_3$ 305.0147; found 305.0140.

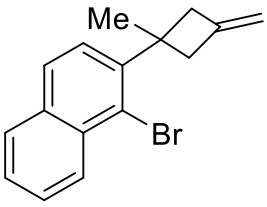

1k. Colourless oil. FC eluent: *n*Hex 100%. Yield = 79% (0.79 mmol, 226.6 mg). **^{1}H NMR** (401 MHz, $CDCl_3$) δ 8.41 (d, *J* = 8.6 Hz, 1H), 7.82 – 7.78 (m, 2H), 7.60 (t, *J* = 7.7 Hz, 1H), 7.51 (t, *J* = 7.5 Hz, 1H), 7.31 (d, *J* = 8.5 Hz, 1H), 4.95 (s, 2H), 3.36 – 3.26 (m, 2H), 3.06 – 2.93 (m, 2H), 1.63 (s, 3H). **^{13}C NMR** (101 MHz, $CDCl_3$) δ 146.2, 144.6, 133.0, 132.8, 127.9, 127.7, 127.4, 126.9, 126.0, 125.6, 121.3, 106.4, 45.8 (2C), 42.2, 26.5. **HRMS (*ESI)*** m/z: $[M+H]^+$ calcd. for $C_{16}H_{16}Br$ 287.0430; found 287.0438.

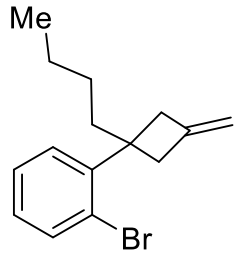

1l. Colourless oil. FC eluent: *n*Hex 100%. Yield = 90% (0.90 mmol, 251.4 mg). **^{1}H NMR** (401 MHz, $CDCl_3$) δ 7.52 (d, *J* = 7.9 Hz, 1H), 7.29 – 7.22 (m, 1H), 7.10 (d, *J* = 7.8 Hz, 1H), 7.05 (td, *J* = 7.6, 1.7 Hz, 1H), 4.86 (s, 2H), 3.17 – 3.07 (m, 2H), 3.00 – 2.82 (m, 2H), 1.94 (bs, 2H), 1.30 – 1.14 (m, 2H), 0.97 (bs, 2H), 0.82 (t, *J* = 7.3 Hz, 3H). **^{13}C NMR** (101 MHz, $CDCl_3$) δ 146.1, 145.3, 133.9, 129.6, 127.4, 126.6, 121.9, 106.1, 44.6, 43.8 (b, 2C), 37.4, 27.4, 23.0, 14.0. **HRMS (*ESI)*** m/z: $[M+H]^+$ calcd. for $C_{15}H_{20}Br$ 279.0743; found 279.0759.

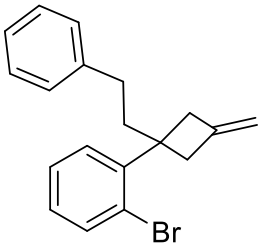

1m. Colourless oil. FC eluent: *n*Hex 100%. Yield = 75% (0.75 mmol, 244.5 mg). **^{1}H NMR** (401 MHz, $CDCl_3$) δ 7.58 (dd, *J* = 7.9, 1.3 Hz, 1H), 7.34 – 7.28 (m, 1H), 7.28 – 7.22 (m, 2H), 7.22 – 7.14 (m, 2H), 7.14 – 7.07 (m, 3H), 4.91 (s, 2H), 3.27 – 3.13 (m, 2H), 3.07 – 2.94 (m, 2H), 2.32 (bs, 4H). **^{13}C NMR** (101 MHz, $CDCl_3$) δ 145.5, 144.7, 142.3, 134.1 (2C), 129.6, 128.2, 128.2, 127.7, 126.7, 125.6 (2C), 121.9, 106.5, 44.7, 43.9 (b, 2C), 39.5, 31.8. **HRMS (*ESI)*** m/z: $[M+H]^+$ calcd. for $C_{19}H_{20}Br$ 327.0743; found 327.0755.

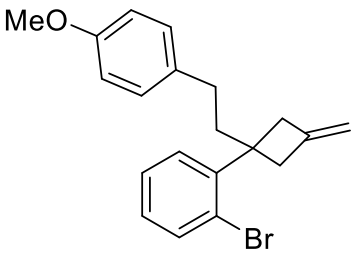

1n. Colourless oil. FC eluent: *n*Hex 100%. Yield = 70% (0.70 mmol, 249.3 mg). **^{1}H NMR** (401 MHz, $CDCl_3$) δ 7.61 – 7.54 (m, 1H), 7.33 – 7.28 (m, 1H), 7.21 – 7.16 (m, 1H), 7.13 – 7.06 (m, 1H), 7.05 – 6.98 (m, 2H), 6.83 – 6.75 (m, 2H), 4.89 (s, 2H), 3.78 (s, 3H), 3.24 – 3.14 (m, 2H), 3.05 – 2.92 (m, 2H), 2.38 – 2.14 (bm, 4H). **^{13}C NMR** (101 MHz, $CDCl_3$) δ 157.6, 145.5, 144.7, 134.3, 134.1, 129.6, 129.1 (2C), 127.6, 126.7, 121.9, 113.7 (2C), 106.4, 55.2, 44.7 (b, 2C), 43.2, 39.7, 30.8. **HRMS (*ESI)*** m/z: $[M+H]^+$ calcd. for $C_{20}H_{22}OBr$ 357.0849; found 357.0851.

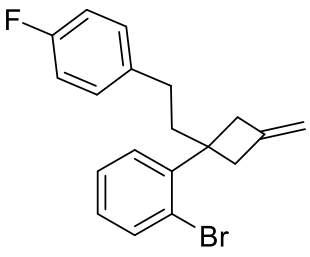

1o. Colourless oil. FC eluent: *n*Hex 100%. Yield = 62% (0.62 mmol, 214.4 mg). **^{1}H NMR** (401 MHz, $CDCl_3$) δ 7.58 (d, *J* = 7.9 Hz, 1H), 7.31 (t, *J* = 7.5 Hz, 1H), 7.19 (dd, *J* = 7.8, 1.6 Hz, 1H), 7.11 (t, *J* = 7.6, 1.7 Hz, 1H), 7.08 – 7.02 (m, 2H), 6.97 – 6.90 (m, 2H), 4.92 (s, 2H), 3.30 – 3.15 (m, 2H), 3.08 – 2.91 (m, 2H), 2.30 (bm, 4H). **^{13}C NMR** (101 MHz, $CDCl_3$) δ 161.1 (d, *J* = 243.1 Hz), 145.3, 144.6, 137.8 (d, *J* = 3.2 Hz), 134.1, 129.6, 129.5 (d, *J* = 7.7 Hz, 2C), 127.7, 126.8, 121.9, 114.9 (d, *J* = 21.1 Hz, 2C), 106.6, 44.7, 43.8 (b, 2C), 39.6, 31.0. **^{19}F NMR** (377 MHz, $CDCl_3$) δ -118.0 (m, 1F). **HRMS (*ESI)*** m/z: $[M+H]^+$ calcd. for $C_{19}H_{19}BrF$ 345.0649; found 345.0645.

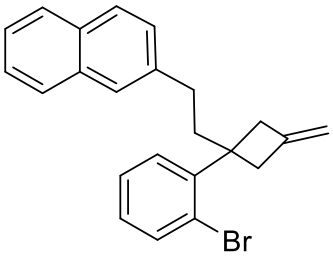

1p. Colourless oil. FC eluent: *n*Hex 100%. Yield = 68% (0.68 mmol, 260.1 mg). **^{1}H NMR** (401 MHz, $CDCl_3$) δ 7.82 – 7.70 (m, 3H), 7.58 (d, *J* = 7.9 Hz, 1H), 7.53 (s, 1H), 7.47 – 7.37 (m, 2H), 7.32 (td, *J* = 7.7, 1.3 Hz, 1H), 7.26 – 7.20 (m, 2H), 7.11 (td, *J* = 7.6, 1.7 Hz, 1H), 4.90 (s, 2H), 3.31 – 3.13 (m, 2H), 3.11 – 2.92 (m, 2H), 2.56 – 2.26 (bm, 4H). **^{13}C NMR** (101 MHz, $CDCl_3$) δ 145.5, 144.7, 139.8, 134.1, 133.6, 131.9, 129.7, 127.7, 127.7 127.5,127.3, 127.3, 126.8, 126.1, 125.8, 125.0, 122.0, 106.5, 44.8, 43.8 (b, 2C), 39.4, 32.0. **HRMS (*ESI)*** m/z: $[M+H]^+$ calcd. for $C_{23}H_{22}Br$ 377.0899; found 377.0905.

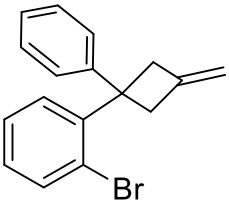

1q. Pale yellow oil. FC eluent: *n*Hex 100%. Yield = 63% (0.63 mmol, 188.8 mg). **^{1}H NMR** (401 MHz, $CDCl_3$) δ 7.56 (d, *J* = 7.9 Hz, 1H), 7.51 (d, *J* = 6.5 Hz, 1H), 7.40 (t, *J* = 8.1 Hz, 1H), 7.34 – 7.24 (m, 4H), 7.23 – 7.11 (m, 2H), 4.95 (s, 2H), 3.62 – 3.52 (m, 2H), 3.50 – 3.38 (m, 2H). **^{13}C NMR** (101 MHz, $CDCl_3$) δ 146.5, 146.4, 143.9, 134.3, 129.3, 128.1 (2C), 128.0, 127.0, 126.1 (2C), 125.8, 123.7, 106.3, 48.3, 46.4 (2C). **HRMS (*ESI)*** m/z: $[M+H]^+$ calcd. for $C_{17}H_{16}Br$ 299.0430; found 299.0425.

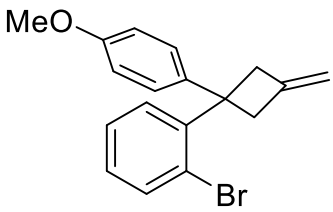

1r.[315] Colourless oil. FC eluent: *n*Hex 100%. Yield = 77% (0.77 mmol, 253.6 mg). **^{1}H NMR** (401 MHz, $CDCl_3$) δ ^{1}H NMR 7.66 (d, *J* = 7.9 Hz, 1H), 7.60 (d, *J* = 7.8 Hz, 1H), 7.47 (t, *J* = 7.5 Hz, 1H), 7.36 (d, *J* = 8.8 Hz, 2H), 7.20 (t, *J* = 7.6 Hz, 1H), 6.95 - 6.92 (m, 2H), 5.08 (s, 2H), 3.85 (s, 3H), 3.71 – 3.61 (m, 2H), 3.59 – 3.45 (m, 2H). **^{13}C NMR** (101 MHz, $CDCl_3$) δ 157.5, 146.6, 143.9, 138.4, 134.1, 129.1, 127.8, 127.1 (2C), 126.9, 123.4, 113.3 (2C), 106.1, 54.9, 47.6, 46.3 (2C). **HRMS (*ESI)*** m/z: $[M+H]^+$ calcd. for $C_{18}H_{18}OBr$ 329.0536; found 329.0541.

[315] Isolated along with about 12% of monochlorinated alkylidene cyclobutane (deriving from the preparation, inseparable mixture). This chlorinated impurity does not affect the catalytic process, nor it is involved in it, therefore the corresponding product **2r** could be easily purified and isolated.

5.1.4 Preparation of Nickel Precatalyst

A flame dried Schlenk tube equipped with a magnetic stirring bar under a continuous N_2 flow was charged with dry THF (5 mL). $NiCl_2$·glyme (0.2 mmol) was added, followed by **L1** (2 equiv, 0.4 mmol, 86.4 mg); the tube was then sealed, and the mixture was refluxed 16 h. The resulting suspension was purified by centrifugation (8000 rpm, 3 min) washing with EtOAc (2 x 10 mL). The obtained complex was then transferred to the final vessel and dried under vacuum for several hours. Complex [Ni(**L1**)$_2$Cl$_2$] was thus obtained as a pale green fine powder in quantitative yield (0.2 mmol, 112.2 mg). The mother liquor from all the washings was evaporated, and the residues were filtered over a short Celite pad and analysed by ^{1}H NMR spectroscopy. If no traces of ligand **L1** were detected, the 1:2 (Ni: **L1**) stoichiometry of the complex was assumed to be correct. Structural elucidation was successively conducted by single-crystal X-ray diffraction analysis (*vide infra*) **(Fig. 67**).

Figure 67. Nickel precatalyst preparation

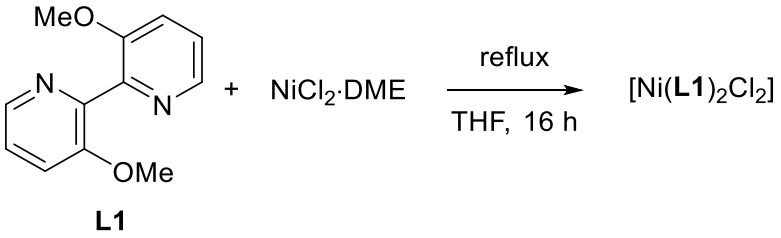

5.1.5 General procedure for the nickel catalyzed reaction

A heat-gun dried Schlenk tube, was charged with anhydrous DMF (1mL), under a constant CO_2 flow; then, under a vigorous stirring (1000 rpm, two magnetic stirring bars) $AlCl_3$ (4.5 equiv, 0.45 mmol, 60.0 mg) was added and the Schlenk tube warmed to 60°C for one minute, in order to solubilize all the solid. The Schlenk tube was then allowed to cool to room temperature. and three vacuum/CO_2 cycles were performed to remove traces of HCl generated. Under a constant flow of CO_2, nickel catalyst [Ni(**L1**)$_2$Cl$_2$] was added (10 mol%, 0.01 mmol, 5.6 mg), followed by the desired starting material **1** (0.1 mmol) and zinc powder (3 equiv, 0.30 mmol, 19.8 mg). A Pasteur pipette connected to the Schlenk line was used to bubble CO_2 in the reaction mixture for ca. 10 seconds and then, the tube was screw capped and warmed at 45°C (**Fig. 68**).

Figure 68. nickel catalyzed reaction set-up.

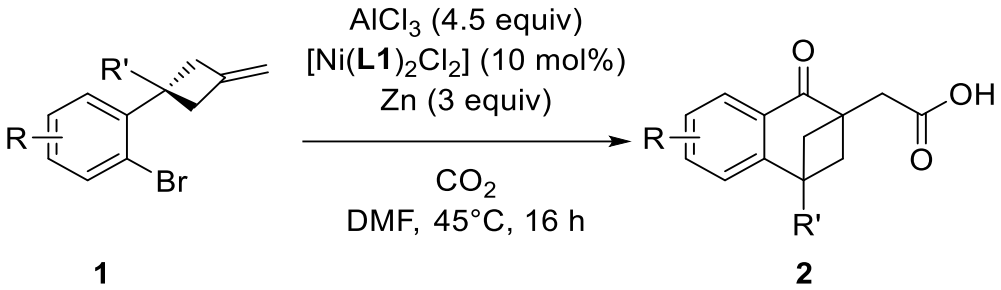

After 16 hours the reaction mixture was quenched with HCl (2 M, 5 mL) and extracted with EtOAc (3 x 5 mL), the organic phase was washed with HCl (0.2 M, 3x15 mL) to remove the DMF, dried over Na_2SO_4 and evaporated *in vacuo*. The crude mixture was purified by flash chromatography on silica gel (FC, hexane: EtOAc mixtures added with 1% HCOOH).

Notes:

- *This nickel catalyzed procedure requires strict control during the set up and is extremely sensitive to air and moisture. We suggest operating a deep cleaning of all apparatus and to thoroughly drying them before use.*
- *Sometimes we observed a white solid formation after $AlCl_3$ addition, exacerbated by air and moisture exposure. If this occurs to a limited extent and just some turbidity is observed the set might go on, otherwise the reaction was not performed if thick insoluble residue were formed.*
- *Zn is added as first reagent to avoid any side reaction prior nickel addition.*

5.1.6 Characterization data of products

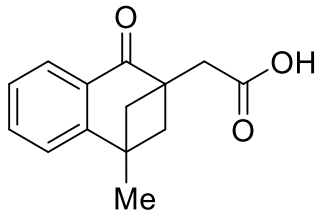

2a. White crystalline solid. FC eluent: *n*Hex/EtOAc 8:2 + 1% HCOOH. Yield = 69% (0.069 mmol, 15.9 mg). **^{1}H NMR** (400 MHz, $CDCl_3$) δ 8.01 (dd, *J* = 7.6, 1.1 Hz, 1H), 7.50 (td, *J* = 7.5, 1.4 Hz, 1H), 7.36 (td, *J* = 7.5, 1.1 Hz, 1H), 7.27 - 7.25 (m, 1H, partially overlapped with the residual solvent signal), 2.79 (s, 2H), 2.72 – 2.62 (m, 2H), 2.55 – 2.47 (m, 2H), 1.56 (s, 3H); the COOH proton signal was not detected. **^{13}C NMR** (101 MHz, $CDCl_3$) δ 201.3, 175.6, 153.5, 133.3, 128.3, 127.0, 126.8, 121.9, 53.5 (2C), 49.1, 39.5, 38.3, 22.1. **HRMS (*ESI)*** m/z: $[M-H]^-$ calcd. for $C_{14}H_{13}O_3$ 229.0870; found 229.0875.

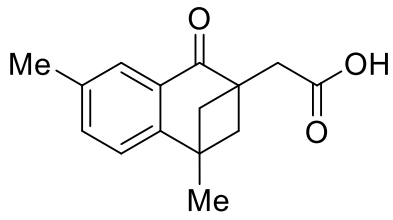

2b. White crystalline solid. FC eluent: *n*Hex/EtOAc 8:2 + 1% HCOOH. Yield = 62% (0.062 mmol, 15.1 mg). **^{1}H NMR** (400 MHz, $CDCl_3$) δ 7.82 (s, 1H), 7.31 (d, *J* = 7.8 Hz, 1H), 7.14 (d, *J* = 7.8 Hz, 1H), 2.78 (s, 2H), 2.66 – 2.59 (m, 2H), 2.53 – 2.45 (m, 2H), 2.39 (s, 3H), 1.54 (s, 3H); the COOH proton signal was not detected. **^{13}C NMR** (101 MHz, $CDCl_3$) δ 201.6, 175.8, 150.8, 136.5, 133.9, 128.1, 127.4, 121.8, 53.7 (2C), 49.1, 39.2, 38.4, 22.1, 20.9. **HRMS (*ESI)*** m/z: $[M-H]^-$ calcd. for $C_{15}H_{15}O_3$ 243.1027; found 243.1033.

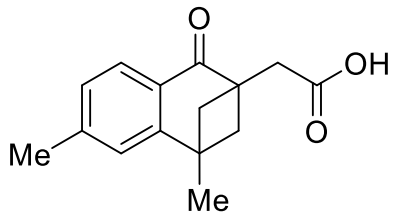

2c. White crystalline solid. FC eluent: *n*Hex/EtOAc 8:2 + 1% HCOOH. Yield = 67% (0.067 mmol, 16.3 mg). **^{1}H NMR** (400 MHz, $CDCl_3$) δ 7.90 (d, *J* = 7.7 Hz, 1H), 7.16 (d, *J* = 7.7 Hz, 1H), 7.05 (s, 1H), 2.77 (s, 2H), 2.66 – 2.59 (m, 2H), 2.52 – 2.46 (m, 2H), 2.42 (s, 3H), 1.54 (s, 3H)¸ the COOH proton signal was not detected. **^{13}C NMR** (101 MHz, $CDCl_3$) δ 201.1, 176.3, 153.6, 144.1, 127.4, 127.1, 125.9, 122.7, 53.5 (2C), 48.9, 39.3, 38.4, 22.1, 22.1. **HRMS (*ESI)*** m/z: $[M-H]^-$ calcd. for $C_{15}H_{15}O_3$ 243.1027; found 243.1022.

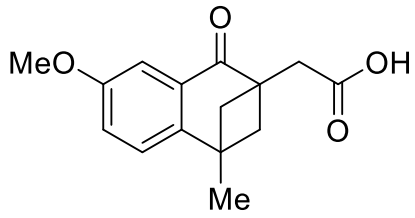

2d. White crystalline solid. FC eluent: *n*Hex/EtOAc 7:3 + 1% HCOOH. Yield = 64% (0.064 mmol, 16.7 mg). **^{1}H NMR** (400 MHz, acetone-d_6) δ 7.45 (d, *J* = 2.8 Hz, 1H), 7.28 (d, *J* = 8.4 Hz, 1H), 7.12 (dd, *J* = 8.4, 2.8 Hz, 1H), 3.88 (s, 3H), 2.74 (s, 2H), 2.63 – 2.53 (m, 4H), 1.56 (s, 3H)¸ the COOH proton signal was not detected. **^{13}C NMR** (101 MHz, acetone-d_6) δ 200.5, 172.5, 159.2, 146.9, 130.2, 123.8, 119.5, 110.9, 55.5, 53.9 (2C), 49.7, 39.4, 38.0, 22.0. **HRMS (*ESI)*** m/z: $[M-H]^-$ calcd. For $C_{15}H_{15}O_4$ 259.0976; found 259.0985.

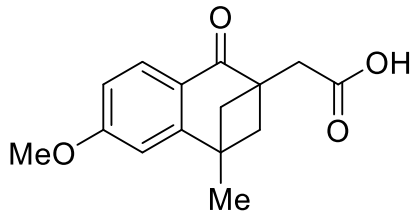

2e. White crystalline solid. FC eluent: *n*Hex/EtOAc 7:3 + 1% HCOOH. Yield = 53% (0.053 mmol, 13.8 mg). **^{1}H NMR** (400 MHz, $CDCl_3$) δ 7.99 (d, *J* = 8.5 Hz, 1H), 6.83 (dd, *J* = 8.5, 2.4 Hz, 1H), 6.74 (d, *J* = 2.4 Hz, 1H), 3.89 (s, 3H), 2.78 (s, 2H), 2.66 – 2.59 (m, 2H), 2.52 – 2.44 (m, 2H), 1.53 (s, 3H)¸ the COOH proton signal was not detected. **^{13}C NMR** (101 MHz, $CDCl_3$) δ 200.6, 175.6, 163.7, 156.0, 129.5, 121.6, 111.1, 108.5, 55.5, 53.4 (2C), 48.7, 39.6, 38.6, 22.1. **HRMS (*ESI)*** m/z: $[M-H]^-$ calcd. for $C_{15}H_{15}O_4$ 259.0976; found 259.0981.

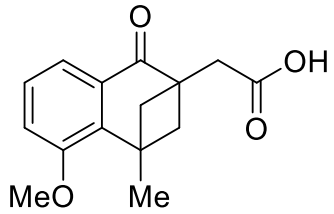

2f. White crystalline solid. FC eluent: *n*Hex/EtOAc 8:3 + 1% HCOOH. Yield = 32% (0.032 mmol, 8.3 mg). **^{1}H NMR** (400 MHz, $CDCl_3$) δ 7.68 (dd, *J* = 7.6, 1.1 Hz, 1H), 7.27 (t, *J* = 7.9 Hz, 1H, partially overlapped with the residual solvent signal), 7.06 (d, *J* = 8.2 Hz, 1H), 3.80 (s, 3H), 2.76 (s, 2H), 2.75 – 2.71 (m, 2H), 2.45 – 2.37 (m, 2H), 1.77 (s, 3H)¸ the COOH proton signal was not detected. **^{13}C NMR** (101 MHz, $CDCl_3$) δ ^{13}C NMR (101 MHz, cdcl$_3$) δ 201.4, 175.6, 156.0, 139.9, 130.5, 127.4, 119.9, 117.8, 55.9, 55.2 (2C), 48.8, 40.4, 38.3, 26.9. **HRMS (*ESI)*** m/z: [M-H]$^-$ calcd. for $C_{15}H_{15}O_4$ 259.0976; found 259.0980.

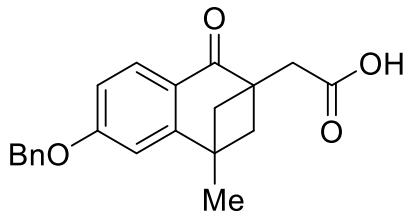

2g. White crystalline solid. FC eluent: *n*Hex/EtOAc 8:2 + 1% HCOOH. Yield = 49% (0.049 mmol, 16.5 mg). **^{1}H NMR** (400 MHz, acetone-d_6) δ 7.87 (d, *J* = 8.4 Hz, 1H), 7.52 (d, *J* = 7.3 Hz, 2H), 7.46 – 7.39 (m, 2H), 7.38 – 7.32 (m, 1H), 7.00 (dd, *J* = 8.4, 2.3 Hz, 1H), 6.91 (d, *J* = 2.3 Hz, 1H), 5.24 (s, 2H), 2.68 (s, 2H), 2.60 – 2.47 (m, 4H), 1.53 (s, 3H)¸ the COOH proton signal was not detected. **^{13}C NMR** (101 MHz, acetone-d_6) δ 199.4, 172.4, 163.1, 156.8, 137.5, 129.1, 129.1 (2C), 128.6, 128.3 (2C), 122.6, 112.6, 109.6, 70.5, 53.2 (2C), 49.1, 40.1, 37.8, 21.9. **HRMS (*ESI)*** m/z: [M-H]$^-$ calcd. for $C_{21}H_{19}O_4$ 335.1289; found 335.1296.

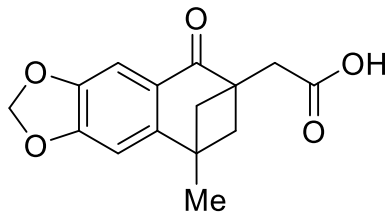

2h. White crystalline solid. FC eluent: *n*Hex/EtOAc 7:3 + 1% HCOOH up to 6:4 + 1% HCOOH. Yield = 74% (0.074 mmol, 20.3 mg). **^{1}H NMR** (400 MHz, acetone-d_6) δ 7.33 (s, 1H), 6.87 (s, 1H), 6.12 (s, 2H), 2.70 (s, 2H), 2.61 – 2.50 (m, 4H), 1.54 (s, 3H)¸ the COOH proton signal was not detected.**^{13}C NMR** (101 MHz, acetone-d_6) δ 199.1, 172.3, 151.9, 151.6, 146.8, 123.3, 106.2, 103.6, 102.3, 54.0 (2C), 49.0, 39.8, 37.7, 22.1. **HRMS (*ESI)*** m/z: [M-H]$^-$ calcd. for $C_{15}H_{13}O_5$ 273.0768; found 273.0762.

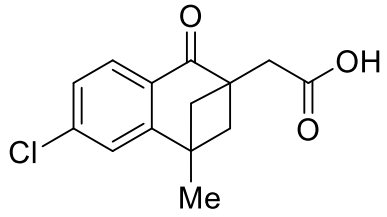

2i. White crystalline solid. FC eluent: *n*Hex/EtOAc 8:2 + 1% HCOOH up to 100% EtOAc + 1% HCOOH. Yield = 62% (0.062 mmol, 16.4 mg). **^{1}H NMR** (400 MHz, DMSO) δ 8.04 – 7.89 (m, 2H), 7.85 (s, 1H), 2.66 (s, 2H), 2.62 – 2.56 (m, 2H), 2.52 – 2.44 (m, 2H), 1.56 (s, 3H)¸ the COOH proton signal was not detected. **^{13}C NMR** (101 MHz, DMSO) δ 200.9, 173.3, 168.5, 154.4, 131.0, 128.4, 126.8, 123.5, 53.5 (2C), 50.0, 41.1, 38.5, 22.5. **HRMS (*ESI)*** m/z: [M-H]$^-$ calcd. for $C_{14}H_{12}{}^{35}ClO_3$ 263.0480; found 263.0477; calcd. for $C_{14}H_{12}{}^{37}ClO_3$ 265.0450; found 265.0439.

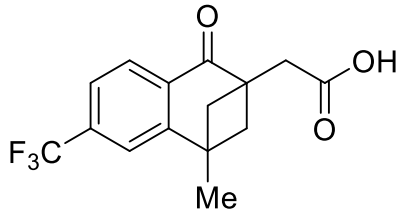

2j. White crystalline solid. FC eluent: *n*Hex/EtOAc 8:2 + 1% HCOOH. Yield = 33% (0.033 mmol, 9.8 mg). **^{1}H NMR** (400 MHz, $CDCl_3$) δ 8.10 (d, *J* = 7.8 Hz, 1H), 7.62 (d, *J* = 7.5 Hz, 1H), 7.49 (s, 1H), 2.78 (s, 2H), 2.70 – 2.62 (m, 2H), 2.58 – 2.47 (m, 2H), 1.59 (s, 3H)¸ the COOH proton signal was not detected. **^{13}C NMR** (101 MHz, $CDCl_3$) δ 199.8, 175.5, 154.1, 134.1, 131.0 (q, J = 1.0 Hz), 127.5, 127.4 (q, J = 190.8 Hz), 123.8 (q, J = 3.9 Hz), 119.1 (q, J = 3.8 Hz), 53.0 (2C), 39.7, 29.7, 21.9. **^{19}F NMR** (377 MHz, $CDCl_3$) δ -63.9 (s, 3F). **HRMS (*ESI)*** m/z: [M-H]$^-$ calcd. For $C_{15}H_{12}O_3F_3$ 297.0744; found 297.0750.

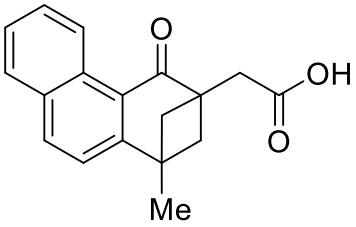

2k. White crystalline solid. FC eluent: *n*Hex/EtOAc 8:2 + 1% HCOOH. Yield = 57% (0.057 mmol, 16.0 mg). **^{1}H NMR** (400 MHz, acetone-d_6) δ 9.62 (d, *J* = 8.2 Hz, 1H), 8.18 (d, *J* = 8.5 Hz, 1H), 8.00 (d, *J* = 8.6 Hz, 1H), 7.68 (t, *J* = 7.1 Hz, 1H), 7.63 (d, *J* = 8.5 Hz, 1H), 7.56 (t, *J* = 7.0 Hz, 1H), 2.81 (s, 2H), 2.80 – 2.74 (m, 2H), 2.70 – 2.62 (m, 2H), 1.70 (s, 3H), the COOH proton signal was not detected. **^{13}C NMR** (101 MHz, acetone-d_6) δ 203.2, 172.5, 157.2, 134.8, 133.8, 132.4, 129.3, 129.2, 126.5, 126.1, 121.5, 121.4, 55.1 (2C), 50.8, 40.6, 38.4, 22.9. **HRMS (*ESI*)** m/z: $[M-H]^-$ calcd. for $C_{18}H_{15}O_3$ 279.1027; found 279.1029.

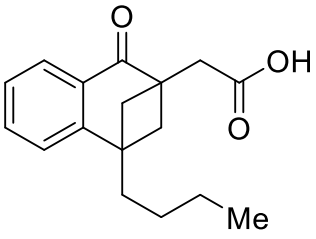

2l. White crystalline solid. FC eluent: *n*Hex/EtOAc 8:2 + 1% HCOOH. Yield = 67% (0.067 mmol, 18.2 mg). **^{1}H NMR** (400 MHz, $CDCl_3$) δ 8.02 (dd, *J* = 7.6, 1.3 Hz, 1H), 7.49 (td, *J* = 7.6, 1.4 Hz, 1H), 7.34 (td, *J* = 7.5, 1.0 Hz, 1H), 7.26 (d, *J* = 7.7 Hz, 1H), 2.78 (s, 2H), 2.63 – 2.55 (m, 2H), 2.55 – 2.46 (m, 2H), 1.93 – 1.85 (m, 2H), 1.51 – 1.35 (m, 4H), 0.99 (t, *J* = 7.0 Hz, 3H), the COOH proton signal was not detected. **^{13}C NMR** (101 MHz, $CDCl_3$) δ 201.1, 176.8, 152.9, 133.1, 128.8, 127.1, 126.6, 122.3, 51.5 (2C), 48.9, 42.8, 38.3, 34.6, 26.8, 23.2, 14.1. **HRMS (*ESI*)** m/z: $[M-H]^-$ calcd. for $C_{17}H_{19}O_3$ 271.1340; found 271.1346.

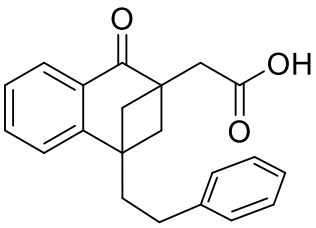

2m. White crystalline solid. FC eluent: *n*Hex/EtOAc 8:2 + 1% HCOOH. Yield = 66% (0.066 mmol, 21.1 mg). **^{1}H NMR** (400 MHz, acetone-d_6) δ 8.00 (d, *J* = 7.5 Hz, 1H), 7.63 (t, *J* = 7.1 Hz, 1H), 7.54 (d, *J* = 7.6 Hz, 1H), 7.46 – 7.34 (m, 5H), 7.25 (t, *J* = 7.0 Hz, 1H), 2.87 – 2.80 (m, 2H), 2.79 (s, 2H), 2.77 – 2.70 (m, 2H), 2.64 – 2.56 (m, 2H), 2.34 – 2.26 (m, 2H); the COOH proton signal was not detected. **^{13}C NMR** (101 MHz, acetone-d_6) δ 200.4, 172.4, 153.3, 142.9, 133.5, 129.7, 129.0 (2C), 128.9 (2C), 127.1, 127.1, 126.4, 123.1, 51.6 (2C), 49.4, 43.3, 37.8, 37.4, 31.3. **HRMS (*ESI*)** m/z: $[M-H]^-$ calcd. for $C_{21}H_{19}O_3$ 319.1340; found 319.1328.

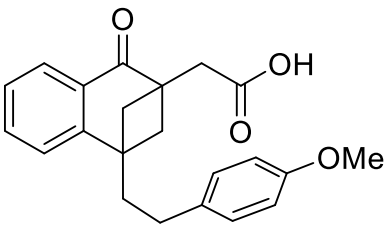

2n. White crystalline solid. FC eluent: *n*Hex/EtOAc 8:2 + 1% HCOOH. Yield = 74% (0.074 mmol, 25.9 mg). **^{1}H NMR** (400 MHz, acetone-d_6) δ 7.93 (d, *J* = 7.5 Hz, 1H), 7.56 (t, *J* = 6.9 Hz, 1H), 7.46 (d, *J* = 7.6 Hz, 1H), 7.38 (t, *J* = 7.5 Hz, 1H), 7.25 (d, *J* = 8.5 Hz, 2H), 6.88 – 6.85 (m, 2H), 3.76 (s, 3H), 2.75 – 2.64 (m, 6H), 2.56 – 2.50 (m, 2H), 2.24 – 2.16 (m, 2H), the COOH proton signal was not detected. **^{13}C NMR** (101 MHz, acetone-d_6) δ 200.4, 172.4, 158.7, 153.4, 134.7, 133.5, 129.8 (2C), 127.1, 127.0, 123.1, 114.4 (2C), 55.1 (2C), 51.6, 49.5, 43.3, 37.8, 37.7, 30.4. **HRMS (*ESI*)** m/z: $[M-H]^-$ calcd. for $C_{22}H_{21}O_4$ 349.1445; found 349.1449.

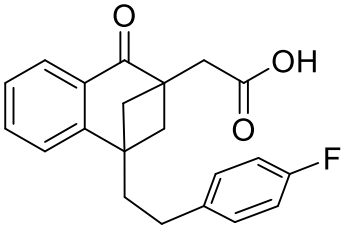

2o. White crystalline solid. FC eluent: *n*Hex/EtOAc 8:2 + 1% HCOOH. Yield = 53% (0.053 mmol, 17.9 mg). **^{1}H NMR** (400 MHz, , acetone-d_6) δ 7.99 (d, *J* = 7.6 Hz, 1H), 7.62 (t, *J* = 7.5 Hz, 1H), 7.53 (d, *J* = 7.6 Hz, 1H), 7.46 – 7.42 (m, 3H), 7.14 – 7.10 (m, 2H), 2.88 – 2.81 (m, 2H), 2.80 – 2.70 (m, 4H), 2.63 – 2.55 (m, 2H), 2.33 – 2.25 (m, 2H), the COOH proton signal was not detected. **^{13}C NMR** (101 MHz, acetone-d_6) δ ^{13}C NMR (101 MHz, acetone-d_6) δ 200.4, 172.4, 161.9 (d, *J* = 241.6 Hz), 153.3, 139.0 (d, *J* =

3.2 Hz), 133.6, 130.6 (d, *J* = 7.9 Hz, 2C), 129.7, 127.2, 127.1, 123.1, 115.5 (d, *J* = 21.1 Hz, 2C), 51.6 (2C), 49.5, 43.3, 37.8, 37.5, 30.5. **^{19}F NMR** (377 MHz, acetone-d_6) -119.17 – -119.30 (m, 1F). **HRMS (*ESI)*** m/z: $[M-H]^-$ calcd. for $C_{21}H_{18}FO_3$ 337.1245; found 337.1237.

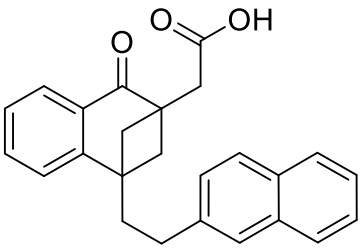

2p. White crystalline solid. FC eluent: *n*Hex/EtOAc 8:2 + 1% HCOOH. Yield = 58% (0.058 mmol, 21.5 mg). **^{1}H NMR** (400 MHz, acetone-d_6) δ 8.01 (d, *J* = 7.5 Hz, 1H), 7.97 – 7.85 (m, 4H), 7.67 – 7.55 (m, 3H), 7.55 – 7.41 (m, 3H), 3.05 – 2.96 (m, 2H), 2.86 – 2.74 (m, 4H), 2.68 – 2.60 (m, 2H), 2.45 – 2.36 (m, 2H), the COOH proton signal was not detected. **^{13}C NMR** (101 MHz, acetone-d_6) δ 200.4, 172.4, 153.4, 140.6, 134.5, 133.6, 132.9, 129.8, 128.6, 128.2, 128.0, 128.0, 127.2, 127.1, 126.8, 126.5, 125.8, 123.2, 51.7 (2C), 49.5, 43.4, 37.9, 37.3, 31.5. **HRMS (*ESI)*** m/z: $[M-H]^-$ calcd. for $C_{25}H_{21}O_3$ 369.1496; found 369.1506.

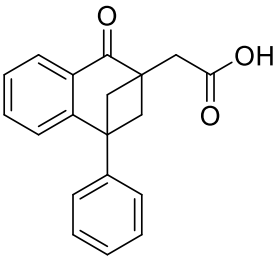

2q. White crystalline solid. FC eluent: *n*Hex/EtOAc 8:2 + 1% HCOOH. Yield = 67% (0.067 mmol, 19.6 mg). **^{1}H NMR** (400 MHz, acetone-d_6) δ 8.03 – 7.96 (m, 1H), 7.53 – 7-50 (m, 2H), 7.44 – 7.39 (m, 3H), 7.30 – 7.28 (m, 2H), 6.52 – 6.45 (m, 1H), 3.14 – 3.06 (m, 2H), 3.03 – 2.96 (m, 2H), 2.84 (s, 2H), the COOH proton signal was not detected. **^{13}C NMR** (101 MHz, acetone-d_6) δ 199.9, 172.4, 155.1, 144.5, 133.4, 129.3 (2C), 129.1, 127.5, 127.4, 127.1 (2C), 126.9, 124.7, 52.4 (2C), 49.6, 48.1, 37.7. **HRMS (*ESI)*** m/z: $[M-H]^-$ calcd. for $C_{19}H_{15}O_3$ 291.1027; found 291.1033.

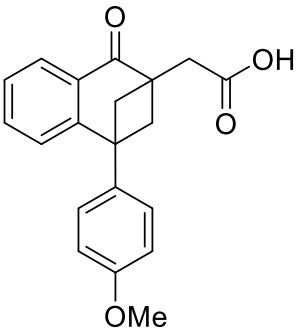

2r. White crystalline solid. FC eluent: *n*Hex/EtOAc 7:3 + 1% HCOOH. Yield = 45% (0.045 mmol, 14.5 mg). **^{1}H NMR** (400 MHz, $CDCl_3$) δ 8.06 – 7.99 (m, 1H), 7.36 – 7.28 (m, 2H), 7.10 – 7-07 (m, 2H), 6.99 – 6-96 (m, 2H), 6.58 – 6.46 (m, 1H), 3.87 (s, 3H), 3.13 – 3.02 (m, 2H), 2.91 – 2.85 (m, 2H), 2.81 (s, 2H), the COOH proton signal was not detected. **^{13}C NMR** (101 MHz, $CDCl_3$) δ 200.5, 175.8, 158.5, 154.3, 135.3, 133.1, 128.0, 127.5 (2C), 126.9, 126.9, 124.3, 114.1 (2C), 55.3 (2C), 52.4, 49.0, 47.0, 29.7. **HRMS (*ESI)*** m/z: $[M+Na]^+$ calcd. for $C_{20}H_{18}O_4Na$ 345.1097; found 345.1094. **HRMS (*ESI)*** m/z: $[M-H]^-$ calcd. for $C_{20}H_{17}O_4$ 321.1132; found 321.1126.

5.2 Synthesis of Benzolactams and Benzolactones

Further relevant information can be found in the SI document of the following work:

Direct Access to Benzolactams and Benzolactones via Nickel Catalyzed Carbonylation with CO_2

R. Giovanelli, G. Monda, S. Kiriakidi, C. Silva López, G. Bertuzzi, M. Bandini,

Chem. Eur. J. **2024**, 30, e202401658.

DOI: 10.1002/chem.202401658

5.2.1 General DFT information

All calculations were computed employing Density Functional Theory (DFT) as implemented in the Gaussian 16 code[316]. The systems were described using the M06[307]/def2svpp[308] level of theory. The structures were fully optimized to either minima or transition states (TSs). The nature of all optimized structures (as minima or TSs) was determined using analysis of the normal modes via diagonalization of the Hessian matrix. In the absence of imaginary frequencies, the corresponding structures were characterized as minima, whereas the structures with exactly one imaginary frequency, connecting the suggested reactants and products were characterized as TSs. The stability of the wave function was also examined in order to verify that the computed wavefunctions are minima in the configuration space of the basis sets used[311]. All geometry optimizations have been optimized using tight convergence criteria in the SCF and an ultrafine grid to guarantee the accuracy of the reported results. The *N*,*N*-dimethylformamide, abbreviated as DMF, was used as the solvent, while solvent effects were modelled using the polarizable continuum model (PCM)[309] with the default parameters implemented in the Gaussian 16 package. The reported thermochemistry values (ΔG and ΔG^{++}) were computed considering 1.0 atm and 298 K to simulate the reaction conditions.

[316] Gaussian 16, Revision C.01, M. J. Frisch, G. W. Trucks, H. B. Schlegel, G. E. Scuseria, M. A. Robb, J. R. Cheeseman, G. Scalmani, V. Barone, G. A. Petersson, H. Nakatsuji, X. Li, M. Caricato, A. V. Marenich, J. Bloino, B. G. Janesko, R. Gomperts, B. Mennucci, H. P. Hratchian, J. V. Ortiz, A. F. Izmaylov, J. L. Sonnenberg, D. Williams-Young, F. Ding, F. Lipparini, F. Egidi, J. Goings, B. Peng, A. Petrone, T. Henderson, D. Ranasinghe, V. G. Zakrzewski, J. Gao, N. Rega, G. Zheng, W. Liang, M. Hada, M. Ehara, K. Toyota, R. Fukuda, J. Hasegawa, M. Ishida, T. Nakajima, Y. Honda, O. Kitao, H. Nakai, T. Vreven, K. Throssell, J. A. Montgomery, Jr., J. E. Peralta, F. Ogliaro, M. J. Bearpark, J. J. Heyd, E. N. Brothers, K. N. Kudin, V. N. Staroverov, T. A. Keith, R. Kobayashi, J. Normand, K. Raghavachari, A. P. Rendell, J. C. Burant, S. S. Iyengar, J. Tomasi, M. Cossi, J. M. Millam, M. Klene, C. Adamo, R. Cammi, J. W. Ochterski, R. L. Martin, K. Morokuma, O. Farkas, J. B. Foresman, and D. J. Fox, Gaussian, Inc., Wallingford CT, 2016.

5.2.2 General procedures for starting materials preparation.

The synthesis of the starting materials **10** was conducted via reductive amination of the corresponding 2-bromobenzaldehydes (or 2-bromoacetophenones) **MM-2** with the desired anilines **MM-3**. The reaction conditions employed have been adapted depending on the aniline and aldehydes reactivity. Starting materials **10a**,[317] **10d, 10f, 10t**,[318], **10g**,[319] **10j**,[320] **10m**,[321], **10u, 10x**[322] **10w**,[323] are already known in literature.

5.2.2.1 Procedure A1

In a 100 mL round bottom flask, the desired 2-bromobenzaldehyde **MM-2** (3 mmol) was dissolved in DCM (10 mL), the desired aniline **MM-3** (3.6 mmol, 1.2 equiv) and glacial acetic acid (4.5 mmol, 1.5 equiv) were then added. The reaction was stirred at room temperature until TLC confirmed complete consumption of **MM-2**. The reaction mixture was then evaporated *in vacuo*, leaving the crude imine **MM-4** to be directly used for the following step. (**Fig. 69**).

Figure 69. Imine formation procedure

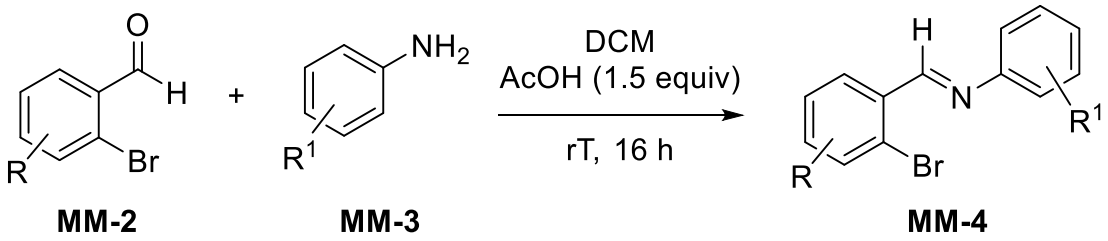

5.2.2.2 Procedure A2:

In a 100 mL round bottom flask, the desired 2-bromobenzaldehyde or 2-bromoacetophenone **MM-2** (3 mmol) was dissolved in DCM (10 mL), the desired aniline **MM-3** (3.6 mmol, 1.2 equiv) and glacial acetic acid (4.5 mmol, 1.5 equiv) were then added. The reaction was then stirred for 16 hours at 70 °C, then evaporated *in vacuo*, leaving the crude imine **MM-4** to be directly used for the following step. (**Fig. 70**).

Figure 70. High temperature imine formation procedure

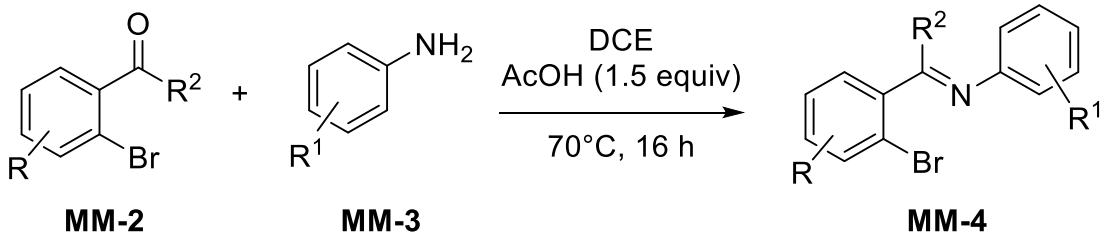

[317] Jiang, M., Li, J., Wang, F., Zhao, Y., Zhao, F., Dong, X., Zhao, W., *Org. Lett.* **2012**, 14, 6, 1420–1423
[318] Glas, C., Wirawan, R., Bracher, F., *Synthesis* **2021**, 53, 11, 1943-1954
[319] De, S., Mishra, S., Kakde, B.N., Dey, D., Bisai, A., *J. Org. Chem*. **2013**, 78, 16, 7823–7844
[320] Linsenmeier, A.M., Williams, C.M., Bräse, S., *European Journal of Organic Chemistry* **2013**, 18, 3847-3856
[321] Chen, K., Pullarkat, S.A., *Org. Biomol. Chem.* **2012**, 10, 6600-6606
[322] De, S., Ghosh, S., Bhunia, S., Sheikh, J.A., Bisai, A., *Org. Lett.* **2012**, 14, 17, 4466–4469
[323] Chelouan, A., Recio, R., Borrego, L.G., Alvarez, E., Khiar, N., Fernandez, I., *Org. Lett.;* **2016**, 18, 13, 3258–3261

5.2.2.3 Procedure B: *(for imine reduction).*

In a round bottom flask, crude imine **MM-4** was dissolved in 7 mL of glacial acetic acid and the mixture was cooled to 0 °C. Then $NaBH_4$ (6 mmol, 2 equiv.) was slowly added to reaction mixture (fast and exothermic hydrogen gas evolution!), and it was stirred for 4 hours at room temperature. After TLC showed complete consumption of **MM-4**, acetic acid was removed *in vacuo*. Then, water (10 mL) and DCM (20 mL) were added, and the pH of the biphasic mixture was adjusted to 12 by addition of NaOH (6M). Then the basic aqueous phase was extracted three times with DCM (20 mL) and the organic phase dried over Na_2SO_4. The crude starting material **1** was then purified via silica gel flash chromatography (**Fig. 71**).

Figure 71. Imine, reduction step.

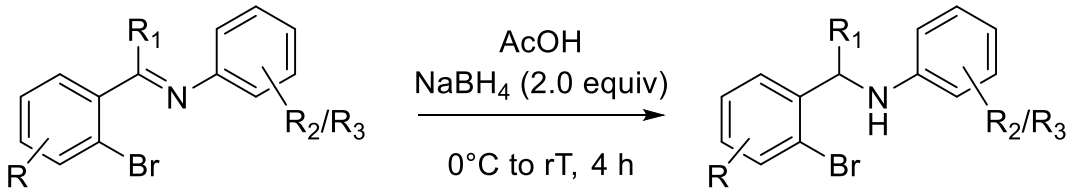

MM-4 **10**

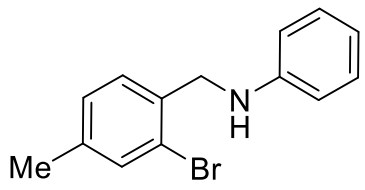

10b. Obtained following **Procedures A1** and **B**. White solid. FC eluent: *n*Hex/EtOAc 25:1. Yield = 78% (2.34 mmol, 646 mg). **^{1}H NMR** (400 MHz, $CDCl_3$) δ 7.43 (s, 1H), 7.28 (d, *J* = 7.8 Hz, 1H), 7.22 – 7.18 (m, 2H), 7.06 (d, *J* = 7.8 Hz, 1H), 6.72 (t, *J* = 7.4 Hz, 1H), 6.65 – 6.64 (m, 2H), 4.39 (s, 2H), 4.22 (bs, 1H), 2.34 (s, 3H). **^{13}C NMR** (101 MHz, $CDCl_3$) δ 147.7, 138.8, 135.0, 133.2, 129.2 (2C), 129.0, 128.3, 123.0, 117.7, 113.0 (2C), 48.1, 20.6. **HRMS *(ESI)*** m/z $[M+H]^+$ calcd. for $C_{14}H_{15}BrN$ 276.0382; found 276.0388. **m.p.** 69 - 70 °C.

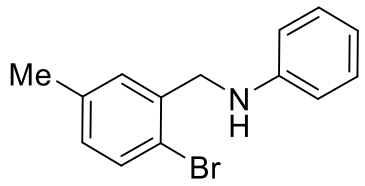

10c. Obtained following **Procedures A1** and **B**. Pale yellow oil. FC eluent: *n*Hex/EtOAc 25:1. Yield = 82% (2.46 mmol, 680 mg). **^{1}H NMR** (400 MHz, $CDCl_3$) δ 7.46 (d, *J* = 8.1 Hz, 1H), 7.25 – 7.18 (m, 3H), 6.97 (dd, *J* = 8.3, 2.3 Hz, 1H), 6.77 – 6.74 (m, 1H), 6.67 – 6.65 (m, 2H), 4.38 (s, 2H), 4.21 (bs, 1H), 2.29 (s, 3H). **^{13}C NMR** (101 MHz, $CDCl_3$) δ 147.8, 137.7, 137.5, 132.5, 130.0, 129.5, 129.2 (2C), 119.9, 117.8, 113.0 (2C), 48.5, 21.0. **HRMS *(ESI)*** m/z $[M+H]^+$ calcd. for $C_{14}H_{15}BrN$ 276.0382; found 276.0387.

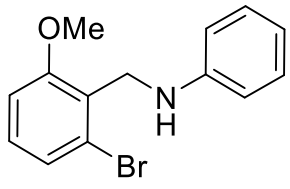

10e. Obtained following **Procedures A2** and **B**. Pale yellow oil. FC eluent: *n*Hex/EtOAc 20:1. Yield = 69% (2.07 mmol, 604 mg). **^{1}H NMR** (400 MHz, $CDCl_3$) δ 7.22 – 7.18 (m, 3H), 7.12 (t, *J* = 8.1 Hz, 1H), 6.85 (dd, *J* = 8.2, 1.2 Hz, 1H), 6.80 – 6.79 (m, 2H), 6.73 (tt, *J* = 7.3, 1.2 Hz, 1H), 4.51 (s, 2H), 3.87 (s, 3H). The NH peak was not detected in the spectrum **^{13}C NMR** (101 MHz, $CDCl_3$) δ 158.8, 148.1, 129.5, 129.1 (2C), 127.1, 125.8, 125.1, 117.7, 113.7 (2C), 109.9, 55.9, 42.9. **HRMS *(ESI)*** m/z $[M+H]^+$ calcd. for $C_{14}H_{15}BrNO$ 292.0332; found 292.0335.

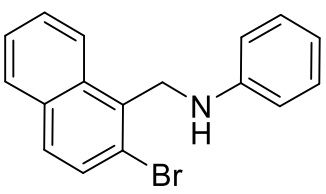

10h. Obtained following **Procedures A2** and **B**. White solid. **m.p.** 99 - 101 °C. FC eluent: *n*Hex/EtOAc 25:1. Yield = 71% (2.13 mmol, 665 mg). **^{1}H NMR** (400 MHz, $CDCl_3$) δ 8.38 (d, *J* = 8.5 Hz, 1H), 7.83 (dd, *J* = 8.1, 1.3 Hz, 1H), 7.78 (d, *J* = 8.4 Hz, 1H), 7.63 (ddd, *J* = 8.5, 6.8, 1.4 Hz, 1H), 7.59 – 7.49 (m, 2H), 7.25 – 7.16 (m, 2H), 6.81 – 6.72 (m, 1H), 6.70 – 6.64 (m, 2H), 4.66 (s, 2H), 4.37 (bs, 1H). **^{13}C NMR** (101 MHz, $CDCl_3$) δ 147.7, 136.5, 133.9, 132.4, 129.3 (2C), 128.1, 127.8, 127.4, 126.9, 126.3, 126.2, 123.0, 117.8, 113.0 (2C), 49.4. **HRMS *(ESI)*** m/z $[M+H]^+$ calcd. for $C_{17}H_{15}BrN$ 312.0382; found 312.0390.

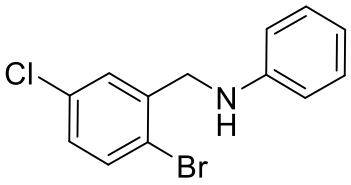

10i. Obtained following **Procedures A1** and **B**. Pale yellow oil. FC eluent: *n*Hex/EtOAc 25:1. Yield = 92% (2.76 mmol, 814 mg). **^{1}H NMR** (400 MHz, $CDCl_3$) δ 7.50 (d, *J* = 8.4 Hz, 1H), 7.43 (d, *J* = 2.6 Hz, 1H), 7.22 – 7.18 (m, 2H7.13 (dd, *J* = 8.4, 2.6 Hz, 1H), 6.79 – 6.75 (m, 1H), 6.62 – 6.60 (m, 2H), 4.39 (s, 2H), 1.57 (bs, 1H). **^{13}C NMR** (101 MHz, $CDCl_3$) δ 147.2, 140.1, 133.8, 133.8, 129.4 (2C), 128.9, 128.7, 120.8, 118.2, 113.1 (2C), 48.4. **HRMS *(ESI)*** m/z $[M+H]^+$ calcd. for $C_{13}H_{12}BrClN$ 295.9836; found 295.9841.

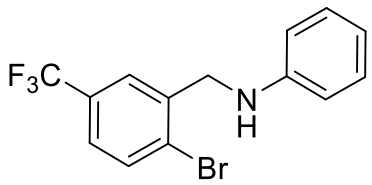

10k. Obtained following **Procedures A1** and **B**. White solid. **m.p.** 87 - 89 °C. FC eluent: *n*Hex/EtOAc 25:1. Yield = 83% (2.49 mmol, 822 mg). **^{1}H NMR** (600 MHz, $CDCl_3$) δ 7.73 - 7.72 (m, 2H), 7.42 (dd, *J* = 8.4, 2.5 Hz, 1H), 7.23 – 7.20 (m, 2H), 6.79 (t, *J* = 7.4 Hz, 1H), 6.64 – 6.62 (m, 2H), 4.47 (s, 2H), 4.26 (bs, 1H). **^{13}C NMR** (101 MHz, $CDCl_3$) δ 147.3, 139.6, 133.3, 130.1 (q, *J* = 32.9 Hz), 129.4 (2C), 126.9, 125.8 (q, *J* = 3.7 Hz), 125.3 (q, *J* = 3.6 Hz), 123.8 (q, *J* = 272.3 Hz) 118.3, 113.0 (2C), 48.5. **^{19}F NMR** (565 MHz, $CDCl_3$) δ -62.59. **HRMS *(ESI)*** m/z $[M+H]^+$ calcd. for $C_{14}H_{12}BrF_3N$ 330.0100; found 330.0105.

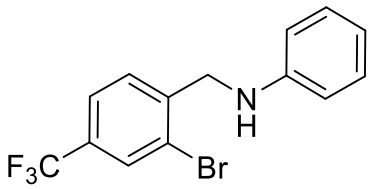

10l. Obtained following **Procedures A1** and **B**. Pale yellow oil. FC eluent: *n*Hex/EtOAc 25:1. Yield = 75% (2.25 mmol, 743 mg). **^{1}H NMR** (400 MHz, $CDCl_3$) δ 7.86 (s, 1H), 7.57 – 7.51 (m, 2H), 7.22 – 7.18 (m, 2H), 6.77 (tt, *J* = 7.4, 1.1 Hz, 1H), 6.60 – 6.58 (m, 2H), 4.47 (s, 2H), 4.32 (bs, 1H). **^{13}C NMR** (101 MHz, $CDCl_3$) δ 147.2, 142.5, 130.8 (q, *J* = 33.1 Hz), 129.7 (q, *J* = 3.9 Hz), 129.4 (2C), 129.0, 124.4 (q, *J* = 3.7 Hz), 123.2 (q, *J* = 272.4 Hz), 123.0, 118.2, 112.9 (2C), 48.3. **^{19}F NMR** (376 MHz, $CDCl_3$) δ -62.58. **HRMS *(ESI)*** m/z $[M+H]^+$ calcd. for $C_{14}H_{12}BrF_3N$ 330.0100; found 330.0095.

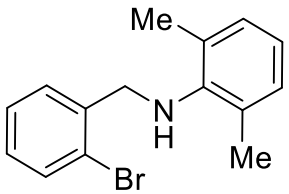

10n. Obtained following **Procedures A2** and **B**. Colourless oil. FC eluent: *n*Hex/EtOAc 25:1. Yield = 49% (1.47 mmol, 368 mg). **^{1}H NMR** (600 MHz, $CDCl_3$) δ 7.60 (dd, J = 7.9, 1.2 Hz, 1H), 7.39 (dd, J = 7.6, 1.7 Hz, 1H), 7.28 (td, J = 7.5, 1.2 Hz, 1H), 7.16 (td, J = 7.7, 1.7 Hz, 1H), 7.03 – 7.01 (m, 2H), 6.91 – 6.84 (m, 1H), 4.23 (s, 2H), 3.49 (bs, 1H), 2.29 (s, 6H). **^{13}C NMR** (151 MHz, $CDCl_3$) δ 145.3 (2C), 139.4, 132.8, 130.2, 130.1, 128.8 (2C + 1C overlapped), 127.5, 123.8, 122.4, 52.5, 18.4 (2C). **HRMS *(ESI)*** m/z $[M+H]^+$ calcd. for $C_{15}H_{17}BrN$ 250.0539; found 250.0543.

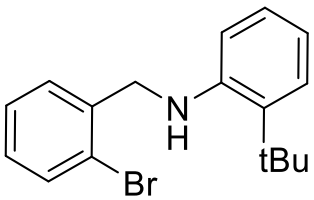

10o. Obtained following **Procedures A2** and **B**. White solid. **m.p.** 116 - 118 °C. FC eluent: *n*Hex/EtOAc 25:1. Yield = 44% (1.32 mmol, 420 mg). **^{1}H NMR** (400 MHz, $CDCl_3$) δ 7.60 (dd, *J* = 7.9, 1.3 Hz, 1H), 7.42 (dd, *J* = 7.7, 1.8 Hz, 1H), 7.33 – 7.24 (m, 2H), 7.16 (td, *J* = 7.6, 1.8 Hz, 0H), 7.10

(ddd, *J* = 8.0, 7.2, 1.6 Hz, 1H), 6.73 (ddd, *J* = 7.8, 7.2, 1.3 Hz, 1H), 6.56 (dd, *J* = 8.1, 1.3 Hz, 1H), 4.49 (s, 2H), 4.43 (bs, 1H), 1.48 (s, 9H). **^{13}C NMR** (101 MHz, $CDCl_3$) δ 145.6, 138.3, 133.3, 132.8, 129.2, 128.7, 127.6, 127.2, 126.3, 123.3, 117.5, 112.0, 48.9, 34.2, 30.0 (3C). **HRMS *(ESI)*** m/z $[M+H]^+$ calcd. for $C_{17}H_{21}BrN$ 318.0852; found 318.0860.

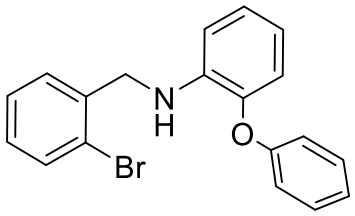

10p. Obtained following **Procedures A2** and **B**. White solid. **m.p.** 133 - 135 °C. FC eluent: *n*Hex/EtOAc 25:1. Yield = 55% (1.65 mmol, 354 mg). **^{1}H NMR** (600 MHz, $CDCl_3$) δ 7.56 (d, *J* = 7.9 Hz, 1H), 7.38 – 7.30 (m, 3H), 7.25 (t, *J* = 7.5 Hz, 1H), 7.13 (dd, *J* = 8.6, 6.8 Hz, 1H), 7.09 (t, *J* = 7.3 Hz, 1H), 7.05 – 6.98 (m, 3H), 6.90 (dd, *J* = 7.9, 1.6 Hz, 1H), 6.68 (td, *J* = 7.7, 1.6 Hz, 1H), 6.64 (dd, *J* = 8.1, 1.7 Hz, 1H), 4.80 (bs, 1H), 4.46 (s, 2H). **^{13}C NMR** (151 MHz, $CDCl_3$) δ 157.6, 143.0, 139.9, 138.0, 132.8, 129.8, 129.7, 128.8, 128.6, 127.5, 125.0, 125.0, 123.2, 122.8, 122.8, 119.4, 119.4, 117.4, 117.4, 117.2, 111.8, 47.9. **HRMS *(ESI)*** m/z $[M+H]^+$ calcd. for $C_{19}H_{17}BrNO$ 354.0488; found 354.0486.

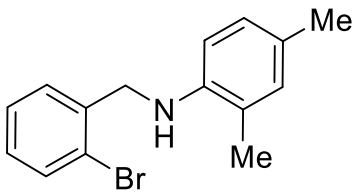

10q. Obtained following **Procedures A2** and **B**. White solid. **m.p.** 111 - 113 °C. FC eluent: *n*Hex/EtOAc 25:1. Yield = 48% (1.44 mmol, 418 mg). **^{1}H NMR** (400 MHz, $CDCl_3$) δ 7.58 (dd, *J* = 7.9, 1.3 Hz, 1H), 7.41 (d, *J* = 7.6 Hz, 1H), 7.27 (td, *J* = 7.6, 1.3 Hz, 1H, partially overlapped with the residual solvent peak), 7.14 (td, *J* = 7.7, 1.8 Hz, 1H), 6.93 (d, *J* = 2.1 Hz, 1H), 6.89 (dd, *J* = 8.2, 2.2 Hz, 1H), 6.46 (d, *J* = 8.1 Hz, 1H), 4.45 (s, 2H), 2.24 (s, 3H), 2.21 (s, 3H). The NH signal was not detected in the spectrum **^{13}C NMR** (101 MHz, $CDCl_3$) δ 150.4, 147.1, 144.5, 142.2, 136.4, 132.8, 131.0, 129.3, 128.6, 127.5, 127.4, 123.4, 48.7, 20.3, 17.5. **HRMS *(ESI)*** m/z $[M+H]^+$ calcd. for $C_{15}H_{17}BrN$ 290.0539; found 290.0532.

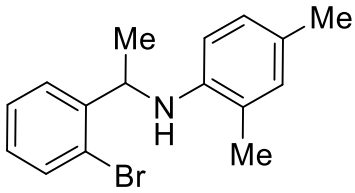

10r. Obtained following **Procedures A2** and **B**. White solid. **m.p.** 103 - 105 °C. FC eluent: *n*Hex/EtOAc 25:1. FC eluent: *n*-hexane/EtOAc 40:1. Yield = 39% (1.17 mmol, 356 mg). **^{1}H NMR** (400 MHz, $CDCl_3$) δ 7.58 (dd, *J* = 7.9, 1.3 Hz, 1H), 7.44 (dd, *J* = 7.8, 1.8 Hz, 1H), 7.24 (td, *J* = 7.5, 1.3 Hz, 1H), 7.10 (td, *J* = 7.6, 1.8 Hz, 1H), 6.91 (s, 1H), 6.78 (dd, *J* = 8.1, 2.2 Hz, 1H), 6.12 (d, *J* = 8.1 Hz, 1H), 4.88 (q, J = 6.6 Hz, 1H), 3.86 (bs, 1H), 2.26 (s, 3H), 2.20 (s, 3H), 1.55 (d, J = 6.6 Hz, 3H). **^{13}C NMR** (101 MHz, $CDCl_3$) δ 143.7, 142.3, 133.0, 130.8, 128.3, 128.0, 127.3, 126.8, 126.1, 122.7, 121.6, 111.1, 52.7, 23.3, 20.3, 17.6. **HRMS *(ESI)*** m/z $[M+H]^+$ calcd. for $C_{16}H_{19}BrN$ 304.0695; found 304.0703.

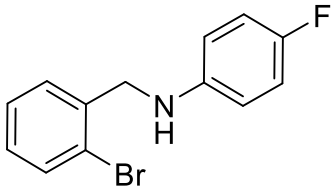

10s. Obtained following **Procedures A2** and **B**. Pale yellow oil. FC eluent: *n*Hex/EtOAc 25:1. Yield = 61% (1.83 mmol, 512 mg). **^{1}H NMR** (400 MHz, $CDCl_3$) δ 7.57 (d, *J* = 8.0 Hz, 1H), 7.38 (d, *J* = 7.7 Hz, 1H), 7.26 (t, *J* = 7.7 Hz, 1H), 7.13 (td, *J* = 7.7, 1.8 Hz, 1H), 6.90 – 6.85 (m, 2H), 6.55 – 6.52 (m, 2H), 4.36 (s, 2H), 4.08 (bs, 1H). **^{13}C NMR** (101 MHz, $CDCl_3$) δ 155.9 (d, *J* = 235.6 Hz), 144.0, 137.9, 132.8, 129.1, 128.7, 127.5, 123.3, 115.7 (d, *J* = 22.4 Hz, 2C), 113.8 (d, *J* = 7.4 Hz, 2C), 49.0. **^{19}F NMR** (376 MHz, $CDCl_3$) δ -127.46. **HRMS *(ESI)*** m/z $[M+H]^+$ calcd. for $C_{13}H_{12}BrFN$ 280.0132; found 280.0133.

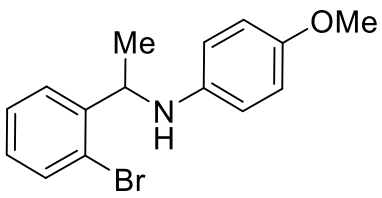

10y. Obtained following **Procedures A2** and **B**. Pale yellow oil. FC eluent: *n*Hex/EtOAc 25:1. Yield = 43% (1.29 mmol, 395 mg). **^{1}H NMR** (400 MHz, $CDCl_3$) δ 7.57 (dd, *J* = 8.0, 1.3 Hz, 1H), 7.47 (dd, *J* = 7.8, 1.7 Hz, 1H), 7.25 (tdd, *J* = 7.8, 1.4, 0.6 Hz, 1H), 7.09 (ddd, *J* = 7.9, 7.3, 1.8 Hz, 1H), 6.72 – 6.70 (m, 2H), 6.43 – 6.41 (m, 2H), 4.81 (q, J = 6.6 Hz, 1H), 3.93 (bs, 1H), 3.70 (s, 3H), 1.49 (d, J = 6.6 Hz, 3H). **^{13}C NMR** (101 MHz, $CDCl_3$) δ 151.9, 143.7, 140.9, 132.9, 128.3, 128.0, 127.0, 122.7, 114.8 (2C), 114.3 (2C), 55.7, 53.3, 23.2. **HRMS *(ESI)*** m/z $[M+H]^+$ calcd. for $C_{15}H_{17}BrNO$ 306.0488; found 306.0492.

5.2.3 General procedure for the nickel catalyzed reaction

A heat-gun dried Schlenk tube under a constant CO_2 flow, was charged with anhydrous DMF (1 mL), then, under a vigorous stirring (1100 rpm, two magnetic stirring bars), $AlCl_3$ (3.4 equiv, 0.34 mmol, 45.0 mg) was added and the Schlenk tube was warmed to 60 °C for one minute, to solubilize all the solid. The Schlenk tube was then allowed to cool to room temperature. Under a constant flow of CO_2, [Ni(**phen**)Cl_2] was added (10 mol%, 0.01 mmol, 3.1 mg), followed by the desired starting material **10** (0.1 mmol) and zinc powder (3 equiv, 0.30 mmol, 19.8 mg). A Pasteur pipette connected to the Schlenk line was used to bubble CO_2 in the reaction mixture for ca. 10 seconds and then DIPEA (1.0 equiv., 0.10 mmol, 17,5 µL was added, the tube was quickly screw capped and stirred at room temperature for 5 hours. Then, reaction mixture was quenched with HCl (2 M, 10 mL) and extracted with EtOAc (3 x 10 mL). A saturated solution of K_2CO_3 (20 mL) was then added to the water phase and the basic aqueous phase was extracted with EtOAc (3 x 10 mL). The organic phases were combined and washed with NH_4Cl (0.1 M, 4 x 20 mL) to remove the DMF, then dried over Na_2SO_4 and evaporated *in vacuo*. The crude mixture was purified by flash chromatography on silica gel (FC, *n*-hexane/EtOAc mixtures).

Figure 72. Nickel catalysed procedure

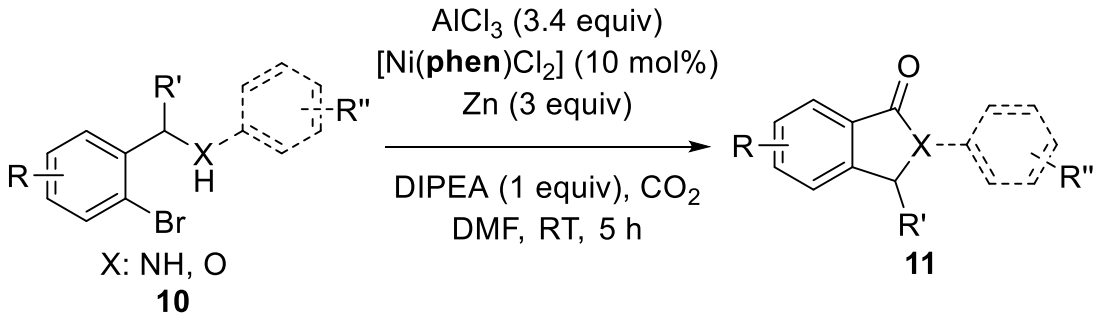

5.2.4 Additional Experiments

Figure 73. Additional tests runned.

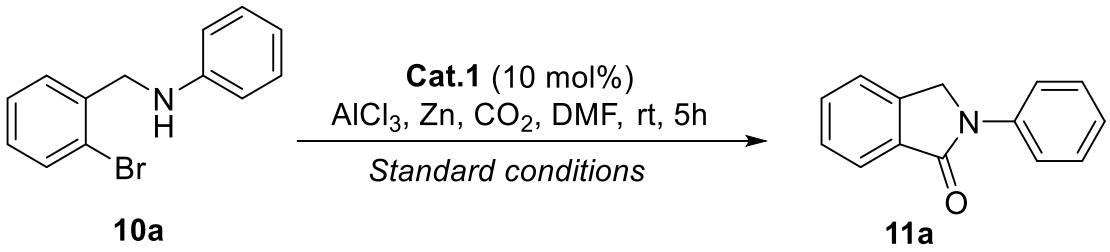

Table 8. Additional optimization runs.

Entry	Variation	Isolated Y(%)
1	-	63
2	**Cat.5** instead of **Cat.1**	58
3	**Cat.6** instead of **Cat.1**	58
4	**Cat.7** instead of **Cat.1**	50
5	**Cat.8** instead of **Cat.1**	46
6	**Cat.9** instead of **Cat.1**	52
7	$AlCl_3$ (4.5 equiv)	57
8	TMSCl (3.4 equiv) instead of $AlCl_3$	32
9	$MgCl_2$ (3.4 equiv)	n.d.
10	$ZnCl_2$ (3.4 equiv)	n.d.
11	Reaction time 1 h instead of 5 h	36
12	Reaction time 2 h instead of 5 h	50
13	Reaction time 3 h instead of 5 h	53
14	Reaction time 16 h instead of 5 h	48

Figure 74. Additional tested nickel precatalysts

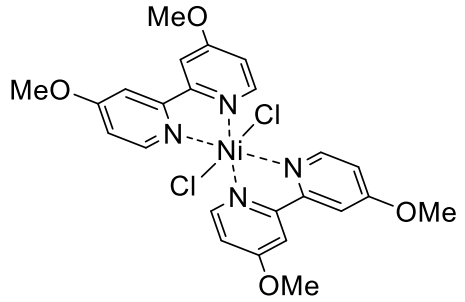

Cat.5

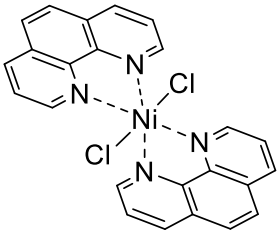

Cat.6

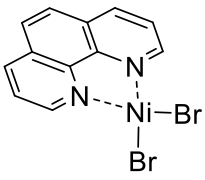

Cat.7

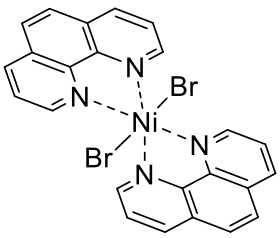

Cat.8

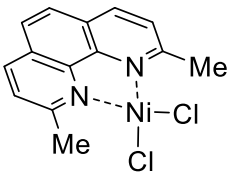

Cat.9

From **Table 8, Fig. 73** and **Fig. 74** it is possible to draw the following trends in the reported carbonylative amidation reaction:

1. The 1:1 ligand/Ni ratio is favourable when phenanthroline-like ligands are applied, while the 2:1 ratio is favourable in the case of bi-pyridine ligands. However, unsubstituted phenanthroline is shown to be the better performing ligand (**entries 1-6**).
2. Other Lewis-acid additives do not promote the desired reaction and the amount of 3.4 equivalents of $AlCl_3$ is optimal for the formation of the desired product (higher amounts can indeed bring to substantial decomposition of both product and starting material).
3. The reaction time is optimal around 3-5 h with the major amount of product formed. Shorter reaction times show incomplete conversion while longer ones lead to decomposition of the formed product (**entries 11-14**).

5.2.5 Characterization data of products

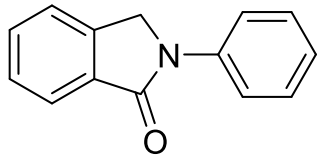

11a. White solid. **m.p.** 169 -171 °C. FC eluent: *n*Hex/EtOAc 8:1. Yield = 63% (0.063 mmol, 13.1 mg). **^{1}H NMR** (600 MHz, $CDCl_3$) δ 7.95 – 7.93 (m, 1H), 7.90 – 7.87 (m, 2H), 7.63 – 7.59 (m, 1H), 7.54 – 7.50 (m, 2H), 7.45 – 7.42 (m, 2H), 7.21 – 7.17 (m, 1H), 4.87 (s, 2H). **^{13}C NMR** (151 MHz, $CDCl_3$) δ 166.5, 139.1, 138.5, 132.2, 131.1, 128.1 (2C), 127.4, 123.5, 123.2, 121.6, 118.5 (2C), 49.7. **HRMS *(ESI)*** m/z $[M+H]^+$ calcd. for $C_{14}H_{12}NO$ 210.0193; found 210.0199.

(*^{13}C*)-2a. Obtained following a modification of the general procedure, as follows. A heat-gun dried Schlenk tube ***under a constant Ar flow*** was charged with anhydrous DMF (1 mL). Then, under vigorous stirring (1000 rpm, two magnetic stirring bars) AlCl3 (3.4 equiv., 0.34 mmol, 45.0 mg) was added and the Schlenk tube was warmed to 60 °C for one minute, to solubilize all the solid. The Schlenk tube was then allowed to cool to room temperature and ***three vacuum/Ar cycles*** were performed. ***Under a constant flow of Ar***, $[Ni(phen)Cl_2]$ was added (10 mol%, 0.01 mmol, 3.1 mg), followed by **1a** (1.0 equiv, 0.1 mmol, 26.2 mg), zinc powder (3.0 equiv, 0.30 mmol, 19.8 mg) and DIPEA (1.0 equiv., 0.10 mmol, 17,5 μL) was added. Then, a mild vacuum was created in the Schlenk tube that was promptly sealed. The vacuum line was switched with a line directly connected to a low pressure (2.54 atm) flask of $^{13}CO2$ and opened to let the gas flow in. The operation was repeated once more, then, the tube was screw capped and stirred at room temperature for 5 hours. After the usual work-up reported in the general procedure,

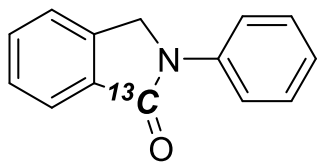

(*13C*)-11a was obtained as a white solid in 65% yield. **^{1}H NMR** (600 MHz, $CDCl_3$) δ 7.86 (ddt, *J* = 7.6, 2.8, 1.0 Hz, 1H), 7.82 – 7.78 (m, 2H), 7.53 (td, *J* = 7.5, 1.1 Hz, 1H), 7.47 – 7.41 (m, 2H), 7.39 – 7.34 (m, 2H), 7.11 (tt, *J* = 7.4, 1.1 Hz, 1H), 4.79 (s, 2H). **^{13}C NMR** (151 MHz, $CDCl_3$) δ 166.5 (>95% 13C abundance), 139.1 (d, *J* = 5.9 Hz), 138.5, 132.2 (d, *J* = 67.7 Hz), 131.1, 128.2, 127.4 (d, *J* = 4.2 Hz), 123.5, 123.2 (d, *J* = 3.5 Hz), 121.6 (d, *J* = 3.4 Hz), 118.5 (d, *J* = 1.5 Hz), 49.7 (d, *J* = 6.5 Hz). **HRMS (*ESI)*** m/z: $[M+H]^+$ calcd. for $^{12}C_{13}$***^{13}C***H12NO 211.0947; found 211.0940.

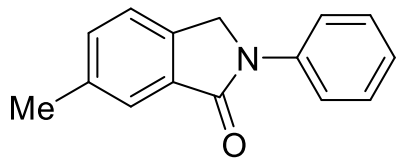

11b. White solid. **m.p.** 166 - 167 °C. FC eluent: *n*Hex/EtOAc 8:1. Yield = 65% (0.065 mmol, 14.5 mg). **^{1}H NMR** (600 MHz, $CDCl_3$) δ 7.89 - 7.87 (m, 2H), 7.74 (s, 1H), 7.45 – 7.40 (m, 4H), 7.19 (tt, *J* = 7.4, 1.2 Hz, 1H), 4.83 (s, 2H), 2.48 (s, 3H). **^{13}C NMR** (151 MHz, $CDCl_3$) δ 167.7, 139.6, 138.4, 137.3, 133.4, 133.1, 129.1 (2C), 124.4, 124.3, 122.3, 119.4 (2C), 50.5, 21.4. **HRMS *(ESI)*** m/z $[M+H]^+$ calcd. for $C_{15}H_{14}NO$ 224.1070; found 224.1075.

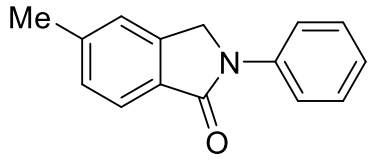

11c. White solid. **m.p.** 160 -163 °C. FC eluent: *n*Hex/EtOAc 8:1. Yield = 46% (0.046 mmol, 10.3 mg). **^{1}H NMR** (600 MHz, $CDCl_3$) δ 7.88 – 7.87 (m, 2H), 7.82 (d, *J* = 8.1 Hz, 1H), 7.45 – 7.42 (m, 2H), 7.33 -7.31 (m, 2H), 7.18 (t, *J* = 7.4 Hz, 1H), 4.82 (s, 2H), 2.50 (s, 3H). **^{13}C NMR** (151 MHz, $CDCl_3$) δ 167.6, 142.8, 140.5, 139.7, 130.7, 129.4, 129.1 (2C), 124.3, 123.9, 123.0, 119.3 (2C), 50.5, 22.0. **HRMS *(ESI)*** m/z $[M+H]^+$ calcd. for $C_{15}H_{14}NO$ 224.1070; found 224.1068.

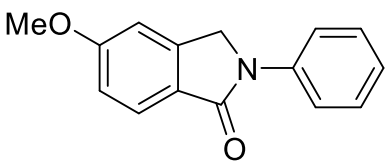

11d. White solid. **m.p.** 150 - 152 °C. FC eluent: *n*Hex/EtOAc 7:1. Yield = 30% (0.03 mmol, 7.2 mg). **^{1}H NMR** (600 MHz, $CDCl_3$) δ 7.87 – 7.84 (m 3H), 7.44 – 7.42 (m, 2H), 7.17 (t, *J* = 7.4 Hz, 1H), 7.04 (d, *J* = 8.6 Hz, 1H), 7.00 (s, 1H), 4.82 (s, 2H), 3.91 (s, 3H). **^{13}C NMR** (151 MHz, $CDCl_3$) δ 167.4, 163.3, 142.4, 139.7, 129.1 (2C), 125.9, 125.6, 124.1, 119.2 (2C), 115.1, 107.4, 55.7, 50.5. **HRMS *(ESI)*** m/z $[M+H]^+$ calcd. for $C_{15}H_{14}NO_2$ 240.1019; found 240.1011.

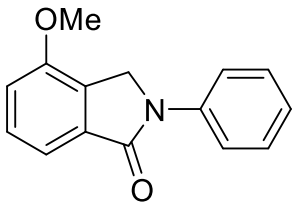

11e. White solid. **m.p.** 140 - 141 °C. FC eluent: *n*Hex/EtOAc 7:1. Yield = 63% (0.063 mmol, 15.1 mg). **^{1}H NMR** (600 MHz, $CDCl_3$) δ 7.90 – 7.89 (m, 2H), 7.53 (dd, *J* = 7.6, 0.8 Hz, 1H), 7.48 – 7.42 (m 3H), 7.18 (tt, *J* = 7.4, 1.1 Hz, 1H), 7.06 (d, J = 7.2 Hz, 1H), 4.80 (s, 2H), 3.95 (s, 3H). **^{13}C NMR** (151 MHz, $CDCl_3$) δ 167.5, 154.4, 139.6, 134.8, 130.0, 129.1 (2C), 128.3, 124.3, 119.3 (2C), 116.1, 113.1, 55.5, 48.6. **HRMS *(ESI)*** m/z $[M+H]^+$ calcd. for $C_{15}H_{14}NO_2$ 240.1019; found 240.1012.

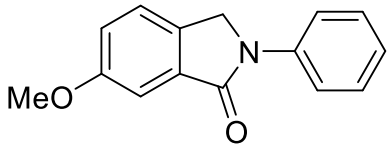

11f. White solid. **m.p.** 171 - 173 °C. FC eluent: *n*Hex/EtOAc 7:1. Yield = 44% (0.044 mmol, 10.5 mg). **^{1}H NMR** (600 MHz, $CDCl_3$) δ 7.88 – 7.86 (m, 2H), 7.45 – 7.40 (m, 4H), 7.20 – 7.16 (m, 2H), 4.81 (s, 2H), 3.90 (s, 3H). **^{13}C NMR** (151 MHz, $CDCl_3$) δ 167.5, 160.2, 139.6, 134.6, 132.3, 129.1 (2C), 124.5, 123.5, 120.7, 119.4 (2C), 106.6, 55.7, 50.3. **HRMS *(ESI)*** m/z $[M+H]^+$ calcd. for $C_{15}H_{14}NO_2$ 240.1019; found 240.1027.

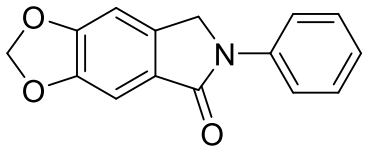

11g. White solid. **m.p.** 195 -196 °C. FC eluent: *n*Hex/EtOAc 5:1. Yield = 81% (0.081 mmol, 20.3 mg). **^{1}H NMR** (600 MHz, DMSO) δ 7.86 – 7.85 (m, 2H), 7.43 – 7.40 (m, 2H), 7.20 (s, 1H), 7.19 (s, 1H), 7.16 – 7.13 (m, 1H), 6.17 (s, 2H), 4.88 (s, 2H). **^{13}C NMR** (151 MHz, $CDCl_3$) δ 166.3, 151.5, 148.0, 139.6, 136.8, 128.9 (2C), 126.0, 123.7, 118.9 (2C), 103.5, 102.5, 102.1, 50.0. **HRMS *(ESI)*** m/z $[M+H]^+$ calcd. for $C_{15}H_{14}NO_3$ 254.0812; found 254.0806.

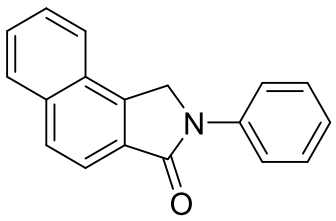

11h. White solid. **m.p.** 165 -167 °C. FC eluent: *n*Hex/EtOAc 9:1. Yield = 78% (0.078 mmol, 19.8 mg). **^{1}H NMR** (600 MHz, $CDCl_3$) δ 9.31 (d, J = 8.4 Hz, 1H), 8.03 (d, J = 8.3 Hz, 1H), 7.93 - 7.91 (m, 3H), 7.70 (ddd, *J* = 8.3, 6.8, 1.3 Hz, 1H), 7.59 (ddd, *J* = 8.1, 6.8, 1.3 Hz, 1H), 7.54 (d, *J* = 8.3 Hz, 1H), 7.47 – 7.44 (m, 2H), 7.19 (tt, *J* = 7.4, 1.1 Hz, 1H), 4.87 (s, 2H). **^{13}C NMR** (151 MHz, $CDCl_3$) δ 168.5, 140.9, 139.6, 133.2, 133.0, 129.5, 129.1 (2C), 128.2, 128.1, 126.8, 126.7, 124.2, 123.7, 119.7, 119.3 (2C), 50.4. **HRMS *(ESI)*** m/z $[M+H]^+$ calcd. for $C_{18}H_{14}NO$ 260.1070; found 260.1079.

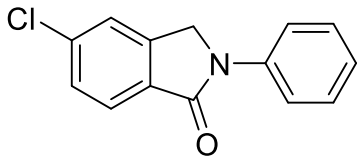

11i. White solid. **m.p.** 157 - 159 °C. FC eluent: *n*Hex/EtOAc 8:1. Yield = 50% (0.05 mmol, 12.2 mg). **^{1}H NMR** (600 MHz, $CDCl_3$) δ 7.87 – 7.84 (m, 3H), 7.52 (s, 1H), 7.51 -7.49 (m, 1H), 7.46 – 7.43 (m, 2H), 7.22 – 7.19 (m, 1H), 4.85 (s, 2H). **^{13}C NMR** (151 MHz, $CDCl_3$) δ 166.4, 141.6, 139.2, 138.4, 131.7, 129.2 (2C), 129.1, 125.4, 124.8, 123.1, 119.5 (2C), 50.3. **HRMS *(ESI)*** m/z $[M+H]^+$ calcd. for $C_{15}H_{11}ClNO$ 244.0524; found 244.0518.

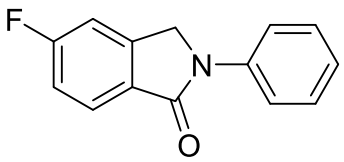

11j. White solid. **m.p.** 137 -138 °C. FC eluent: *n*Hex/EtOAc 8:1. Yield = 58% (0.058 mmol, 13.2 mg). **^{1}H NMR** (600 MHz, $CDCl_3$) δ 7.94 – 7.91 (m, 1H), 7.85 – 7.84 (m, 2H), 7.46 – 7.43 (m, 2H), 7.23 - 7.19 (m, 3H), 4.86 (s, 2H). **^{13}C NMR** (151 MHz, $CDCl_3$) δ 166.4, 165.5 (d, *J* = 252.2 Hz), 142.4 (d, *J* = 10.3 Hz), 139.3, 129.3 (d, *J* = 2.1 Hz), 129.2 (2C), 126.3 (d, *J* = 9.8 Hz), 124.6, 119.4 (2C), 116.3 (d, *J* = 23.4 Hz), 110.0 (d, *J* = 24.4 Hz), 50.4 (d, *J* = 2.8 Hz). **^{19}F NMR** (565 MHz, $CDCl_3$) δ -106.48 - -106.52 (m). **HRMS *(ESI)*** m/z $[M+H]^+$ calcd. for $C_{14}H_{11}FNO$ 228.0819; found 228.0810.

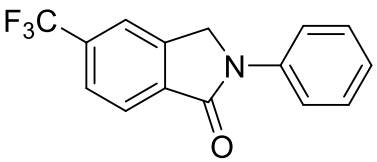

11k. White solid. **m.p.** 220 -224 °C. FC eluent: *n*Hex/EtOAc 8:1. Yield = 86% (0.086 mmol, 23.8 mg). **^{1}H NMR** (600 MHz, acetone-d_6) δ 8.06 (s, 1H), 8.02 – 7.99 (m, 3H), 7.92 – 7.90 (m, 1H), 7.47 - 7.45 (m, 2H), 7.22 – 7.20 (m, 1H), 5.15 (s, 2H). **^{13}C NMR** (151 MHz, acetone-d_6) δ 166.3, 142.7, 140.6, 137.6, 133.9 (q, *J* = 32.2 Hz), 129.8 (2C), 126.2 (q, *J* = 3.8 Hz), 125.1 (q, *J* = 272.6 Hz), 125.3, 125.1, 121.5 (q, *J* = 3.9 Hz), 120.2 (2C), 51.3. **^{19}F NMR** (565 MHz, acetone-d_3) δ -62.90. **HRMS *(ESI)*** m/z $[M+H]^+$ calcd. for $C_{15}H_{11}F_3NO$ 278.0787; found 278.0795.

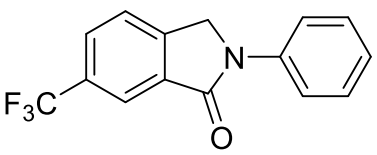

11l. White solid. **m.p.** 198 - 201 °C. FC eluent: *n*Hex/EtOAc 8:1. Yield = 62% (0.062 mmol, 17.2 mg). **^{1}H NMR** (600 MHz, $CDCl_3$) δ 8.22 (s, 1H), 7.88 – 7.85 (m, 3H), 7.68 – 7-66 (m, 1H), 7.47 – 7.44 (m, 2H), 7.24 – 7.22 (m, 1H), 4.94 (s, 2H). **^{13}C NMR** (151 MHz, $CDCl_3$) δ 166.0, 143.4, 139.0, 134.0, 131.4 (q, *J* = 33.1 Hz), 129.3 (2C), 128.8 (q, *J* = 3.3 Hz), 125.0, 123.7 (q, *J* = 272.0 Hz), 123.4, 121.5 (q, *J* = 3.9 Hz), 119.6 (2C), 50.7. **^{19}F NMR** (565 MHz, $CDCl_3$) δ -62.35. **HRMS *(ESI)*** m/z $[M+H]^+$ calcd. for $C_{15}H_{11}F_3NO$ 278.0787; found 278.0781.

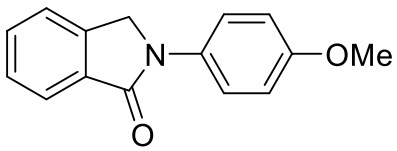

11m. White solid. **m.p.** 175 - 177 °C. FC eluent: *n*Hex/EtOAc 6:1. Yield = 32% (0.032 mmol, 7.7 mg). **^{1}H NMR** (600 MHz, $CDCl_3$) δ 7.93 (d, *J* = 8.1 Hz, 1H), 7.76 – 7.74 (m, 2H), 7.59 (td, *J* = 7.4, 1.1 Hz, 1H), 7.52 – 7.50 (m, 2H), 6.98 – 6.97 (m, 2H), 4.83 (s, 2H), 3.84 (s, 3H). **^{13}C NMR** (151 MHz, $CDCl_3$) δ 167.2, 156.6, 140.1, 133.3, 132.7, 131.8, 128.3, 124.0, 122.5, 121.5 (2C), 114.3 (2C), 55.5, 51.2. **HRMS *(ESI)*** m/z $[M+H]^+$ calcd. for $C_{15}H_{14}NO_2$ 240.1019; found 240.1010.

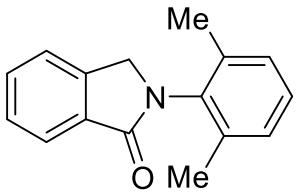

11n. White solid. FC eluent: *n*Hex/EtOAc 8:1. Yield = 25% (0.025 mmol, 5.9 mg). **^{1}H NMR** (600 MHz, $CDCl_3$) δ 7.99 (dt, *J* = 7.6, 1.0 Hz, 1H), 7.63 (td, *J* = 7.5, 1.2 Hz, 1H), 7.57 – 7.51 (m, 2H), 7.23 (dd, *J* = 8.4, 6.6 Hz, 1H), 7.19 – 7.15 (m, 2H), 4.61 (s, 2H), 2.21 (s, 6H). **^{13}C NMR** (151 MHz, $CDCl_3$) δ 167.8, 141.7, 136.8, 135.5, 132.4, 131.6, 128.6 (2C), 128.5, 128.2, 124.4, 122.9 (2C), 51.2, 18.0 (2C). **HRMS *(ESI)*** m/z $[M+H]^+$ calcd. for $C_{16}H_{16}NO$ 238.1226; found 238.1231. **m.p.** 120 - 121 °C.

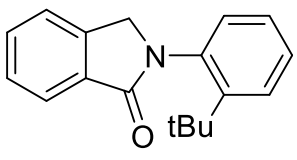

11o. White solid. FC eluent: *n*Hex/EtOAc 11:1. Yield = 76% (0.076 mmol, 20.2 mg). **^{1}H NMR** (600 MHz, $CDCl_3$) δ 8.16 (dd, *J* = 7.8, 1.1 Hz, 1H), 7.59 – 7.52 (m, 2H), 7.42 (td, *J* = 7.8, 1.6 Hz, 1H), 7.30 (dd, *J* = 7.9, 1.4 Hz, 1H), 7.11 (ddd, *J* = 8.6, 7.2, 1.5 Hz, 1H), 6.77 (td, *J* = 7.6, 1.3 Hz, 1H), 6.71 (dd, *J* = 8.1, 1.2 Hz, 1H), 4.79 (s, 2H), 1.46 (s, 9H). **^{13}C NMR** (151 MHz, $CDCl_3$) δ 172.1, 145.5,

141.5, 134.1, 133.4, 132.3, 129.3, 128.5, 127.5, 127.2, 126.4, 118.2, 113.3, 48.4, 34.1, 30.1 (3C). **HRMS *(ESI)*** m/z $[M+H]^+$ calcd. for $C_{18}H_{20}NO$ 266.1539; found 266.1544. **m.p.** 135 - 137 °C.

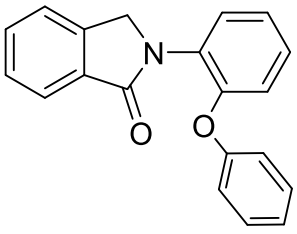

11p. White solid. **m.p.** 155 - 158 °C. FC eluent: *n*Hex/EtOAc 8:1. Yield = 87% (0.087 mmol, 26.2 mg). **^{1}H NMR** (600 MHz, $CDCl_3$) δ 8.11 (dt, *J* = 7.7, 1.0 Hz, 1H), 7.55 – 7.49 (m, 2H), 7.40 – 7.36 (m, 1H), 7.32 – 7.27 (m, 2H), 7.05 (tt, *J* = 7.4, 1.1 Hz, 1H), 7.01 (td, *J* = 7.7, 1.5 Hz, 1H), 6.99 – 6.95 (m, 2H), 6.88 (dd, *J* = 8.0, 1.5 Hz, 1H), 6.74 (dd, *J* = 8.1, 1.5 Hz, 1H), 6.69 (td, *J* = 7.7, 1.5 Hz, 1H), 4.76 (s, 2H). **^{13}C NMR** (151 MHz, $CDCl_3$) δ 171.9, 157.5, 143.3, 141.6, 139.7, 133.3, 132.3, 129.7 (2C), 129.0, 128.1, 127.3, 124.9, 122.7, 119.5, 117.7, 117.2 (2C), 112.7, 47.0. **HRMS *(ESI)*** m/z $[M+H]^+$ calcd. for $C_{20}H_{16}NO_2$ 302.1176; found 302.1181.

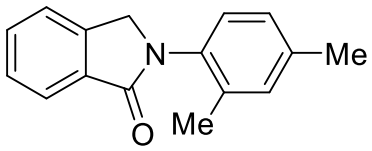

11q. White solid. **m.p.** 145 - 146 °C. FC eluent: *n*Hex/EtOAc 8:1. Yield = 38% (0.038 mmol, 9.0 mg). **^{1}H NMR** (600 MHz, $CDCl_3$) δ 7.96 (d, J = 7.5 Hz, 1H), 7.61 (t, *J* = 7.4 Hz, 1H), 7.54 – 7.51 (m, 2H), 7.16 – 7.14 (m, 2H), 7.09 (d, *J* = 7.8 Hz, 1H), 4.71 (s, 2H), 2.37 (s, 3H), 2.23 (s, 3H). **^{13}C NMR** (151 MHz, $CDCl_3$) δ 167.7, 141.5, 138.1, 136.0, 134.3, 132.5, 131.9, 131.6, 128.2, 127.5, 127.2, 124.2, 122.7, 53.1, 21.1, 18.1. **HRMS *(ESI)*** m/z $[M+H]^+$ calcd. for $C_{16}H_{16}NO$ 238.1226; found 238.1221.

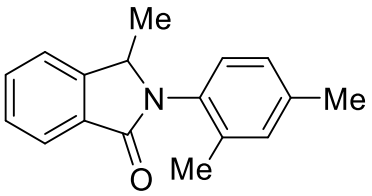

11r. White solid. **m.p.** 125 - 127 °C. FC eluent: *n*Hex/EtOAc 8:1. Yield = 73% (0.073 mmol, 18.3 mg). **^{1}H NMR** (600 MHz, $CDCl_3$) δ ^{1}H NMR (600 MHz, $CDCl_3$) δ 7.95 (d, *J* = 7.5 Hz, 1H), 7.61 (td, *J* = 7.5, 1.2 Hz, 1H), 7.52 (t, *J* = 7.5 Hz, 1H), 7.49 (dd, *J* = 7.6, 1.0 Hz, 1H), 7.17 (s, 1H), 7.14 – 7.02 (m, 2H), 5.03 + 4.79 (couple of bs, attributable to the presence of rotamers, 1H), 2.37 (s, 3H), 2.32 – 2.09 (bm attributable to the presence of rotamers, 3H), 1.45 – 1.35 (bm attributable to the presence of rotamers, 3H). **^{13}C NMR** (151 MHz, $CDCl_3$) δ 166.5, 147.2, 137.7, 137.1, 132.9, 131.9, 131.7, 131.6, 130.0, 128.2, 127.4, 126.4, 124.1, 122.0, 59.6 + 57.8 (two peaks attributable to the presence of rotamers, 1C), 21.1, 18.4, 18.0. Some peaks appear broad due to the presence of rotamers. **HRMS *(ESI)*** m/z $[M+H]^+$ calcd. for $C_{17}H_{18}NO$ 252.1383; found 252.1390.

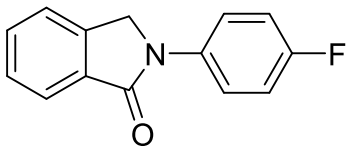

11s. White solid. **m.p.** 145 - 146 °C. FC eluent: *n*Hex/EtOAc 8:1. Yield = 80% (0.080 mmol, 18.2 mg). **^{1}H NMR** (600 MHz, $CDCl_3$) δ 7.93 (d, *J* = 8.2 Hz, 1H), 7.84 – 7.82 (m, 2H), 7.61 (td, *J* = 7.5, 1.1 Hz, 1H), 7.53 – 7.51 (m, 2H), 7.14 – 7.11 (m, 2H), 4.84 (s, 2H). **^{13}C NMR** (151 MHz, $CDCl_3$) δ 167.4, 159.5 (d, *J* = 244.4 Hz), 140.0, 135.6 (d, *J* = 2.8 Hz), 133.0, 132.1, 128.5, 124.2, 122.6, 121.3 (d, *J* = 7.8 Hz, 2C), 115.8 (d, *J* = 22.4 Hz, 2C), 51.0. **^{19}F NMR** (565 MHz, $CDCl_3$) δ -117.80 - -117.84 (m). **HRMS *(ESI)*** m/z $[M+H]^+$ calcd. for $C_{14}H_{11}FNO$ 228.0819; found 228.0822.

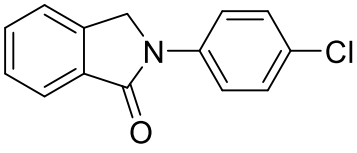

11t. White solid. **m.p.** 181 - 184 °C. FC eluent: *n*Hex/EtOAc 8:1. Yield = 67% (0.067 mmol, 16.3 mg). **^{1}H NMR** (600 MHz, $CDCl_3$) δ 7.92 – 7.91 (m, 1H), 7.84 – 7.83 (m, 2H), 7.61 (td, *J* = 7.5, 1.2 Hz, 1H), 7.53 – 7.50 (m, 2H), 7.39 – 7.37 (m, 2H), 4.83 (s, 2H). **^{13}C NMR** (151 MHz, $CDCl_3$) δ 167.5, 139.9, 138.1, 132.9, 132.3, 129.5, 129.1 (2C), 128.5, 124.2, 122.6, 120.4 (2C), 50.6. **HRMS *(ESI)*** m/z $[M+H]^+$ calcd. for $C_{15}H_{11}ClNO$ 244.0524; found 244.0529.

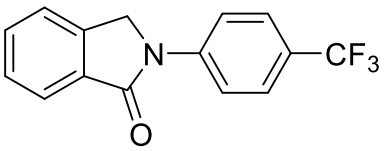

11u. White solid. **m.p.** 190 - 192 °C. FC eluent: *n*Hex/EtOAc 8:1. Yield = 44% (0.044 mmol, 12.2 mg). **^{1}H NMR** (600 MHz, $CDCl_3$) δ 8.06 – 8.04 (m, 2H), 7.95 (d, *J* = 7.5 Hz, 1H), 7.70 – 7.68 (m, 2H), 7.65 (t, *J* = 7.4 Hz, 1H), 7.56 – 7.53 (m, 2H), 4.91 (s, 2H). **^{13}C NMR** (151 MHz, $CDCl_3$) δ 167.8, 142.5, 139.9, 132.7, 132.7, 128.7, 126.4 (q, J = 3.8 Hz, 2C), 126.0 (q, *J* = 32.7 Hz), 124.4, 124,1 (q, *J* = 271.4 Hz) 122.7, 118.6 (2C), 50.5. **^{19}F NMR** (565 MHz, $CDCl_3$) δ -62.35. **HRMS *(ESI)*** m/z $[M+H]^+$ calcd. for $C_{15}H_{11}F_3NO$ 278.0787; found 278.0795.

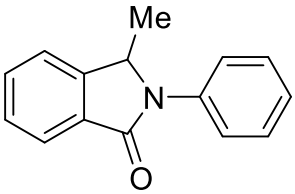

11w. White solid. **m.p.** 147 - 149 °C. FC eluent: *n*Hex/EtOAc 8:1. Yield = 52% (0.052 mmol, 11.6 mg). **^{1}H NMR** (600 MHz, $CDCl_3$) δ 7.95 (dt, *J* = 7.5, 1.0 Hz, 1H), 7.64 – 7.60 (m, 3H), 7.54 – 7.50 (m, 2H), 7.48 -7.45 (m, 2H), 7.25 (tt, *J* = 7.4, 1.2 Hz, 1H), 5.23 (q, J = 6.7 Hz, 1H), 1.47 (d, J = 6.7 Hz, 3H). **^{13}C NMR** (151 MHz, $CDCl_3$) δ 166.9, 146.3, 137.1, 132.0, 131.8, 129.1 (2C), 128.4, 125.4, 124.2, 123.4 (2C), 122.0, 56.9, 18.8. **HRMS *(ESI)*** m/z $[M+H]^+$ calcd. for $C_{15}H_{14}NO$ 224.1070; found 224.1075.

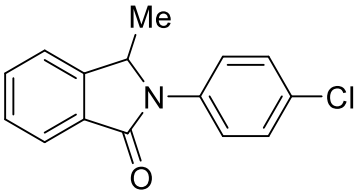

11x. White solid. **m.p.** 135 - 137 °C. FC eluent: *n*Hex/EtOAc 8:1. Yield = 66% (0.066 mmol, 17.0 mg). **^{1}H NMR** (600 MHz, $CDCl_3$) δ 7.93 (dt, *J* = 7.5, 1.0 Hz, 1H), 7.63 (td, *J* = 7.5, 1.2 Hz, 1H), 7.58 – 7.56 (m, 2H), 7.54 – 7.50 (m, 2H), 7.43 - 7.42 (m, 2H), 5.19 (q, J = 6.7 Hz, 1H), 1.47 (d, J = 6.7 Hz, 3H). **^{13}C NMR** (151 MHz, $CDCl_3$) δ 166.9, 146.1, 135.7, 132.3, 131.5, 130.6, 129.2 (2C), 128.5, 124.3 (2C), 124.2, 122.0, 56.8, 18.7. **HRMS *(ESI)*** m/z $[M+H]^+$ calcd. for $C_{15}H_{13}ClNO$ 258.0680; found 258.0674.

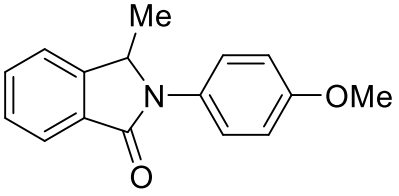

11y. White solid. **m.p.** 155 - 156 °C. FC eluent: *n*Hex/EtOAc 8:1. Yield = 66% (0.066 mmol, 16.7 mg). **^{1}H NMR** (600 MHz, $CDCl_3$) δ 7.93 (dt, *J* = 7.5, 1.0 Hz, 1H), 7.61 (td, *J* = 7.5, 1.2 Hz, 1H), 7.52 – 7.48 (m, 2H), 7.46 -7.45 (m, 2H), 7.00 -6.99 (m, 2H), 5.11 (q, J = 6.7 Hz, 1H), 3.85 (s, 3H), 1.44 (d, J = 6.7 Hz, 3H). **^{13}C NMR** (151 MHz, $CDCl_3$) δ 166.9, 157.5, 146.3, 131.9, 131.8, 129.9, 128.3, 125.5 (2C), 124.0, 121.9, 114.4 (2C), 57.5, 55.5, 18.8. **HRMS *(ESI)*** m/z $[M+H]^+$ calcd. for $C_{16}H_{16}NO_2$ 254.1176; found 254.1170.

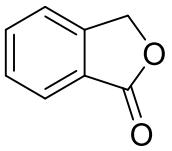

12a. Colourless sticky solid. FC eluent: *n*Hex/EtOAc 10:1. Yield = 64% (0.064 mmol, by ^{1}H NMR using mesitylene as internal standard). **^{1}H NMR** (600 MHz, $CDCl_3$) δ 7.95 (d, *J* = 7.7 Hz, 1H), 7.70 (td, *J* = 7.5, 1.1 Hz, 1H), 7.55 (td, *J* = 7.5, 0.9 Hz, 1H), 7.51 (dt, *J* = 7.7, 0.9 Hz, 1H), 5.34 (s, 2H). **^{13}C NMR** (151 MHz, $CDCl_3$) δ 171.1, 146.5, 134.0, 129.0, 125.8, 125.8, 122.1, 69.6. **HRMS *(ESI)*** m/z $[M+H]^+$ calcd. for $C_8H_7O_2$ 135.0441; found 135.0435.

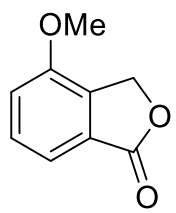

12b. White solid. **m.p.** 110 - 111 °C. FC eluent: *n*Hex/EtOAc 6:1. Yield = 62% (0.062 mmol, 10.2 mg). **^{1}H NMR** (600 MHz, $CDCl_3$) δ 7.51 – 7.48 (m, 2H), 7.13 – 7.10 (m, 1H), 5.27 (s, 2H), 3.93 (s, 3H). **^{13}C NMR** (151 MHz, $CDCl_3$) δ 171.2, 154.2, 134.9, 130.8, 127.4, 117.3, 114.7, 68.1, 55.6. **HRMS *(ESI)*** m/z $[M+H]^+$ calcd. for $C_9H_9O_3$ 165.0546; found 165.0539.

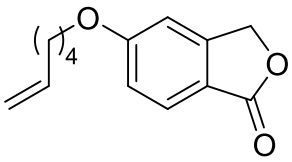

12c. Colourless sticky solid. FC eluent: nHex/EtOAc 5:1. Yield = 58% (0.058 mmol, 13.5 mg). **^{1}H NMR** (600 MHz, $CDCl_3$) δ 7.33 (d, J = 8.7 Hz, 1H), 6.98 (d, J = 3.1 Hz, 1H), 6.64 (dd, J = 8.7, 3.1 Hz, 1H), 5.75 (ddt, J = 16.9, 10.2, 6.6 Hz, 1H), 4.96 (dq, J = 17.1, 1.7 Hz, 1H), 4.91 (ddt, J = 10.2, 2.1, 1.2 Hz, 1H), 4.63 (s, 2H), 3.89 (t, J = 6.5 Hz, 2H), 2.09 – 2.03 (m, 2H), 1.77 – 1.66 (m, 2H), 1.53 – 1.46 (m, 2H). **^{13}C NMR** (151 MHz, $CDCl_3$) δ 177.9, 158.8, 140.7, 138.5, 133.1, 115.3, 114.9, 114.8, 112.4, 68.1, 65.1, 33.4, 28.6, 25.3. **HRMS (*ESI*)** m/z [M+H]+ calcd. for C14H17O3 233.1172; found 233.1177

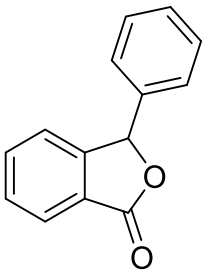

12d. White solid. **m.p.** 160 - 162 °C. FC eluent: *n*Hex/EtOAc 8:1. Yield = 63% (0.063 mmol, 13.2 mg). **^{1}H NMR** (600 MHz, $CDCl_3$) δ 7.98 (dt, *J* = 7.6, 1.0 Hz, 1H), 7.66 (td, *J* = 7.5, 1.1 Hz, 1H), 7.57 (t, *J* = 7.5 Hz, 1H), 7.40 – 7.39 (m, 3H), 7.35 – 7.34 (m, 1H), 7.30 – 7.28 (m, 2H), 6.42 (s, 1H). **^{13}C NMR** (151 MHz, $CDCl_3$) δ 170.5, 149.7, 136.4, 134.3, 129.3, 129.0 (2C), 128.5, 127.5, 127.0 (2C), 125.7, 122.8, 82.7. **HRMS *(ESI)*** m/z $[M+H]^+$ calcd. for $C_{14}H_{11}O_2$ 211.0754; found 211.0755.

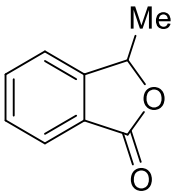

12e. Colourless sticky solid. FC eluent: *n*Hex/EtOAc 8:1. Yield = 61% (0.061 mmol, 9.0 mg). **^{1}H NMR** (600 MHz, $CDCl_3$) δ 7.91 (dt, *J* = 7.6, 1.0 Hz, 1H), 7.69 (td, *J* = 7.5, 1.1 Hz, 1H), 7.54 (tt, *J* = 7.6, 0.8 Hz, 1H), 7.45 (dq, *J* = 7.7, 0.9 Hz, 1H), 5.58 (q, *J* = 6.7 Hz, 1H), 1.65 (d, *J* = 6.7 Hz, 3H). **^{13}C NMR** (151 MHz, $CDCl_3$) δ 170.4, 151.2, 134.0, 129.1, 125.8, 125.7, 121.5, 77.7, 20.4. **HRMS *(ESI)*** m/z $[M+H]^+$ calcd. for $C_9H_9O_2$ 149.0597; found 149.0606.

5.3 Direct Access to α-aryl-α-trifluoromethyl Benzyl Alcohols

Further relevant information can be found in the SI document of the following work**:**

Direct Synthesis of α-Aryl-α-Trifluoromethyl Alcohols via Nickel Catalyzed Cross Electrophile Coupling

L. Lombardi, A. Cerveri, R. Giovanelli, M. Castiñeira Reis, C. Silva López, G. Bertuzzi, M. Bandini,

Chem. Int. Ed. **2022**, *61*, e202211732; *Angew. Chem.* **2022**, *134*, e202211732.

DOI: 10.1002/anie.202211732

5.3.1 General DFT information

We have used the Density Functional Theory (DFT) in the Kohn-Sham formulation to optimize all the stationary points presented in this manuscript. Geometries of all the stationary points were fully optimized at the M06[307]/def2svpp[308] computational level. The effect of solvent (DMA) was modelled using the polarizable continuum model (PCM)[309] with the default parameters implemented in the Gaussian 09 package.[310] Explicit solvation was also included in some instances since the solvent has the potential ability to coordinate the metallic center and even aid in hydrogen transferences.

All geometry optimizations have been performed using tight convergence criteria in the SCF and requesting a pruned (99.590) grid to guarantee the accuracy of the reported results. Moreover, calculations were performed considering 1.0 atm and 298.1 K to properly simulate the reaction conditions.

Frequency analysis was used to establish the nature of all optimized structures as either minima or transition structures. For all stationary points, the stability of the wave function was examined.[311] When different spin-states are possible for a stationary point those states were explored by running single point energy calculations starting from the optimized structure with the expected multiplicity. Single point energies for the different possible multiplicities are specified in the Cartesian section.

IRC calculations[312] were conducted for important transition states to ensure their connectivity with the expected reactants and products. The nudged elastic band method was used to locate difficult transition states[324] When the substrates showed conformational freedom, conformational analysis was performed manually, it must be indicated that only the most stable conformer of each stationary point was considered and reported unless otherwise indicated. The visualization of the reported structures was performed using MOLDEN.[325] The representation of the structures here presented was generated using CYLView.[313]

[324] a) Sheppard, D., Terrell, R., Henkelman, G., *J. Chem. Phys*. **2008**, 128, 134106. b) Henkelman, G., Jóhannesson, G., Jónsson, H., "Methods for Finding Saddle Points and Minimum Energy Paths" in Progress on Theoretical Chemistry and Physics, Ed. S. D. Schwartz, 269–300 (Kluwer Academic Publishers, **2000**). c) Henkelman, G., Uberuaga, B.P., Jónsson, H., *J. Chem. Phys.* **2000**, 113, 9901. d) Henkelman, G., Jónsson, H., *J. Chem. Phys*., **2000**, 113, 9978. e) Jónsson, H., Mills, G., Jacobsen, K.W., "Nudged Elastic Band Method for Finding Minimum Energy Paths of Transitions" in Classical and Quantum Dynamics in Condensed Phase Simulations, Ed. B. J. Berne, G. Ciccotti and D. F. Coker, 385 (World Scientific, **1998**).
[325] Schaftenaar, G., Vlieg, E., Vriend, G., *J. Comput. Aided. Mol. Des*. **2017**, 31, 789–800

5.3.1.1 Computational evaluation of Zn aggregation

The reduction steps constitute a troublesome point in this research since they involve metallic Zn. We have worked here under the consideration that in the presence of such a coordinating solvent such as DMA part of the metallic Zn will be efficiently solvated and leached in the form of $Zn(DMA)_3$. Different numbers of solvent molecules coordinated to the metal center have been explored obtaining that three is the enthalpically preferred coordination (**Tab. 9**).

Table 9. Data on the solvation of metallic Zn. [a]SCF energies correspond to the electronic energies expressed in a.u. Imaginary frequencies are expressed in cm-1. [b] H denotes the Sum of electronic and thermal Enthalpies. [c] G denotes the Sum of electronic and thermal Free Energies.

ID	Im. Freqs	Stable	SCF[a]	SCF+ZPVE	H[b]	G[c]
DMA	-	Yes	-287.4093664	-287.280614	-287.272025	-287.312298
Zn	-	Yes	-1779.098406	-1779.098406	-1779.096045	-1779.114283
Zn(DMA)	-	Yes	-2066.517272	-2066.387867	-2066.377097	-2066.425476
$Zn(DMA)_2$	-	Yes	-2353.937241	-2353.676407	-2353.657118	-2353.723942
$Zn(DMA)_3$	-	Yes	-2641.356003	-2640.965713	-2640.937012	-2641.026676

5.3.1.2 Computational evaluation of xix evolution

Figure 75a. 3D representation of the explored reacting surface related to the H-shift step from **xix** to **xixa** via the NEB method. Arbitrary units used in the configuration space and Hartrees (Eh) used in the energy axis.

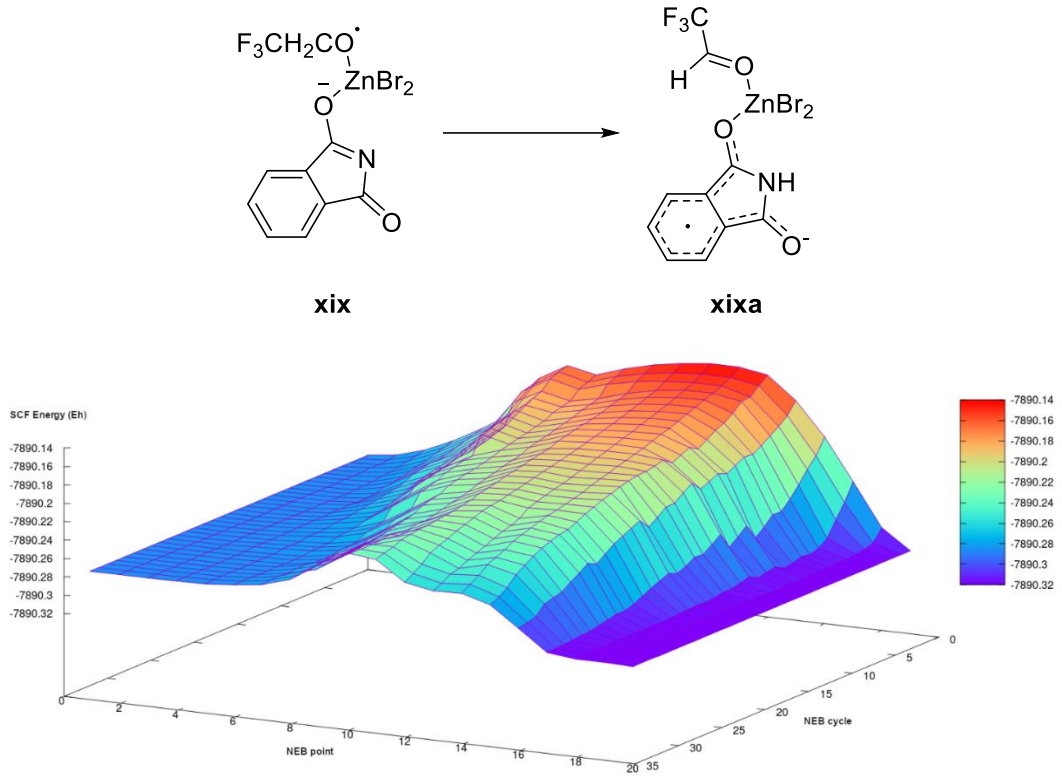

Figure 75b. MEP for the for the conversion of **xix** to **xixa** obtained using the NEB. Y-axis contains the SCF energies expressed in a.u. and X-axis represents the reaction points.

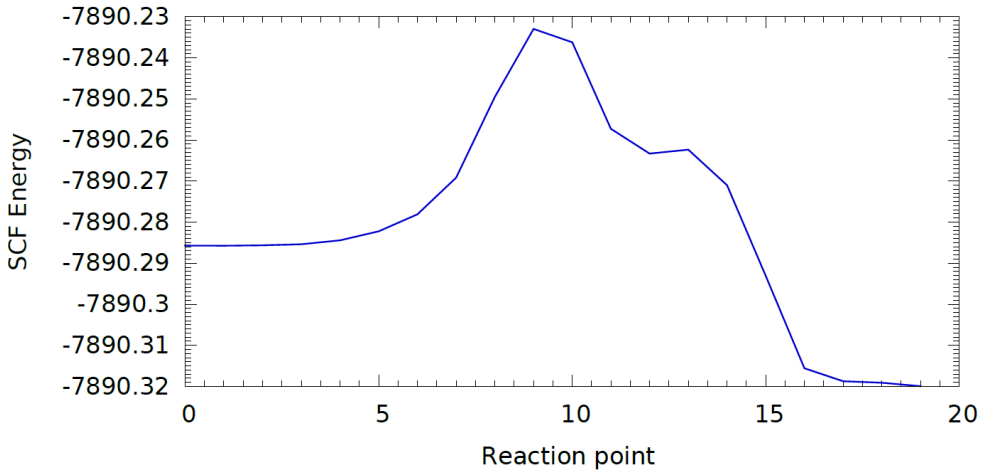

5.3.2 General procedures for preparation of Starting Materials.

Synthesis of compound 14

Compound **14** was synthetized from *N*-hydroxyphthalimide (NHPI) and 2,2,2-trifluoroethyl trifluoromethanesulfonate according to the literature.[326] The latter was prepared from trifluoroethanol (TFE) and triflic anhydride following a described procedure (**Fig. 76**).[327]

Figure 76. Trifluoroethanole triflate preparation.

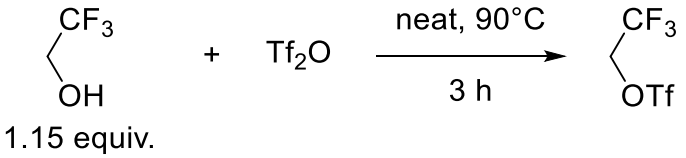

In a heat-gun dried, 25 mL two-necked round bottom flask under N_2 atmosphere equipped with reflux condenser were added TFE (4.17g, 3.0 mL, 41.7 mmol, 1.15 eq) and triflic anhydride (10.0 g, 6 mL, 35.7 mmol, 1 eq). The mixture was stirred for 15 minutes at rt (**CAUTION! Heat is produced when mixing the two liquids**) and then refluxed for 3 hours at 90 °C.

Under N_2 flow, the reflux condenser was removed, and the flask connected to a previously heat-gun dried distillation apparatus equipped with two receiving flasks also under N_2 flow.

Fractionate distillation under N_2 atmosphere at atmospheric pressure was conducted (oil bath temperature ca. 120 °C), discarding the head distillate (ca. 0.5 mL, containing residual TFE) to obtain pure 2,2,2-trifluoroethyl trifluoromethanesulfonate (7.46 g, 32.1 mmol, 90 % yield). Spectral data are in accordance with the literature.

Figure 77. preparation of redox active ether **14.**

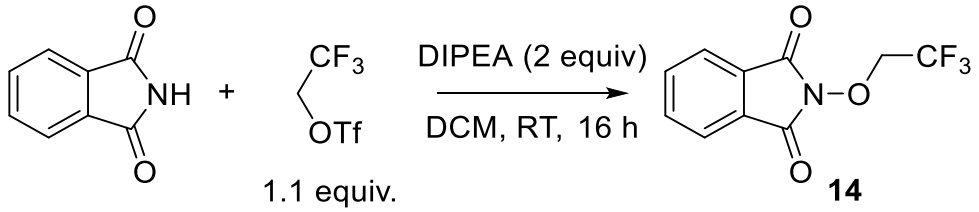

A 250 mL three -necked round bottom flask was evacuated and back-filled with N_2 for three times. NHPI (2.90 g, 17.8 mmol, 1 eq) was added to the flask, followed by DCM (50 mL). DIPEA (4.60 g, 6.2 mL, 35.6 mmol, 2 eq) was added slowly to the suspension, immediately producing a color change to orange/red, indicating formation of NHPI anion. The mixture was stirred until homogeneous (5 to 10 minutes). At this point 2,2,2-trifluoroethyl trifluoromethanesulfonate (4.53 g, 19.5 mmol, 1.1 eq) was added in one portion, and the mixture was stirred overnight under N_2 atmosphere.

The reaction was quenched with H_2O, transferred to a separatory funnel, the aqueous phase extracted with DCM, the combined organic phases dried on anhydrous Na_2SO_4, and the solvent removed under reduced pressure. Flash chromatography on silica gel (5:1 until a 365 nm light absorbing impurity is

[326] Shu, C., Noble, A. and Aggarwal, V.K., *Nature* **2020**, *586*, 714–719

[327] Son, J.C., Kim, B.J., Kim, J.H., Lee I.Y., Yun, C.S., Lee, S.H., Lee, C.K., Novel Antiviral Pyrrolopyridine Derivatives and Method for Preparing the Same. US 2014/249162 A1, September 4, **2014**.

eluted, then 3.5:1) furnished *N*-trifluoroethoxyphthalimide as a white, fluffy solid. (3.14 g, 12.8 mmol, 72 % yield). Spectral data are in accordance with the literature (**Fig. 77**).[326]

Notes:

- *Care must be taken to properly sealing all the glass joints before the distillation. This is to avoid any leakage of TfOH that would react with grease in the joints, making the system not well sealed, ultimately leading to very slow distillation, loss of product as well as posing safety issues.*
- *We noticed that compound **14** is not stable in the reaction crude upon dryness, probably due to sensitivity to strongly basic conditions. Therefore, solvent should be evaporated only right before flash chromatography. Anyway, compound **14** resulted stable in the reaction mixture in the presence of solvent for at least one day.*

Aryl iodides **13a-c, 13e, 13f, 13k, 13m-r, 13t, 13v-x** are commercially available and were used without as received.

Aryl iodides **13c**[328], **13d**[329], **13g**[330], **13u**[331] were prepared from 4-iodophenol according to the literature.

Aryl iodides **13h**[332], **13j**[333], **13l**[334] were prepared from 4-iodoaniline according to the literature.

Aryl iodide **13s**[335] was prepared from 4-iodobenzoic acid according to the literature.

Aryl iodide **13y**[336] was prepared from 1,4-diiodobenzene according to the literature.

Aryl iodides **13ad**[337] and **13ac**[338] were prepared following a literature procedure by a two-step sequence: Suzuki cross coupling between 4-(trimethylsilyl)phenylboronic acid and 4-iodobenzonitrile (**15ad**) or 3-fluoroiodobenzene (**13ac**) followed by *ipso*-iodination with ICl.

Aryl iodides **13aa**[339], **13ab**[340] and **13ae**[341] were prepared from 4-iodobenzoyl chloride and the corresponding alcohol or amine according to the literature.

---

[328] Denton, R.M., Scragg, J.T., Saska, J., *Tetrahedron Lett.* **2011**, *52*, 2554–2556
[329] Yuan, H., Bi, K., Chang, W., Yue R., Li, B., Ye, J., Sun, Q., Jin, H., Shan. L., Zhang, W., *Tetrahedron* **2014**, 70, 9084–9092
[330] Yeung, C.S., Dong, V.M., *J. Am. Chem. Soc.* **2008**, 130, 7826–7827
[331] Lee, Y.H., Morandi, B., *Angew. Chem. Int. Ed.* **2019**, 58, 6444–6448
[332] Goldup, S.M., Leigh, D.A., Lusby,P.J., McBurney, R.T., Slawin, A,M.Z., *Angew. Chem. Int. Ed.* **2008**, 47, 3381–3384
[333] Melissaris, A.P., Litt, M.H., *J. Org. Chem.* **1994**, 59, 5818–5821
[334] Boehm, P., Roediger, S., Bismuto, A., Morandi, B., *Angew. Chem. Int. Ed.* **2020**, 59, 17887–17896
[335] Suzuki, T., Ota, Y., Ri, M., Bando, M., Gotoh, A., Itoh, Y., Tsumoto, H., Tatum, P.R., Mizukami, T., Nakagawa, H., Iida, S., Ueda, R., Shirahige, K. and Miyata, N., *J. Med. Chem.* **2012**, 55, 9562–9575
[336] Montoro-García, C., Mayoral, M.J., Chamorro, R., González-Rodríguez, D., *Angew. Chem. Int. Ed.* **2017**, 56, 15649–15653
[337] Liu, T., Yu, S., Shen, X., Li, Y., Liu, J., Huang, C., Cheng, F., *Synthesis* **2022**, 54, A–L
[338] Li, H.L., Kuninobu, Y., *Adv. Synth. Catal.* **2020**, 362, 2637–2641
[339] Han, Y.Q., Yang, X., Kong, K.X., Deng, Y.T., Wu, L.S., Ding, Y., Shi, B.F., *Angew. Chem. Int. Ed.* **2020**, 59, 20455–20458
[340] Zhao, Q.W., Yang, Z.F., Fu, X.P., Zhang, X., *Synlett* **2021**, 32, 1565–1569
[341] Landge, V.G., Grant, A.J., Fu, Y., Rabon, A.M., Payton, J.L., Young, M.C., *J. Am. Chem. Soc.* **2021**, 143, 10352–10360

5.3.3 Nickel precatalyst preparation

Figure 78. L5 preparation

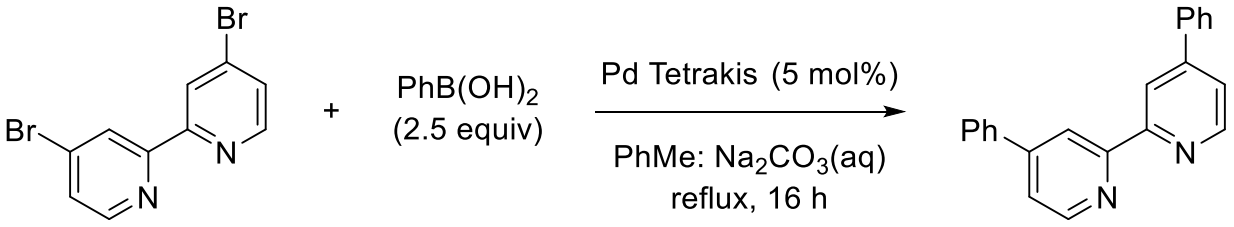

MM-5 **L5**

Ligand **L5** was prepared according to the literature from 4,4'-dibromo-2,2'-bipyridine **MM-5** and phenyl boronic acid via Suzuki Cross Coupling (**Fig. 78**).[342]

Figure 79. Precatalyst nickel complex preparation

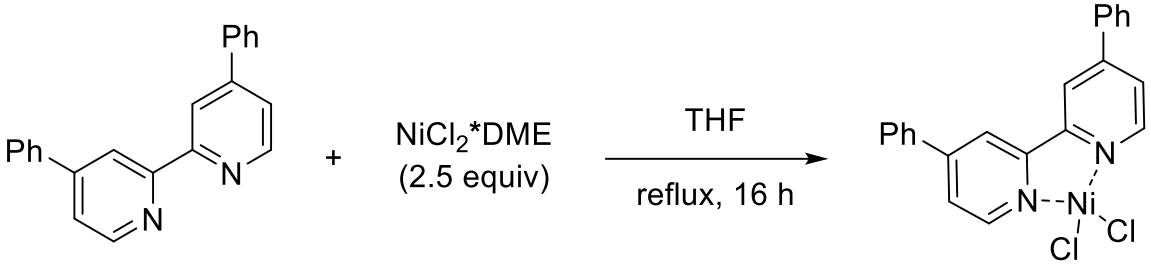

L5

Nickel complex [Ni(**L5**)Cl_2] was prepared via modification of a described procedure for the synthesis of [Ni(dtbbpy)Cl_2][343] as follows: in a heat-gun dried Schlenk tube were added **L5** (0.3 mmol, 92.4 mg, 1 eq), $NiCl_2$(glyme) (0.3 mmol, 65.9 mg, 1 eq) and dry THF (2 mL). The heterogeneous mixture was refluxed for 18 h, cooled to room temperature and diluted with EtOAc (6 mL). The solid was separated by centrifugation, washed with EtOAc, and dried under vacuum to obtain [Ni(**L5**)Cl_2] as a pale green solid (0.285 mmol, 124.8 mg, 95% yield) (**Fig. 79**).

[342] Han, W.S., Han, J.K., Kim, H.Y., Choi, M.J., Kang, Y.S., Pac, C., Kang, S.O., *Inorg. Chem.* **2011**, 50, 3271–3280

[343] Hsu, C.M., Lee, S.C., Tsai, H.E., Tsao, Y.T., Chan, C.L., Minoza, S., Tsai, Z.N., Li, L.Y., Liao, H.H., *J. Org. Chem.* **2022**, 87, 3799–3803

5.3.4 General procedure for the nickel catalyzed reaction

A heat-gun dried pressure Schlenk under N_2 atmosphere was charged with [Ni(**L5**)Cl_2] (4.4 mg, 0.01 mmol, 0.1 eq), and dry/degassed DMA (0.5 mL). The mixture was stirred until the complete dissolution of the metal complex to yield an emerald-green solution (few minutes) (**Figure 81**, top left).

N-trifluoroethoxyphthalimide **14** (73.5 mg, 0.3 mmol, 3 eq), Zn dust (13 mg, 0.2 mmol, 2 eq), NaI (15 mg, 0.1 mmol, 1 eq) and, if solid, aryl iodide **13** (0.1 mmol, 1 eq) were added at once (due to its hygroscopic nature, NaI was weighted last). For liquid aryl iodides, they were added with a 50 µL Hamilton syringe after the solids (**Figure 81**, top right). The heterogeneous mixture appears olive green and turbid (**Figure 81**, bottom left). TMSCl (12.5 µL, 0.1 mmol, 1 eq) was added, and within seconds, a sudden change of color to deep red occurs (**Figure 81**, bottom right) (**Fig. 80**).

The Schlenk was sealed and the mixture stirred at 1250 rpm for the indicated time (until **14** disappeared, judged by TLC).

Figure 80. Nickel catalyzed reaction conditions.

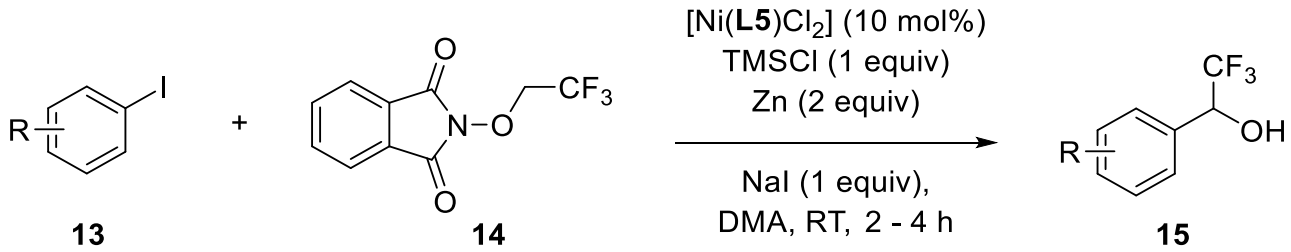

Figure 81. Top Left: [Ni(**L5**)Cl_2] solution in DMA. Top right: Solid reagents (**14**, **13p**, Zn, NaI). Bottom left: Reaction mixture after addition of all solids. Bottom right: Reaction mixture few seconds after the addition of TMSCl.

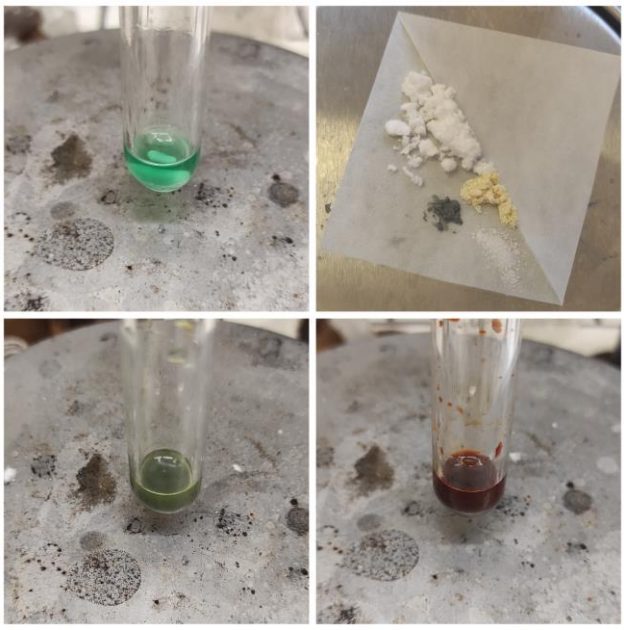

After the indicated time, the Schlenk was opened to air and EtOAc was added, followed by 2N HCl, and the biphasic mixture was shaken and stirred until all Zn was consumed (ca. 5 minutes). The red

color of the organic phase gradually disappears to give a pale-yellow solution. For ^{19}F-NMR yield determination, $PhCF_3$ was added to the reaction mixture as an internal standard and an aliquot was taken without solvent evaporation. To isolate the product, the biphasic mixture was directly transferred to a separatory funnel, the aqueous phase extracted with EtOAc (10 mL x 3), and then the combined organic phases were washed twice with diluted HCl (ca 0.1 N, 10 mL x 2). The organic layer was separated, dried on anhydrous Na_2SO_4, and the solvent removed under reduced pressure. Flash chromatography on silica gel with the appropriate eluent yields the product.

Notes:

- *In our experience, the observation of the color change towards red does not guarantee high yields, but usually indicates initiation of the reaction and full or almost full conversion of* ***14*** *is observed when it occurs. When it does not occur, the reaction provides low yields and low conversion. Addition of TMSCl is not mandatory to observe this change in color, but we noticed that in its presence it always occurs readily, while when it is not added, this phenomenon seems to be more substrate- and conditions dependent.*
- *Vigorous stirring (1250 rpm) is beneficial given the heterogeneous nature of the reductant used, and the reaction should not be run at lower stirring speeds.*[344]
- *For product* ***15h****, due to its basic nature, the aqueous phase was brought to pH = 10 by adding saturated Na_2CO_3 solution prior to extraction.*
- *For products* ***15g, 15i, 15j, 15t, 15x, 15z, 15ac, 15ad,*** *chromatographic separation from phthalimide coproduct was troublesome, therefore after FC a basic wash (aqueous 1N NH_3 / Et_2O) was conducted to obtain pure compounds.*
- *Products* ***15a****,* ***15b****,* ***15c****,* ***15e****,* ***15f****,* ***15m****,* ***15n****,* ***15o****,* ***15p****,* ***15q, 15r*** *are volatile, therefore thorough drying under reduced pressure was not possible. Spectra of these compounds present occasionally solvent peaks; however, this does not prevent full comprehension of the spectroscopic data.*
- *For product* ***15x*** *the General Procedure was slightly modified by doubling the amount of [Ni(****L5****)Cl_2], Zn and* ***14****.*

[344] Lin, Q., Diao, T., *J. Am. Chem. Soc.* **2019**, *141*, 17937−17948

5.3.5 Characterization data of products

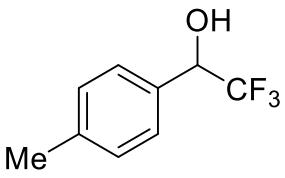

15a. Viscous colourless oil. Reaction time: 2 h. FC eluent: *n*Hex/EtOAc: 7:1. Yield = 88%, (0.088 mmol, 16.7 mg). **^{1}H NMR** (400 MHz, $CDCl_3$) δ = 7.38 – 7.31 (m, 2H), 7.23 – 7.18 (m, 2H), 4.97 (q, *J* = 6.8 Hz, 1H), 2.54 (bs, 1H), 2.36 (s, 3H); **^{13}C NMR** (100 MHz, $CDCl_3$) δ = 139.5, 131.0, 129.3 (2C), 127.3 (q, *J* = 1.0 Hz, 2C), 124.3 (q, *J* = 282.0 Hz), 72.7 (q, *J* = 31.9 Hz), 21.2; **^{19}F NMR** (377 MHz, $CDCl_3$) δ = -78.47 (d, *J* = 6.7 Hz, 3F).

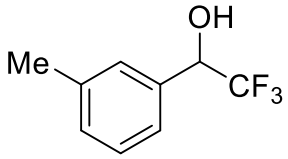

15b. Viscous colourless oil. Reaction time: 3 h. FC eluent: *n*Hex/EtOAc: 7:1. Yield = 62%, (0.062 mmol, 11.8 mg). **^{1}H NMR** (400 MHz, $CDCl_3$) δ = 7.31 – 7.25 (m, 3H), 7.23 – 7.19 (m, 1H), 4.97 (q, *J* = 6.7 Hz, 1H), 2.51 (bs, 1H), 2.37 (s, 3H); **^{13}C NMR** (100 MHz, $CDCl_3$) δ = 138.4, 133.9, 130.3, 128.5, 128.0 (q, *J* = 1.4 Hz), 124.5 (q, *J* = 1.1 Hz), 124.2 (q, *J* = 282.1 Hz), 72.9 (q, *J* = 31.9 Hz), 21.4; **^{19}F NMR** (377 MHz, $CDCl_3$) δ = -78.32 (d, *J* = 6.8 Hz, 3F).

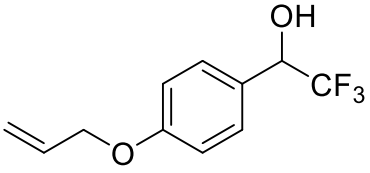

15c. White solid. Reaction time: 5 h. FC eluent: *n*Hex/EtOAc: 6:1. Yield = 50%, (0.050 mmol, 11.8 mg). **MP** = 51 – 53 °C. **^{1}H NMR** (400 MHz, $CDCl_3$) δ = 7.41 – 7.36 (m, 2H), 6.99 – 6.92 (m, 2H), 6.05 (ddt, *J* = 17.3, 10.5, 5.3 Hz, 1H), 5.42 (dq, *J* = 17.3, 1.7 Hz, 1H), 5.30 (dq, *J* = 10.5, 1.4 Hz, 1H), 4.96 (qd, *J* = 6.6, 3.6 Hz, 1H), 4.55 (dt, *J* = 5.3, 1.6 Hz, 2H), 2.47 (d, *J* = 4.3 Hz, 1H); **^{13}C NMR** (100 MHz, $CDCl_3$) δ = 158.5, 131.9, 127.7 (2C), 125.2, 123.3 (q, *J* = 282.2 Hz), 116.9, 113.8 (2C), 71.46 (q, *J* = 32.1 Hz), 67.8; **^{19}F NMR** (377 MHz, $CDCl_3$) δ = -78.53 (d, *J* = 6.8 Hz, 3F).

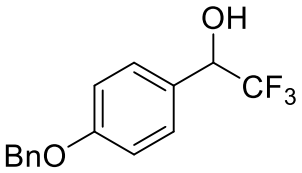

15d. White solid. Reaction time: 5 h FC eluent: *n*Hex/EtOAc: 6:1. Yield = 63%, (0.063 mmol, 17.8 mg). **MP** = 101 – 103 °C. **^{1}H NMR** (400 MHz, $CDCl_3$) δ = 7.45 – 7.29 (m, 7H), 7.03 – 6.96 (m, 2H), 5.07 (s, 2H), 4.97 – 4.91 (m, 1H), 2.56 (d, *J* = 4.1 Hz, 1H); **^{13}C NMR** (100 MHz, $CDCl_3$) δ ^{13}C NMR (101 MHz, $CDCl_3$) δ 159.7, 136.6, 128.8 (2C), 128.6 (2C), 128.1, 127.5 (2C), 126.3, 124.30 (q, *J* = 282.0 Hz), 114.9 (2C), 72.5 (q, *J* = 32.0 Hz), 70.1; **^{19}F NMR** (377 MHz, $CDCl_3$) δ = -78.54 (d, *J* = 6.8 Hz, 3F).

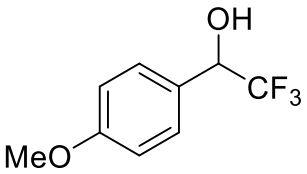

15e. Viscous colourless oil. Reaction time: 3 h. FC eluent: *n*Hex/EtOAc: 6:1. Yield = 61%, (0.061 mmol, 12.6 mg). **^{1}H NMR** (400 MHz, $CDCl_3$) δ = 7.42 – 7.33 (m, 2H), 6.97 – 6.88 (m, 2H), 4.95 (qd, *J* = 6.7, 4.2 Hz, 1H), 3.81 (s, 3H), 2.53 (d, *J* = 4.3 Hz, 1H); **^{13}C NMR** (100 MHz, $CDCl_3$) δ = 160.5, 128.7 (q, *J* = 1.0 Hz, 2C), 126.1 (q, *J* = 1.1 Hz), 124.3 (q, *J* = 281.9 Hz), 114.0 (2C), 72.5 (q, *J* = 32.0 Hz), 55.3; **^{19}F NMR** (377 MHz, $CDCl_3$) δ = -78.60 (d, *J* = 6.8 Hz, 3F).

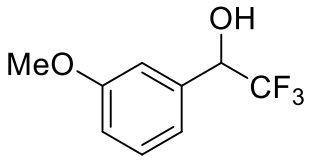

15f. Colourless oil. Reaction time: 6 h. FC eluent: *n*Hex/EtOAc: 6:1. Yield = 64%, (0.064 mmol, 13.2 mg). **^{1}H NMR** (400 MHz, $CDCl_3$) δ = 7.35 – 7.28 (m, 1H), 7.07 – 6.99 (m, 2H), 6.93 (ddd, *J* = 8.4, 2.6, 1.1 Hz, 1H), 4.98 (q, *J* = 6.7 Hz, 1H), 3.81 (s, 3H), 2.63 (bs, 1H); **^{13}C NMR** (100 MHz, $CDCl_3$) δ = 159.7, 135.4 (q, *J* = 1.2 Hz), 129.7, 124.2 (q, *J* = 282.1 Hz),

119.7 (q, *J* = 0.8 Hz), 115.09, 112.9 (q, *J* = 1.0 Hz), 72.7 (q, *J* = 32.0 Hz), 55.3; **^{19}F NMR** (377 MHz, $CDCl_3$) δ = -78.38 (d, *J* = 6.7 Hz, 3F).

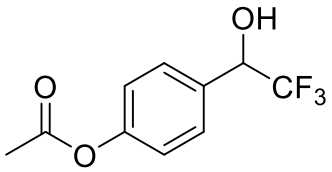

15g. White solid. Reaction time: 5 h. FC eluent: *n*Hex/EtOAc: 4.5:1. Yield = 62%, (0.062 mmol, 14.5 mg). **MP** = 95 – 98 °C. **^{1}H NMR** (400 MHz, $CDCl_3$) δ = 7.52 – 7.45 (m, 2H), 7.17 – 7.08 (m, 2H), 5.01 (q, *J* = 6.7 Hz, 1H), 2.66 (bs, 1H), 2.29 (s, 3H); **^{13}C NMR** (100 MHz, $CDCl_3$) δ = 169.2, 151.5, 131.5, 128.6 (2C), 124.1 (q, *J* = 282.2 Hz), 121.8 (2C), 72.3 (q, *J* = 32.2 Hz), 21.1; **^{19}F NMR** (377 MHz, $CDCl_3$) δ = -78.46 (d, *J* = 6.8 Hz, 3F).

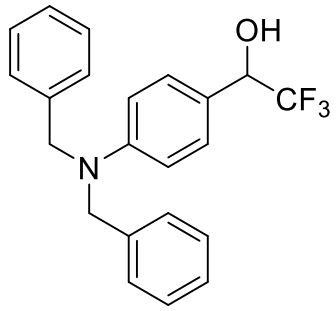

15h. White solid. Reaction time: 3 h. FC eluent: *n*Hex/EtOAc: 4:1. Yield = 73%, (0.073 mmol, 27.1 mg). **MP** = 152 – 154 °C. **^{1}H NMR** (400 MHz, $CDCl_3$) δ = 7.32 – 7.23 (m, 4H), 7.22 – 7.14 (m, 8H), 6.68 – 6.64 (m, 2H), 4.79 (q, *J* = 7.0 Hz, 1H), 4.60 (s, 4H), 2.27 (bs, 1H); **^{13}C NMR** (150 MHz, $CDCl_3$) δ = 149.0, 137.0 (2C), 127.7 (4C), 127.6 (2C), 126.0 (2C), 125.5 (4C), 123.5 (q, *J* = 281.8 Hz), 120.8, 111.1 (2C), 71.70 (q, *J* = 32.0 Hz), 53.1 (2C); **^{19}F NMR** (565 MHz, $CDCl_3$) δ = -78.3 (d, *J* = 6.9 Hz, 3F); **HRMS (*ESI*)** m/z: $[M+H]^+$ calcd. for $C_{22}H_{20}F_3NO$ 372.1575; found 372.1567.

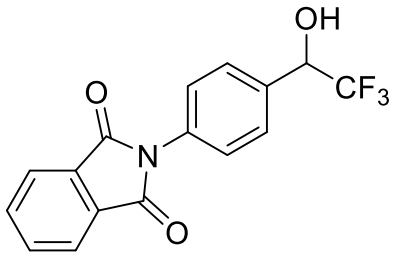

15i. White solid. Reaction time: 16 h. FC eluent: *n*Hex/EtOAc: 2:1. Yield = 74%, (0.074 mmol, 23.8 mg). **MP** = 202 – 204 °C. **^{1}H NMR** (400 MHz, acetone-d_6) δ = 7.97 – 7.93 (m, 2H), 7.93 – 7.90 (m, 2H), 7.74 – 7.68 (m, 2H), 7.61 – 7.54 (m, 2H), 5.97 (d, *J* = 5.4 Hz, 1H), 5.32 (qd, *J* = 7.1, 5.2 Hz, 1H); **^{13}C NMR** (100 MHz, acetone-d_6) δ = 166.8 (2C), 135.3 (q, *J* = 1.6 Hz), 134.5 (2C), 133.0, 132.0 (2C), 128.1 (q, 0.8 Hz, 2C), 126.8 (2C), 125.0 (q, *J* = 281.9 Hz), 123.3 (2C), 71.2 (q, *J* = 31.2 Hz); **^{19}F NMR** (377 MHz, acetone-d_6) δ = -78.64 (d, *J* = 7.0 Hz, 3F); **HRMS (*APCI*)** m/z: $[M+H]^+$ calcd. for $C_6H_{11}F_3NO_3$ 322.0691; found 322.0682.

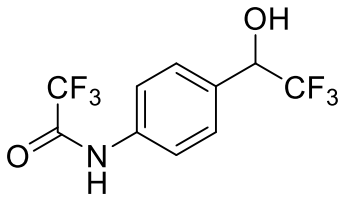

15j. White solid. Reaction time: 16 h. FC eluent: *n*Hex/EtOAc: 3:1. Yield = 63%, (0.063 mmol, 18.1 mg). **MP** = 147 – 150 °C. **^{1}H NMR** (400 MHz, acetone-d_6) δ = 10.32 (bs, 1H), 7.79 – 7.71 (m, 2H), 7.58 – 7.53 (m, 2H), 5.93 – 5.85 (m, 1H), 5.23 – 5.15 (m, 1H), peaks at 10.32 ppm and 5.89 ppm show an integral value lower than unity, probably due to partial H-D exchange with the solvent; **^{13}C NMR** (100 MHz, acetone-d_6) δ = 154.8 (q, *J* = 37.1 Hz, two isotopomeric signals), 137.1 (two isotopomeric signals), 134.1, 128.3 (2C), 125.0 (q, *J* = 282.1 Hz), 120.5 (2C, (two isotopomeric signals), 116.0 (q, *J* = 288.1 Hz), 71.0 (q, *J* = 31.4 Hz, (two isotopomeric signals), some signals appear split due to partial H-D exchange with the solvent giving rise to two isotopomers; **^{19}F NMR** (377 MHz, $CDCl_3$) δ = -76.12 – -76.34 (m, 3F, two isotopomeric signals), -78.73 – -78.85 (m, 3F, two isotopomeric signals); **HRMS (*ESI*)** m/z: $[M-H]^-$ calcd. for $C_{10}H_6F_6NO_2$ 286.0308; found 286.0323.

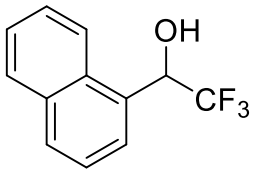

15k. Colourless oil. Reaction time: 16 h. FC eluent: *n*Hex/EtOAc: 9:1. Yield = 61%, (0.061 mmol, 13.8 mg). **^{1}H NMR** (400 MHz, $CDCl_3$) δ = 8.05 (d, *J* = 8.4 Hz, 1H), 7.95 – 7.87 (m, 2H), 7.83 (d, *J* = 7.3 Hz, 1H), 7.60 – 7.42 (m, 3H), 5.89 (q, *J* = 6.5 Hz, 1H), 2.84 (bs, 1H); **^{13}C NMR** (100 MHz, $CDCl_3$) δ = 133.7, 131.1, 130.1, 130.0 (q, *J* = 0.9 Hz), 129.0, 126.8, 125.9, 125.8 (q, *J* = 1.3 Hz), 125.2, 124.7 (q, *J* = 282.6 Hz), 122.8 (q, *J* = 1.4 Hz), 69.0 (q, *J* = 32.3 Hz); **^{19}F NMR** (377 MHz, $CDCl_3$) δ = -76.93 (d, *J* = 6.6 Hz, 3F).

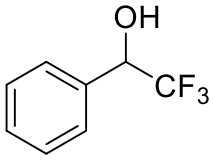

15l. Reaction time: 4 h. Compound **3t** was found to be too volatile to be isolated on 0.1 mmol scale. The yield given (70%) was determined by ^{19}F NMR analysis on the crude reaction mixture. This is a known compound and spectral data observed in the crude is in accordance with the literature.[286]

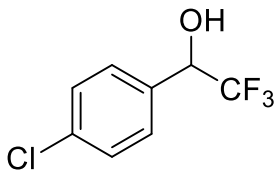

15m. Colourless oil. Reaction time: 16 h. FC eluent: *n*Hex/EtOAc: 10:1. Yield = 56%, (0.056 mmol, 11.8 mg). **^{1}H NMR** (400 MHz, $CDCl_3$) δ = 7.44 – 7.39 (m, 2H), 7.39 – 7.35 (m, 2H), 5.00 (q, *J* = 6.2 Hz, 1H), 2.69 (s, 1H); **^{13}C NMR** (100 MHz, $CDCl_3$) δ = 135.5, 132.3 (q, *J* = 1.0 Hz), 128.8 (2C), 128.8 (q, *J* = 0.9 Hz, 2C) 124.0 (q, *J* = 281.9 Hz), 72.1 (q, *J* = 32.1 Hz); **^{19}F NMR** (377 MHz, $CDCl_3$) δ = -78.59 (d, *J* = 6.4 Hz, 3F).

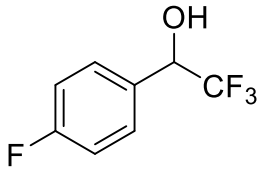

15n. Colourless oil. Reaction time: 16 h. FC eluent: *n*Hex/EtOAc: 7:1. Yield = 55%, (0.055 mmol, 10.7 mg). **^{1}H NMR** (400 MHz, $CDCl_3$) δ = 7.50 – 7.40 (m, 2H), 7.15 – 7.04 (m, 2H), 5.01 (q, *J* = 6.6 Hz, 1H), 2.64 (bs, 1H); **^{13}C NMR** (100 MHz, $CDCl_3$) δ = 163.4 (d, *J* = 248.5 Hz), 129.7 – 129.6 (m), 129.3 (dq, *J* = 8.6, 0.9 Hz, 2C), 124.1 (qd, *J* = 281.8, 1.1 Hz), 115.6 (d, *J* = 21.8 Hz, 2C), 72.2 (q, *J* = 32.2 Hz); **^{19}F NMR** (377 MHz, $CDCl_3$) δ = -76.93 (d, *J* = 6.6 Hz, 3F), -111.81 – -111.89 (m, 1F).

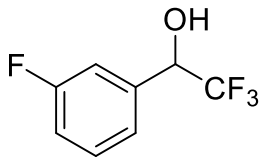

15o. Viscous colourless oil. Reaction time: 16 h. FC eluent: *n*Hex/EtOAc: 7:1. Yield = 65%, (0.065 mmol, 12.6 mg). **^{1}H NMR** (400 MHz, $CDCl_3$) δ = 7.40 – 7.33 (m, 1H), 7.25 – 7.19 (m, 2H), 7.09 (tdd, *J* = 8.4, 2.6, 1.0 Hz, 1H), 5.07 – 4.98 (m, 1H), 2.70 (d, *J* = 4.4 Hz, 1H); **^{13}C NMR** (100 MHz, $CDCl_3$) δ = 162.7 (d, *J* = 246.8 Hz), 136.2 (d, *J* = 8.7 Hz), 130.1 (d, *J* = 8.1 Hz), 124.0 (q, *J* = 282.4 Hz), 123.2 – 123.0 (m), 116.5 (d, *J* = 21.2 Hz), 114.5 (dq, *J* = 22.6, 1.0 Hz), 72.1 (qd, *J* = 32.4, 1.7 Hz); **^{19}F NMR** (377 MHz, $CDCl_3$) δ = -78.45 (d, *J* = 6.5 Hz, 3F), -112.18 (td, *J* = 9.0, 5.6 Hz, 1F).

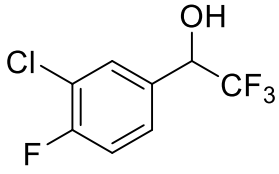

15p. Viscous colourless oil. Reaction time: 16 h. FC eluent: *n*Hex/EtOAc: 10:1. Yield = 65%, (0.065 mmol, 14.8 mg). **^{1}H NMR** (600 MHz, $CDCl_3$) δ = 7.76 (dd, *J* = 6.7, 2.3 Hz, 1H), 7.71 – 7.66 (m, 1H), 7.26 (t, *J* = 9.2 Hz, 1H), 5.09 (q, *J* = 6.5 Hz, 1H), 2.94 (bs, 1H); **^{13}C NMR** (150 MHz, $CDCl_3$) δ = 157.7 (d, *J* = 251.3 Hz), 129.8 (d, *J* = 4.0 Hz), 128.9, 126.3 (d, *J* = 7.6 Hz), 122.9 (q, *J* = 282.1 Hz), 120.5 (d, *J* = 18.1 Hz), 115.8 (d, *J* = 21.6 Hz), 70.6 (q, *J* = 32.4 Hz); **^{19}F NMR** (565 MHz, $CDCl_3$) δ = -78.62 (d, *J* = 6.8 Hz, 3F), -113.87 – -113.93 (m, 1F).

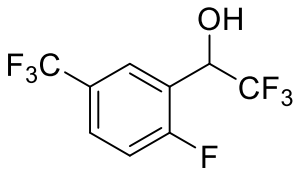

15q. Viscous colourless oil. Reaction time: 16 h. FC eluent: *n*Hex/EtOAc: 10:1. Yield = 43%, (0.043 mmol, 11.3 mg). **^{1}H NMR** (600 MHz, $CDCl_3$) δ = 7.57 (dd, *J* = 7.0, 2.2 Hz, 1H), 7.36 (ddd, *J* = 8.1, 4.2, 2.2 Hz, 1H), 7.18 (t, *J* = 8.6 Hz, 1H), 5.01 (q, *J* = 6.5 Hz, 1H), 2.83 (bs, 1H); **^{13}C NMR** (150 MHz, $CDCl_3$) δ = 159.3 (dq, *J* = 259.0, 2.1 Hz), 132.0 (d, *J* = 8.9 Hz), 129.1 (d, *J* = 3.8 Hz), 125.5 (q, *J* = 5.2 Hz), 122.8 (q, *J* = 282.0 Hz) partially overlapped with 121.2 (q, *J* = 272.4 Hz), 117.8 (qd, *J* = 33.4, 12.9 Hz), 116.3 (d, *J* = 20.9 Hz), 70.5 (q, *J* = 32.4 Hz); **^{19}F NMR** (565 MHz, $CDCl_3$) δ = -61.57 (d, *J* = 12.2 Hz, 3F), -78.72 (d, *J* = 6.8 Hz, 3F), -112.98 – -113.10 (m, 1F); **HRMS (*ESI*)** m/z: $[M+HCOO]^-$ calcd. for $C_{10}H_6F_7O_3$ 307.0211; found 307.0216.

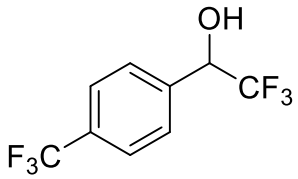

15r. Colourless oil. Reaction time: 16 h. FC eluent: *n*Hex/EtOAc: 10:1. Yield = 58%, (0.058 mmol, 14.2 mg). **^{1}H NMR** (400 MHz, $CDCl_3$) δ = 7.69 – 7.64 (m, 2H), 7.63 – 7.58 (m, 2H), 5.14 – 5.06 (m, 1H), 2.81 (bs, 1H); **^{13}C NMR** (100 MHz, $CDCl_3$) δ = 137.6 – 137.5 (m), 131.7 (q, *J* = 32.6 Hz), 127.8 (q, *J* = 0.9 Hz, 2C), 125.5 (q, *J* = 3.8 Hz, 2C), 123.9 (q, *J* = 282.1 Hz) partially overlapped with 123.8 (q, *J* = 272.4 Hz), 72.2 (q, *J* = 32.3 Hz); **^{19}F NMR** (377 MHz, $CDCl_3$) δ = -62.90 (s, 3F), -78.59 (d, *J* = 6.4 Hz, 3F).

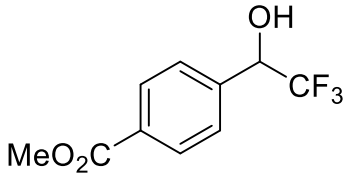

15s. White solid. Reaction time: 16 h. FC eluent: *n*Hex/EtOAc: 5:1. Yield = 73%, (0.073 mmol, 17.1 mg). **MP** = 46 – 49 °C. **^{1}H NMR** (400 MHz, $CDCl_3$) δ = 8.08 – 8.01 (m, 2H), 7.58 – 7.51 (m, 2H), 5.08 (q, *J* = 6.6 Hz, 1H), 3.91 (s, 3H), 3.02 (bs, 1H); **^{13}C NMR** (100 MHz, $CDCl_3$) δ = 166.6, 138.6 (q, *J* = 1.2 Hz), 131.1, 129.7 (2C), 127.5 (q, *J* = 0.9 Hz, 2C), 124.0 (q, *J* = 282.3 Hz), 72.3 (q, *J* = 32.1 Hz), 52.29; **^{19}F NMR** (377 MHz, $CDCl_3$) δ = -78.24 (d, *J* = 6.7 Hz, 3F).

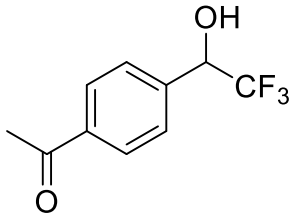

15t. White solid. Reaction time: 16 h. FC eluent: *n*Hex/EtOAc: 5:1. Yield = 68%, (0.068 mmol, 14.8 mg). **MP** = 97 – 99 °C. **^{1}H NMR** (400 MHz, $CDCl_3$) δ = 8.01 – 7.93 (m, 2H), 7.61 – 7.55 (m, 2H), 5.10 (q, *J* = 6.7 Hz, 1H), 2.88 (bs, 1H), 2.60 (s, 3H); **^{13}C NMR** (100 MHz, $CDCl_3$) δ = 197.7, 138.8 (q, *J* = 1.1 Hz), 138.0, 128.6 (2C), 127.8 (q, *J* = 0.9 Hz, 2C), 124.0 (q, *J* = 282.3 Hz), 72.3 (q, *J* = 32.2 Hz), 26.7; **^{19}F NMR** (377 MHz, $CDCl_3$) δ = -78.23 (d, *J* = 6.7 Hz, 3F).

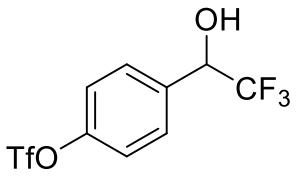

15u. Viscous colourless oil. Reaction time: 7 h. FC eluent: *n*Hex/EtOAc: 7:1. Yield = 61%, (0.061 mmol, 19.8 mg). **^{1}H NMR** (400 MHz, $CDCl_3$) δ = 7.61 – 7.55 (m, 2H), 7.35 – 7.28 (m, 2H), 5.07 (q, *J* = 6.8 Hz, 1H), 2.89 (bs, 1H); **^{13}C NMR** (100 MHz, $CDCl_3$) δ = 150.1, 134.3 (q, *J* = 1.0 Hz), 129.5 (q, *J* = 0.8 Hz, 2C), 123.8 (q, *J* = 282.2 Hz), 121.6 (2C), 118.7 (q, *J* = 320.6 Hz), 71.8 (q, *J* = 32.4 Hz); **^{19}F NMR** (377 MHz, $CDCl_3$) δ = -72.85 (s, 3F), -78.54 (d, *J* = 6.3 Hz, 3F); **HRMS (*ESI*)** m/z: $[M+HCOO]^-$ calcd. for $C_{10}H_7F_6O_6S$ 368.9873; found 368.9889.

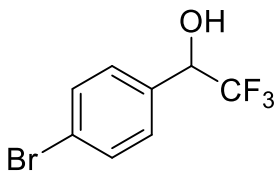

15v. Colourless oil. Reaction time: 16 h. FC eluent: *n*Hex/EtOAc: 10:1. Yield = 60%, (0.060 mmol, 15.2 mg). **^{1}H NMR** (600 MHz, $CDCl_3$) δ = 7.50 – 7.46 (m, 2H), 7.31 – 7.26 (m, 2H), 4.93 (qd, *J* = 6.7, 3.8 Hz, 1H), 2.86 (bs, 1H); **^{13}C NMR** (150 MHz, $CDCl_3$) δ = 136.7, 130.8 (2C), 128.1 (2C), 123.0 (q, *J* = 282.3 Hz), 122.7, 71.2 (q, *J* = 32.2 Hz); **^{19}F NMR** (565 MHz, $CDCl_3$) δ =

-78.52 (d, *J* = 6.8 Hz, 3F). (This compound was isolated as an inseparable 9:1 mixture with the corresponding *p*-iodo derivative. Relevant signals in the ^{1}H NMR spectrum for this compound are: 7.69 – 7.66 (m, 2H) and 7.16 – 7.14 (m, 2H). The ^{19}F NMR spectrum for this compound shows a doublet at -78.49 ppm. This is a known compound, and spectral data are in accordance with the literature.[345]

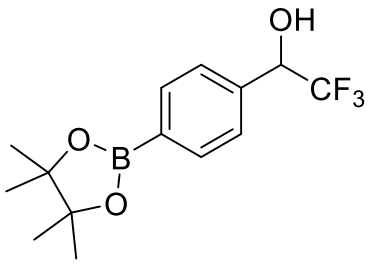

15w. White solid. Reaction time: 16 h. FC eluent: *n*Hex/EtOAc: 5:1. Yield = 43%, (0.043 mmol, 7.5 mg). **MP** = 84 – 87 °C. **^{1}H NMR** (400 MHz, $CDCl_3$) δ = 7.86 – 7.80 (m, 2H), 7.49 – 7.43 (m, 2H), 5.02 (qd, *J* = 6.7, 4.6 Hz, 1H), 2.59 (d, *J* = 4.6 Hz, 1H), 1.33 (s, 12 H); **^{13}C NMR** (100 MHz, $CDCl_3$) δ = 136.7 (q, *J* = 1.0 Hz), 135.0 (2C), 126.7 (2C), 124.1 (q, *J* = 282.3 Hz), 84.0 (2C), 72.8 (q, *J* = 31.9 Hz), 24.8 (4C), the quaternary carbon connected to the B atom is too broad and was not detected; **^{19}F NMR** (377 MHz, $CDCl_3$) δ = -78.27 (d, *J* = 6.7 Hz, 3F); **HRMS (*ESI*)** m/z: $[M+HCOO]^-$ calcd. for $C_{15}H_{19}BF_3O_5$ 347.1283; found 347.1291.

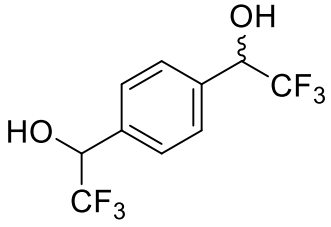

15x. White solid. Reaction time: 16 h. FC eluent: *n*Hex/EtOAc: 8:1. Yield = 73%, (0.073 mmol, 20.0 mg), 1:1 *dr*. **^{1}H NMR** (400 MHz, $CDCl_3$) δ = 7.53 (s, 4H), 5.05 (q, *J* = 6.7 Hz, 2H), 2.65 (bs, 2H), the signals of the two diastereoisomers overlap completely, appearing as a single compound; **^{13}C NMR** (100 MHz, $CDCl_3$) δ = 135.2 (2C), 127.7 (4C), 124.1 (q, *J* = 282.0 Hz, 2C), 72.4 (q, *J* = 32.3 Hz, 2C, two diastereomeric signals), The signals of the two diastereoisomers overlap in some cases, appearing as a single compound, in other cases (as specified in the list) they split; **^{19}F NMR** (377 MHz, $CDCl_3$) δ = -78.38 (d, *J* = 6.5 Hz, 6F), the signals of the two diastereoisomers overlap completely, appearing as a single compound.

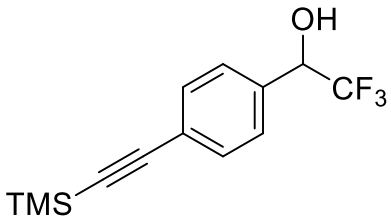

15y. Yellow solid. Reaction time: 16 h. FC eluent: *n*Hex/EtOAc: 8:1. Yield = 65%, (0.065 mmol, 17.7 mg). **MP** = 58 – 60 °C. **^{1}H NMR** (400 MHz, $CDCl_3$) δ = 7.52 – 7.45 (m, 2H), 7.43 – 7.36 (m, 2H), 5.00 (q, *J* = 6.7 Hz, 1H), 2.66 (bs, 1H), 0.24 (s, 9H); **^{13}C NMR** (100 MHz, $CDCl_3$) δ = 133.9 (q, *J* = 1.1 Hz), 132.1 (2C), 127.2 (q, *J* = 0.8 Hz, 2C), 124.5, 124.0 (q, *J* = 282.2 Hz), 104.2, 95.5, 72.5 (q, *J* = 32.1 Hz), -0.14 (3C); **^{19}F NMR** (377 MHz, $CDCl_3$) δ = -78.38 (d, *J* = 6.7 Hz, 3F)

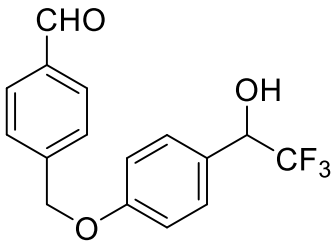

15z. White solid. Reaction time: 16 h. FC eluent: nHex/EtOAc: 3:1. Yield = 50% (0.050 mmol, 15.5 mg). MP = 114 – 117 °C. **^{1}H NMR** (400 MHz, $CDCl_3$) δ = 9.86 (s, 1H), 7.86 – 7.78 (m, 2H), 7.53 – 7.49 (m, 2H), 7.48 – 7.44 (m, 2H), 7.10 – 7.02 (m, 2H), 5.16 (s, 2H), 5.04 (q, J = 6.8 Hz, 1H), 2.90 (s, 1H); **^{13}C NMR** (100 MHz, $CDCl_3$) δ = 190.9, 163.5, 137.4, 134.1, 132.0 (2C), 130.2, 127.8 (2C), 127.5 (2C), 124.2 (q, J = 282.3 Hz), 115.1 (2C), 72.5 (q, J = 31.9 Hz), 69.7; **^{19}F NMR** (377 MHz,

[345] Aspnes, G.E., Dow, R.L., Munchhof, M.J., 4-Amino-7,8-Dihydropyrido[4,3-d]pyrimidin-5(6H)-one Derivatives. US 2010/197591 A1, August 5, **2010**

$CDCl_3$) δ = -78.4 (d, J = 6.7 Hz); **HRMS (*ESI*)** m/z: [M+HCOO] - calcd. for $C_{17}H_{14}F_3O_5$ 355.0799; found 355.0788.

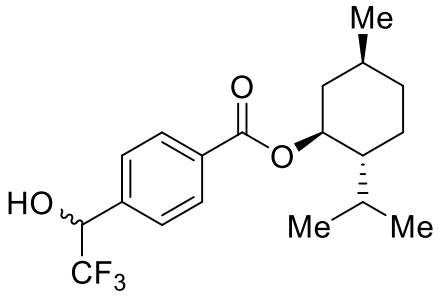

15aa. White solid. Reaction time: 16 h. FC eluent: *n*Hex/EtOAc: 5:1. Yield = 46%, (0.046 mmol, 16.5 mg), 1:1 *dr*. **^{1}H NMR** (400 MHz, $CDCl_3$) δ = 8.09 – 8.02 (m, 2H), 7.58 – 7.51 (m, 2H), 5.08 (q, *J* = 6.6 Hz, 1H), 4.92 (td, *J* = 10.9, 4.4 Hz, 1H), 2.84 (bs, 1H), 2.15 – 2.05 (m, 1H), 1.98 – 1.85 (m, 1H), 1.77 – 1.67 (m, 2H), 1.65 – 1.47 (m, 2H), 1.18 – 1.02 (m, 2H), 0.92 (d, *J* = 4.8 Hz, 3H), 0.90 (d, *J* = 5.4 Hz, 3H) overlapped with 0.93 – 0.88 (m, 1H), 0.77 (d, *J* = 6.9 Hz, 3H), the signals of the two diastereoisomers overlap completely, appearing as a single compound; **^{13}C NMR** δ = 165.6, 138.3, 131.9, 129.7 (2C), 127.4 (2C), 124.0 (q, *J* = 282.2 Hz), 75.2, 72.4 (q, *J* = 32.3, Hz) and 72.3 (q, *J* = 31.8 Hz, two diastereomeric signals), 47.2, 40.9, 34.3, 31.4, 26.5 (two diastereomeric signals), 23.6 (two diastereomeric signals), 22.0, 20.7 (two diastereomeric signals), 16.5 (two diastereomeric signals). The signals of the two diastereoisomers overlap in some cases, appearing as a single compound, in other cases (as specified in the list) they split; **^{19}F NMR** (377 MHz, $CDCl_3$) δ = -78.25 (d, *J* = 6.5 Hz, 3F) and -78.26 (d, *J* = 6.4 Hz, 3F), two partially overlapped diastereomeric signals; **HRMS (*ESI*)** m/z: $[M+HCOO]^-$ calcd. for $C_{20}H_{26}F_3O_5$ 403.1738; found 403.1741.

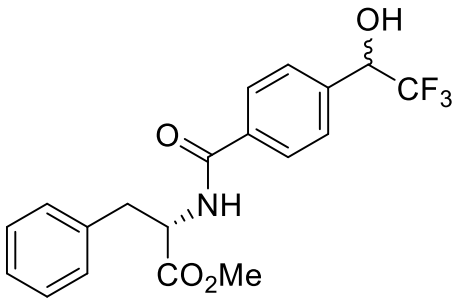

15ab. White solid. Reaction time: 16 h. FC eluent: *n*Hex/EtOAc: 3:1. Yield = 65%, (0.065 mmol, 24.8 mg), 1:1 *dr*. **^{1}H NMR** (400 MHz, $CDCl_3$) δ = 7.70 – 7.62 (m, 2H), 7.51 – 7.44 (m, 2H), 7.32 – 7.21 (m, 3H), 7.14 – 7.07 (m, 2H), 6.60 (d, *J* = 7.6 Hz, 1H), 5.10 – 4.98 (m, 2H), 3.76 (s, 3H), 3.28 (bs, 1H) partially overlapped with 3.26 (dd, *J* = 13.9, 5.7 Hz, 1H), 3.18 (dd, *J* = 13.9, 5.5 Hz, 1H), the signals of the two diastereoisomers overlap completely, appearing as a single compound; **^{13}C NMR** δ = 172.0 (two diastereomeric signals), 166.4 (two diastereomeric signals), 137.8, 135.6, 134.7 (two diastereomeric signals), 129.3 (2C), 128.7 (2C), 127.7 (2C), 127.3, 127.1 (2C, two diastereomeric signals), 124.1 (q, *J* = 282.3 Hz), 72.10 (q, *J* = 31.8 Hz, two diastereomeric signals) 53.6 (two diastereomeric signals), 52.5, 37.8, the signals of the two diastereoisomers overlap in some cases, appearing as a single compound, in other cases (as specified in the list) they split; **^{19}F NMR** (377 MHz, $CDCl_3$) δ = -78.25 (d, *J* = 6.8 Hz, 3F), and -78.26 (d, *J* = 6.8 Hz, 3F), two partially overlapped diastereomeric signals; **HRMS (*ESI*)** m/z: $[M+Na]^+$ calcd. for $C_{19}H_{18}F_3NNaO_4$ 404.1086; found 404.1079.

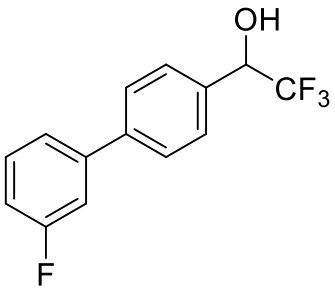

15ac. White solid. Reaction time: 16 h. FC eluent: *n*Hex/EtOAc: 8:1. Yield = 75% (0.075 mmol, 20.3 mg) reaction run on 0.1 mmol scale. Yield = 81% (0.81 mmol, 218.7 mg) reaction run on 1.0 mmol scale (unmodified protocol except for 4.0 mL of DMA employed as the solvent). **MP** = 67 – 70 °C. **^{1}H NMR** (400 MHz, $CDCl_3$) δ = 7.63 – 7.58 (m, 2H), 7.57 – 7.52 (m, 2H), 7.44 – 7.33 (m, 2H), 7.27 (ddd, *J* = 10.2, 2.5, 1.6 Hz, 1H), 7.09 – 7.02 (m, 1H), 5.07 (q, *J* = 6.7 Hz, 1H), 2.75 (s, 1H); **^{13}C NMR** (100 MHz, $CDCl_3$) δ = 163.2 (d, *J* = 246.0 Hz), 142.6 (d, *J* = 7.6 Hz), 141.2 (d, *J* = 2.3 Hz), 133.4 (q, *J* = 1.1 Hz), 130.3 (d, *J* = 8.5 Hz), 128.0 (q, *J* = 0.9 Hz,

2C), 127.3 (2C), 124.2 (q, *J* = 281.9 Hz), 122.8 (d, *J* = 3.0 Hz), 114.5 (d, *J* = 21.2 Hz), 114.0 (d, *J* = 22.1 Hz), 72.5 (q, *J* = 32.1 Hz); **^{19}F NMR** (377 MHz, $CDCl_3$) δ = -78.32 (d, *J* = 6.7 Hz), -112.89 (ddd, *J* = 10.0, 8.3, 5.5 Hz).

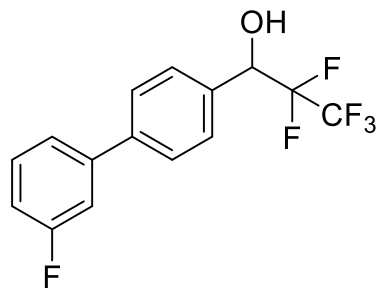

15ac'. White solid. Reaction time: 16 h. FC eluent: nHex/EtOAc: 10:1. Yield = 22% (0.022 mmol, 7.0 mg). MP = 65 – 68 °C. **^{1}H NMR** (400 MHz, $CDCl_3$) δ = 7.66 – 7.60 (m, 2H), 7.59 – 7.52 (m, 2H), 7.45 – 7.36 (m, 2H), 7.30 (dt, J = 10.1, 2.1 Hz, 1H), 7.10 – 7.02 (m, 1H), 5.19 (ddd, J = 16.6, 7.2, 4.9 Hz, 1H), 2.56 (d, J = 5.0 Hz, 1H); **^{13}C NMR** (100 MHz, $CDCl_3$) δ = 163.2 (d, J = 246.0 Hz), 142.5 (d, J = 7.6 Hz), 141.3 (d, J = 2.1 Hz), 133.4, 130.3 (d, J = 8.4 Hz), 128.4 (2C), 127.3 (2C), 122.8 (d, J = 3.0 Hz), 114.5 (d, J = 21.3 Hz), 114.1 (d, J = 22.1 Hz), 71.7 (dd, J = 28.1, 22.6 Hz), the CF_2 and CF_3 carbons of the pentafluoroethyl group were not detected; **^{19}F NMR** (377 MHz, $CDCl_3$) δ = -81.20 (s, 3F), -112.87 (td, J = 9.3, 5.6 Hz, 1F), -121.66 (dd, J = 275.9, 7.3 Hz, 1F), -129.27 (dd, J = 276.0, 16.6 Hz, 1F); **HRMS (*ESI*)** m/z: [M+HCOO] - calcd. for $C_{16}H_{11}F_6O_3$ 365.0618; found 365.0625

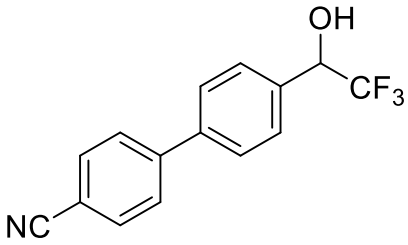

15ad. White solid. Reaction time: 16 h. FC eluent: *n*Hex/EtOAc: 5:1. Yield = 58% (0.058 mmol, 16.1 mg). **MP** = 152 – 154 °C. **^{1}H NMR** (400 MHz, $CDCl_3$) δ = 7.75 – 7.70 (m, 2H), 7.69 – 7.65 (m, 2H), 7.64 – 7.56 (m, 4H), 5.09 (q, *J* = 6.7 Hz, 1H), 2.79 (bs, 1H); **^{13}C NMR** (100 MHz, $CDCl_3$) δ = 144.8, 140.3, 134.3, 132.7 (2C), 128.2 (q, *J* = 1.0 Hz, 2C), 127.8 (2C), 127.4 (2C), 124.1 (q, *J* = 282.2 Hz), 118.8, 111.3, 72.4 (q, *J* = 32.1 Hz); **^{19}F NMR** (377 MHz, $CDCl_3$) δ = -78.33 (d, *J* = 6.6 Hz); **HRMS (*ESI*)** m/z: $[M+HCOO]^-$ calcd. for $C_{16}H_{11}F_3NO_3$ 322.0697; found 322.0700.

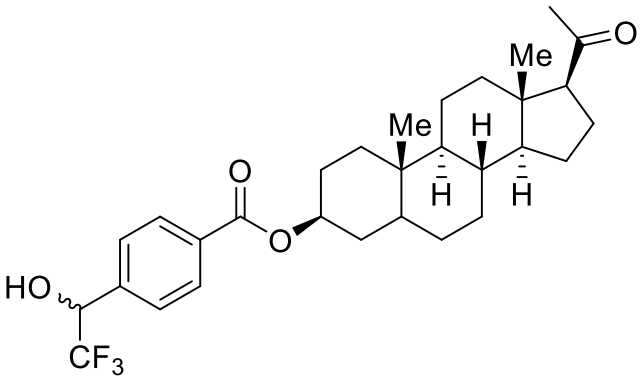

15ae. White solid. Reaction time: 16 h. FC eluent: *n*Hex/*i*PrOAc: 2:1. Yield = 32%, (0.032 mmol, 16.6 mg), 1:1 *dr*. **^{1}H NMR** (400 MHz, $CDCl_3$) δ = 8.09 – 8.03 (m, 2H), 7.60 – 7.50 (m, 2H), 5.44 – 5.37 (m, 1H), 5.09 (q, *J* = 6.6 Hz, 1H), 4.85 (dtd, *J* = 16.3, 8.4, 4.5 Hz, 1H), 2.98 (s, 1H), 2.53 (t, *J* = 8.9 Hz, 1H), 2.45 (d, *J* = 7.2 Hz, 2H), 2.21 – 2.13 (m, 1H), 2.11 (s, 3H), 2.07 – 1.96 (m, 3H), 1.91 (dt, *J* = 13.4, 3.5 Hz, 1H), 1.80 – 1.39 (m, 7H), 1.31 – 1.13 (m, 4H), 1.05 (s, 3H) overlapped with 1.07 – 1.01 (m, 1H), 0.62 (s, 3H), the signals of the two diastereoisomers overlap completely, appearing as a single compound; **^{13}C NMR** δ = 209.8, 165.4, 139.5, 138.4, 131.8, 129.7 (2C), 127.4 (2C), 124.0 (q, *J* = 282.6 Hz), 122.6, 74.7, 72.4 (q, *J* = 32.1 Hz), 63.7, 56.8, 49.9, 44.0, 38.8, 38.1, 37.0, 36.6, 31.8, 31.8, 31.5, 27.8, 24.5, 22.8, 21.0, 19.3, 13.2, the signals of the two diastereoisomers overlap completely, appearing as a single compound; **^{19}F NMR** (377 MHz, $CDCl_3$) δ = -78.25 (d, *J* = 6.3 Hz, 3F), the signals of the two diastereoisomers overlap completely, appearing as a single compound; **HRMS (*ESI*)** m/z: $[M+HCOO]^-$ calcd. for $C_{31}H_{38}F_3O_6$ 563.2626; found 563.2633.

A short but due acknowledgment is made to Dr. Giulio Bertuzzi for his continuous support and whom great passion toward chemistry has always echoed in me, his guidance has proved essential throughout this wonderful journey.

[i] Riccardo Giovanelli acknowledge for fundings:

Borsa di dottorato del Programma Operativo Nazionale Ricerca e Innovazione 2014-2020 (CCI 2014IT16M2OP005), risorse FSE REACT-EU, Azione IV.4 "Dottorati e contratti di ricerca su tematiche dell'innovazione" e Azione IV.5 "Dottorati su tematiche Green". Codice borsa e n°: DOT1303815-3. CUP: J35F21003060006